UNIVERSITÀ DEGLI STUDI DI PAVIA

Doctorate in Biomedical Sciences

Department of Molecular Medicine
Unit of Biochemistry

Generation and phenotyping of two different murine models for chondrodysplasias caused by defects in proteoglycan biosynthesis

Supervisor
Prof. Antonio Rossi

Experimental PhD thesis by
Rossella Costantini

XXXI cycle- Academic Year 2017/2018

TABLE OF CONTENTS

LIST OF ABBREVIATIONS

ACG1B = Achondrogenesis type 1B

ADAMTSs = metalloproteinase with thrombospondin motifs

AMAC = 2-amminoacridone

AO2 = Atelosteogenesis type 2

BMP = bone morphogenetic protein

COMP = cartilage oligomeric matrix proteins

CS = chondroitin sulfate

DMMB = dimethylmethylene blue

DS = dermatan sulfate

DTD = Diastrophic dysplasia

DTDST = diastrophic dysplasia sulfate transporter

ΔDi-0S = 3-O-β (D-gluc-4-eneuronosyl)-N-acetylgalactosamine

ΔDi-4S = derivatives of ΔDi-0S with a sulfate at the 4 position of hexosamine moiety

ΔDi-6S = derivatives of ΔDi-0S with a sulfate at the 6 position of hexosamine moiety

ECM = extracellular matrix

ER = endoplasmic reticulum

ERAD = ER-associated protein degradation

FACIT = Fibril-associated collagens with interrupted triple helices

FGF = fibroblast growth factor

GAG = glycosaminoglycan

Gal = galactose

GalNAc = N-acetylgalatosamine

GlcNAc = N-acetylglucosamine

GlcUA = glucuronic acid

gSULT = Golgi sulfotransferases

HA = hyaluronan

HS = heparan sulfate

IdoUA = iduronic acid

KS = keratan sulfate

LP = link proteins

MIM = Mendelian inheritance in man

MMP = matrix metalloproteinases

MSC = mesenchymal stem cell

NRC = nucleotidase conserved regions

PAP = phosphoadenosine phosphate

PAPS = 3'-phosphoadenosine 5'-phosphosulfate

PAPSS = PAPS synthase

PAPST = PAPS antiporters

PG = proteoglycan

PTHrP = parathyroid hormone-related peptide

rMED = recessive multiple epiphyseal dysplasia

SBD-F = 7-fluorobenzofurazan-4-sulfonic acid ammonium salt

SLRPs = small leucine rich repeat proteoglycans family

T.E.M = transmission electron microscopy

TGF-β = transforming growth factor β

TIMPs = tissue inhibitors of metalloproteinases

VEGF = vascular endothelial growth factor

V_t = total volume

wt = wild types

Xyl = xylose

Abstract

Skeletal dysplasias are rare diseases that affect a small number of patients but still represent one of the largest classes of birth defects. More than 350 disease genes have been identified encoding for proteins involved in a wide spectrum of biological functions in cartilage and bone and 436 different disorders have been clustered in 42 different groups depending on molecular and/or clinical features. Among the recent classification of genetic skeletal disorders, there is a cluster of diseases such as, Desbuquois dysplasia, diastrophic dysplasia and recessive Larsen syndrome that display common features including short stature, dysplasia of skeletal elements, and congenital joint dislocations. At biochemical level all these disorders are characterized by defects in proteoglycans (PGs) that represent, with collagen, the most important components of the cartilage extracellular matrix.

They play several crucial roles maintaining cartilage physical and mechanical properties; moreover, PGs can bind growth factors regulating chondrocyte proliferation and differentiation. For these reasons alterations of PG synthesis, due to mutations in genes encoding for enzymes or proteins involved in the process, lead to the onset of genetic diseases affecting cartilage.

The molecular basis of many skeletal disorders are poorly understood, thus mechanistic studies using an *in vivo* approach is necessary to investigate the role of the disease gene in the disorder. Moreover since skeletal dysplasias are rare diseases and patients' biopsies are unavailable, the generation of animal models to elucidate the pathogenesis of dysplasias and to develop novel less invasive treatments are crucial.

Among this scenario, this work has been focused, using *in vivo* models, on the study of two chondrodysplasias in which proteoglycan synthesis is impaired: Chondrodysplasia with joint dislocation gPAPP type and Desbuquois dysplasia type 1. Chondrodysplasia with joint dislocation gPAPP type is a recessive osteochondrodysplasia caused by mutations in *IMPAD1* gene that encodes for a Golgi resident adenosine 3',5'-bisphosphate phosphatase crucial for

proteoglycan sulfation. Desbuquois dysplasia type 1 is a rare chondrodysplasia caused by mutations in the *CANT1* gene encoding for calcium-activated nucleotidase 1, a Golgi protein that preferentially hydrolyzes UDP.

The molecular knowledge of the two disorders is different; thus, in this thesis the two models have been used to pursue different objectives: I) the generation and characterization of a conditional knock-in mouse as model for the study of the chondrodysplasia with joint dislocations gPAPP type, II) the validation of a Cant1 knock-out mouse (dbqd mouse) as an animal model of Desbuquois dysplasia type 1 and the study of Cant1 role in PG biosynthesis.

In this work, we have tested an innovative strategy called "the Cre-mediated genetic switch" *in vivo,* with the aim to generate a Impad1 conditional knock-in mouse for a missense mutation already reported in a 23 years old patient. The Cre-mediated genetic switch combines the ability of Cre recombinase to stably invert or excise a DNA fragment depending upon the orientation of flanking mutant loxP sites. Targeting constructs were generated in which the *Impad1* exon 2 and an inverted exon 2 containing the point mutations, were flanked by mutant loxP sites in a head-to-head orientation. When the Cre recombinase is present, the DNA flanked by the mutant loxP sites is expected to be stably inverted leading to the activation of the mutated exon. The targeting vectors were used to generate heterozygous floxed mice in which inversion of the wild-type with the mutant exon has not occurred yet. To generate *Impad1* knock-in mice, floxed animals were mated to a global Cre-deleter mouse strain for stable inversion and activation of the mutation. Heterozygous mice were than mated to further generate homozygous mouse for the mutation. Unexpectedly the phenotype of homozygous *Impad1* knock-in animals overlaps with the lethal phenotype described previously in *Impad1* knock-out mice. Expression studies by qPCR and RT-PCR demonstrated that mutant mRNA underwent abnormal splicing leading to the synthesis of non-functional proteins. Thus, the skeletal phenotypes were not caused by the missense mutations, but by aberrant splicing. Our data demonstrate that the Cre mediated genetic switch strategy

should be considered cautiously for the generation of conditional knock-in mice.

The dbqd mouse, an animal model of human Desbuquois dysplasia type I, was previously generated by our research group.

The clinical phenotype of *Cant1* knock-out (dbqd) mice showed the same typical features of patients with Desbuquois dysplasia type 1 confirming the dbqd mouse as an animal model of the human disorder. Biochemical studies performed on dbqd mouse cartilage and chondrocyte cultures highlighted the contribution of CANT1 in PG synthesis. As it was demonstrated, glycosaminoglycan (GAG) synthesis was reduced and GAG chains were shorter and oversulfated compared with wild type mice. The defect in GAG chain synthesis caused reduced PG secretion altering therefore the extracellular matrix properties and composition.

In conclusion, the dbqd mouse can be considered an appropriate animal model of Desbuquois dysplasia type 1 since it resemble the same typical features observed in patients such as reduced size, growth retardation and delta phalanx. Moreover, biochemical studies have demonstrated that CANT1 is involved in PG metabolism since when CANT1 is impaired, PG and GAG synthesis are decreased and PG secretion delayed.

Chapter I

Cartilage and chondrodysplasias

1. CARTILAGE

Cartilage is a highly specialized connective tissue formed during the early embryonic stage of development as a template for bone formation and growth. Cartilage persist in some parts of the body, playing structural, morphological and mechanical roles: it reduces friction, bearing and transferring load between bones, and it is a high flexible and elastic tissue capable of resistance to traction and pressure forces. The main components of cartilage are extracellular matrix (ECM), whose main components are collagens and proteoglycans (PGs), water and inorganic ions, and specialized cells, chondrocytes, that produce and are embedded in the cartilage ECM. [1] Cartilage is an avascular tissue since it lacks blood vessels and nerves, therefore nutrients to chondrocyte are sustained by diffusion throughout the ECM. According to the absence of vessels, cartilage grows and repairs more slowly compared to other connective tissues. [2] A layer of connective tissue, called perichondrium, can be found around the perimeter of elastic cartilage and hyaline cartilage. The perichondrium consists of fibroblasts, which produce collagenous fibers, and undifferentiated cells that can generate chondrocytes or osteoblasts. Perichondrium is absent in articular cartilage and it plays a role in growth and repair of cartilage.

Depending on ECM composition and the mechanical and physical properties, three types of cartilage can be distinguished: hyaline cartilage, fibrocartilage and elastic cartilage.

Hyaline cartilage is the most present type of cartilage in the body. It can be found in trachea, larynx, in costal cartilage and most prominently in the joints where named as articular cartilage. In embryo during the endochondral ossification give rise to the anlage forming the skeleton.

It is mainly composed of water (70–80%) recalled by ECM components such as proteoglycans, collagens, and other macromolecules. This structure is responsible for the unique mechanical properties of the tissue.

Fibrocartilage is the strongest cartilage in the body, present in the intervertebral disks, pubic symphysis, meniscus, and at the interface between ligaments and tendons with bone. This type of cartilage is characterized by a large amount of collagen type I which forms, with collagen II, a dense longitudinal and circular network.

Elastic cartilage is present in the trachea, in the ear and in the epiglottis. The elasticity is provided by elastin fibers, randomly oriented within the tissue. The main role of the elastic cartilage is to maintain the shape and the flexibility of the organs. [1]

1.1 Articular cartilage

Articular cartilage has a highly organized layered structure produced upon maturation as a result of applied and generated hydrostatic forces through the tissue. This layered structure is composed of four different zones that varies according to the ECM composition as well as chondrocyte morphology. Each of these zones possesses unique structural, functional and mechanical properties [3] and can be divided as following: (1) the top layer, also denoted as a superficial or tangential zone, (2) the middle or transitional zone, (3) the deep or radial zone, and (4) the calcified zone. [4,5] (**Figure.1**)

The articulating surface of cartilage, also known as lamina splendens, is covered by a thin layer composed of proteins and has an acellular and non-fibrous character. The lamina splendens is made by the progressive accumulation of proteins from the synovial fluid and it serves mainly to preserve cartilage from low-friction, but its precise role is still unknown. [6]

Under the lamina splendens, in the superficial zone (10–20% of the cartilage thickness), the collagen type II fibers are densely packed and aligned parallel. The concentration of proteoglycans in this zone is low, therefore the permeability of the tissue is higher in comparison to other deeper layers. [7] The chondrocytes within the region appear flattened and elongated, and are

arranged parallel to the surface, densely packed along the collagen fibers. This architecture is optimized to dissipate high shear forces, protecting deeper layers from deformation. [8]

Right underneath the superficial zone there is the middle zone (40-60% of the cartilage thickness), characterized by a low density and spherical chondrocytes expressing a large amount of collagen II and proteoglycans such as aggrecan. Type II collagen is organized in thick fibers having an oblique orientation randomly distributed. The middle zone has the highest proteoglycan content of all other zones.

In the deep zone together with the calcified zone (20–50% of the cross sectional length) chondrocytes are elongated and organized in short columns perpendicularly orientated to the surface. Chondrocytes produce and release less collagen II, but start to produce collagen X. The deep zone is divided to the calcified zone by a thin layer called tidemark. The calcified zone contains hypertrophic chondrocytes that start to deposit hydroxyapatite. This zone serves as a transition zone between the cartilage and hard bone. (**Figure.1**)

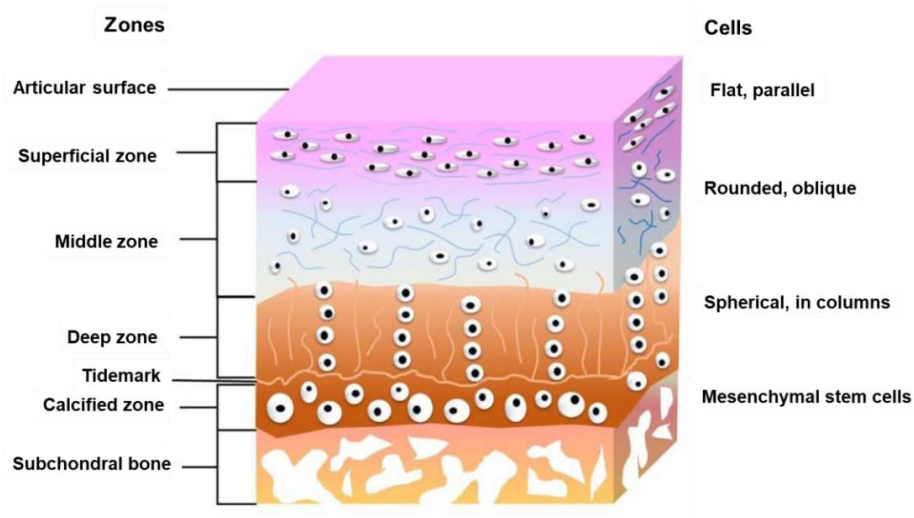

Figure 1: Structure of mature articular cartilage zones.

Schematic illustration of the depth-dependent structure of articular cartilage, highlighting the different cell organization throughout the four horizontal layers. From *Ng HY et al. 2017.*[135]

Articular cartilage has a secondary microstructure, called chondron, that varies according to the radial distance from the chondrocytes.

The chondron is constituted by chondrocytes surrounded by a narrow matrix region that is compositionally and structurally distinct from the surrounding bulk ECM. This region is approximately 2 to 4 μm thick and is called the "pericellular matrix" (PCM). The PCM then integrates with the adjacent tissue via the "territorial matrix" (Tm), connecting in the end, the PCM to the "interterritorial matrix" (Im). The PCM has high concentration of aggrecan, link protein and hyaluronan, and a collagen type II content that forms thicker collagen II bundles. Together with collagen II, collagen type IX and VI are present in the pericellular matrix in high concentrations. [9]

This architecture is thought to modulate the environmental signals before they reach the chondrocytes playing a key role in chondrocyte gene expression and epigenetic state. In the interterritorial matrix collagen II appears as small-diameter fibers (10–15 nm) that form a tight interlinked structure, the pericellular capsule. [10] This architecture is thought to be a hydrodynamic protection for chondrocytes, serving as a flexible cushion supporting the load by reversible deformation. [11]

The territorial matrix (Tm) has a composition similar to the interterritorial matrix, but with thinner collagen II fibrils and higher proteoglycan concentration that is rich in chondroitin sulfate. [12] (**Figure 1.1**)

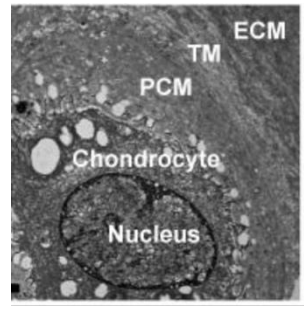

Fig 1.1: Structure and morphology of the chondron. Transmission electron microscopy (TEM) showing the chondrocyte within the pericellular (PCM), territorial (TM), and extracellular matrix (ECM) (scale bar = 1 μm). Adapted from *Wilusz et al. 2014* [137]

1.2 Endochondral ossification and growth plate

During embryonic development, mesenchymal stem cells (MSCs) are derived from the mesoderm and form the components of the appendicular skeleton such as the limbs. [13] Upon development of the limbs, MSCs undergo to a condensation of cells and further mitosis, thus increasing the cell density within the condensate. In the center, the MSCs of the condensate undergo differentiation into prechondrogenic cells giving rise to the cartilage anlage for the new bone. The cells at the edges differentiate into fibroblasts forming the perichondrium. Chondrocytes proliferate producing the typical cartilage ECM with collagen II and abundant aggrecan, producing the enlargement of the anlage; At the start of the fetal period, chondrocytes at the center of the cartilaginous templates stop proliferating, becoming bigger producing collagen type X, and undergo hypertrophy and lastly apoptosis. During this phase hypertrophic chondrocytes release the vascular endothelial growth factor (VEGF) inducing the invasion of blood vessels, osteoclasts, osteoblast progenitors and hematopoietic cells from perichondrium. Additionally VEGF not only promotes angiogenesis, but also stimulates cartilage matrix resorption by osteoclasts activity [14]. The concomitant activity of osteoclast, that degrade the cartilage extracellular matrix, and the differentiation of osteoblast progenitors in osteoblast secreting collagen I, give rise to the mineralization of the cartilage remnants. Simultaneously, hematopoietic cells and blood vessels form the bone marrow [15]. All these events give rise to the formation of the primary ossification center, that further develops into the trabecular bone, from which the bone continues to lengthen, while in the perichondrium osteoblast progenitors differentiate in osteoblast that start bone mineralization creating a bone collar around the cartilage anlage. Around the time of birth, at the other end of the cartilage anlage, a second ossification center is formed in the middle of the epiphyses at the ends of long bones, resulting in compartmentalization of epiphyseal cartilage into articular cartilage peripherally, and a central portion of

cartilage, named growth plate, whose main role is to ensure long bones growth. (**Figure 2)**

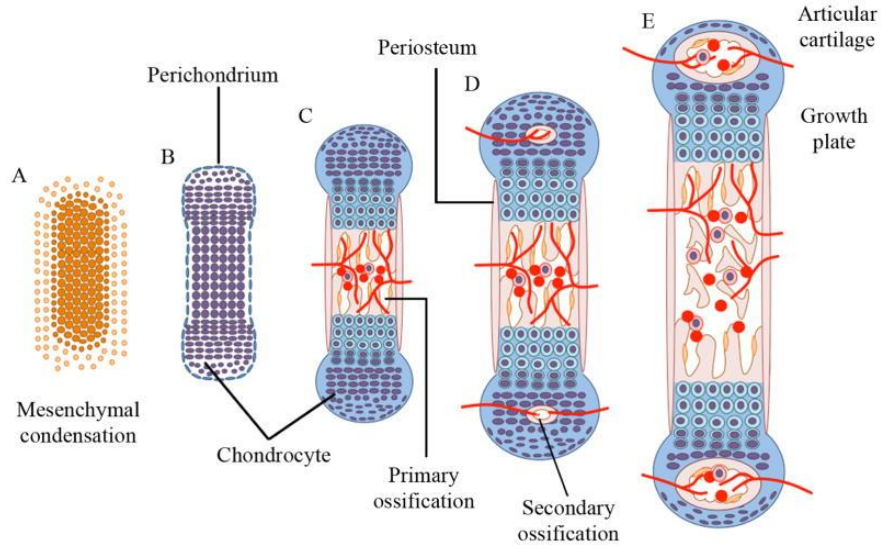

Figure 2: Schematic representation of endochondral ossification. (A) Endochondral ossification starts with the formation of mesenchymal condensation and (B) mesenchymal cells differentiate in chondrocytes that proliferate forming a cartilage anlage for new bone. (C) In the centre of cartilage anlage chondrocytes undergo hypertrophy and promote the vascular invasion and formation of primary ossification centre. (D) After birth the secondary ossification centre is formed. (E) Between the two centres of ossification growth plate is entrapped allowing the bone growth. A*dapted from Usami et al. 2016* .[136]

The growth plate can be subdivided into three stratified zones according to chondrocyte size, shape, organization, and function (**Figure 2.1**). The resting zone is the first and the closest zone to the secondary ossification center. In this zone chondrocytes are relatively mitotically inactive, flattened and express markers such as Col2a1 (encoding for type II collagen). Below this zone, chondrocytes quickly proliferate and express Col2a1 and Acan (aggrecan) at high level. Chondrocytes start undergo to a clonal expansion, dividing three to five times and organizing in parallel columns. Next, chondrocytes exit the cell cycle and become prehypertrophic, expressing Col10a1 (type X collagen) and Ihh (Indian Hedgehog) [16]. Prehypertrophic chondrocytes increase in size, to

become hypertrophic cells that stop expressing Col2a1 but continue expressing Col10a1. Hypertrophic chondrocytes eventually stop expressing Col10a1 and reach terminal stages, undergoing apoptosis, autophagic cell death, or transdifferentiation. During hypertrophy chondrocytes change morphology and metabolism: chondrocytes increase in height and cellular volume but reduce the cellular density because of the increase in surface of the organelles such as RER and Golgi apparatus; volume of extracellular matrix drop drastically until chondrocytes undergo apoptosis, autophagy or transdifferentiation in osteoblast, concluding the hypertrophic process. Hypertrophic chondrocytes express several proteinases such as MMP13, MMP9, ADAMTS, cathepsins and calpain allowing the degradation of ECM surrounding the cells. The matrix degradation is an important process required by volume expansion of hypertrophic chondrocytes and vascular invasion [17]. Towards the bone diaphysis and below the hypertrophic zone, matrix calcification and bone tissue formation occurs. In fact at the end of the hypertrophic zone, blood vessels can invade and, concurrently, osteoblasts can deposit bone allowing skeletal growth. The rapid chondrocyte loss is balanced by rapid proliferation and hypertrophy of chondrocytes within the growth plate [18]. Until the puberty the growth plate grows and endochondral ossification continues allowing bones growth.

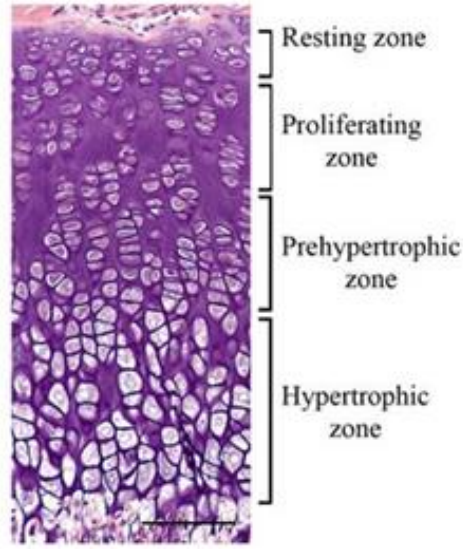

Figure 2.1: The growth plate.

Histological section of cartilage growth plate stained with hematoxylin and eosin. Growth plate is organised in several zones. Adapted from *Usami et al. 2016* [136]

The signaling cascade involved in skeletal development need to be finely tuned because it allows developmental signals from the environment to transduce into proper spatial- and temporal-specific cellular responses. These signaling cascades converge on master chondrocyte transcription factors, including Sox9, Runx2, and Osterix. Two of the most important pathways that regulate proliferation and hypertrophy in growth plate chondrocytes are Ihh and parathyroid hormone-related peptide (PTHrP) signaling that interact through a negative feedback. Ihh is synthesized by pre-hypertrophic and early hypertrophic chondrocytes and binding its receptor Patched-1 activates directly chondrocyte proliferation and expression of PTHrP. Instead PTHrP is synthesised by perichondral cells and early proliferating chondrocytes and acts on chondrocytes in the proliferative zone to stimulate proliferation and delay hypertrophy. Chondrocytes, that are distant from PTHrP-producing cells, cannot receive the PTHrP signal and thus they start the hypertrophic process and produce Ihh. Moreover Ihh can also stimulate osteoblasts differentiation in

the perichondrium near the hypertrophic zone of the growth plate leading to bone collar formation [17,19]. For correct Ihh signaling a morphogen gradient within the growth plate is necessary. The ability of HS and CS to bind Ihh allows the formation of the Ihh gradient. Indeed near Ihh producing cells there is an high concentration of HS that binds with high affinity Ihh causing a local retention. CS chains of aggrecan in the cartilage ECM can bind Ihh allowing its diffusion throughout the growth plate and preventing its degradation. Finally HS attached to cell-surface PGs on target cells can bind Ihh and favours the binding to its receptor [20].

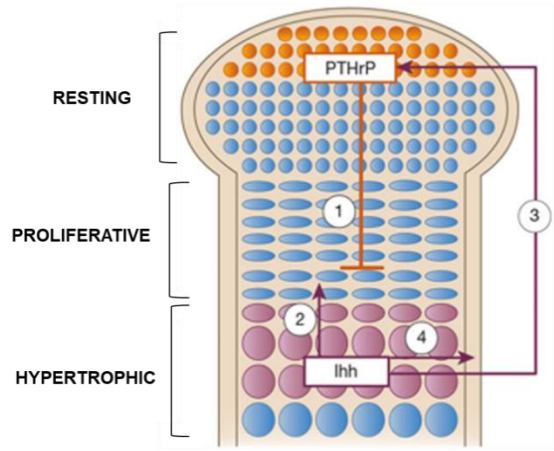

Fig. 2.2: Model of PTHrP and IHH regulation.

PTHrP is made by undifferentiated and proliferating chondrocytes at the ends of long bones. It acts through the PTH1R on proliferating and prehypertrophic chondrocytes to delay their differentiation, maintain their proliferation, and delay the production of IHH, which is made by hypertrophic cells (1). IHH, in turn, increases the rate of chondrocyte proliferation (2) and stimulates the production of PTHrP at the ends of the bone (3). IHH also acts on perichondral cells to generate osteoblasts in the bone collar (4). Adapted from *Kronenberg H. M.et al.* 2003[19]

TGFβ signaling is another important signaling pathway involved in the inhibition of chondrocyte hypertrophy, stimulating expression and maintenance of SOX9 [21]. For instance TGFβ2 mediates the signaling of Ihh, but on the other hand TGFβ1 stimulates non-apoptotic physiological death [22]. TGFβ

acts on perichondrium cells and proliferating chondrocytes of the growth plate where TGFβR1 and 2 are present on the cell membrane [23]. BMP, another member of TGFβ superfamily, is crucial to endochondral ossification since BMP signaling stimulates cartilage condensation and also regulates the proliferation and differentiation of growth plate chondrocytes [17]. In particular BMP signaling stimulates resting chondrocytes to proliferate. Moreover it induces hypertrophic differentiation playing an antagonist role to the TGFβ pathway and acting independently to Ihh/PTHrP signaling [23]. The antagonist of BMP signaling is the FGF pathway that inhibit chondrocytes proliferation and promote hypertrophy and vascular invasion. Most important members of the FGF family in the growth plate are FGF9 and 18 with redundant functions: FGF18 stimulates chondrocytes proliferation and hypertrophy in early stages of gestation, while in late gestation inhibits them [21]. In the growth plate WNT can act through two pathways: a canonical pathways allowing β-catenin to translocate in nucleus and activate gene expression and a non-canonical pathway including planar cell polarity (PCP). Through WNT canonical pathway β-catenin antagonizes SOX9 activity regulating chondrocytes differentiation. On the other hand non-canonical WNT signaling inhibits canonical ones promoting chondrocyte differentiation and induces column formation by growth plate chondrocytes [21].

1.3 Chondrocyte: the cartilage cellular component

Chondrocytes are the only resident cells in the articular cartilage [19]. Usually they are rounded cells, with a diameter of 15-30 µm, but they can also assume a flattened or elliptical shape depending on the cartilage region in which they are resident. All chondrocytes have the same features related to gene and protein expression, surface markers and metabolic activity. However, they can show differences depending on the specific region in which they are located, especially along the depth of the cartilage tissue [1]. Since the chondrocyte has to synthesize and turnover a large matrix volume comprising collagens, glycoproteins and proteoglycan, they display typical features of a metabolically active cells. Chondrocytes are characterized by a highly expanded Golgi apparatus with numerous mitochondria, evident centrioles, and vesicular nuclei with several nucleoli. Other specific features present are the possession of a primary cilium and the relatively high matrix to cell volume ratio: the chondrocytes occupying about the 1-5% of the total tissue volume. Chondrocyte appear isolated within a voluminous extracellular matrix (ECM) that is neither vascularized nor innervated. As a consequence, nutrient/waste exchange occurs through diffusion and, the cell is able to exist in a low oxygen tension environment. During embryo development, mesenchymal progenitors that originate from the mesoderm give rise to the limb skeleton formation. The molecular events that regulate the differentiation of mesenchymal cells into chondrocytes are complex and not well characterized yet. Initially the chondrogenic differentiation is determined by the fibroblast growth factor 2 (FGF-2). The condensate mesenchymal cells express the transcription factor Sox9, which is a key regulator of chondrogenesis, and give rise to cartilage primordia consisting of round immature chondrocytes that continue to express Sox9 [24]. Therefore Sox9 is considered to be the principal chondrogenic transcription factor because its expression is found at high level in the MSCs progenitors [20, 21]. Moreover Sox9 interacts with many other transcription

factors such as SOX5/SOX6 [25], CREB/p300[26] and cMaf [27] regulating the gene expression of main cartilage ECM molecules as collagen II [28], IX [29], XI [30], aggrecan[31] and cartilage link protein [32]. Chondrocytes are well differentiated cells whose phenotype is highly regulated by interactions with the surrounding ECM [33]. Another group of transcription factors, SOXC, composed of SOX4, SOX11 and SOX12, are responsible to antagonize the chondrogenic action of SOX9, inhibiting the chondrogenesis. Therefore they downregulates Sox9 expression acting with canonical WNT signaling [34].

2. CARTILAGE EXTRACELLULAR MATRIX

The cartilage extracellular matrix (ECM) contains a set of related molecules interacting to form a complex networks. Depending on the different assembly of the specific molecules, different extracellular matrix are present in all the tissues. For long time ECM was considered a matrix present to fulfill space around cells, instead ECM has more complex functions such as regulating cell behavior and proliferation, binding growth factor or allowing the interaction of growth factors with cellular receptors. The major protein forming the ECM are fibril forming collagens and other proteins that interact all together [35]. Specifically the collagens fibrils are collagen II, and for approximately the 5% of the fibrils, collagen XI [36]. Other types of collagen, such as collagen IX, can interact with collagen fibrils and bind other ECM molecules. Fibril formation and stability is tuned by other ECM proteins, mainly belonging to the small leucine rich repeat proteoglycans family (SLRPs) such as decorin [37], biglycan [38], fidromodulin [39] and lumican [40], thrombospondin [41] and matrilins [42]. Other non-collagenous proteins present in cartilage ECM are proteoglycans (PGs), mainly aggrecan, which is assembled to large aggregates interacting with hyaluronan (HA) [43]. Cartilage ECM homeostasis is maintained by a continuous remodeling thanks to a perfect combination and balance between new molecules synthesis and matrix degradation due to the activity of matrix metalloproteinases (MMPs). ECM degradation is also regulated and inhibited by inhibitors of MMPs [44]. (**Figure 3**)

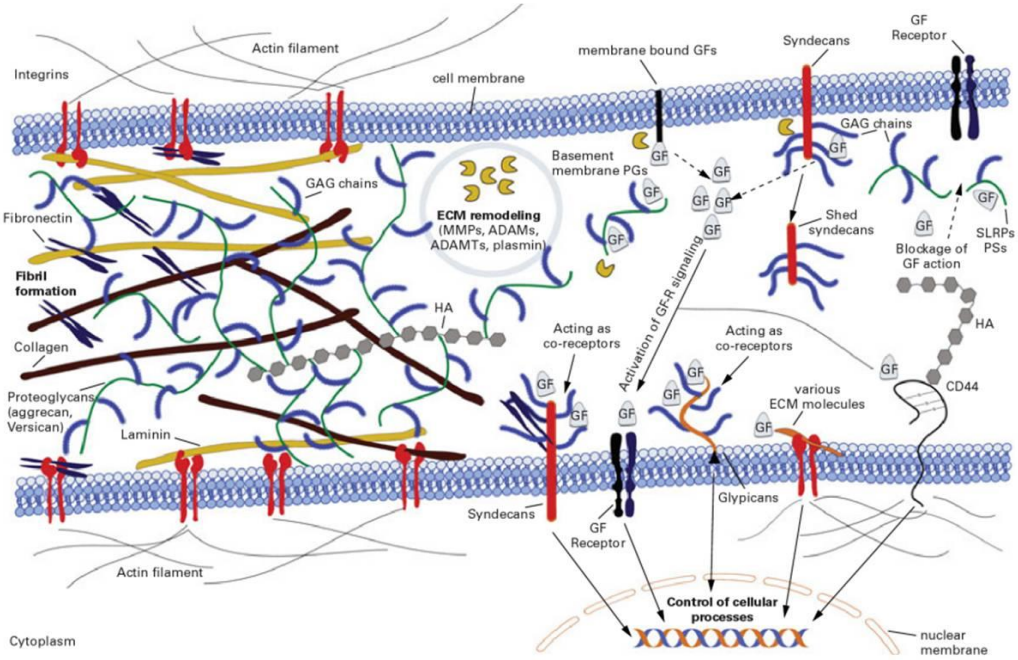

Figure 3. Schematic representation of the major components of cartilage extracellular matrix. Proteoglycans and collagen form a high organized meshwork in which other molecules are immersed. This network confers shape and mechanical characteristics to cartilage extracellular matrix, providing an adequate substrate for chondrocyte growth and differentiation. Adapted from *Theocharis A. et al.* [138].

2.1 Proteoglycans

Proteoglycans (PGs) are a class of multifunctional macromolecules present in the ECM of different tissues and on the cell membrane with a great effect on cell life and behavior. PGs are composed of a core protein onto which a variable number of polysaccharide chains, called glycosaminoglycans (GAGs), are covalently attached. GAG chains can differ in number and size according to the status of cell or tissue [45]. PGs are classified depending on cellular and subcellular location, the presence of specific protein modules within their respective protein cores, and GAGs structure. According to this, four major proteoglycan classes include nearly all the known proteoglycans. Based on cellular and subcellular localization, there is only one PG intracellular located: serglycin. It is the only proteoglycan that brings heparin side chains and forms a

class on its own for this unique properties. Serglycin is packaged in the granules of mast cells [46]. Associated with the cell surface or the pericellular matrix there are Heparan sulfate proteoglycans (HSPGs). The HSPGs associated with the plasma membranes of cells function as major biological modifiers of growth factors, while the HSPGs located in the basement membrane zone interact with each other and with key constituents of the basement membrane, participating in the generation and maintenance of gradients for morphogens during embryogenesis and regenerative processes. Moving away from the cells, proteoglycans constituents of extracellular matrices are chondroitin- and dermatan sulfate containing proteoglycans (CSPGs and DSPGs, respectively). They provide the typical mechano-physical and chemical properties of the matrices. Moreover the extracellular matrix contains the biggest class of proteoglycans, the so-called small leucine-rich proteoglycans (SLRPs) which are the most abundant products in terms of gene number. SLRPs can function both as structural constituent and as signaling molecules [46]. (**Figure 3.1**)

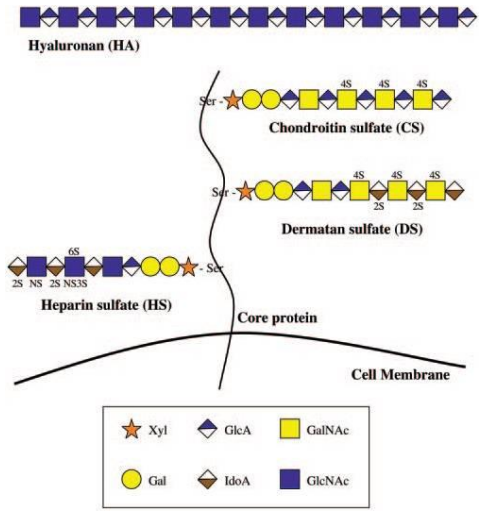

Figure 3.1: Disaccharide composition of glycosaminoglycan chains and their attachment to core protein of proteoglycans. Adapted from *Taylor K.R. and Gallo R. L.* [139].

Glicosaminoglycans (GAGs) are linear unbranched polysaccharide chains whose disaccharides units consist of an amino sugar, N-acetylglucosamine (GlcNAc) or N-acetylgalactosamine (GalNAc), and an uronic acid, glucuronic acid (GlcUA) or iduronic acid (IdoUA). Depending on the different organization of these sugar moieties, GAGs may differ with each other. [47] GAGs usually have a strong negative charge conferred by the acidic sugar moieties and the sulfate groups present in different positions along the GAG chains [48]. GAGs can be divided according to the presence of sulfate groups in: sulfated glycosaminoglycans represented by chondroitin sulfate (CS), keratan sulfate (KS), dermatan sulfate (DS) and heparin sulfate (HS) and non-sulfated glycosaminoglycans such as hyaluronan.

The more relevant sulfated GAG in cartilage is represented by chondroitin that is composed by repeated disaccharide unit of glucuronic acid and N-acetylgalactosamine linked by a β1-3 glycosidic bond. Generally GalNAc residues are sulfated in C-4, forming chondroitin A, or in C-6, forming chondroitin sulfate C. On the contrary disulfated disaccharides, with sulfate groups in C-2 of GlcUA and in C-6 of GalNAc (D unit) or in C-4 and C-6 of GalNAc (E unit) are rare [49].

The chondroitin chain is subjected to modifications such as epimerization of the GlcUA in iduronic acid forming Dermatan sulfate (DS) GAG. The repeated disaccharide unit of IdoUAα1-3GalNac may be mono- or di-sufated on the C-4 and C-6 of GalNac or disulfated in positions C-2 of IdoUA and in C-6 of GalNac and in C-2 of IdoUA and C-4 of GalNac but the latter is very rare [49]. DS is present in different tissues such as blood vessels and heart valves, skin and tendon.

Heparan sulfate assemble as GlcNaAcα1–4GlcUAβ1-4 disaccharide and then is subjected to widespread modifications reactions including sulfation/deacetylation of GlcNaAc forming $GlcNSO_3$ and epimerization of GlcUA to IdoUA. Sulfation can occur in C-2 of GlcUA/ IdoUA and in C-3 C-6 of GlcNAc. The modifications occur in clusters during HS biosynthesis, giving

rise to different domains of N-acetylated (NA), N-sufated (NS) and mixed domains (NA/NS) flanked by non-modified regions. The HS structure and amount depends strictly by the cell type and on the developmental stage. [50,51]

CS, DS and HS GAGs are linked to a serine residue in core proteins via tetrasaccharide linkage region (Xyl-Gal-Gal-GlcUA). A specific consensus sequence does not exist but generally a glycine stands at the C-terminal end of the serine residue and other two amminoacid are present.

Keratan sulfate is made up of repeated disaccharides of sulfated GlcNAC and galactose (Gal) linked directly to the core protein through either N-glycosylation bonds to asparagine residue, forming KSI, or O-glycosylation bond to serine or threonine, forming KSII and KSIII. The disaccharides units may be both sulfated on C-6 carbon, but GlcNAc is the most abundant. KS is express in cartilage, bones, cornea and in the brain [48].

Hyaluronic acid (HA) is a non-sulfated GAG without covalent protein attachment. HA is a long polimer made up of repeated disaccharides units of GlcUA and GlcNAc. Moreover the synthesis of HA is peculiar since, in contrast to the biosynthesis of the other GAGs that occurs in the Golgi, HA is synthesized on the inner surface of the plasma membrane and then directly released. HA is abundant in extracellular matrices and at the cell surface, where it can modulate a large number of molecules, maintaining the cartilage mechanical properties and functions. Furthermore it interacts to RHAMM receptor (CD44 HA-mediate motility receptor) and TLR (toll-like receptors) mediating also angiogenesis and inflammatory response. HA is present in connective and epithelial tissues in the synovial fluid of joints, in the vitreous humor of the eye and also in the neural tissue [52].

2.1 Proteoglycan biosynthesis and degradation

The proteoglycan synthesis is a complex and multistep process that can be divided in four main steps: core protein synthesis, GAG synthesis, GAG sulfation and PG secretion. (**Figure 4**)

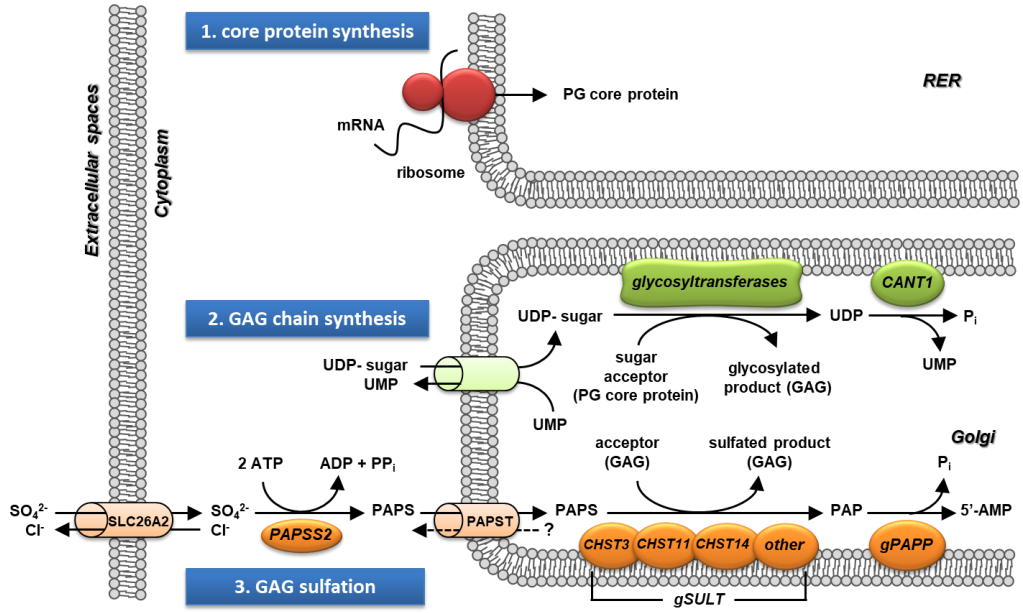

Figure 4: Schematic representation of the proteoglycan synthesis process. The core protein of PG is synthesized in ER lumen and then it moves to Golgi, where synthesis and sulfation of GAG chains occur. Once synthesized PGs can be secreted in ECM.

The protein component of PGs is synthesized by ribosomes on the rough endoplasmic reticulum and then translocated into the lumen where the modifications required for protein secretion, such as the addition of the N-linked oligosaccharides, begins. Once the core protein is synthesized, it moves to the Golgi apparatus where GAG chains synthesis take place. CS, DS and HS, the main GAGs present in PGs have the presence of a tetrasaccharides, made of one xylose, two galactose and one glucuronic acid, through which they are attached to a serine residue. β-Xylosyltransferase (XylT), encoded by *XYLT1* gene, catalyzes the attachment of the serine residue to the core protein using UDP-xylose as donor. After xylose addition two galactose residues are added

from UDP-Gal by β1,4-galactosyltransferase-I (GalT I) and β1,3-galactosyltransferase-II (GalT II), that are encoded respectively by *B4GALT7* and *B3GALT6* genes. The transfer of GlcUA from UDP-GlcUA to the second Gal is catalyzes by β1,3-Glucuronosyltransferase-I (GlcAT-I) encoded by *B3GAT3* gene [53,54] .

Modifications such as 2-O-phosphorylation of Xyl residues, or sulfation at C-6 on the first Gal and at C-4 and C-6 on the second Gal may occur on tetrasaccharides. Phosphorylation can be transient and together with sulfation regulate the activity of GalT-I and GlcAT-I suggesting a role in processing or sorting of GAG [45].

After tetrasaccharide linkage region assembles, GAG biosynthesis can start with the repeated disaccharide units. To obtain chondroitin sulfate, β1,4-N-acetylgalactosaminyltransferase-I (GalNAcT-I) catalyzes GalNAc transfer from UDP-GalNAc, on GlcUA residue. After that, polymerization of the CS backbone occurs to construct the repeated disaccharide region consisting of GalNAc β1–4 GlcA. These reactions are catalyzed by a CS polymerase complex composed of various combinations of synthase enzymes, including chondroitin synthase (ChSy), chondroitin polymerizing factor (ChPF), and other four family members [55] [56]. The catalytic activities for the addition of GlcA and GalNAc, performed by these enzymes, have been named CSGlcAT-II and GalNAcT-II respectively.

Sulfation of disaccharide unit is catalysed by different sulfotransferases (SULTs). Three sulfotransferases specific for C-4 sulfation of GalNAc are present: Chondroitin-4-O-sulfotransferase 1, 2 and 3 (C4ST1-3); whereas just one for C-6 sulfation of GalNAc, Chondroitin-6-O-sulfotransferase (C6ST) has been identified, for disulfated GalNAc, GalNAc-4-O-sulfate-6-O-sulfotransferase (GalNAc4S-6ST) and for sulfation at C-2 position of GlcUA, uronosyl-2-O-sulfotransferase (UST) [57]. To synthesize DS chains, GlcA residues are epimerized to IdoA by an enzyme named DS C5-epimerase (DSE). The epimerization reaction is accompanied by an anomeric change of the

glycosidic linkage of GlcA from β to α. DS is sulfated by dermatan-4-O-sulfotransferase (D4ST) and UST [54]. Both the modifications occur during GAG synthesis or before PG secretion[45].

HS polymerization begin with the addition of a GlcNAc on the linkage tetrasaccharide catalyzed by α1,4-N-acetylglucosaminyltransferase-I (GlcNAcT-I). Then HS-β1,4-glucuronyltransferase-II (HS-GlcAT-II) and α1,4-N-acetylglucosaminyltransferase-II (GlcNAcT-II) transfer GlcUA and GlcNAc from UDP-GlcUA and UDP-GlcNAc on HS chain. HS undergoes a large number of modifications such as epimerization of GlcUA in IdoUA by HS-glucuronyl-C5-epimerase, deacetylation of GalNAc residue by N-deacetylase, and sulfations at C-2 of uronic acid and C-3 and C-6 of GlcN by HS-2-O-sulfatransferase, HS-3-O-sulfatransferase and HS-6-O sulfatransferase [45]. Additionally HS-6-O-endosulfatase removes the sulfate group from 6-O-sulfated GlcNS in HS chain changing its structure to regulate several biological event as cell signaling and tumour growth [58,59,60].

Keratan sulfate is linked through D-GalNAc to serine or threonine residues of the core protein and then for its synthesis follows the addition of the disaccharide units composed of Gal and GlcNAc. At least two sulfotransferases, GlcNAc-6-O-sulfotransferase and galactose-6-O-sulfotransferase catalyze the sulfation reaction on KS chain [61]. GlcNAc-6-O-sulfation occurs only on the nonreducing terminal, while galactose sulfation occurs on the nonreducing terminal and on internal galatose adjacent the sulfated GlcNAc [61]. Remarkably sulfation on the nonreducing terminal galactose might block KS chain elongation providing a mechanism for controlling the chain length [45].

Hyaluronan synthesis occurs at the inner surface of plasma membrane through the activity of three different isoenzymes, named HA synthases 1, 2 and 3 (HAS1, HAS2 and HAS3). HASs are integral membrane proteins with two different active site that can bind the two UDP-sugars therefore they catalyze the transfer of GlcUA and GlcNAC from UDP-GlcUA and UDP-GlcNAc. Different isoenzymes produce HA with different molecular weight [62,63].

The sulfation is the next and important step in PGs biosynthesis because it confers to the molecules their biological effects. Sulfotransferases enzyme located in the Golgi lumen (gSULT), catalyzes the attachment of sulfate groups to the GAG growing chains. These sulfotransferases use 3'-phosphoadenosine-5'-phosphosulfate (PAPS) as universal sulfate donor, transferring the sulfate group present on PAPS to sulfate acceptor substrates. The maintenance of PAPS concentration is important for sulfotransferase reactions and a continuous uptake and activation of inorganic sulfate is required. PAPS is synthesized in the cytoplasm starting from adenosine triphosphate (ATP) and inorganic sulfate. (**Figure 4.1**)

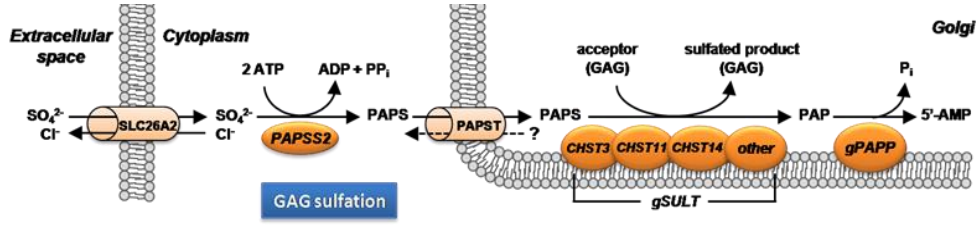

Figure 4.1: Schematic representation of the sulfate activation pathway.

Sulfate enters the cells trough SLC26A2 sulfate/chloride antiporter and it is activated to PAPS by PAPS synthase II. PAPS moves to Golgi where it is used for macromolecules sulfation, especially GAGs, by Golgi sulfotransferases (gSULT). The residual PAP is then hydrolyzed to 5'-adenosine monophosphate (5'-AMP) and inorganic phosphate by a Golgi 3'-phosphoadenosine 5'-phosphate-phosphatase (gPAPP) enzyme. Then, 5'AMP and inorganic phosphate can exit from the Golgi.

The intracellular sulfate pool depend on extracellular concentration and only for a small amount can come from the catabolism of sulfur-containing amino acids. Inorganic sulfate enters in the cell [64]. PAPS synthesis requires two serial reactions, the first is the conjugation of one inorganic sulfate molecule with one ATP molecule, resulting in adenosine 5'-phosphosulfate (APS) and pyrophosphate formation, reaction catalyzed by the action of ATP sulfurylase [65]. The second reaction in PAPS formation is catalyzed by APS kinase and requires another ATP molecule, which reacts with APS, forming PAPS. In

mammals, ATP sulfurylase and APS kinase are grouped together forming a multi enzymatic complex termed PAPS synthase (PAPSS) [66].

Once PAPS is synthesized in the cytoplasm, it is transported to the Golgi apparatus, where sulfate can be donated for sulfotransferase reactions. PAPS transport is mediated by two specific PAPS antiporters (PAPST) exchanging PAPS with phosphoadenosine phosphate (PAP) or adenosine monophosphate (AMP) [67,68]. As a result, for each reaction there is the attachment of one sulfate group to the GAG growing chains and as secondary product, the production of one molecule of 3'-phosphoadenosine-5'-phosphate (PAP). PAP is then hydrolyzed to 5'-adenosine monophosphate (5'-AMP) and inorganic phosphate by a Golgi 3'-phosphoadenosine 5'-phosphate-phosphatase (gPAPP) enzyme [69,70]. 5'AMP and inorganic phosphate can exit from the Golgi and, in the cytoplasm, they can be recycled and reused in other cellular mechanisms. At the end of GAG chain synthesis, newly synthesized PGs are secreted in ECM through secretory vesicles, where they perform their functions.

PG degradation is a high complex process finely regulated by different enzymes for core protein and GAG catabolism. PGs degradation begin in ECM where proteolytic enzymes are present in latent forms [45] and their activity is finely tuned by tissue inhibitors of metalloproteinases (TIMPs). Once these enzymes are activated, they produce proteoglycan fragments [71,72] digesting PGs in different sites within the core protein. These fragments are then endocytosed and degradation continues in lysosomes. The core protein is catabolized by lysosomal proteases, whereas GAGs are hydrolyzed by the lysosomal glycosidases that are specific for the hydrolysis of each monosaccharide type. Moreover a specific sulfatase catalyzes the sulfate group removal from the sulfated monosaccharide [45].

2.2 Cartilage proteoglycans

In cartilage the 10% of tissue dry weight is represented by proteoglycans, among which aggrecan is the main. It is a large proteoglycan possessing a core protein of 250kDa and numerous glycosaminoglycan chains that confer the ability to form aggregates in association with hyaluronan. All aggrecan molecules are composed of three globular domain termed G1, G2 and G3, with a small interglobular domain (IGD) separating G1 from G2, and a long GAG-attachment region separating G2 fromG3 [73]. (**Figure 5**)

The G1 region is in the N- terminal portion of the aggrecan core protein, and is responsible for the interaction with HA. It is composed of three disulfide-bonded domains termed A, B and B' [74]. The B and B' domains are responsible for the interaction with HA, while the A domain is responsible for the stabilization of the interaction with the HA. The G1 region can be glycosylated by N-linked oligosaccharides or KS [75]. The spacer region between G1 and G2 domain is termed IGD domain and it is susceptible to proteinases cleavage. The IGD domain can also be glycosylated by both N-linked and O-linked oligosaccharides or KS [75].

It is not clear until now the functional role of the G2 region, which is composed of two disulphide-bonded B and B' similar to those in G1 domain domains, but they do not interact with HA. The GAG-attachment site is constituted by a KS-rich and CS-rich domains. In particular, following the G2 region there is the KS-rich domain in which about 30 KS are O-linked to serine residues. It is a region constituted of a sequenced repetition of six amino acid (E-E/K-P-F-P-S), that contains proline and serine [76]. Aggrecan possesses two adjacent CS-rich domains termed CS1 and CS2, different for the aminoacid composition. In the CS-rich domain about 100 CS are bound to the core protein where a regular repetition of serine and glycine is present and may represent the attachment site of the CS [77,78].

The G3 region is formed at the C-terminal portion of the core protein. It is composed of several disulfide-bonded domains with homology to the epidermal growth factor (EGF), c-type lectin and complement regulatory protein (CRP) [79] and appears to be essential for normal trafficking of the molecule through the cell and subsequent secretion [80]. (**Figure 5**)

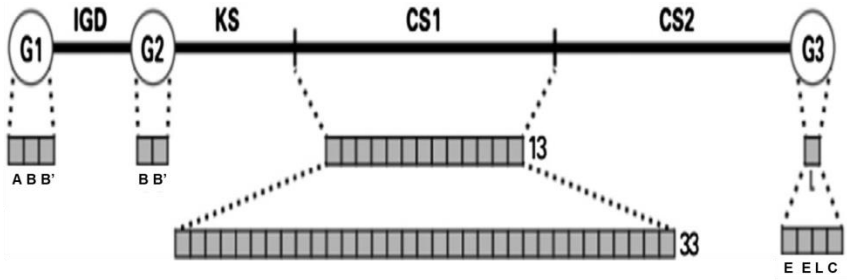

Fig. 5: **The domain structure of aggrecan**.

The figure depicts the aggrecan core protein with 3 globular regions (G1, G2 and G3) and 4 extended domains (IGD, KS, CS1 and CS2). The G1 region is divided into three domains (A, B and B′) and the G2 region is divided into 2 domains (B and B′). The G3 region can possess 4 domains (E, E, L and C; though the 2 E domains and the C domain may be absent due to alternative splicing). The CS1 domain is composed of between 13 and 33 repeat sequences. IGD, interglobular domain; KS, keratan sulfate-rich domain; CS1, chondroitin sulfate-rich domain 1; CS2, chondroitin sulfate-rich domain 2; E, epidermal growth factor-like domain; L, lectin-like domain; C, complement regulatory protein-like domain. From *Sivan et al.2014* [79]

Aggrecan presents many different functions in cartilage tissues. The major function is to create a large osmotic swelling pressure by an extremely high fixed charge density that retains water into the tissue. This occurs mainly because all the negatively charged sulfate groups on the CS chains attract mobile counter ions such as sodium and calcium creating a gradient in ion concentration between cartilage and the adjacent tissue. Consequently water is drawn into cartilage because of this osmotic imbalance and because of the limited diffusion of aggrecan, that is immobile and unable to redistribute itself, causing the swelling and expansion of the cartilage. This expansion is counterbalanced by the presence of the tensile force of the collagen fibers [81]. Then when a compressive load is applied, water draws out from the tissue

leading to an increase in aggrecan concentration, that allows water return after load removal. (**Figure 5.1**)

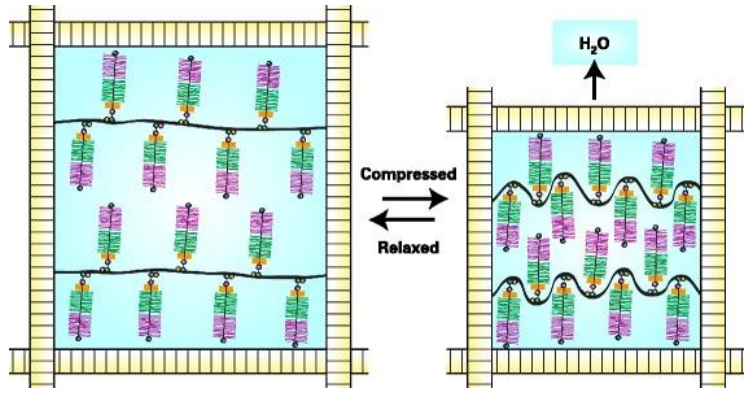

Figure 5.1: Representation of the aggrecan functional role in cartilage ECM. Highly negative charged PGs binds counter ions such as Na2+ and Ca2+ allowing the incoming of water in cartilage. When a load force is applied, water goes out from the tissue giving to cartilage its compressive ability. Adapted from *Roughley et al. 2014* [140

In addition aggrecan inhibits hydroxyapatite deposition since calcium is used as counter ion for sulfate reducing the amount of free calcium ions that allow mineral deposition [79]. Age-related changes in aggrecan are related to the altered tissue content, different ratio of C-4 and C-6 sulfation [82], impaired ability to interact with HA and fragmentation [79].

Decorin and biglycan belongs to the largest family of SLRPs class and they are characterized by a protein core of 40 kDa and encompassing a central region constituted by leucine-rich repeats (LRRs) on the binding site for one or two GAG chains, respectively. The type and amount of CS and DS chains is dependent from tissues and cell types in which they are expressed. For instance, in skin they contain DS, while in cartilage and bone only CS chains, even if decorin bears DS in articular cartilage.

Decorin and biglycan bind collagen during fibril formation through their N-terminal domain and regulate its assembly determining the rate and the end stage of this process. Both molecules may protrude out of collagen fibres, once they are formed, and may interact with other ECM molecules such as matrilins.

Decorin binds collagen fibers and reduces collagen fibrillogenesis *in vitro,* while biglycan does not bind collagen nor influence fibrillogenesis process. Furthermore decorin and biglycan can bind growth factors sequestering them in the ECM. In particular decorin binds transforming growth factor β (TGF-β) and biglycan binds bone morphogenetic protein-4 (BMP-4) regulating cartilage metabolism [45].

Other than decorin and biglycan, other member of SLRPs class in cartilage is fibromodulin. It contains one or two KS bounded through N-glycosidic linkage to its core protein. The N-terminal portion of the core protein contains nine sulfated tyrosine that with other acid amino acids form a cluster. These cluster function as polyanionic domain that interact with different growth factors such as FGF-2 and interleukin 10 (IL-10) sequestering them in the matrix and releasing them after cartilage degradation [35]. Moreover, through its leucine rich repeat region fibromodulin binds collagen fibrils [35,83].

Osteoadherin and chondroadherin are other members of SLRPs class resident in cartilage and bone that bind integrin cell receptors α5β3 [84] and α2β1 [85] respectively, modulating intracellular signals. Osteoadherin is widespread expressed in the bone-cartilage interface [86], whereas chondroadherin is mainly present in cartilage.

2.3 Cartilage collagens

Collagens are a widespread protein family and represent one of the fundamental elements of ECM in all tissues. In articular cartilage the tissue's strength is conferred by the extensions of collagen crosslinks. Collagen components do not vary among the different zones of articular cartilage, but they vary during maturation: fibrils of young growth cartilage are composed of more collagen IX and XI and less collagen II than the ticker fibrils of mature cartilage [36]. The major type of collagen present in cartilage is the Collagen II. It is a homotrimer composed of three identical α1(II) collagen chains encoded by the *COL2A1*

gene [87]. These collagen form a fibrillar structure that in cartilage ECM creates a massive network interacting also with other type of collagen such as collagen IX and XI. Its importance in cartilage is well demonstrated by diseases related to mutatios in *COL2A1* [88].

Collagen XI is a fibrillar collagen also widely expressed in cartilage. It is a heterotrimer composed of α1(XI), α2(XI) and α3(XI) chains. The first two α chains are encoded by *COL11A1* and *COL11A2* genes, whereas α3 chain is encoded by *COL2A1* gene and it is identical with α1 chain of collagen II changing only in post-translational modifications [87]. Collagen XI seems to be more concentrated in thin fibrils of the pericellular region of cartilage and it also presents binding sites with high-affinity for heparan sulfate [89].

Collagen IX is a Fibril-associated collagens with interrupted triple helices (FACIT) collagen and a heterotrimer composed of three different α1(IX), α2(IX) and α3(IX) chains encoded by *COL9A1, COL9A2* and *COL9A3* genes [87]. The role of collagen IX in the matrix requires the molecule to be covalently linked to the surface of collagen II/XI fibrils and it can regulate interactions between collagen fibrils and other ECM molecules increasing network mechanical integrity and providing a stability for PGs osmotic swelling [36]. Collagen VI is the most present in fibrocartilage such as the meniscus and intervertebral disc the protein is a heterotrimer composed mainly of α1(VI), α2(VI) and α3(VI) chains, but other chains presenting high homology with α3 chain are found (α4, α5 and α6 chains) and may form additional isoforms [90]. This protein trimers form dimers, tetramers and filamentous networks most concentrated around cells. Collagen X is a homotrimer composed of three identical α1(X) chains encoded by the *COL10A1* gene [87]. The protein is mainly expressed by hypertrophic chondrocytes forming a network in the pericellular matrix necessary for the retention of the correct type and amount of ECM molecules. Collagen X can be considered a marker of terminal chondrocyte differentiation: it is present in the hypertrophic zone of growth plate and it binds calcium ions at the early stage of the calcification process.

Mutations in *COL10A1* gene cause Schmid metaphyseal chondrodysplasia indicating the main role of collagen X in skeletal development [91].

2.4 Other cartilage extracellular matrix molecules

Cartilage contains proteins, other than collagen and proteoglycans, that are necessary for maintaining tissue properties and functions.

In particular, the matrilins family are a group of oligomeric adaptor proteins that are most strongly expressed in cartilage and in many other extracellular matrices. The matrilins family includes four different members (matrilin 1-4) that all share a structure made up of three or four subunits, forming therefore a multimeric protein [92]. Typically matrilin 1 is present in tracheal cartilage, while matrilin 3 in articular cartilage.

The proteins contain as the key functional domain one or two von Willebrand factor A motifs, through which may interact with different ECM molecules, they contains also an epidermal growth factor motif and a C-terminal coiled-coil domain allowing the homo- or hetero-oligomerization [92]. They present also an important high affinity interaction with biglycan and decorin that are linked to collagen VI. Thus matrilins appear interspersed between collagen VI via biglycan/decorin on one side and on the other side to collagen II fibrils [35]. Other roles of matrilins include the binding to collagen IX and cartilage oligomeric matrix proteins (COMP).

The cartilage extracellular matrix contains also proteins termed COMP or thrombospondin 5. COMP consists of five identical subunits linked together by N-terminal coiled-coil domains and reinforced by disulfide-bonds. The COMP subunit has EGF-like and thrombospondin type 3 repeats and a C-terminal globular domain which functions to bind other ECM molecules [87]. COMP has five binding sites with high affinity for collagen I and II and thus it can simultaneously interacts with five collagen molecules accelerating collagen fibril formation [41]. Notably COMP does not bind collagen fibrils, it appears

that it dissociates from the forming fibers at the very beginning, representing just a catalyst that bring together collagen fibers. COMP interacts tightly also with matrilin, which in turn have collagen binding activity. Therefore the COMP molecule facilitates the early association of collagen molecules, while in the adult cartilage with reduced collagen turnover the molecule appears to play a role in the stability of the collagen network [35,41] .

3. SKELETAL DYSPLASIAS

Skeletal dysplasias are a group of heterogeneous genetic disorders caused by mutations in different genes encoding for ECM components [93].

Their main characteristics are defects in the skeleton such as skeletal malformations, metabolic bone and cartilage disorders and dysostoses. Currently 436 disorders have been described linked to mutations in 364 genes, classified in 42 groups on the basis of clinical and radiological features [94]. The skeletal dysplasia are classified as rare disorder, showing an incidence of 1 of 5,000 births each year [93]. The severity of skeletal dysplasias can vary from mild forms characterized by short stature, to lethal forms in the foetal period generally associated with respiratory insufficiency [95]. Further than the skeletal phenotype, these disorders can show some others typical tracts as auditory, visual, pulmonary, cardiac, renal and mental complications [93].

3.1 Glycosaminoglycan chain synthesis related disorders

GAG chains constitute a fundamental component of PGs and confer characteristic biochemical properties to them, as well as to cartilage tissues in which they are expressed. Dysfunctions in GAG chain formation and attachment to PG core protein lead to the onset of various human disorders, [54,49].

GENE	CHR REGION	CODED ENZYME OR PROTEIN	DISORDERS	MIM N°	CLINICAL FEATURES	REFs	ANIMAL MODELs	REFs
XYLT1	16p12.3	Xylosyltransferase (XylT)	Desbuquois dysplasia type2, Short stature syndrome	608124	Short stature, joint laxity flat face with prominent eyes	[109,110]	YES	[145]
B4GALT7	5q35.2 5q35.3	beta 1,4-galactosyltransferase7 (GalT-I)	Ehlers-Danlos syndrome progeroid type1, Larsen of Reunion Island syndrome	604327	aged appearance, developmental delay, short stature, craniofacial disproportion, generalized osteopenia, defective wound healing, hypermobile joints, hypotonic muscles and loose but elastic skin	[96,97]	NONE	/
B3GAT3	11q12.3	Beta-1,3-glucuronyltransferase3 (GlcAT-I)	Larsen-like syndrome, B3GAT3 type	603381	joints dislocations mainly affecting the elbow, congenital heart defects	[98]	NONE	/

GENE	CHR REGION	CODED ENZYME OR PROTEIN	DISORDERS	MIM N^{O}	CLINICAL FEATURES	REF$_{S}$	ANIMAL MODELs	REF$_{S}$
CSGALNACT1	8p21.3	Chondroitin *N*-acetylgalactosaminyltransferase1 (GalNAcT-I)	Hereditary motor and sensory neuropathy unknown type Bell's palsy	/	Intermittent postural tremor reduction in compound muscle action potentials neurodegenerative disorders spasticity of the lower limbs	[99]	YES	[146]
SLC35D1	1p31.3	UDP-glucuronic acid UDP-N-acetylgalactosamine transporter	Schneckenbecken dysplasia	610804	platyspondyly with oval-shaped vertebral bodies extremely short long bones with dumbbell-like appearance small ilia with snail-like appearance	[100,101]	YES	[100]

GENE	CHR REGION	CODED ENZYME OR PROTEIN	DISORDERS	MIM N^{O}	CLINICAL FEATURES	REF$_{S}$	ANIMAL MODELs	REF$_{S}$
CANT1	17q25.3	Soluble calcium-activated nucleotidase1	Desbuquois dysplasia Epiphyseal dysplasia, multiple7	613165	multiple epiphyseal dysplasia severe prenatal and postnatal growth retardation, joint laxity short extremities round face prominent bulging eyes short long bones with metaphyseal splay 'Swedish key' appearance of the proximal femur advance carpal and tarsal bone age	[102-105]	YES	Cant1 Knock-in and knock-out here discussed

3.2 Desbuquois dysplasia

Desbuquois dysplasia (DBQD) is an autosomal recessive chondrodysplasia first described in 1966 by Desbuquois [107]. It is a rare severe chondrodysplasia with a prevalence of 1 on 1,000,000 in worldwide population and it belongs to the multiple dislocation group in the International Nosology of Genetic Skeletal Disorder [94]. The disorder is characterized by growth retardation both in prenatal and postnatal period, joint laxity, short extremities, flat midface, micrognathia, cleft palate and progressive scoliosis and a high lethality rate, due to respiratory failure [106] or to cardiopulmonary complications secondary to thorax hypoplasia [103]. Radiological analyses of patients show thoracic hypoplasia, vertebral and metaphyseal abnormalities, joint laxity, dislocations and disorganised ossification of hand and feet bones [107]. Orthopaedic complications are often present and include proximal femurs with exaggerated trochanter and "Swedish key" appearance, hypoplasia of thorax and ilia, scoliosis, marked lordosis and ambulatory difficulties that require surgical approach [108]. DBQD is a disorder considered clinically and radiographically heterogeneous and two variants have been described [109]. DBQD type I is characterized by the presence of typical hand anomalies, such as extra ossification centers distal to the second metacarpal, delta phalanx, bifid distal thumb phalanx and dislocation of the interphalangeal joints. DBQD type II, instead, does not show peculiar hand deformities, patients only present minor changes of the hand, such as malalignment of the interphalangeal joints and brachydactly. (**Figure 6**)

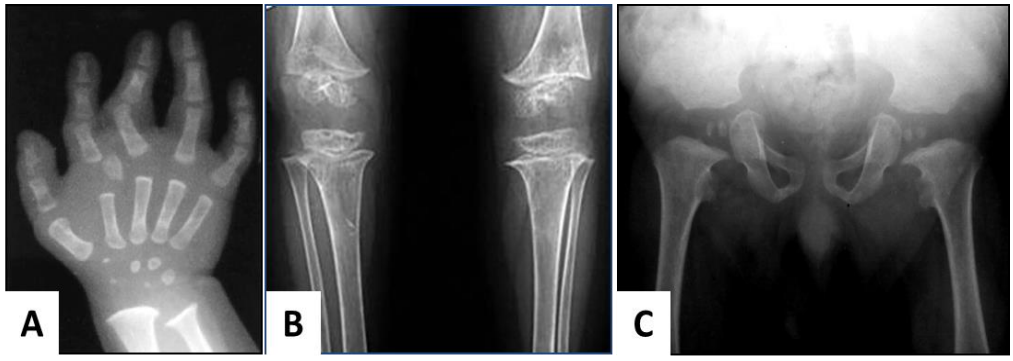

Figure 6: Radiological features of Desbuquois dysplasia type 1.

X-ray of patients with typical clinical features of Desbuquois dysplasia type 1: (**A**) hand with advanced carpal ossification and delta phalanx, (**B**) metaphyseal irregularities of knee and horizontal acetabular roofs and (**C**) hip with "Swedish key" appearance of proximal femur. Adapted from *Huber et al. 2009* . [102]

Desbuquois dysplasia type 1 is caused by mutations in *CANT1* gene that encodes for a calcium-activated nucleotidase 1 (CANT1) [102]. It is a ER and Golgi nucleotidase whose physiological role is still unclear. Desbuquois dysplasia type II is caused by mutations in *XYLT1* gene, which encodes for the xylosyltransferase 1 (XYLT1), a glycosyltransferase that is involved in GAG synthesis. *XYLT1* mutations lead to a complete or partial loss of function of XYLT1 causing PG synthesis impairment [110].

3.2.1 The Calcium activated nucleotidase 1 (CANT1) and its role in Desbuquois dysplasia type I eziopathogenesis

Calcium-activated nucleotidase 1 is a member of apyrase family and hydrolyses preferentially UDP followed by GDP and UTP.

Two forms of CANT1 have been reported, one bounded to the membrane of the endoplasmic reticulum and Golgi apparatus, and the other is a secreted soluble form. Both forms show high activity when dimers are assembled and their activity could be modulated by calcium concentration [111].

CANT1 gene is composed of five exons encoding for a protein of 401 amino acids with eight nucleotidase conserved regions (NRC).

Many types of *CANT1* mutations have been reported in homozygous or composite heterozygous state that include nonsense and missense mutations, among them Arg300Cys or Arg300His substitutions are the most frequent, rarely an intronic splice site mutation that alters a splice donor site in 5'UTR [102,104], and also frameshift mutations [106].

It has been demonstrated that several *CANT1* missense mutations linked to Desbuquois dysplasia are located in the NCR7-encoding region. Within the NCR7 domain there is a pentapeptide composed of five positively and negatively charged amino acids alternately organized forming four salt bridges involved in the catalytic site. Mutations causing amino acid substitutions in this domain lead to decrease enzyme activity [102]. Since Desbuquois dysplasia shows a phenotype similar to diastrophic dysplasia and other pathologies associated to altered GAG synthesis and sulfation, it has been suggested that CANT1 may play a role in PG metabolism. Moreover Studies on fibroblasts of Desbuquois dysplasia patients demonstrated reduced PGs synthesis and GAGs with lower molecular mass [104].

Therefore a model to explain the involvement of CANT1 in the onset of DBQD (**Figure 7**) has been proposed [104]. In this model CANT1 is associated to the endoplasmic reticulum or Golgi compartment and hydrolyzes UDP to UMP and inorganic phosphate. UDP-sugars enter in the Golgi apparatus through a transporter in antiport with UMP. Once inside the Golgi apparatus, UDP-sugars are used in glycosyltransferase reactions necessary for protein glycosylation and GAG synthesis. The byproduct of these reactions is UDP that needs to be hydrolyzes by CANT1 in UMP and inorganic phosphate. (**Figure 7**)

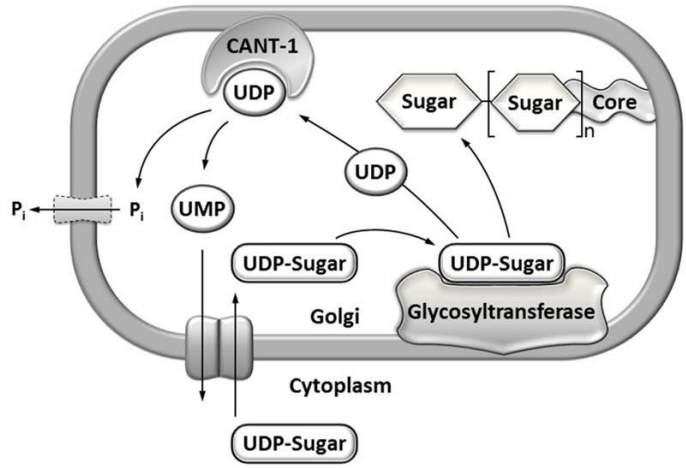

Figure 7: Schematic representation of the suggested role of CANT1 in proteoglycan metabolism. UDP sugars are transported into the lumen of the Golgi apparatus where sugars are transferred by specific glycosyltransferases to the growing GAG chains. UDP is hydrolyzed to UMP and inorganic phosphate (Pi) by CANT1. Thanks to UDP hydrolysis, glycosyltransferase reactions are not inhibited by the product (negative feedback) and UMP is exchanged with cytosolic UDP sugars through an antiporter exchanger. Adapted from *Nizon M. et al.* [104].

If CANT1 function is impaired due to mutations in *CANT1* gene, as in DBQD1, the UDP concentration increases inside the Golgi, inhibiting glycosyltransferase reactions via negative feedback, resulting in a reduced protein glycosylation and GAG synthesis. In addition, the missing UDP hydrolysis to UMP and inorganic phosphate causes the lack of UMP inside the Golgi, resulting in the impairment of the UDP-sugars / UMP antiporter. Thus, UDP-sugars cannot enter the Golgi and glycosyltransferases lack of substrates necessary for their reactions.

Moreover, since uridine nucleotides as well as UDP-sugars are also recognized as extracellular signaling molecules, the soluble secreted form suggests that the enzyme may also modulate cellular responses to UDP via specific pyrimidinergic receptors (P2Y family) [112].

3.2.2 Dbqd mouse models

To provide new insight on the role of CANT1 in the development and homeostasis of the skeleton and to contribute to the understanding of the molecular mechanism causing the DBQD1, our group generated the first *Cant1* knock-out mouse strain.

The transgenic mice generated carry the p.R302H substitution, homologous to the p.R300H substitution in the active site of human CANT1. The same mutation was detected at the homozygous state in two patients with different ethnic origin affected by a moderate form of DBQD1 [102]. To knock-in the missense mutation a c.G905A transition in a cloned fragment containing exon 4 of the murine *Cant1* gene was introduced by site directed mutagenesis. The gene targeting vector for the generation of the knock-in was designed in order to generate also a knock-out mouse. In fact, exon 3 and 4, encoding for the enzyme active site, were flanked by loxP sequences for their possible excision by Cre recombinase. Offspring were mated to an Flp deleter mouse strain to remove the positive selection cassette leading to the generation of heterozygous *Cant1* knock-in mice (*Cant1*$^{+/R302H}$ mouse) bearing the R302H missense mutation. In the knock-in strain *Cant1* exons 3 and 4 were flanked by Cre recombination sites. (**Figure 8A**) Thus, the heterozygous *Cant1* knock-out mice (*Cant1*$^{+/-}$ mouse) was generated by mating heterozygous knock-in animals with a Cre deleter murine strain (**Figure 8B**).

One of the objective of the thesis is the characterization of the knock-out model henceforth generated.

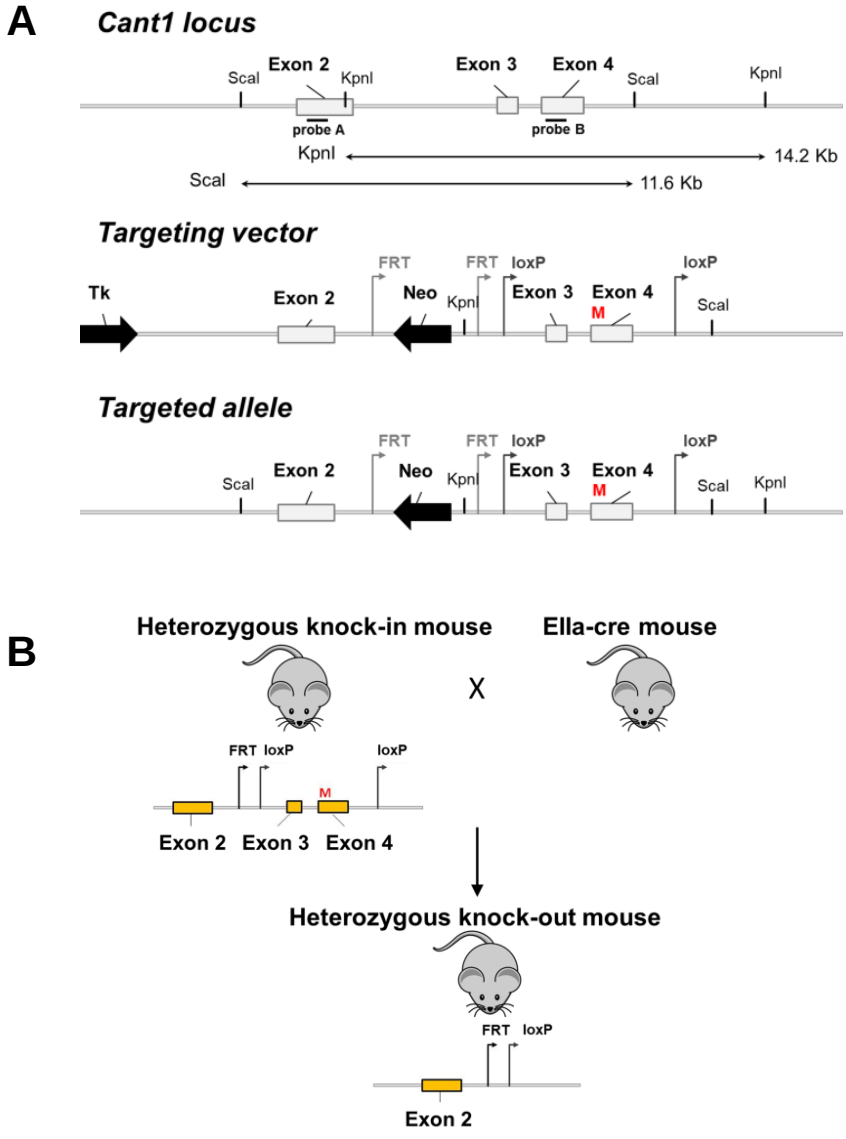

Fig. 8: Generation of *Cant1* knock-in and knock-out mice. (A) Schematic representation of *Cant1* locus and targeting vector used for the generation of *Cant1* knock-in (*Cant1*$^{R302H/R302H}$) and knock-out (*Cant1*$^{-/-}$) mice. A c.G905A transition (M) causing the R302H substitution was inserted in *Cant1* exon 4 to generate the *Cant1* knock-in mouse, while exon 3 and 4 were flanked by loxP sites to allow the generation of the *Cant1* knock-out mouse by Cre recombinase excision.
(B) Schematic diagram of heterozygous *Cant1* knock-out mice generation by the excision of exon 3 and 4 obtained mating heterozygous *Cant1* knock-in mice with Cre deleter mice.

3.3 Glycosaminoglycan sulfation related disorders

Among the several human disorders caused by defects in cell sulfate uptake, in sulfate activation pathway and in sulfotransferase reactions, there are some skeletal dysplasia caused by mutations affecting crucial enzyme involved in the biosynthesis and sulfation of CS/DS side chains, demonstrating the crucial role of a proper GAG chain sulfation. All these alterations lead to the synthesis of under sulfated PGs which affects connective tissue properties. The table below summarizes the main skeletal disorders related to sulfation defects and the animal model generated [49].

GENE	CHR REGION	CODED ENZYME OR PROTEIN	DISORDERS	MIM N°	CLINICAL FEATURES	REFs	ANIMAL MODELs	REFs
SLC26A2	5q32	Diastrophic dysplasia sulfate transporter (DTDST)	Achondrogenesis type IB	600972	invariably lethal during the foetal period shortly after birth with severe underdevelopment of the skeleton extreme micromelia. Fingers and toes are similarly short, stubby and feet are rotated inward.	[113]	none	/
SLC26A2	5q32	Diastrophic dysplasia sulfate transporter (DTDST)	Atelosteogenesis type II	256050	lethal during the foetal period or shortly after birth. tapering of the distal humeri short limbs adducted feet, and the “hitchhiker thumb.	[114]	none	/

GENE	CHR REGION	CODED ENZYME OR PROTEIN	DISORDERS	MIM N^{O}	CLINICAL FEATURES	REF$_{S}$	ANIMAL MODELs	REF$_{S}$
SLC26A2	5q32	Diastrophic dysplasia sulfate transporter (DTDST)	Diastrophic dysplasia	222600	short stature with severe shortening of the limbs and mild shortening of the trunk, cleft palate, brachydactyly, "hitchhiker" thumb" kyphoscoliosis, frequent contractures at joints.	[115-117]	yes	[118]
SLC26A2	5q32	Diastrophic dysplasia sulfate transporter (DTDST)	Multiple epiphyseal dysplasia, AR type	226900	The mildest form. clubfoot and hip dysplasias at birth, with no palatal clefting, "hitchhiker" thumb, and digital deformities.	[119]	no	/

GENE	CHR REGION	CODED ENZYME OR PROTEIN	DISORDERS	MIM N°	CLINICAL FEATURES	REFs	ANIMAL MODELs	REFs
PAPSS2	10q23.2-10q23.31	PAPS synthase-2	Spondyloepimetaphyseal dysplasia, Pakistani type	612847	short stature, short and bowed lower limbs with enlarged knee joints, kyphoscoliosis, mild brachydactyly, delayed ossification of the epiphyses and osteoarthritis	[120]	yes	[121]
PAPSS2	10q23.2-10q23.31	PAPS synthase-2	Brachyolmia AR type	612847	short trunk short stature generalized platyspondyly rounding vertebral bodies	[122]	yes	[121]

GENE	CHR REGION	CODED ENZYME OR PROTEIN	DISORDERS	MIM N°	CLINICAL FEATURES	REFs	ANIMAL MODELs	REFs
CHST3	10q22.1	Chondroitin 6-O-sulfotransferase C6ST-1	Spondyloepiphyseal dysplasia (SED) – Omani type Larsen syndrome, AR type humerospinal dysostosis (HSD) chondrodysplasia with multiple dislocations (CDMD) – Megarbane type	143095 603799	Short stature, severe kyphoscoliosis, osteoarthritis, secondary dislocation of large joints, rhizomelia, fusion of carpal bones, mild brachydactyly,metacarpal shortening, ventricular septal defect.	[123-127]	yes	[128]

GENE	CHR REGION	CODED ENZYME OR PROTEIN	DISORDERS	MIM N°	CLINICAL FEATURES	REFs	ANIMAL MODELs	REFs
CHST14	15q15.1	Dermatan 4-O-sulfotransferase (D4ST-1)	Ehlers-Danlos syndrome - musculocontractural type 1, Adducted thumb-clubfoot syndrome	608429	skin hyperextensibility, articular hypermobility, and tissue fragility craniofacial dysmorphism, congenital contractures of thumbs and fingers, clubfeet, severe kyphoscoliosis, muscular hypotonia, wrinkled palms.	[129]	none	/

GENE	CHR REGION	CODED ENZYME OR PROTEIN	DISORDERS	MIM N^{O}	CLINICAL FEATURES	REF$_{S}$	ANIMAL MODELs	REF$_{S}$
IMPAD1	8q12.1	3'-Phosphoadenosine 5'-phosphate 3'-phosphatase-gPAPP	chondrodysplasia with joint dislocations -gPAPP type	614010	short stature, chondrodysplasia with brachydactyly, congenital joint dislocations, micrognathia, cleft palate and facial dysmorphism.	[70]	Impad1 knock-out and Knock-in	[69,130]

3.3.1 Chondrodysplasia with joint dislocations - gPAPP type

Chondrodysplasia with joint dislocations gPAPP type is an autosomal recessive skeletal disorder belonging to the sulfation disorder group according to the International classification of skeletal dysplasias with a reported prevalence of <1 / 1 000 000. Vissers at al. (2011) reported for the first time four individuals from three unrelated consanguineous families showing a phenotype like Desbuquois dysplasia, diastrophic dysplasia and Larsen syndrome, caused by defective sulfation of proteoglycans [70] . They were characterized by prenatal onset of disproportionate short stature, shortening of the limbs, congenital joint dislocations, micrognathia, posterior cleft palate, brachydactyly, short metacarpals and irregular size of the metacarpal epiphyses, supernumerary carpal ossification centers and dysmorphic facial features. The absence of significant vertebral anomalies may help in distinguishing gPAPP deficiency from Desbuquois syndrome and from CHST3 deficiency, and the presence of knee dislocations and a facial phenotype may distinguish it from diastrophic dysplasia. By whole-exosome sequencing three individuals carried homozygous missense mutations in *IMPAD1* gene; a fourth unrelated patient was subsequently found to be homozygous for a premature termination codon. In 2012 Nizon et al [104] reported other 2 unrelated Turkish patients with a Catel-Manzke syndrome-like phenotype, in whom they identified homozygous loss-of-function mutations in the *IMPAD1* gene. They had severe growth retardation with short and abnormal extremities, cleft palate with micrognathia, and knee hyperlaxity. Chondrodysplasia with joint dislocations- gPAPP type is caused by mutation in *IMPAD1* gene located on chromosome 8q12.1 in humans that encodes for a Golgi resident enzyme 3'-phosphoadenosine 5'-phosphate-phosphatase (gPAPP), responsible for the hydrolysis of 3'-phosphoadenosine 5'-phosphate (PAP) in AMP e P_i. [70]

Fig. 9 Clinical Features of Individuals with *IMPAD1* mutation. (A) 3 years old patient affected by chondrodysplasia with joint dislocations gPAPP type. The hands and feet are short, the right leg is shorter than the left because of hip dislocation. (B and C) Hands and feet of patient. Note the marked brachydactyly associated with shortened metacarpals, as well as the proximal insertion and radial deviation of digit I (so called ‘‘hitch-hiker thumb’’). The feet are short, with forefoot adduction. (D and E) The median posterior palatal cleft in patient. From *Vissers et al 2011* [70]

Unfortunately cells or cartilage biopsies from these patients were not available, but this condition is associated with defective synthesis of sulfated proteoglycans; in fact *Impad1*inactivation in mice has previously been shown to produce skeletal defects, abnormal joint formation and impaired proteoglycan sulfation.[70]

3.3.2 gPAPP enzyme and its role in the eziopathogenesis of Chondrodysplasia with joint dislocations

IMPAD1 is completely conserved throughout evolution. In humans it is located on chromosome 8q12.1 and the coding sequence of the *IMPAD1* gene is divided in six exons. The structure of the phosphatase has been predicted by similarity with other related proteins, and from molecular cloning of the mouse gPAPP. The deduced mouse protein has 359 AA with the residues 176–179 as substrate binding domain, a short N-terminal tail, a transmembrane domain, and an N-glycosylation site. The enzyme is widespread express in embryo, mostly in brain, spinal cord, lung, kidney, and cartilage. Immunofluorescence analysis of human skin fibroblasts revealed colocalization of endogenous gPAPP with markers of the Golgi compartment. Even if the enzyme is ubiquitously expressed in all tissues recessive mutations of *IMPAD1* cause problems mainly in cartilage tissue. To explain the sulfation defect associated with gPAPP inactivation, Frederick [69]suggested that the physiologic role of gPAPP might be to remove the PAP that remains after the transfer of the high-energy sulfate group from PAPS to the sulfation substrate (such as the nascent chondroitin chains) in the Golgi. The degree of functional impairement of *IMPAD1* is related to mutations with different effects on the protein. for instance the mutations reported (p.Asp177Asn and Thr183Pro) were located in, and close to, the substrate binding pocket, directly disturbing the phosphatase activity, causing a partial loss of function of the enzyme. Other (p.Arg187Stop) mutations lead to the truncation of the protein with the loss of 173 amino acid residues, and therefore the total loss of function. (**Figure 10**)

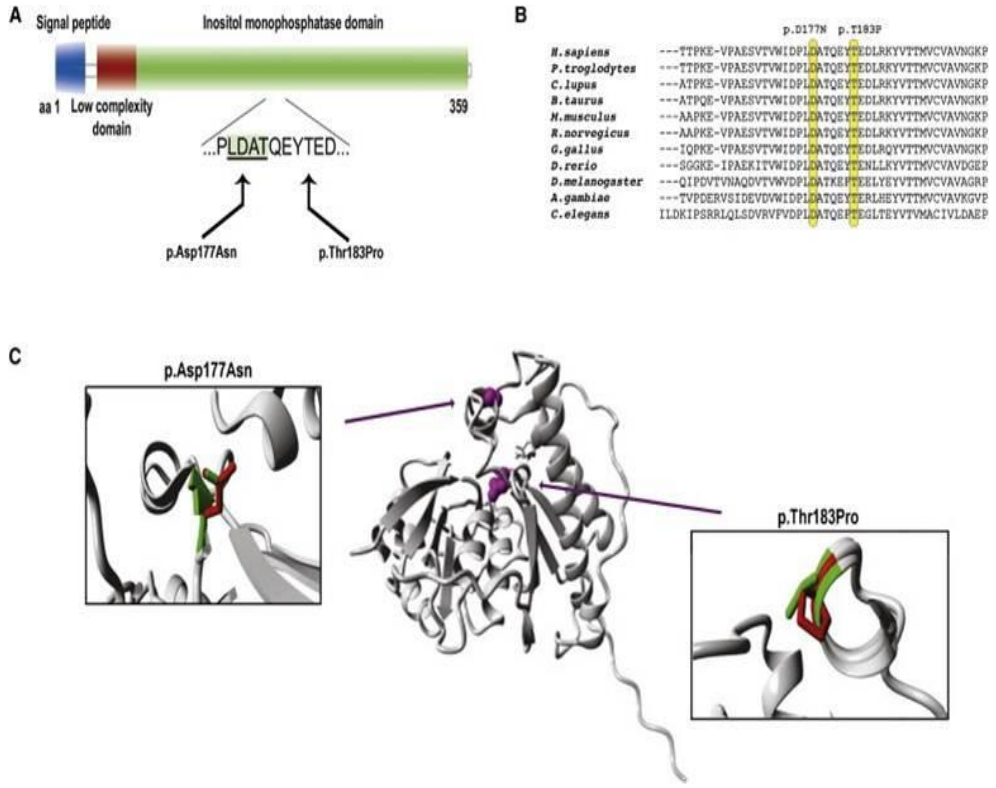

Fig 10: Schematic Representation and Protein Modeling of IMPAD1 p.Asp177Asn and p.Thr183Pro Mutations. (A) Schematic representation of the domains provided in different colors, with the binding domain harboring the mutations indicated by an underlined protein sequence in a green shaded box. (B) Evolutionary conservation of the protein sequence throughout evolution. Mutated amino acids are indicated by yellow boxes. (C) Overview of the protein in ribbon presentation. Middle: the protein is colored gray, and the side chains of the mutated residue are colored magenta. Left and right: Close-up of the p.Thr183Pro and p.Asp177Asn mutations. Side chains of both the wild-type and the mutant residue are shown and are colored green and red, respectively. From *Vissers et al. 2011* [70]

3.3.3 The gPAPP knock-out mouse

Impad1 inactivation has been associated with skeletal dysplasia and abnormal joint formation in mice by three independent groups. Mitchell et al. applied a modified gene trap approach to systematically analyze the functions *in vivo* of large numbers of genes encoding secreted and membrane protein [142]. By screening the phenotypes obtained from about 60 gene trapped ES cell lines they identified a strain with neonatal lethality displaying craniofacial defects and shortened limbs and body axis. Mutant mice were homozygous for an insertion in a novel membrane protein with similarity to inositol monophosphatases. Sohaskey et al. studied this mouse strain in more depth and observed a severe chondrodysplasia including ectopic interphalangeal joints, leading to the denomination of the phenotype as "*JAWS* " for "*joints abnormal with splitting*." [130] (**Figure 11**). They observed delayed and disorganized maturation of growth-plate chondrocytes, impaired sulfation of chondroitin, and abnormal metabolism of the chondroitin sulfate proteoglycan aggrecan, but a functional characterization of the specific enzymatic function of *Impad1* was not performed. Frederick et al. explored the enzymatic properties of *Impad1 in vitro* and showed that when targeted to the Golgi, *Impad1* had a strong phosphoadenosine phosphate 3-nucleotidase (or PAP phosphatase, PAPP) activity. Subsequently, they made use of a different *Impad1* gene-trap cell line to generate transgenic mice and noted that the chondrodysplasia phenotype was associated with markedly reduced sulfation of chondroitin and heparan proteoglycans. Both groups of researchers placed their findings in the context of skeletal dysplasias related to proteoglycan undersulfation and suggested that the *Impad1*-inactivated mouse was a possible model for a human disorder yet to be identified. Predictions made on the basis of these mutuant strain were confirmed by

Vissers et al. who had identified the patients bearing the same mutations in *IMPAD1*, that showed the same skeletal phenotype.

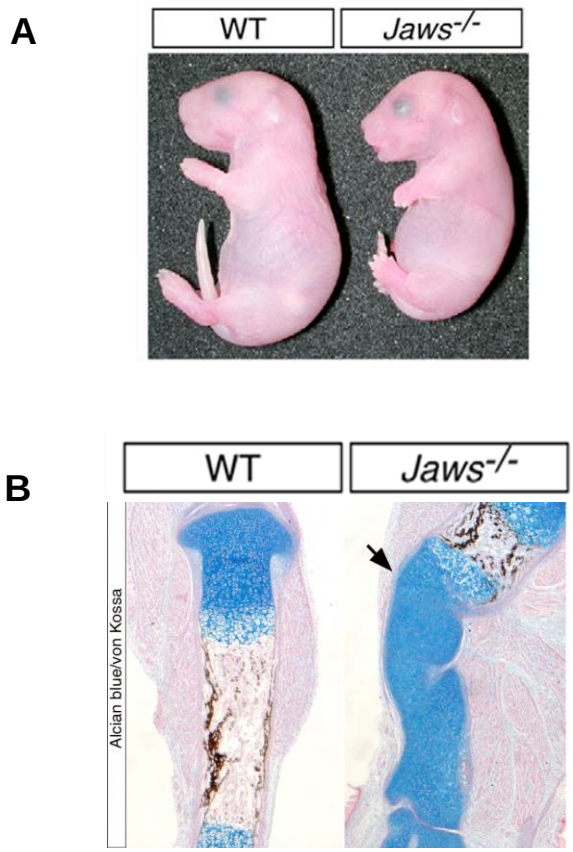

Fig 11: (A) Visual inspection of wildtype (WT) and Jaws$^{-/-}$ embryos (E18.5).
(B) Failure of knee joint formation and tibial development in *Jaws-/-* mice with Alcian blue/von Kossa staining. Arrow indicate the region of the presumptive knee joint in the *Jaws-/-* hindlimb. From *Sohaskey et al* 2008 [130]

Chapter II

Research objectives

The cartilage extracellular matrix is a complex network composed of collagens and other proteins that provides structural support to the tissue. Among cartilage ECM components, proteoglycans are the most abundant proteins. They play several important roles maintaining cartilage physical and mechanical properties. PGs, through their highly negative charge, regulate osmotic pressure conferring to cartilage the ability to resist to compressive loads. Furthermore, PGs can bind growth factors regulating chondrocyte proliferation and differentiation. For these reasons, it is clear how mutations in genes encoding for enzymes or proteins involved in the PG synthesis process, lead to the onset of genetic diseases affecting the cartilage. Currently, little is known about the molecular bases that contribute to the pathogenesis of different forms of chondrodysplasias, moreover since they are rare diseases, that affect a small number of patients, the study of these disorders on patient's samples is extremely difficult. Thus, the generation of animal models to elucidate the pathogenesis of dysplasias and to develop novel less invasive treatments is crucial. Using in vivo models, this work has been focused on two chondrodysplasias in which proteoglycan synthesis is impaired: chondrodysplasia with joint dislocation - gPAPP type and Desbuquois dysplasia type 1. Both disorders are caused by mutations in enzymes involved in two different steps of the GAG biosynthesis: *CANT1* is involved in the elongation of the GAG growing chain, while *IMPAD1* is involved in the GAG sulfation pathway. The disease gene in Chondrodysplasia with joint dislocation - gPAPP type has been identified only in 2011[70], but since no biochemical data are available because of the unavailability of tissue biopsies from patients, the only information about the molecular bases of the disorder comes from a knock-out mouse model lethal at birth. Conversely, the disease gene in Desbuquois dysplasia type 1 has been identified in 2009 [102], but the information on the molecular basis of the disease are still poor and do not allow to devise any therapeutic approach.

In conclusion, the molecular knowledge of the two disorders is different; thus, in this thesis the two models have been used to pursue different objectives: I) the generation of *Impad1* conditional Knock-in mouse model to define the physiological function of *IMPAD1* and its role in the etiology of chondrodysplasia with joint dislocation - gPAPP type. II) the validation of a *Cant1* knock-out mouse, already available in the laboratory, as an animal model of Desbuquois dysplasia type 1.

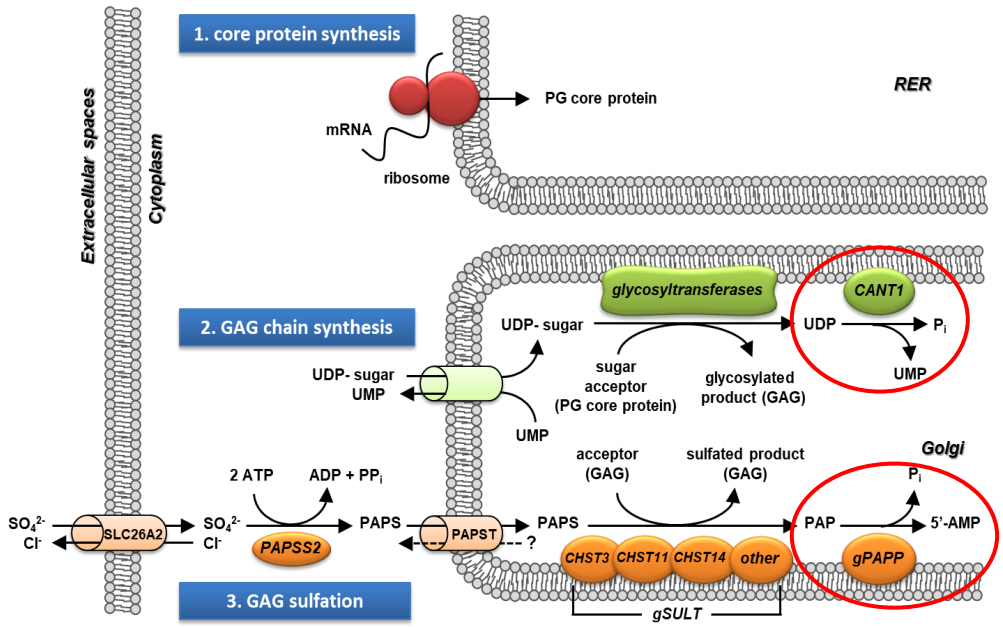

Chapter III

Generation of a conditional knock-in mice using the “Cre-mediated genetic switch”

1. Aim of the work

Chondrodysplasia with joint dislocations gPAPP type is a rare recessive skeletal disorder caused by mutations in the *IMPAD1* gene encoding for gPAPP, a Golgi-resident phosphoadenosine phosphate 3'-phosphatase that hydrolyzes phosphoadenosine phosphate (PAP), the by-product of sulfotransferase reactions, to AMP; thus, this enzyme is involved in the GAG sulfation pathway. Mutation in *IMPAD 1* has been reported for the first time in 2011 by Vissers et al. in three patients characterized by short stature, brachydactyly, joint dislocations and cleft palate [70]. No biochemical data are available because of the lack of tissue biopsies from patients, therefore the only data comes from the generation of a Impad1 knock-out (KO) mouse by two different research groups in 2008 [69;130]. Unfortunately the phenotype of KO mice was lethal at birth due to severe pulmonary defects and skeletal deformities. Moreover the formation of ectopic joints in the phalanges, not reported in patients, suggests an important role of *IMPAD1* in the correct orientation and positioning of the phalanges. Mutant mice were characterized by a severe chondrodysplasia, a growth plate that lacks the peculiar organization and the presence of undersulfated proteoglycans. Because of KO lethality at birth the authors studied only the embryonic skeletal development, but they cannot study post-natal skeletal development, and therefore the KO mouse cannot be considered a good model of chondrodysplasia with joint dislocations gPAPP type. Since the pathology in patients is not lethal at birth, a knock-in mouse model is required. One of the aim of this work has been the generation and characterization of a conditional Impad1 knock-in mouse by morphological, biochemical and molecular biology approaches in order to validate the animal as a model of human chondrodysplasia with joint dislocations - gPAPP type and to elucidate the role of the enzyme in proteoglycan metabolism.

2. Results

2.1 Generation of the Cre mediated genetic switch allele in mice.

In collaboration with Polygene, (Rumlag, Switzerland), the conditional knock-in mouse was generated using a combination of two partially mutated lox sites in the head-to-head orientation. This strategy guarantees stable inversion of DNA between the lox sites since after Cre recombination a wild-type loxP site and a double mutant lox, no longer recognized by the enzyme, are generated (**Figure 12 A**). First the combination lox71 and loxKR3, reported previously by Araki et al [141] in a head to head orientation was tested for recombination efficiency in a Cre expressing E.coli strain. Different clones were isolated from each transformation and analyzed via restriction analysis with BstBI. All clones analyzed showed the expected restriction pattern corresponding to the inverted version of the test vector (**Figure 12 B**). The targeting vector was then generated based on the lox71/loxKR3 construct (**Figure 12 C**). The missense mutation knocked-in the murine Impad1 was the p.Asp175>Asn corresponding to the p.Asp177>Asn detected previously in a patient [70].

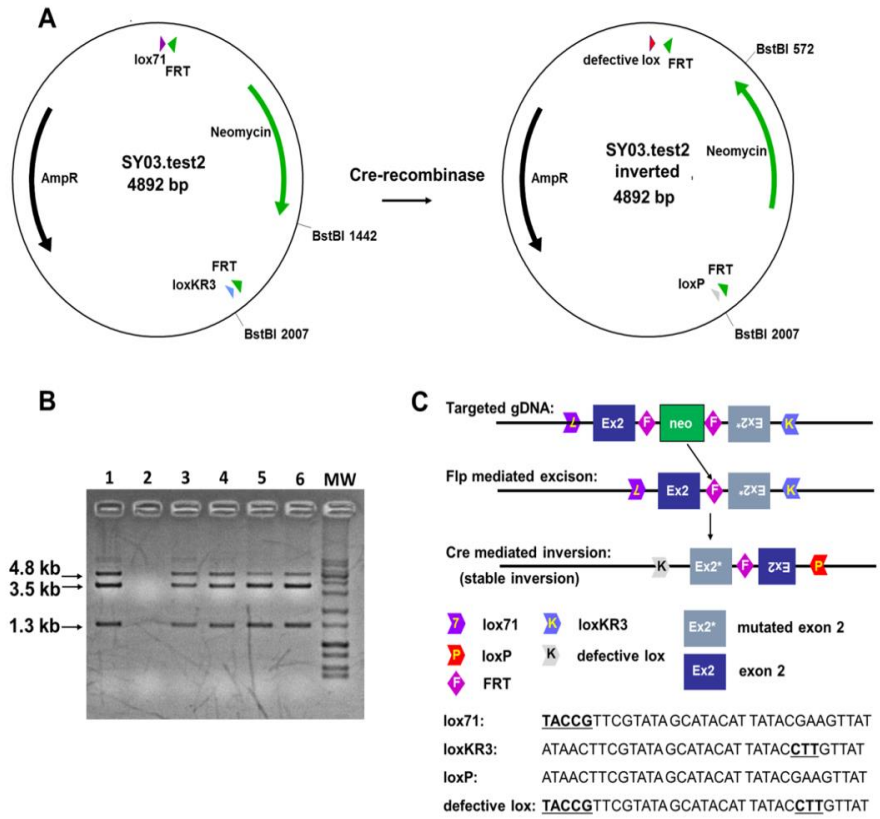

Fig 12: Strategy for conditional knock-in generation via inversion. (A) Scheme of the plasmid used to test recombination and stable inversion with *lox71* and *loxKR3*. Magenta arrowhead: *lox71*; light blue arrowhead: *loxKR3*; grey arrowhead: *loxP*; red arrowhead: double mutant *lox*; green arrowhead: *FRT* site. (B) Restriction fragment analysis with *BstBI* of the plasmid (4.8 kb) after transformation in Cre-expressing E.c*oli*. The correctly inverted plasmid results in restriction fragments of 3.5 kb and 1.3 kb. Lanes 1, 3-6: positive clones; lane 2: blank (water); MW: DNA molecular weight marker. (C) Two versions of the targeted exon (wild-type and mutated) are inserted in head-to-head orientation between a *loxKR3* and a *lox71* site. The two versions of the exon are separated by an FRT-flanked *neomycin* cassette. After targeting the *neomycin* cassette is deleted via Flp-mediated recombination *in vivo*. The mutation is activated by stable inversion of the two exons mediated by Cre-recombinase. The targeted exon in the *Impad1* conditional knock-in is exon 2, as shown in the figure.The sequences of *lox* sites used in this study are reported and mutated sequences are indicated by bold and are underlined. *Lox71* carries mutations in the left element, while *loxKR3* carries mutations in the right element.

Homologous recombination was performed in C57Bl/6N-based ES cells and confirmed by Southern blot analysis. Proper targeted ES cell clones were injected into grey C57Bl/6N blastocysts and the resulting chimeras were bred to FLP-deleter mice for neomycin cassette deletion. The heterozygous offspring, termed "floxed" mice, were then confirmed by the presence of the lox71 site (**Figure 13 A-C**) and the deletion of the neomycin cassette (not shown).

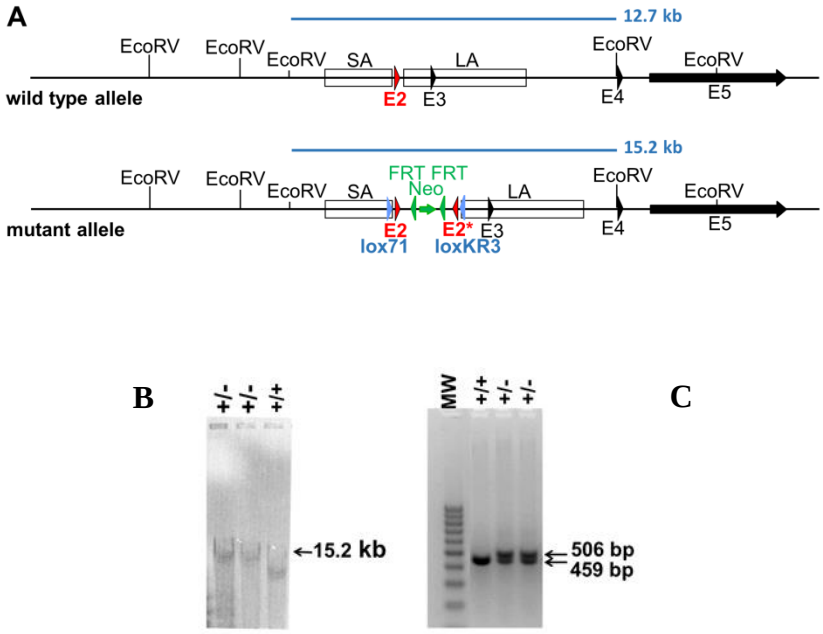

Fig 13: Generation of the *Impad1* mouse lines. (A) Schematic drawing of the wild type and targeted loci for *Impad1*. *EcoRV* restriction sites and fragments for Southern blot analyses are indicated in light blue. (B) Southern blot analysis of *Impad1* targeted ES cells after *EcoRV* digestion using a *neomycin* specific probe; the 15.2 kb fragment corresponding to correct homologous recombination is indicated. (C) Genotyping PCR analysis for heterozygous *Impad1* floxed pups using primers SY08.20 and SY08.21 flanking the *lox71* site. The wild-type and floxed allele result in PCR products of 459 bp and 506 bp, respectively. Black arrowhead: exon; green arrowhead: FRT site; light blue arrowhead: *lox71* or *loxKR3* site; red arrowhead: targeted exon 2 in *Impad1*; green arrow: *neomycin* cassette; SA: short arm; LA: long arm; E#: exon number; MW: DNA molecular weight marker.

To generate an Impad1 knock-in, floxed Impad1 mice were mated to a global Cre mouse strain for stable inversion and activation of the mutation.

2.2 Morphological characterization of Impad1 knock-in mouse

Mice heterozygous for the *Impad1* mutation did not show any phenotypic alteration by X-ray analysis and visual inspection, as human carriers of *IMPAD1* mutations and were no further studied. Homozygous mutant animals died at birth and were smaller compared to wild type and heterozygous littermates; visual inspection and X-ray analysis demonstrated growth retardation and skeletal defects (**Figure 14 A-B**). Mutant animals showed severe hypoplasia of the skeleton: the length of the axial skeleton and of the limbs were reduced. By X-rays and alcian blue and alizarin red skeletal staining was observed that the femur, tibia and fibula were markedly shorter compared to wild-type animals; furthermore, reduced sternal length and diminished rib spacing were evident (**Figure 14 B and 14 D**). Moreover, knock-in mice showed cleft palate already observed in patients with chondrodysplasia with joint dislocations - gPAPP type (**Figure 14 C**). Surprisingly, the knock-in mouse showed the same peculiar phenotype described previously in the *Impad1* knock-out mouse [69,130]. Thus, we further investigated the molecular and biochemical basis causing neonatal lethality in our animal model.

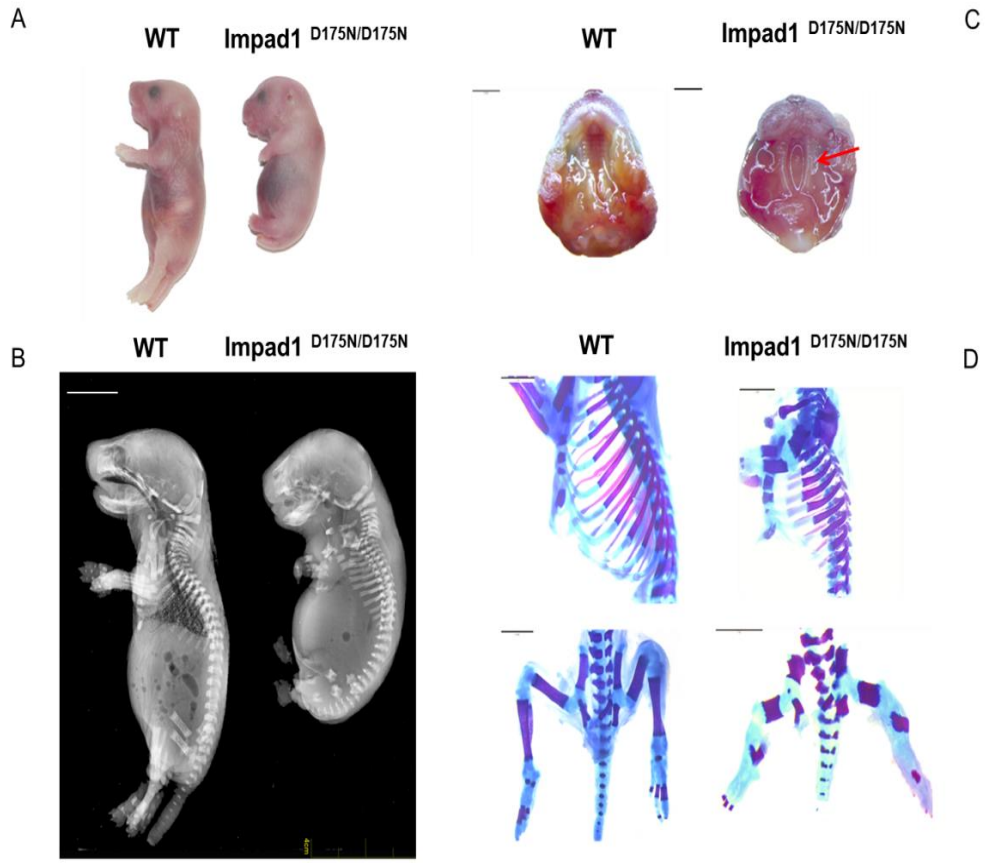

Fig 14: Phenotypic characterization of the *Impad1*$^{D175N/D175N}$ mouse. (A) Gross morphology of wild type and *Impad1*$^{D175N/D175N}$ newborn mice. Mutant animals die at birth and are considerably smaller than wild type littermates demonstrating severe growth retardation. (B) X-rays of wild type and mutant mice at birth. The mutant shows skeletal defects and growth retardation. (C) In *Impad1*$^{D175N/D175N}$ mice cleft palate is observed (arrow). Scale bars: 2 mm. (D) Alcian blue and alizarin red skeletal staining of *Impad1*$^{D175N/D175N}$ and wild type bones at birth; the femur, tibia and fibula are markedly shorter compared to wild-type animals; rib cages of mutant mice display skeletal defects characterized by reduced sternal length and diminished rib spacing. Scale bars: 2mm

2.3 Disaccharide sulfation analysis

Impad1 encodes for a Golgi 3'-phosphoadenosin 5'-phosphate phosphatase crucial for macromolecular sulfation. In whole embryo and in the limbs of the *Impad1* knock-out mouse severe undersulfation of chondroitin sulfate proteoglycans was demonstrated compared to wild-type mice [69,130]. For this reason, proteoglycan sulfation was measured by HPLC disaccharide analysis in femoral head cartilage of wild type and mutant knock-in mice and, for comparison, in the Frederick's *Impad1* knock-out [130]. Glycosaminoglycans were purified by digestion of cartilage with papain. Then glycosaminoglycans were digested with chondroitinase and released disaccharides separated by HPLC after derivatization with a fluorescent tag. A dramatic increase in the relative amount of the non-sulfated disaccharide (ΔDi-0S: 3-O-β(D-gluc-4-eneuronosyl)-N-acetylgalactosamine) relative to the total amount of disaccharides (ΔDi-0S plus ΔDi-4S and ΔDi-6S: derivatives of ΔDi-0S with a sulfate at the 4 or 6 position of hexosamine moiety respectively) was observed in newborn mutant mice compared to wild-type animals indicating chondroitin sulfate undersulfation (61 ± 9.2% and 14 ± 1.6% ΔDi-0S, respectively; $P < 0.001$ n=3). Remarkably, the level of proteoglycan undersulfation in knock-in mice was similar to *Impad1* knock-out animals (63 ± 1.6% ΔDi-0S, n=3) (**Figure 15**).

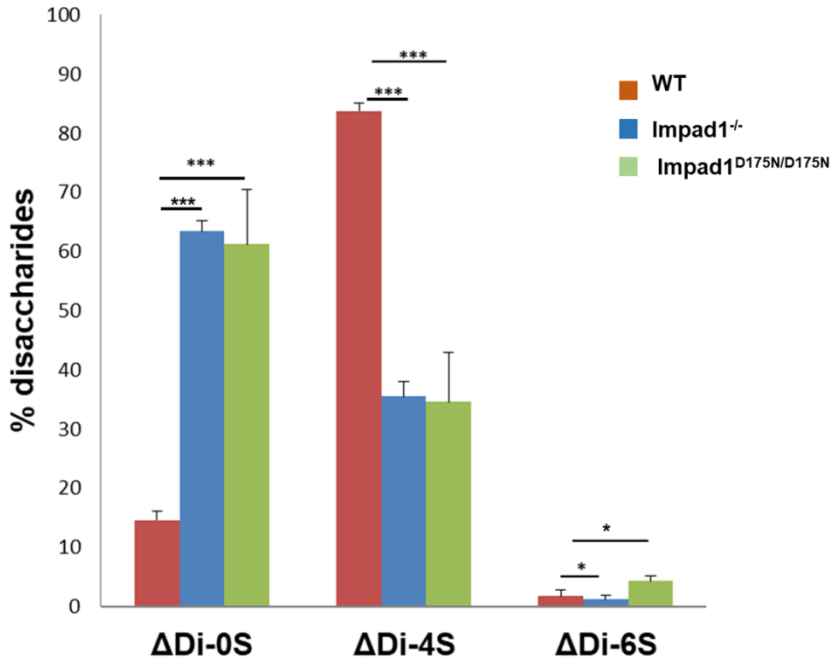

Fig 15: Sulfation of chondroitin sulfate proteoglycans from femoral head cartilage. Sulfation of proteoglycans was determined by HPLC disaccharide analysis after digestion by chondroitinase ABC and ACII of chondroitin sulfate proteoglycans from the femoral head cartilage of wild-type (WT) and *Impad1*$^{D175N/D175N}$ mice at birth. In parallel the same analysis was performed also in the *Impad1* knock-out (*Impad1*$^{-/-}$) mouse. The amount of non-sulfated disaccharide (ΔDi-0S) relative to the total amount of disaccharides (ΔDi-0S, ΔDi-4S and ΔDi-6S) is significantly increased in mutant mice compared to the wild-types indicating proteoglycan undersulfation. Interestingly, the level of proteoglycan undersulfation in mutants is similar to the Frederick's knock-out mouse [69]. Three mice per group were used; data are reported as mean ± SD; significance was determined by Student's t-test, * $P < 0.05$; ** $P < 0.01$; *** $P < 0.001$.

2.4 *Impad1* expression analysis

Since the clinical and biochemical phenotype of knock-in mutant animals overlaps with *Impad1* knockouts, the expression of Impad1 was measured by qPCR with primers spanning exon 2 and 3. Impad1 mRNA was absent in knock-in mice compared with wild-types; Impad1 expression level in heterozygous mice was half compared to wild-types (**Figure 16**).

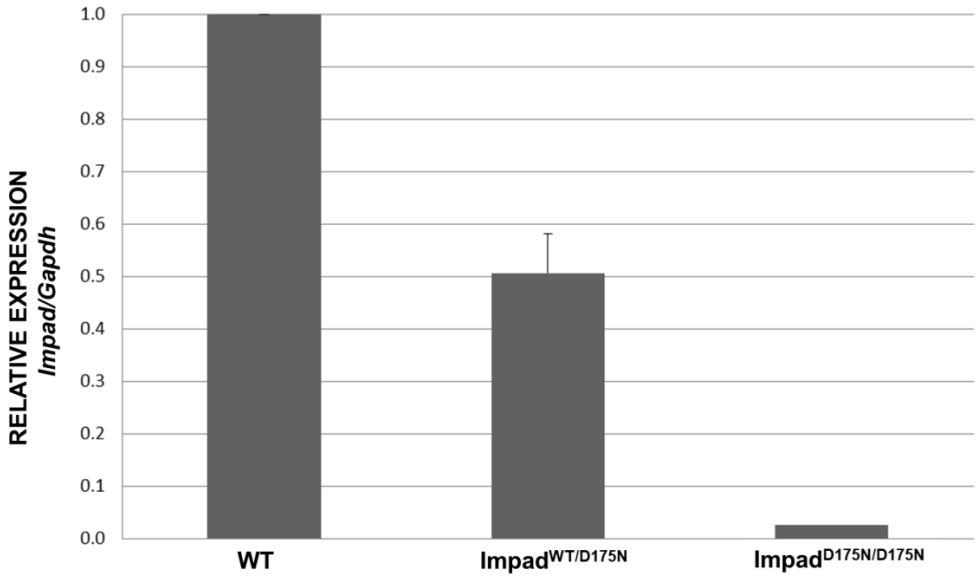

Fig 16: Relative expression analysis of the *Impad1* gene. RT-qPCR on total RNA isolated from skin of wild-type (WT), heterozygous (*Impad1*$^{WT/D175N}$) and *Impad1*$^{D175N/D175N}$ newborn mice was performed with primers spanning exon 2 and exon 3. Expression of *Impad1* mRNA normalized to *Gapdh* is absent in homozygous mutant animals compared to wild-types. Three mice per genotype were used; each sample was run in triplicate and three different experiments were performed.

Since in knock-in mice no *Impad1* transcript was detected by qPCR, we checked whether the modified *Impad1* locus impairs correct RNA splicing. Thus, we considered potential alternative splicing of Impad1 exons by RT-PCR using two primers spanning exon 1 to 5 encompassing the whole coding sequence (**Figure 17 A**). Results demonstrated that in wild-type animals one

band, 639 bp long, corresponding to a unique transcript including the 5 coding exons was present. This band was not detected in mutant mice; conversely two different bands, 477 bp and 383 bp long, respectively were observed (**Figure 17 A**). Sequencing of the two bands demonstrated that the two transcript variants lack exon 2 or exon 2 and exon 3 (**Figure 17 B**) causing putative frameshift mutations leading to premature stop codons (p.Ile128ArgfsX13 and p.Ile128LeufsX5, respectively).

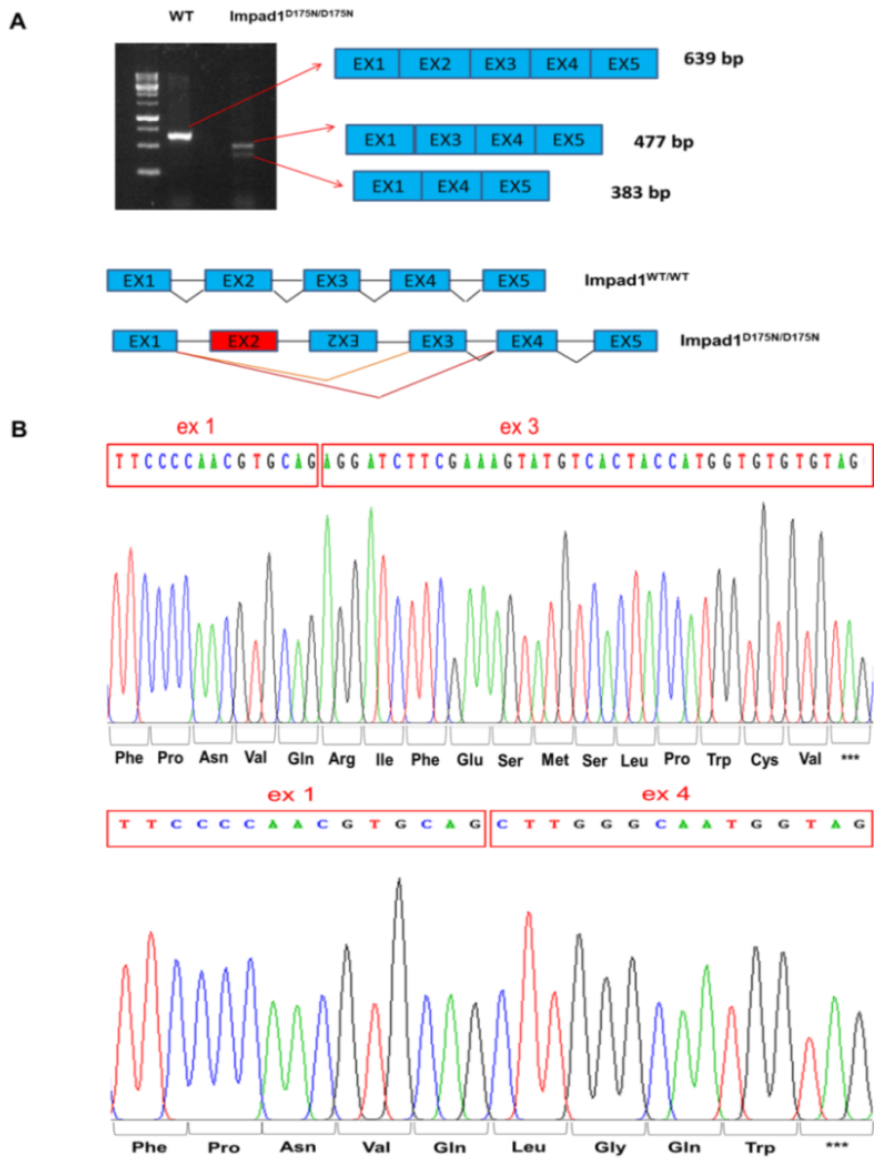

Fig 17: Alternative splicing analysis of Impad1 mRNA. (A) RT-PCR using primers that amplify a region spanning exon 1 to exon 5 was performed from skin total RNA of wild-type and *Impad1*$^{D175N/D175N}$ newborn mice and analysed by 1.5% agarose gel. In wild-type animals one band, 639 bp long, corresponding to the correctly spliced *Impad1* transcript including the 5 coding exons is present. This band is not detected in mutant mice, conversely two different bands, 477 bp and 383 bp long, respectively are observed. (B) Sequencing of the two bands demonstrated that the two transcript variants lack exon 2 or both exon 2 and exon 3.

3. DISCUSSION

In these work we have tested an innovative strategy named “Cre-mediated genetic switch” combining the ability of Cre recombinase to invert a DNA fragment, depending upon the orientation of the flanking *loxP* sites, and the use of wild-type and mutant *loxP* sites in order to make recombination irreversible. The concept was that Cre recombinase-mediated inversion would place the exon bearing the missense mutation into a position where it would be spliced properly, while the inverted wild-type exon would be spliced out. We have used this strategy to generate a conditional knock-in mice for the *Impad1*. Mutations in this gene causes in human a skeletal disorder called chondrodysplasia with joint dislocations - gPAPP type. *Impad1* encodes for a Golgi resident adenosine 3’,5’-bisphosphate phosphatase crucial for macromolecular sulfation [69,130]. The missense mutation knocked-in the murine Impad1 was the p.Asp175>Asn corresponding to the p.Asp177>Asn detected previously in a patient [70].The mouse model generated through this strategy resulted in an unexpected severe skeletal phenotype. Heterozygous floxed *Impad1* (*Impad1*$^{Flox/WT}$) mice were mated to a Cre deleter mouse strain in order to generate *Impad1*$^{D175N/WT}$ animals. Heterozygous *Impad1* (*Impad1*$^{D175N/WT}$) mice were mated; *Impad1*$^{D175N/D175N}$ mice died at birth with severe hypoplasia of the skeleton and at the biochemical level cartilage proteoglycans were dramatically undersulfated. The phenotype overlapped with the lethal phenotype described previously in *Impad1* knock-out mice generated by a gene trap approach [69,130]. Expression studies by qPCR and RT-PCR demonstrated that the mutant *Impad1* mRNA underwent abnormal splicing with loss of exon 2 or exons 2 and 3; no mutant full length mRNA spanning exons 1-5 as in normal *Impad1* mRNA was detected. This may results in activation of non-sense mediated decay or anyway to the synthesis of transcript encoding for a non-

functional enzyme since the active site of the phosphatase is encoded by exon 2. The skeletal phenotype resemble the phenotypes of the knock-out mice suggesting that the skeletal defects were not due to the missense mutation, but to aberrant splicing causing the synthesis of non-functional proteins. It is tempting to speculate that the two exons in opposite orientation generate a hairpin loop leading to the skipping of both exons. A similar strategy was devised previously in order to generate a conditional knock-in of the cAMP response element binding protein (CBP) [131]. To achieve the Cre recombinase-mediated mutation $CBP^{Tyr658Ala}$, a targeting construct containing the wild-type exon 5 of the CBP and a mutated exon 5 (p.Tyr658>Ala) in an inverted orientation was generated. These sequences were flanked by two mutated *loxP* sites, which were positioned in a head-to-head orientation. The authors demonstrated that in ES cells the genetic switch worked properly when cells were transfected with a plasmid expressing Cre-recombinase, but unfortunately, no data were available regarding the expression at the mRNA or protein level. The generation and further characterization of transgenic animals from these ES cells has never been reported to date. In conclusion, the Cre mediated genetic switch strategy has paved the way to the engineering of sophisticated genetic modifications including conditional point mutation, conditional rescue, conditional gene replacement and recombinase mediated cassette exchange, which have been used successfully *in vitro*. However, it is worth noting that modifying the genome of eukaryotic cells to generate Cre mediated switch alleles may have some drawbacks. The repetition of endogenous splicing sites in the antisense orientation may also induce the occurrence of aberrantly spliced mRNA. In any case, it is probably safe to reduce DNA repetitions as much as possible and to test for functionality in transiently transfected cells when possible, or in ES cell clones before further proceeding to blastocyst injections.

Chapter IV
Phenotyping of a *Cant1* knock-out mouse as animal model for Desbuquois dysplasia type 1

1. Aim of the work

CANT1 is a Golgi-resident calcium-activated nucleotidase, encoded by *CANT1* gene, that preferentially hydrolyzes UDP in UMP and phosphate allowing the Golgi uptake of UDP-sugars, substrates of glycosyltransferases. The physiological role is still uncertain, but *CANT1* impairment leads to the onset of a rare chondrodysplasia called Desbuquois dysplasia type 1. A molecular model to explain the role of CANT1 in Desbuquois dysplasia has been suggested. CANT1 is involved in preventing the inhibition of glycosyltransferase reactions allowing the Golgi uptake of UDP-sugars, substrates of glycosyltransferases. When its activity is impaired or absent, the increased Golgi UDP level inhibits, through negative feedback, glycosyltransferases thus reducing the synthesis of GAGs. Moreover, the low UMP level reduces the Golgi supply of UDP-sugars decreasing the activity of UDP-sugar/UMP antiporters [102].

Skin fibroblasts from Desbuquois dysplasia type 1 patients revealed reduced PG synthesis and GAG chains with a lower hydrodynamic size compared to controls [104]. Even if these results support CANT1 role in PG metabolism, more evidences *in vivo* and *in vitro* are required and the generation of an appropriate animal model is essential to better explore CANT1 role in the pathogenesis of Desbuquois dysplasia. For this reason a *Cant1* knock-out mouse, termed dbqd mouse, has been generated through the excision of exon 3 and 4, encoding for the active site of the enzyme. One of the aim of this thesis has been the characterization of the *Cant1* knock-out mouse in order to validate the animal as a model of human Desbuquois dysplasia type 1 and to elucidate the role of the nucleotidase in proteoglycan metabolism.

2. Results

2.1 Morphological characterization of dbqd mice

The skeletal phenotype was studied first by double staining with alcian blue and alizarin red in mice at different ages from birth to postnatal days (P) 21 to stain cartilage and bone. Homozygous mutant (Cant1$^{-/-}$) mice from P1 to P21 were smaller compared with wild types (wt) indicating a skeletal growth defect (**Figure 18 A**). By x-ray analysis in Cant1$^{-/-}$ mice, the presence of moderate thoracic kyphosis was also observed at P60 (**Figure 18 B**). Moreover, in the hind limbs of P7, P14 and P21 Cant1$^{-/-}$ mice the medial deviation of the first digit with the formation of an additional rudimentary phalanx, named "delta phalanx" (**Figure 18 C**) was clearly evident. This is a distinctive tract of patients with Desbuquois dysplasia type 1. These data demonstrated a chondrodysplastic phenotype with growth retardation and anomalies in bone extremities in Cant1$^{-/-}$ mice, reminiscent of the clinical features of Desbuquois dysplasia type 1.

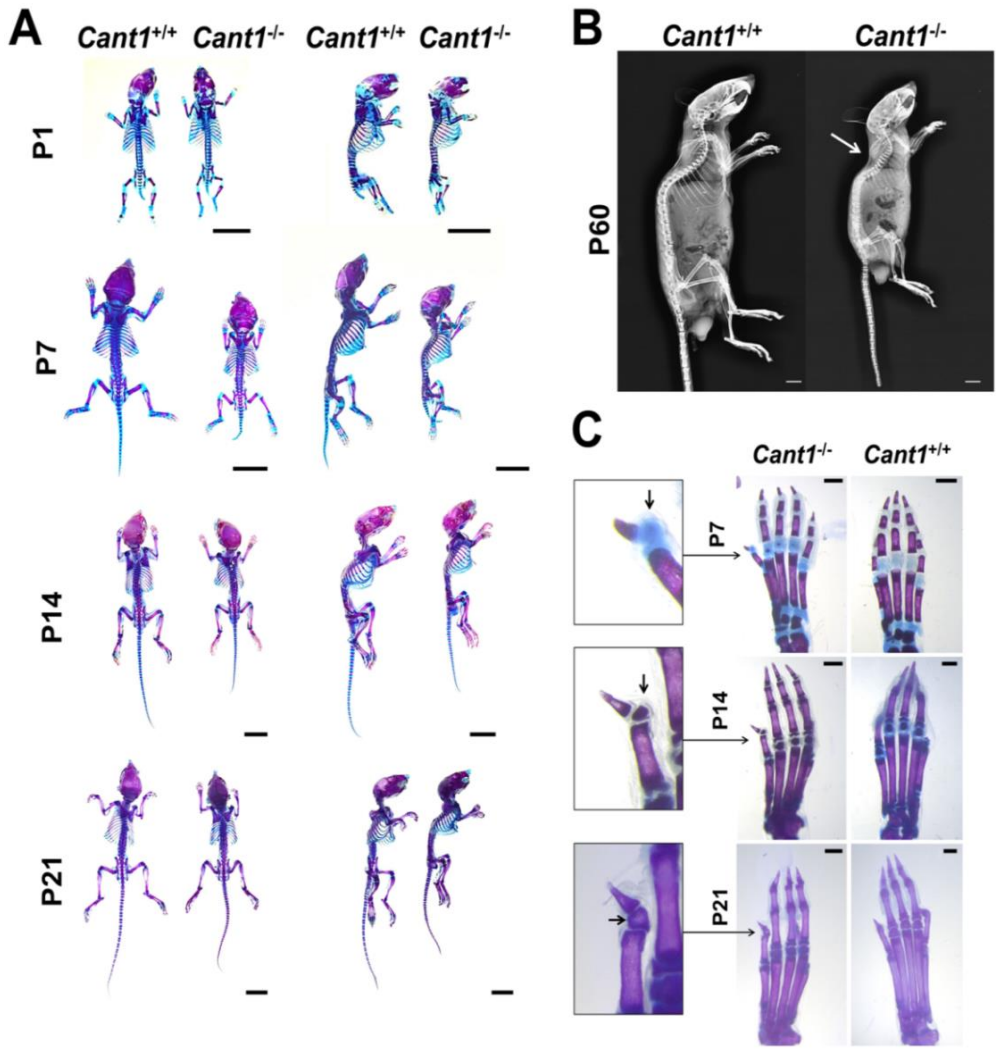

Fig. 18: The skeletal phenotype of *Cant1* knock-out mice is reminiscent of patients phenotype. (A) Double staining with alcian blue and alizarin red of mice from birth to P21 showed that *Cant1*$^{-/-}$ mice were smaller compared with age matched wild type (*Cant1*$^{+/+}$) animals. Scale bars = 1 cm. (B) X-ray analysis of two month old (P60) *Cant1*$^{-/-}$ and *Cant1*$^{+/+}$ mice demonstrated reduced growth of *Cant1*$^{-/-}$ compared with wild type animals. A moderate thoracic kyphosis (arrow) in *Cant1*$^{-/-}$ mice was observed. Scale bars = 1 cm. (C) Double staining with alcian blue and alizarin red of extremities of hind limbs from *Cant1*$^{-/-}$ and Cant1+/+ mice at different ages revealed the presence of delta phalanx (arrow) in Cant1-/- mice at all ages considered. Scale bars = 1 mm.

2.2 Morphometric analysis of long bones in Cant1$^{-/-}$ mice

Morphometric analysis on representative long bones (tibia, femur and ilium) in skeleton preparations from birth to P21, stained with alcian blue and alizarin red were performed. In mutant newborn mice the width of tibia and femur were significantly decreased in Cant1$^{-/-}$ mice compared with wild type newborns. At P7, P14 and P21 both length and width of tibiae and femurs were significantly decreased in Cant1$^{-/-}$ mice compared with wt animals. Moreover, a significant reduction in ilium length and width was found in mutant animals compared with wild types (**Figure 19**).

Bone morphometric measurements confirmed the growth defect in long bones of Cant1$^{-/-}$ mice suggesting a defect in endochondral ossification.

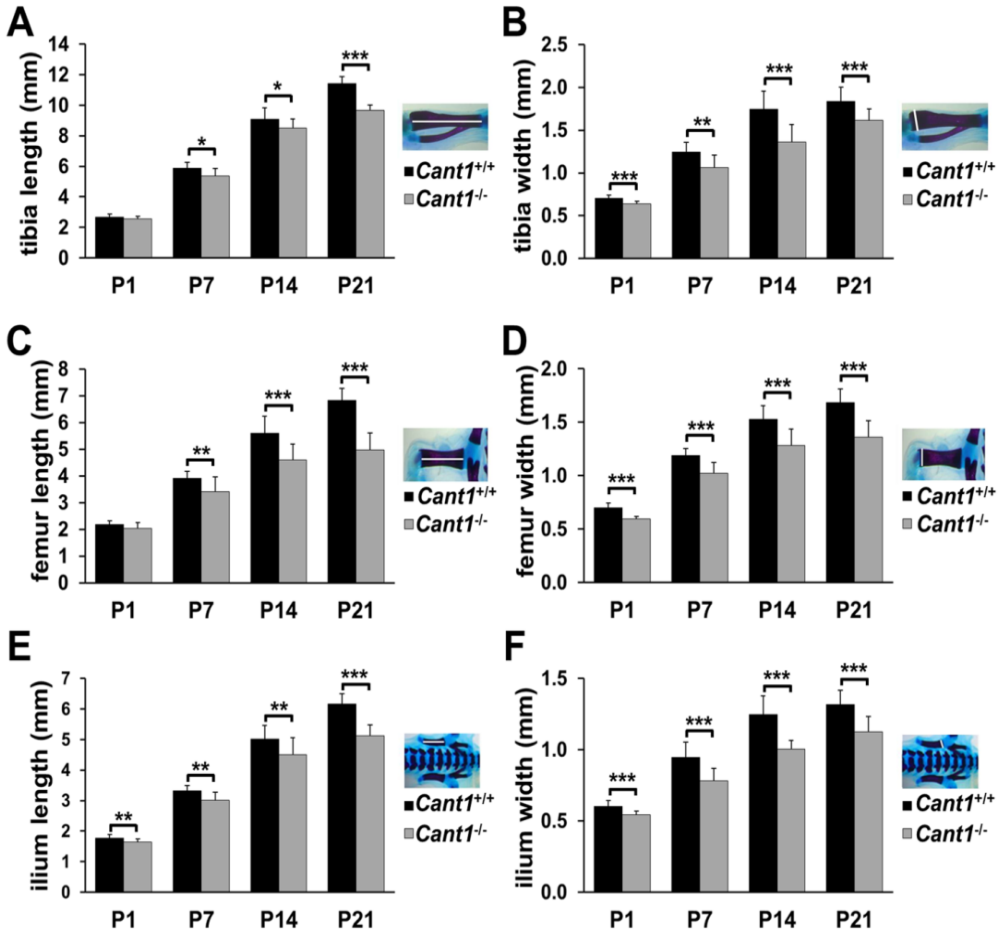

Fig. 19: *Cant1*$^{-/-}$ mice show growth defects in long bones. (A – F) Morphometric analysis on alcian blue and alizarin red skeletal preparations. (A) Tibia length was significantly decreased in *Cant1*$^{-/-}$ mice starting from one week of life, while (B) tibia width was reduced from birth. Same results were observed for (C, D) femur, whereas (E) ilium length and (F) width were significantly decreased in *Cant1*$^{-/-}$ mice from birth. Data are presented as mean ± SD, significance was determined by Student's t-test, * $P < 0.05$; ** $P < 0.01$; *** $P < 0.001$; n = 5

2.3 Analysis of proteoglycan synthesis in dbqd mice

Proteoglycan synthesis studies were performed in primary chondrocyte cultures from rib cartilage of mutant and wild type mice at P4 by metabolic labeling with ^{35}S-sulfate for 24 hours. PGs were purified by DEAE-Sephacel step gradient chromatography and the ^{35}S-activity was measured and normalised to cell layer proteins determined with the BCA protein assay. In basal conditions (MEM), PG synthesis was reduced in Cant1$^{-/-}$ chondrocytes compared with wild type cells ($P < 0.01$, $n = 3$). The defect was even more enhanced when cells were metabolically labelled in MEM containing p-nitrophenyl-β-D-xylopyranoside (β-D-xyloside) ($P < 0.001$, $n = 3$) (**Figure 20 A and B**).

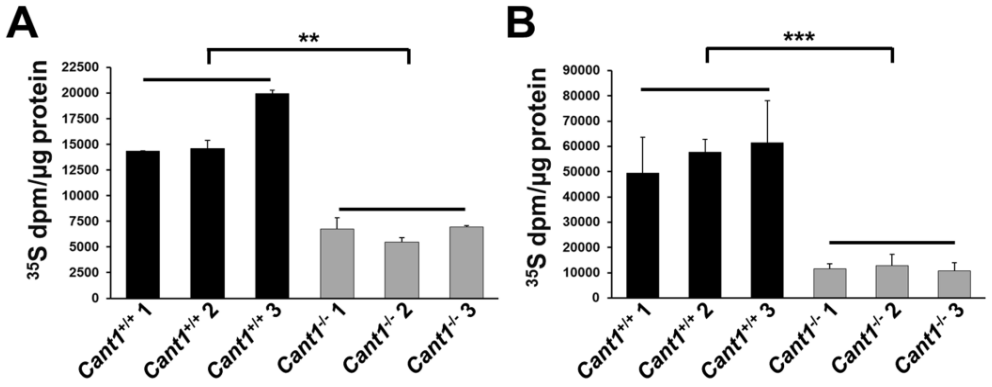

Fig 20: Proteoglycan synthesis is reduced in *Cant1*$^{-/-}$ mice. (A) Rib chondrocyte cultures were metabolically labelled with ^{35}S-sulfate for 24 h in basal medium. Then, the amount of newly synthesised PGs was determined on the basis of ^{35}S-activity and normalised to the protein content demonstrating that *Cant1*$^{-/-}$ chondrocytes produced less PGs compared with wild type cells. Data are representative of two independent experiments and reported as mean ± SD. Significance was determined by Student's t-test; ** $P < 0.01$. (B) Rib chondrocyte cultures were metabolically labelled with ^{35}S -sulfate for 24 h in basal medium containing 1 mM p-nitrophenyl-β-D-xylopyranoside. Samples were analysed as described in 6A demonstrating that the reduced PG synthesis in *Cant1*$^{-/-}$ chondrocytes was more evident in presence of β-D-xyloside. Data are representative of two independent experiments and reported as mean ± SD. Student's t-test was performed, *** $P < 0.001$.

2.4 Analysis of glycosaminoglycan content in Cant1$^{-/-}$ mice

To evaluate if CANT1 affects PG synthesis also *in vivo*, we measured the GAG content of cartilage from mutant and wild type mice. Femoral head cartilage from P4 mice was dissected and digested with proteinase K to remove all proteins and release GAGs. Then GAGs were quantified with the dimethylmethylene blue (DMMB) assay and the results were normalised to the DNA content determined with the Quant-iT PicoGreen dsDNA Kit.

The GAG content of cartilage from dbqd mice was reduced compared with wild type animals (92.28 ± 15.46 µg GAGs/µg DNA and 115.32 ± 18.25 µg GAGs/µg DNA respectively, P < 0.01) (**Figure 21**).

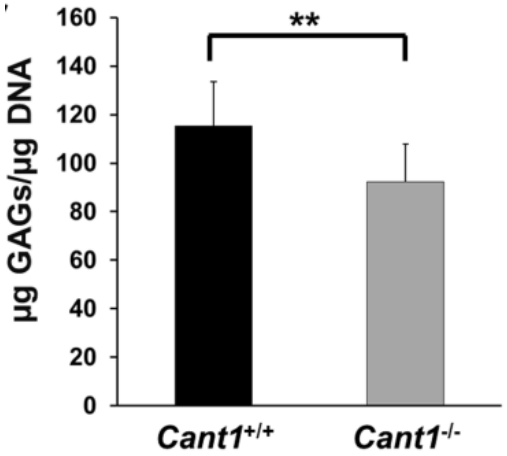

Fig 21: The GAG content in femoral head cartilage from 4 day old mice was analyzed by dimethylmethylene blue assay and normalized to DNA content showing reduced GAG content in *Cant1*$^{-/-}$ cartilage. Data are representative of three independent experiments and reported as mean ± SD. Student's t-test was performed, ** $P < 0.01$; n = 10.

2.5 Analysis of glycosaminoglycan sulfation in dbqd mice

To check whether CANT1 defect also affects other structural properties of PGs such as proteoglycan sulfation, we analysed the level of GAG sulfation in primary chondrocytes by HPLC analysis of chondroitin sulfate disaccharides.

The percentage of monosulfated disaccharides (ΔDi-4S and ΔDi-6S) relative to the total amount of disaccharides (ΔDi-0S, ΔDi-4S and ΔDi-6S), was increased in *Cant1*$^{-/-}$ chondrocytes compared with wt ones, in both cell layer (88.43 ± 1.91% and 76.92 ± 3.47%, respectively; $P < 0.01$) and medium fractions (92.22 ± 1.36% and 73.62 ± 3.03%, respectively; $P < 0.001$) demonstrating chondroitin sulfate oversulfation in *Cant1*$^{-/-}$ chondrocytes compared with wild-type cells (**Figure 22 A**).

To confirm the result in vivo, sulfation of chondroitin sulfate from femoral head cartilage of P4 *Cant1*$^{-/-}$ and wt mice was analyzed by HPLC. Results showed a significant increase of the relative amount of monosulfated disaccharides in *Cant1*$^{-/-}$ mouse cartilage compared with wild type (94.05 ± 0.56% and 86.01 ± 0.49%, respectively; $P < 0.001$) and a parallel reduction of the relative amount of non-sulfated disaccharide (5.95 ± 0.56% and 13.99 ± 0.49%, respectively; $P < 0.001$) confirming PG oversulfation in *Cant1*$^{-/-}$ mouse cartilage (**Figure 22 B**).

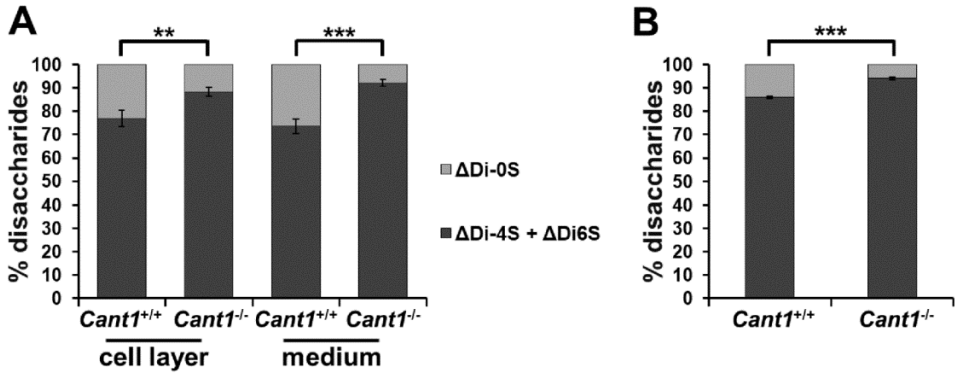

Fig 22: Chondroitin sulfate proteoglycans are oversulfated in *Cant1*$^{-/-}$ mice.
(A) Sulfation of chondroitin sulfate proteoglycans extracted from cell layer and medium of P4 *Cant1*$^{-/-}$ and *Cant1*$^{+/+}$ chondrocyte cultures was analysed by reverse-phase HPLC after digestion with chondroitinase ABC and ACII. The percentage of monosulfated disaccharides (ΔDi-4S and ΔDi-6S) was significantly increased in *Cant1*$^{-/-}$ cells compared with wild type ones. Data are reported as mean ± SD and significance was determined by Student's t-test, $^{**}P < 0.01$, $^{***}P < 0.001$; n = 3. (B) Chondroitin sulfate proteoglycans were extracted from P4 *Cant1*$^{-/-}$ and *Cant1*$^{+/+}$ femoral head cartilage and their sulfation was analysed by reverse-phase HPLC after digestion with chondroitinase ABC and ACII. The percentage of monosulfated disaccharides (ΔDi-4S and ΔDi-6S) was significantly increased and correspondingly the percentage of non-sulfated disaccharides (ΔDi-0S) was reduced in *Cant1*$^{-/-}$ cartilage compared with wild type. Data are reported as mean ± SD and Student's t-test was performed, $^{***}P < 0.001$; n = 6.

2.6 Analysis of the hydrodynamic size of glycosaminoglycans in dbqd mice

Since GAG content and sulfation were altered in cartilage and in chondrocyte cultures from *Cant1*$^{-/-}$ mice, we also considered the hydrodynamic size of GAGs. Starting from chondrocyte cultures labelled with ^{35}S-sulfate and incubated in presence or in absence of β-D-xyloside, newly synthesized PGs were β-eliminated in order to release GAGs. Then GAGs were analyzed by gel filtration chromatography on a Sepharose 6 10/300 GL column and ^{35}S-activity was measured in each fraction of the eluate by scintillation counting.

When chondrocytes were incubated in basal medium, the hydrodynamic size of GAG chains both in *Cant1*$^{-/-}$ and wt cells was the same (K_{av} 0.50 and 0.53, respectively), even if a slight peak broadening towards the total volume (V_t) was evident in *Cant1*$^{-/-}$ chromatograms indicating a fraction of GAGs with lower molecular mass compared with wild type (**Figure 23 A**). Remarkably, when cells were metabolically labelled in presence of β-D-xyloside, GAGs from *Cant1*$^{-/-}$ chondrocytes showed a significant shift toward the V_t compared with wild type (K_{av} 0.81 ± 0.02 and 0.63 ± 0.05, respectively; $P < 0.01$), (**Figure 23 B**). This result demonstrated the smaller size of newly synthesised GAG in *Cant1*$^{-/-}$ chondrocytes compared with control cells when oligosaccharide synthesis was enhanced.

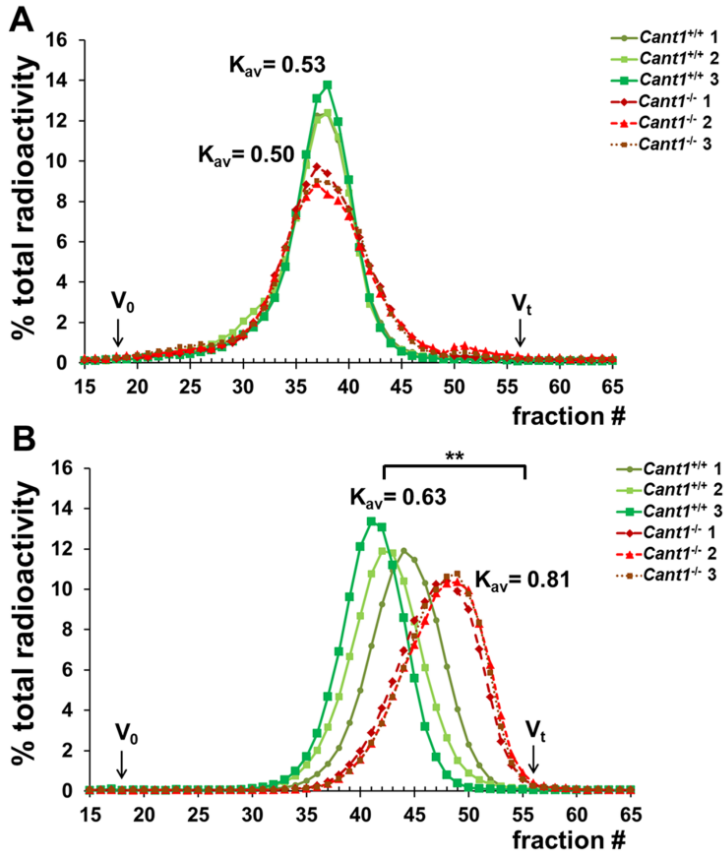

Fig 23: GAG hydrodynamic size is reduced in *Cant1*$^{-/-}$ mice.
(A) Chondrocyte cultures were metabolically labelled with ^{35}S-sulfate for 24 hours in basal medium. GAGs were released from PGs by β-elimination and their hydrodynamic size was analysed by gel filtration chromatography. GAG hydrodynamic size of *Cant1*$^{-/-}$ chondrocytes was comparable with *Cant1*$^{+/+}$ cells even if a slight peak broadening toward the total volume (V_t) was observed. Data are representative of two independent experiments. (B) *Cant1*$^{-/-}$ and *Cant1*$^{+/+}$ chondrocyte cultures were metabolically labelled with ^{35}S-sulfate in basal medium containing 1 mM p-nitrophenyl-β-D-xylopyranoside, an enhancer of GAG synthesis. GAG hydrodynamic size was analysed by gel filtration chromatography. A marked shift toward the V_t was found in *Cant1*$^{-/-}$ chromatograms demonstrating that *Cant1*$^{-/-}$ GAGs have reduced size compared with wild type ones. Data are representative of two independent experiments and K_{av} is reported as mean. Significance was determined by Student's t-test, ** $P < 0.01$.

2.7 Analysis of proteoglycan secretion in *Cant1*$^{-/-}$ mice

Results described above demonstrated defects in different steps of PG and GAG synthesis in *Cant1*$^{-/-}$ chondrocytes; therefore PG secretion was also measured. In a pulse chase experiment primary rib chondrocytes from P4 *Cant1*$^{-/-}$ and wt mice were incubated with ^{35}S-sulfate for 2 hours. Then the medium was replaced with medium containing an excess of cold sulfate and cells were harvested at different time points: 0.5, 2.5 and 5 hours. At each time point ^{35}S-proteoglycans were purified from free ^{35}S-sulfate by gel filtration chromatography and the percentage of ^{35}S-radioacticity in the medium to the total count (medium and cell layer) was determined. A significant reduction in PG secretion was demonstrated in mutant chondrocytes compared with wild type cells ($P < 0.05$, n = 3) (**Figure 24**).

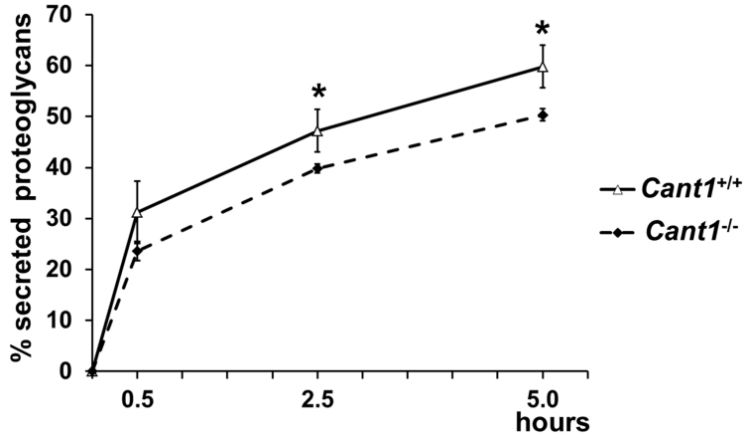

Fig 24: Proteoglycan secretion is delayed in *Cant1*$^{-/-}$ mice. Chondrocyte cultures were metabolically labelled with ^{35}S-sulfate for 2 hours and cells were harvested after 0.5, 2.5 and 5 hours. The percentage of ^{35}S-PGs in the medium to total labelled PGs (in medium and cell layer) was considered demonstrating a delayed secretion of PGs in *Cant1*$^{-/-}$ chondrocytes. Data are reported as mean ± SD and significance was determined by Student's t-test, * $P < 0.05$; n = 3.

2.8 Transmission electron microscopy of dbqd cartilage

To better characterize the defects in proteoglycan synthesis and secretion observed *in vitro*, a study of chondrocytes at the ultrastructural level by transmission electron microscopy (T.E.M.) was performed.

T.E.M. analysis of cartilage sample from P4 dbqd and wild type mice was performed in collaboration with professor Marco Biggiogera from the Department of Biology and Biotechnology of the University of Pavia, Italy.

In dbqd cartilage sections, chondrocytes showed huge vacuoles and endoplasmic reticulum (ER) enlargement with proteinaceous material inside, confirming results previously obtained on patient fibroblasts (**Figure 25**). Interestingly, on the same sections from dbqd femoral head cartilage a less dense ECM compared with wild type samples was observed (**Figure 25**) confirming reduced GAG content in dbqd cartilage observed by the DMMB assay (**Figure 21**).

These results were in line with biochemical data demonstrating defects in proteoglycan metabolism and secretion.

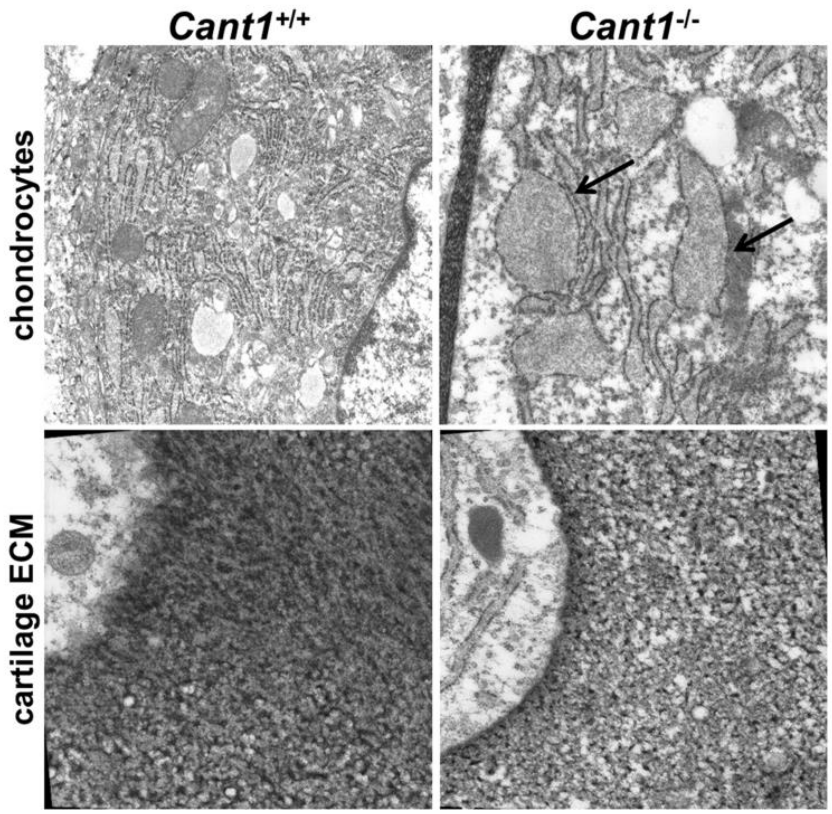

Fig 25: ER enlargement is present in *Cant1*$^{-/-}$ cartilage. Femoral head cartilage sections of P4 *Cant1*$^{-/-}$ and *Cant1*$^{+/+}$ mice were analysed by TEM. In *Cant1*$^{-/-}$ samples the presence of ER enlargement in chondrocytes (arrows) and a less dense cartilage ECM compared with wild type sections were observed. Three animals for each genotype were analysed. Magnification in chondrocyte images: 12,000x and in cartilage images: 20,000x.

3. DISCUSSION

In this work a *Cant1* knock-out mouse (dbqd mouse) generated previously in my research group, was deeply characterized to define the physiological role of CANT1 and to better understand the pathophysiology of Desbuquois dysplasia type 1. At birth dbqd mice were smaller compared with wild type newborns and the growth defect persist after birth. The morphological characterization of dbqd mice by double staining with alcian blue and alizarin red and by X-ray demonstrated a chondrodysplastic phenotype reminiscent of patients affected by Desbuquois dysplasia type 1. Moreover at the extremities of dbqd mice at P7, P14 and P21 the presence of an additional phalanx in the first digit, the so called "delta phalanx", was observed; this is a typical hand anomaly present in Desbuquois dysplasia type 1 patients [102]. Thus, the phenotypical features validate the mutant mouse as an animal model of Desbuquois dysplasia type 1.

Since PGs play a crucial role in cartilage growth plate development and homeostasis [36], we investigated the role of CANT1 in PG biosynthesis using mouse tissues and primary cultures of rib chondrocytes from mutant and wild type mice. PGs were metabolic labeled with ^{35}S-sulfate to study the biosynthetic process: dbqd chondrocytes synthesized less PGs compared with wild type cells and the defect was even more enhanced after incubation of cells with basal medium containing 1 mM p-nitrophenyl-β-D-xylopyranoside (β-D-xyloside), a compound that increases GAG synthesis acting as an artificial chain initiator [134]. The *in vitro* results were confirmed by *ex vivo* analysis in mutant mice. In fact the GAG content in femoral head cartilage of P4 dbqd mice was reduced compared with wild type mice. The defect in GAG biosynthesis was deeply characterized by studying their hydrodynamic size and sulfation. Gel filtration chromatography of newly synthesised GAGs from dbqd cells showed a peak broadening toward the total volume of the

column indicating that a small fraction of GAGs from dbqd cells were smaller in size compared with wild type cells; the defects was dramatically enhanced when β-D-xyloside was present. Sulfation analysis demonstrated that GAGs in dbqd chondrocytes were oversulfated compared with wild type cells. These results were confirmed also *in vivo* by chondroitin sulfate disaccharide analysis in femoral head cartilage of P4 dbqd and wild type mice. Since different intracellular steps of GAG biosynthesis were altered, PG secretion was also considered. PG secretion was analyzed by a pulse chase experiments and a delay of PG secretion was demonstrated in dbqd chondrocytes compared with wild type cells.

To further investigate the molecular basis of the PG secretion defects, transmission electron microscopy on cartilage samples was performed. In semi-thin sections of dbqd femoral head cartilage, chondrocytes showed huge vacuoles and ER enlargement with electrodense material inside confirming potential PG retention. Since the presence of vacuoles and ER enlargement was already reported in fibroblasts from patients [102] , this result provided an additional evidence that dbqd mice are reminiscent of human Desbuquois dysplasia type 1.

Furthermore, the possible PG retention and the ER enlargement observed by T.E.M. analysis suggested that ER stress might be involved in the pathogenesis of the disorder.

The defects in different intracellular steps of GAG biosynthesis caused a delay of PG secretion in *Cant1*$^{-/-}$ chondrocytes compared with wild type cells. Interestingly, we demonstrated that in the absence of CANT1, GAG chains are oversulfated both *in vitro* and *in vivo.* Thus, we postulate that the oversulfation of chondroitin sulfate chains in cartilage of mutant mice is caused by the delay of PG secretion. In particular, PGs spend more time in the Golgi apparatus of *Cant1*$^{-/-}$ chondrocytes, where sulfotransferases have more time to catalyse GAG sulfation.

Reduced PG synthesis and short GAG chains detected in dbqd mice were already observed in fibroblast cultures from patients affected by Desbuquois dysplasia type 1 [102]. Consequently, our findings on dbqd chondrocytes confirmed at the biochemical level the phenotypic similarities with the disorder in humans. All these data provide final evidence of CANT1 involvement in PG biosynthesis.

In conclusion, the dbqd mouse can be considered an appropriate animal model for Desbuquois dysplasia type 1 since it is reminiscent of typical features of patients such as reduced size, growth retardation and delta phalanx. Moreover, biochemical studies demonstrated that CANT1 plays a role in PG metabolism since when CANT1 is impaired, PG and GAG synthesis is decreased and PG secretion delayed.

Chapter V

Materials and methods

1. ANIMALS

1.1 Generation of Impad1 knock-in mouse model

The Impad1 mouse is a knock-in generated by the insertion of a c.726G>A transition (NCBI Ref. Seq. NM_177730.4) in the *Impad1* gene, leading to substitution of p.Asp175>Asn in exon 2. In addition close to the mutation two silent mutations, c.716T>C and c.719C>T respectively, were inserted to generate a *ClaI* restriction site useful for animal genotyping. A vector for the stable inversion mediated by Cre-recombinase was generated by Polygene (AG, Rumlang, Switzerland) using gene synthesis method, with a combination of *lox71* as LE mutant *loxP* (carrying mutations in the left-inverted repeat region) and *loxKR3* as RE mutant *loxP* (carrying mutations in the right-inverted repeat region) in a head-to-head orientation [132]. For testing, an FRT-flanked *neomycin* resistance cassette was cloned between the *lox*-sites using *EcoRV* and *EcoRI* restriction enzymes. The resulting vector was transformed in *E.coli* expressing Cre-recombinase where efficient recombination was confirmed by inversion *in vivo*. Next, the *lox71*/*loxKR3* vector was used for the assembly of the Impad1 conditional knock-in gene targeting construct. Briefly, the vector contained homology arms for the *Impad1* genes of about 5 kb and 2.7 kb; The homologous sequences flanked a duplicated region of the mutated and wild type exon 2, which were introduced in a head to head orientation. They were flanked by the head to head *lox71* and *loxKR3* sites and separated by an FRT-flanked neomycin cassette. The targeting vector bearing the *Impad1* mutation were electroporated into 2 x 10^7 C57Bl/6N-based ES cells. After selection with 200 µg/ml neomycin (G418) for 8 days, ES cell clones were isolated and analyzed via PCR screening. Positive ES cell clones in which correct

homologous recombination has occurred were identified via long range PCR and Southern blot analysis.

Two positive ES cell clones were injected into grey C57Bl/6N derived blastocysts. The resulting chimeras were bred to C57Bl/6N-based Flp-deleter mice (B6gr Tg (ACTFLPe) 9205Dym/NPg) and the resulting black offspring was analyzed via PCR analyses. Several positive mice that lost the FRT-flanked neomycin cassette via Flp-recombination were identified (called "floxed" mice). Deletion of the neomycin cassette was demonstrated by PCR using primers Neo3-for and Neo4-rev

Neo3-for: 5'-CAAGCTCTTCAGCAATATCACGGG-3'

Neo4-rev: 5'-CCTGTCCGGTGCCCTGAATGAACT-3'

moreover the presence of the floxed allele was confirmed by the presence of the *lox71* site checked by PCR with primers SY08.20 and SY08.21.

SY08.20: 5'-TGGCCTGAGACACATTCC-3'

SY08.21: 5'-CTGCTGGTACCTCCTTAG-3'

100 ng of genomic DNA were added to the PCR mix, which includes 1X Taq DNA Polymerase buffer (GenScript), 0,2 mM dNTPs, 0,01 U/µl Taq DNA Polymerase (GenScript) and 0,4 pmol/µl primers. The PCR cycle starts with 5 minutes of denaturation at 94°C, followed by 35 cycles of:

- denaturation of 30 seconds at 94°C
- annealing of 30 seconds at 56°C
- extension of 45 seconds at 72°C

and terminates with other 5 minutes of extension at 72°C. The PCR products were checked by electrophoresis on a 1.5% (w/v) agarose gel in TBE buffer, pH 8.0 (88 mM Tris, 89 mM boric acid, 2 mM disodium EDTA). The wild type band is 459 bp long, the mutated one is 506 bp long. Floxed mice were mated to a Cre mouse strain (B6.FVB-Tg(EIIa-cre)C5379Lmgd) to generate the stable knock-in of the p.Asp175>Asn mutation.

1.2 Animal care and sacrifice

Animals were bred with free access to water and standard pelleted food. Care and use of mice for this study was in compliance with relevant animal welfare institutional guidelines in agreement with EU Directive 2010/63/EU for animals and the Italian Legislative Decree 4.03.2014, n.26. The experimental protocol was approved by the Italian Ministry of Health (Animal protocol n. 844/2017-PR and n. 95/2017-PR). Mice were humanely sacrificed by CO_2 inhalation. The Impad1 knockout strain, generated by Frederick et al. [69] was provided by "The Jackson Laboratories", Bar Harbor, Maine, USA.

1.3 Genomic DNA extraction from tissue

DNA used for mouse genotyping was extracted from tail clips. Samples were digested in 500 µl of lysis buffer (100 mM Tris-HCl, 5 mM EDTA, 0.2% SDS (w/v), 200 mM NaCl, pH 8.5) and 20 µl of 15 mg/ml proteinase K (Sigma) and incubated at 55°C overnight. Specimens were then centrifuged at 12,000 rpm for 15 minutes to remove undigested materials. DNA was precipitated with 500 µl of isopropanol and centrifuged at 12,000 rpm for 10 minutes. The DNA pellet was washed gently with 900 µl of 70% ethanol (v/v) and samples were centrifuged at 12,000 rpm for 5 minutes. The DNA was air-dried for at least 20 minutes and resuspended in 150 µl of Tris-EDTA buffer (10 mM Tris-HCL, 1 mM EDTA, pH 8.0). The DNA concentration was determined by absorbance at 260 nm with the NanoDrop ND-1000 spectrophotometer.

1.4 Impad1 mouse genotyping

Mice were genotyped by PCR using genomic DNA from mouse tail or ear clips. The mutant allele was detected by digestion with *ClaI* of a PCR product generated with primers Imp3 and Imp8.

IMP3: 5’-GTTAGATTAGAAAGTACTTGAAG-3’

IMP8: 5’-CTAGTCTGCTTGTCTGGAAACC-3’

100 ng of genomic DNA were added to the PCR mix, which includes 1X Taq DNA Polymerase buffer (GenScript), 0,2 mM dNTPs, 0,01 U/µl Taq DNA Polymerase (GenScript) and 0,4 pmol/µl primers. The PCR cycle starts with 5 minutes of denaturation at 94°C, followed by 35 cycles of:

- denaturation of 30 seconds at 94°C
- annealing of 30 seconds at 59°C
- extension of 50 seconds at 72°C

and terminates with other 5 minutes of extension at 72°C. The PCR products were checked by electrophoresis on a 1.5% (w/v) agarose gel in TBE buffer, pH 8.0 (88 mM Tris, 89 mM boric acid, 2 mM disodium EDTA). The wild type band is 430 bp long, the mutated one is 480 bp long. The PCR product was digested with ClaI restriction enzyme (Promega) at 30 ^{o}C O/N. The 480 bp PCR product of the mutant allele was digested by ClaI in two restriction fragments of 124bp and 356bp, respectively. Genotyping of the *Impad1* knockout strain was performed as described previously [69].

2. MORPHOLOGICAL ANALYSIS

2.1 X-rays and image analysis

X-ray analyses were performed using a Faxitron MX-20 cabinet X-ray system (Faxitron X-Ray LLC, Lincolnshire, IL 60069).

The exposure was set at:

- 21 kV for 30 seconds with 4-fold magnification for *Impad1* P0 mice
- 27kV for 19 seconds with 2-fold magnification for *Dbqd* adult mice (P60)

images were analyzed using K-pace Software.

2.2 Differential skeletal staining with alcian blue and alizarin red

Skeletal characterization of mice was performed using the double staining with alcian blue which stains cartilage glycosaminoglycans and alizarin red which binds and stains bone calcium. Mice were sacrificed and dissected to remove skin and internal organs. Skeletons were fixed in 96% ethanol for 14 days and skeletal preparations were defatted in acetone for 2 weeks. The staining was performed using 45 ml of staining solution (1 volume of 0,3% Alcian Blue 8GX in 70% ethanol, 1 volume of 0,1% Alizarin Red S in 95% ethanol, 1 volume of acetic acid and 17 volumes of 70% ethanol) for 3 days at 37°C. After staining, skeletons were rapidly rinsed in tap water and then washed in 1% KOH and 20% glycerol solution until complete tissues clarification, changing the solution every 2-3 days. The subsequent washes were in increasing concentration of glycerol (50% and 80%) and 1% KOH; finally skeletons were stored in 100% glycerol. Mice were then photographed on a Leica M165 FC stereomicroscope connected to a Leica DFC425 C digital camera (Leica Microsystems, Italy).

2.3 Impad1 RT-qPCR and alternative splicing analysis

Skin from newborn mice was homogenized in 1 ml of QIAzol Lysis Reagent (QIAGEN, Italy) and total RNA was extracted according to the manufacturer's instructions. Reverse transcription of 1µg RNA in a final volume of 20 µl was performed using the SuperScript IV First-Strand Synthesis System (Invitrogen, Thermo Fisher Scientific, Italy) according to the manufacturer's instructions. For expression analyses by RT-qPCR, the QuantiFast Primer Assays with validated primer set for *Impad1* and *Gapdh* (QIAGEN) were used with the QuantiTect SYBR Green PCR Kit (QIAGEN)

according to the manufacturer's protocol. The primer set of Impad1 span exon 2 and 3. Each sample was run in triplicate in 96 well plates in three independent experiments with the MX3000P (Stratagene, USA) apparatus. Briefly, RT-qPCR cycle started with 5 min of denaturation at 95 °C, followed by 40 cycles of:

- denaturation of 10 seconds at 95°C
- annealing of 30 seconds at 60°C
- extension of 30 seconds at 72°C

and terminated with the dissociation curve. The expression of *Impad1* relative to the housekeeping *Gapdh* gene was obtained by ΔΔCt method.

For alternative splicing detection total RNA was used for RT-PCR analysis using primers in exon 1 (5'-CGAGAGCAATGTCCTTCACG-3') and exon 5 (5'-TTTTAAGATGGCATTGCCAGC-3') of the *Impad1* gene. PCR cycle started with 5 min of denaturation at 94 °C, followed by 35 cycles of

- denaturation of 30 seconds at 94°C
- annealing of 30 seconds at 58°C
- extension of 1:30 minutes at 72°C

and terminates with other 5 minutes of extension at 72°C. PCR products were analyzed by 1.5% agarose gels. For DNA sequencing of the spliced forms, the PCR products were cloned with the TA cloning kit (Invitrogen) according to the instructions provided by manufacturer, followed by Sanger sequencing.

3. BIOCHEMICAL ANALYSIS

3.1 HPLC analysis of glycosaminoglycan sulfation in cartilage and skin

For disaccharide analysis, cartilage was obtained from the femoral heads of newborn mice by careful dissection under the dissection microscope and skin

was carefully removed from the body. Glycosaminoglycans (GAGs) were recovered by tissue digestion using papain in 0,1 M sodium acetate, pH 5.6, 5 mM EDTA and 5 mM cysteine at 65°C for 48 h. After papain inactivation at 100°C, released GAGs were recovered by precipitation with 1% and cetylpyridinium chloride precipitation. The precipitate was washed three times with 10% potassium acetate in 96% ethanol and three times with 96% ethanol respectively. The precipitate was dried and purified GAGs were digested with 30 mU of both chondroitinase ABC and chondroitinase ACII (Seikagaku Corp., Japan) in 0,1 M sodium acetate, pH 7.35 at 37°C overnight. Undigested products were removed by precipitation by centrifugation. Released disaccharides were lyophilized and redissolved in 40 µl of 12.5 mM 2-aminoacridone (Invitrogen) in 85% DMSO/15% acetic acid and incubated for 15 minutes at room temperature in the dark; then, 40 µl of 1.25 M sodium cyanoborohydride in water was added and the mixture was incubated overnight at 37 °C. Disaccharides were fractioned with a ProntoSIL HPLC column (4.6 mm × 200 mm, Bischoff Chromatography, Germany) using a linear gradient (0 - 42% solvent B in 42 min); mobile phases were 0.1 M ammonium acetate, pH 7.0, (Solvent A) and methanol (Solvent B). The flow rate was 0.7 ml/min at room temperature and the elution profile was monitored by a fluorescence detector (2475 Multy λ Fluorescence Detector, Waters, Italy), with excitation and emission wavelengths of 425 and 525 nm, respectively.

3.2 Extraction of rib chondrocytes

Primary chondrocyte cultures were established from rib cartilage of 4 days old mice. The thoracic cage of mice was harvested and digested with 2 mg/ml collagenase type II (Invitrogen) in Dulbecco's modified Eagle's medium (DMEM) (Sigma) for 1 hour and half at 37°C to remove intercostal muscles. Then under the microscope, cartilage was dissected from each rib and

digested with 2 mg/ml collagenase type II for 3 hours at 37°C. Released chondrocytes were plated and cultured in DMEM with 10% foetal calf serum (FCS) (Euroclone) and antibiotics at 37°C in a 5% CO_2.

3.3 Metabolic labelling of chondrocyte cultures and PG synthesis

For PG labelling, cells were preincubated with or without 1 mM p-nitrophenyl β-D-xylopyranoside in minimal essential medium (MEM) (Sigma) containing 250 μM cold Na_2SO_4 without FCS in 5% CO_2 at 37°C for 2 hours. Cells were then labeled with 50μCi/ml Na2[$^{35}SO_4$] in the same medium for 24 hours as previously described [131]. At the end of the labelling period, an equal volume of 100 mM sodium acetate buffer, pH 5.8, containing 8 M urea, 4% Triton X-100, 20 mM EDTA, 20 mM NEM, 0.1 M aminocaproic acid and 1 mM PMSF was added to the medium. The cell layer was lysed in 50 mM sodium acetate buffer, pH 5.8, containing 2 M urea, 2% Triton X-100 and an aliquot was used to determine the protein content by the BCA Protein Assay (Pierce), whereas the rest was added to the medium. Samples were loaded on 1 ml DEAE Sephacel columns and, after column washing with 50 mM sodium acetate, pH 6.0, 8 M urea, 0.12 M NaCl, 0.5% Triton X-100 and proteinase inhibitors, PGs were eluted with 1 M NaCl in the same buffer. Then PGs were precipitated with 9 volumes of ethanol followed by centrifugation at 17,000 x g for 60 minutes at 4°C. The pellet was washed with 70% ethanol and then solubilized in water. PGs were quantified by measuring the ^{35}S-activity using a liquid scintillation analyzer (TRI-CARB 2300 TR) and normalized to the protein content.

3.4 Size exclusion chromatography of GAG chain

Labelled PGs synthesised by chondrocytes and purified as described above were β-eliminated by alkaline digestion with 0.125 M NaOH followed by

reduction with 1 M $NaBH_4$ at room temperature overnight. After neutralization with acetic acid, samples were lyophilized and dissolved in 4 M guanidinium chloride, 50 mM sodium acetate, pH 6.0, 0.5% Triton X-100. Samples were loaded on a Superose 6 10/300GL (GE) and eluted in the same buffer at 0.2 ml/min. 0.4 ml fraction were collected and ^{35}S-activity was measured by scintillation counting.

3.5 Proteoglycan secretion

In a pulse chase experiment primary chondrocytes were plated in 24 well plates at a cell density of 50,000 cells/well and 24 hours later they were labelled with 30 μCi/well of ^{35}S-sulfate for 2 hours in MEM without FCS in 5% CO2 at 37°C. At the end of the labelling period, the medium was removed, cells were washed with MEM without FCS containing 5 mM cold sulfate and incubated in the same medium for different chase times (0, 0.5, 2.5 and 5 hours) as previously described [132]. At each time point, cell layer and medium were collected separately. To each medium an equal volume of 2% Triton X-100, 8 M guanidinium chloride and protease inhibitor cocktail in 0.2 M sodium acetate, pH 5.8, was added, while each cell layer was scraped in 2% Triton X-100, 4 M guanidinium chloride and protease inhibitors in 0.1 M sodium acetate, pH 5.8. Each medium and cell layer were desalted to remove ^{35}S-sulfate with PD Midi-Trap G-25 columns (GE) equilibrated and eluted with 4 M guanidinium chloride, 0.5%Triton X-100 in 50 mM sodium acetate, pH 6.0. The V_0 for each gel filtration was collected and ^{35}S-radioactivity was measured by scintillation counting. For each time point the percentage of ^{35}S-radioactivity in the medium to the total counts (medium and cell layer) was calculated.

3.6 Cartilage glycosaminoglycan content

GAG content was measured in femoral head cartilage of mice with the dimethylmethylene blue (DMMB) assay according to Farndaèle et al [133]. Briefly, femoral head cartilages of P4 mice were dissected and digested with 100 µl of 5 µg/µl proteinase K in 20 mM sodium acetate buffer, pH 6.8, containing 1 mM EDTA at 55°C overnight. Then to denature proteinase K, samples were incubated at 99°C for 10 minutes. 30 µl of digested samples was used for DMMB assay bringing each sample to a final volume of 60 µl with water and adding 1 ml of DMMB solution (10.7 mg/l DMMB in 55 mM formic acid, pH 3.3). GAG concentration was analysed by reading sample absorbance at 525 nm immediately after DMMB addition. The assay was calibrated by the use of reagent blank and standard containing up to 6 µg chondroitin sulfate in the same buffer as samples. GAG content was normalised to DNA amount analysed on 30 µl of sample by the Quant-iTTM PicoGreen ® dsDNA Assay Kit (Invitrogen), according to the instruction provided by manufacturer.

3.7 Proteoglycan sulfation analysis

To analyze the PG sulfation level, PGs were extracted from cartilage and chondrocyte samples. Femoral head cartilage of mice was carefully dissected under the dissection microscope and digested with 10 U of papain (Sigma) in 300 µl of papain digestion buffer (0.1 M sodium acetate, pH 5.6, 5 mM EDTA and 5 mM cysteine) at 65°C overnight. Chondrocyte cultures were incubated with basal medium without FCS in 5% CO_2 at 37°C for 24 hours. 694 µl of 10x papain digestion buffer (1 M sodium acetate, pH 5.6, 50 mM EDTA), 1 ml 33 mM cysteine and 20 U of papain was added to the medium, while cells were scraped in 5 ml of papain digestion buffer and, then, 20 U of papain was added to sample. Both medium and cell layer were digested at 65°C overnight. After papain inactivation at 100°C for 10 minutes, released

GAGs from all samples (cartilage and chondrocytes) were precipitated, digested with chondroitinase, and dissolved as described above. HPLC analysis was performed using an HPLC binary pump system (Binary HPLC Pump 1525μ, Waters) coupled to a fluorescent detector (Multi λ Fluorescence detector 2475, Waters) set at λex 425 nm and λem 525 nm. Chromatography was carried out with a C18 column LiChroCART® 250-4 Superspher® 100 RP-18 endcapped (Merk) and linked to a LiChroCART® 4-4 LiChrospher ®100 RP-18 endcapped (5μm) (Merk) precolumn. Mobile phase flow was 0.7 ml/min and elution was performed at room temperature using a linear gradient (0 - 45% solvent B in 36 min); mobile phases were 0.1 M ammonium acetate, pH 7.0, (Solvent A) and methanol (Solvent B).

4. HISTOLOGICAL ANALYSIS

4.1 Transmission electron microscopy analysis

Femoral head cartilages were dissected and processed for transmission electron microscopy as reported in literature [144]. Cartilage was fixed with 2% (v/v) glutaraldehyde and 0.7% (w/v) ruthenium hexamine trichloride (RHT) in 0.1 M cacodylate buffer, pH 7.4 at room temperature for 3 hours. Later samples were washed with 0.7% RHT in 0.1 M cacodylate buffer, pH 7.4. Samples were post-fixed in 0.7% RHT and 2% (w/v) OsO_4 in 0.1 M cacodylate buffer at room temperature for 2 hours, rinsed in distilled water and dehydrated in ethanol. Specimens were infiltrated with LR White acrylic resin at 4°C overnight and polymerized in gelatin capsules at 60°C for 24 hours. Thin section (60-70 nm tick) were cut on a Reichert OM-U3 ultramicrotome with a diamond knife and collocated on 300-mesh nickel grids. The grids were finally stained with saturated aqueous uranyl acetate followed by lead citrate and observed with a Zeiss EM900 electron microscope.

Biblyography

BIBLYOGRAPHY

1. Camarero-Espinosa S, Rothen-Rutishauser, B., Fostera, E. J. , Weder, C. (2016) Articular cartilage: from formation to tissue engineering. Biomater Sci 4: 734–767.
2. Seibel JM, Robins, P.S., and Bilezikian, P.J. (2006) Supramolecular Structure of Cartilage Matrix. Dynamics of Bone and Cartilage Metabolism. 2 ed.
3. Ulrich-Vinther M, D. Maloney M, M. Schwarz E, Rosier R, O'Keefe RJ (2003) Articular cartilage biology . J Am Acad Orthop Surg 11(6): 421–430.
4. Athanasiou KA, M. DE, C HJ (2009) Articular Cartilage Tissue Engineering. Synthesis Lectures on Tissue Engineering ,. pp. 1-182.
5. Temenoff J, Mikos A (2000) Review: tissue engineering for regeneration of articular cartilage.: Biomaterials. pp. 431-440.
6. Thambyah A, Broom N (2007) On how degeneration influences load-bearing in the cartilageebone system: a microstructural and micromechanical study. Osteoarthritis and Cartilage. pp. 1410-1423.
7. Knudson CB, Warren K (2001) Cartilage proteoglycans. Semin. Cell Dev Biol. pp. 69–78.
8. Eyre DR, Wu JJ (1995) Collagen structure and cartilage matrix integrity.: J Rheumatol Suppl.
9. Guilak F, Nims R, Dicks A, Wu C-L, Ingrid M (2018) Osteoarthritis as a disease of the cartilage pericellular matrix.: Matrix Biology : Journal of the International Society for Matrix Biology. pp. Pages 40-50.
10. Poole AR, Pidoux I, Reiner A, Rosenberg L (1982) An immunoelectron microscope study of the organization of proteoglycan monomer, link protein, and collagen in the matrix of articular cartilage. J Cell Biol 93: 921-937.
11. Poole AR, Matsui Y, Hinek A, Lee ER (1989) Cartilage macromolecules and the calcification of cartilage matrix. Anat Rec 224: 167-179.
12. Hunziker E, Michel M, Studer D (1997) Ultrastructure of adult human articular cartilage matrix after cryotechnical processing.: Microsc Res Tech. pp. 271-284.
13. Hall B, Miyake T (1992) The membranous skeleton: the role of cell condensations in vertebrate skeletogenesis.: Anat Embryol. pp. 107-124.
14. Steadman J, Briggs K, Rodrigo J, Kocher M, Gill T, et al. (2003) Outcomes of microfracture for traumatic chondral defects of the knee: average 11-year follow-up. pp. 477-484.
15. Mithoefer K, McAdams T, Williams R, Kreuz P, Mandelbaum B (2009) Clinical efficacy of the microfracture technique for articular cartilage repair in the knee: an evidence-based systematic analysis.: Am J Sports Med. pp. 2053-2063.
16. Hall B, Miyake T (2000) All for one and one for all: condensations and the initiation of skeletal development.: Bioessays. pp. 138-147.

17. Mackie EJ, Ahmed YA, Tatarczuch L, Chen KS, Mirams M (2008) Endochondral ossification: how cartilage is converted into bone in the developing skeleton. Int J Biochem Cell Biol 40: 46-62.
18. Hunziker EB, Schenk RK, Cruz-Orive LM (1987) Quantitation of chondrocyte performance in growth-plate cartilage during longitudinal bone growth. J Bone Joint Surg Am 69: 162-173.
19. Kronenberg HM (2003) Developmental regulation of the growth plate. Nature 423: 332-336.
20. Cortes M, Baria AT, Schwartz NB (2009) Sulfation of chondroitin sulfate proteoglycans is necessary for proper Indian hedgehog signaling in the developing growth plate. Development 136: 1697-1706.
21. Samsa WE, Zhou X, Zhou G (2017) Signaling pathways regulating cartilage growth plate formation and activity. Semin Cell Dev Biol 62: 3-15.
22. Ahmed YA, Tatarczuch L, Pagel CN, Davies HM, Mirams M, et al. (2007) Physiological death of hypertrophic chondrocytes. Osteoarthritis Cartilage 15: 575-586.
23. Moore ER, Jacobs CR (2017) The primary cilium as a signaling nexus for growth plate function and subsequent skeletal development. J Orthop Res.
24. Akiyama H, Chaboissier MC, Martin JF, Schedl A, de Crombrugghe B (2002) The transcription factor Sox9 has essential roles in successive steps of the chondrocyte differentiation pathway and is required for expression of Sox5 and Sox6. Genes Dev 16: 2813-2828.
25. Lefebvre V, Li P, de Crombrugghe B (1998) A new long form of Sox5 (L-Sox5), Sox6 and Sox9 are coexpressed in chondrogenesis and cooperatively activate the type II collagen gene. EMBO J 17: 5718-5733.
26. Tsuda M, Takahashi S, Takahashi Y, Asahara H (2003) Transcriptional co-activators CREB-binding protein and p300 regulate chondrocyte-specific gene expression via association with Sox9. J Biol Chem 278: 27224-27229.
27. Huang W, Lu N, Eberspaecher H, De Crombrugghe B (2002) A new long form of c-Maf cooperates with Sox9 to activate the type II collagen gene. J Biol Chem 277: 50668-50675.
28. Lefebvre V, Huang W, Harley VR, Goodfellow PN, de Crombrugghe B (1997) SOX9 is a potent activator of the chondrocyte-specific enhancer of the pro alpha1(II) collagen gene. Mol Cell Biol 17: 2336-2346.
29. Zhang P, Jimenez SA, Stokes DG (2003) Regulation of human COL9A1 gene expression. Activation of the proximal promoter region by SOX9. J Biol Chem 278: 117-123.
30. Bridgewater LC, Lefebvre V, de Crombrugghe B (1998) Chondrocyte-specific enhancer elements in the Col11a2 gene resemble the Col2a1 tissue-specific enhancer. J Biol Chem 273: 14998-15006.
31. Sekiya I, Tsuji K, Koopman P, Watanabe H, Yamada Y, et al. (2000) SOX9 enhances aggrecan gene promoter/enhancer activity and is up-regulated by retinoic acid in a cartilage-derived cell line, TC6. J Biol Chem 275: 10738-10744.

32. Kou I, Ikegawa S (2004) SOX9-dependent and -independent transcriptional regulation of human cartilage link protein. J Biol Chem 279: 50942-50948.
33. Hardingham TE, Oldershaw RA, Tew SR (2006) Cartilage, SOX9 and Notch signals in chondrogenesis. J Anat 209: 469-480.
34. Lefebvre V, Bhattaram P (2016) SOXC Genes and the Control of Skeletogenesis. Curr Osteoporos Rep 14: 32-38.
35. Heinegård D (2009) Fell-Muir Lecture: Proteoglycans and more--from molecules to biology. Int J Exp Pathol 90: 575-586.
36. Eyre D (2002) Collagen of articular cartilage. Arthritis Res 4: 30-35.
37. Danielson KG, Baribault H, Holmes DF, Graham H, Kadler KE, et al. (1997) Targeted disruption of decorin leads to abnormal collagen fibril morphology and skin fragility. J Cell Biol 136: 729-743.
38. Schonherr E, Hausser H, Beavan L, Kresse H (1995) Decorin-type I collagen interaction. Presence of separate core protein-binding domains. J Biol Chem 270: 8877-8883.
39. Hedbom E, Heinegard D (1993) Binding of fibromodulin and decorin to separate sites on fibrillar collagens. J Biol Chem 268: 27307-27312.
40. Chakravarti S, Magnuson T, Lass JH, Jepsen KJ, LaMantia C, et al. (1998) Lumican regulates collagen fibril assembly: skin fragility and corneal opacity in the absence of lumican. J Cell Biol 141: 1277-1286.
41. Halász K, Kassner A, Mörgelin M, Heinegård D (2007) COMP acts as a catalyst in collagen fibrillogenesis. J Biol Chem 282: 31166-31173.
42. Wagener R, Ehlen HW, Ko YP, Kobbe B, Mann HH, et al. (2005) The matrilins--adaptor proteins in the extracellular matrix. FEBS Lett 579: 3323-3329.
43. Hardingham TE, Fosang AJ (1992) Proteoglycans: many forms and many functions. FASEB J 6: 861-870.
44. Honke K, Taniguchi N (2002) Sulfotransferases and sulfated oligosaccharides. Med Res Rev 22: 637-654.
45. Vynios DH (2014) Metabolism of cartilage proteoglycans in health and disease. Biomed Res Int 2014: 452315.
46. Iozzo RV, Schaefer L (2015) Proteoglycan form and function: A comprehensive nomenclature of proteoglycans. Matrix Biol 42: 11-55.
47. Esko J, Kimata K, Lindahl U Proteoglycans and Sulfated Glycosaminoglycans. In: Press CSHNCSHL, editor. Essentials of Glycobiology. 2nd ed.
48. Prydz K, Dalen KT (2000) Synthesis and sorting of proteoglycans. J Cell Sci 113 Pt 2: 193-205.
49. Mizumoto S, Sugahara K (2012) Bone and skin disorders caused by a disturbance in the biosynthesis of chondroitin sulfate and dermatan sulfate. In: Ed. by Karamanos N, editor. Extracellular matrix: pathobiology and signaling: Walter de Gruyter GmbH & Co. KG. pp. 98-118.
50. Ledin J, Staatz W, Li JP, Götte M, Selleck S, et al. (2004) Heparan sulfate structure in mice with genetically modified heparan sulfate production. J Biol Chem 279: 42732-42741.

51. Pikas DS, Do A, Deligny A, Dagalv A, Kjellén L (2012) Heparan sulfate design: regulation of biosynthesis. In: K KN, editor. Extracellular matrix: pathobiology and signaling. Göttingen (D): De Gruyter. pp. 84-97.
52. Hascall V, Esko JD (2017) Hyaluronan. In: A V, Rd C, Jd E, editors. Essentials of Glycobiology. 3rd edition ed. New York (USA): Cold Spring Harbor.
53. Mizumoto S, Yamada S, Sugahara K (2015) Mutations in Biosynthetic Enzymes for the Protein Linker Region of Chondroitin/Dermatan/Heparan Sulfate Cause Skeletal and Skin Dysplasias. Biomed Res Int 2015: 861752.
54. Mizumoto S, Yamada S, Sugahara K (2014) Human genetic disorders and knockout mice deficient in glycosaminoglycan. Biomed Res Int 2014: 495764.
55. Kitagawa H, Izumikawa T, Uyama T, Sugahara K (2003) Molecular cloning of a chondroitin polymerizing factor that cooperates with chondroitin synthase for chondroitin polymerization. J Biol Chem 278: 23666-23671.
56. Izumikawa T, Uyama T, Okuura Y, Sugahara K, Kitagawa H (2007) Involvement of chondroitin sulfate synthase-3 (chondroitin synthase-2) in chondroitin polymerization through its interaction with chondroitin synthase-1 or chondroitin-polymerizing factor. Biochem J 403: 545-552.
57. Mikami T, Kitagawa H (2013) Biosynthesis and function of chondroitin sulfate. Biochim Biophys Acta 1830: 4719-4733.
58. Morimoto-Tomita M, Uchimura K, Werb Z, Hemmerich S, Rosen SD (2002) Cloning and characterization of two extracellular heparin-degrading endosulfatases in mice and humans. J Biol Chem 277: 49175-49185.
59. Ohto T, Uchida H, Yamazaki H, Keino-Masu K, Matsui A, et al. (2002) Identification of a novel nonlysosomal sulphatase expressed in the floor plate, choroid plexus and cartilage. Genes Cells 7: 173-185.
60. Dhoot GK, Gustafsson MK, Ai X, Sun W, Standiford DM, et al. (2001) Regulation of Wnt signaling and embryo patterning by an extracellular sulfatase. Science 293: 1663-1666.
61. Funderburgh JL (2002) Keratan sulfate biosynthesis. IUBMB Life 54: 187-194.
62. Weigel PH, DeAngelis PL (2007) Hyaluronan synthases: a decade-plus of novel glycosyltransferases. J Biol Chem 282: 36777-36781.
63. Fouladi-Nashta AA, Raheem KA, Marei WF, Ghafari F, Hartshorne GM (2017) Regulation and roles of the hyaluronan system in mammalian reproduction. Reproduction 153: R43-R58.
64. Hästbacka J, de la Chapelle A, Mahtani MM, Clines G, Reeve Daly MP, et al. (1994) The diastrophic dysplasia gene encodes a novel sulfate transporter: positional cloning by fine-structure linkage disequilibrium mapping. Cell 78: 1073-1087.
65. Sugahara K, Schwartz NB (1979) Defect in 3'-phosphoadenosine 5'-phosphosulfate formation in brachymorphic mice. Proc Natl Acad Sci U S A 76: 6615-6618.

66. Schwartz NB, Lyle S, Ozeran JD, Li H, Deyrup A, et al. (1998) Sulfate activation and transport in mammals: system components and mechanisms. Chem Biol Interact 109: 143-151.
67. Kamiyama S, Suda T, Ueda R, Suzuki M, Okubo R, et al. (2003) Molecular cloning and identification of 3'-phosphoadenosine 5'-phosphosulfate transporter. J Biol Chem 278: 25958-25963.
68. Kamiyama S, Sasaki N, Goda E, Ui-Tei K, Saigo K, et al. (2006) Molecular cloning and characterization of a novel 3'-phosphoadenosine 5'-phosphosulfate transporter, PAPST2. J Biol Chem 281: 10945-10953.
69. Frederick JP, Tafari AT, Wu SM, Megosh LC, Chiou ST, et al. (2008) A role for a lithium-inhibited Golgi nucleotidase in skeletal development and sulfation. Proc Natl Acad Sci U S A 105: 11605-11612.
70. Vissers LE, Lausch E, Unger S, Campos-Xavier AB, Gilissen C, et al. (2011) Chondrodysplasia and abnormal joint development associated with mutations in IMPAD1, encoding the Golgi-resident nucleotide phosphatase, gPAPP. Am J Hum Genet 88: 608-615.
71. Troeberg L, Nagase H (2012) Proteases involved in cartilage matrix degradation in osteoarthritis. Biochim Biophys Acta 1824: 133-145.
72. Struglics A, Hansson M (2010) Calpain is involved in C-terminal truncation of human aggrecan. Biochem J 430: 531-538.
73. Watanabe H, Yamada Y, Kimata K (1998) Roles of aggrecan, a large chondroitin sulfate proteoglycan, in cartilage structure and function. J Biochem 124: 687-693.
74. Watanabe H, Cheung SC, Itano N, Kimata K, Yamada Y (1997) Identification of hyaluronan-binding domains of aggrecan. J Biol Chem 272: 28057-28065.
75. Barry FP, Rosenberg LC, Gaw JU, Koob TJ, Neame PJ (1995) N- and O-linked keratan sulfate on the hyaluronan binding region of aggrecan from mature and immature bovine cartilage. J Biol Chem 270: 20516-20524.
76. Doege KJ, Sasaki M, Kimura T, Yamada Y (1991) Complete coding sequence and deduced primary structure of the human cartilage large aggregating proteoglycan, aggrecan. Human-specific repeats, and additional alternatively spliced forms. J Biol Chem 266: 894-902.
77. Krueger RC, Fields TA, Hildreth J, Schwartz NB (1990) Chick cartilage chondroitin sulfate proteoglycan core protein. I. Generation and characterization of peptides and specificity for glycosaminoglycan attachment. J Biol Chem 265: 12075-12087.
78. Bourdon MA, Krusius T, Campbell S, Schwartz NB, Ruoslahti E (1987) Identification and synthesis of a recognition signal for the attachment of glycosaminoglycans to proteins. Proc Natl Acad Sci U S A 84: 3194-3198.
79. Sivan SS, Wachtel E, Roughley P (2014) Structure, function, aging and turnover of aggrecan in the intervertebral disc. Biochim Biophys Acta 1840: 3181-3189.

80. Zheng J, Luo W, Tanzer ML (1998) Aggrecan synthesis and secretion. A paradigm for molecular and cellular coordination of multiglobular protein folding and intracellular trafficking. J Biol Chem 273: 12999-13006.
81. Hardingham T (2006) Proteoglycans and Glycosaminoglycans. In: J SM, P RS, P BJ, editors. Dynamics of bone and cartilage metabolism Principles and clinical applications. 2nd edition ed. San Diego (USA): Academic Press. pp. 85-98.
82. Bayliss MT, Osborne D, Woodhouse S, Davidson C (1999) Sulfation of chondroitin sulfate in human articular cartilage. The effect of age, topographical position, and zone of cartilage on tissue composition. J Biol Chem 274: 15892-15900.
83. Chakravarti S (2002) Functions of lumican and fibromodulin: lessons from knockout mice. Glycoconj J 19: 287-293.
84. Wendel M, Sommarin Y, Heinegård D (1998) Bone matrix proteins: isolation and characterization of a novel cell-binding keratan sulfate proteoglycan (osteoadherin) from bovine bone. J Cell Biol 141: 839-847.
85. Camper L, Heinegârd D, Lundgren-Akerlund E (1997) Integrin alpha2beta1 is a receptor for the cartilage matrix protein chondroadherin. J Cell Biol 138: 1159-1167.
86. Ramstad VE, Franzén A, Heinegård D, Wendel M, Reinholt FP (2003) Ultrastructural distribution of osteoadherin in rat bone shows a pattern similar to that of bone sialoprotein. Calcif Tissue Int 72: 57-64.
87. Myllyharju J (2014) Extracellular matrix and developing growth plate. Curr Osteoporos Rep 12: 439-445.
88. Melrose J, Shu C, Whitelock JM, Lord MS (2016) The cartilage extracellular matrix as a transient developmental scaffold for growth plate maturation. Matrix Biol 52-54: 363-383.
89. Vaughan-Thomas A, Young RD, Phillips AC, Duance VC (2001) Characterization of type XI collagen-glycosaminoglycan interactions. J Biol Chem 276: 5303-5309.
90. Mienaltowski MJ, Birk DE (2014) Structure, physiology, and biochemistry of collagens. Adv Exp Med Biol 802: 5-29.
91. Warman ML, Abbott M, Apte SS, Hefferon T, McIntosh I, et al. (1993) A type X collagen mutation causes Schmid metaphyseal chondrodysplasia. Nat Genet 5: 79-82.
92. Klatt AR, Becker AK, Neacsu CD, Paulsson M, Wagener R (2011) The matrilins: modulators of extracellular matrix assembly. Int J Biochem Cell Biol 43: 320-330.
93. Krakow D, Rimoin DL (2010) The skeletal dysplasias. Genet Med 12: 327-341.
94. Bonafe L, Cormier-Daire V, Hall C, Lachman R, Mortier G, et al. (2015) Nosology and classification of genetic skeletal disorders: 2015 revision. Am J Med Genet A 167: 2869-2892.
95. Jelin AC, O'Hare E, Blakemore K, Jelin EB, Valle D, et al. (2017) Skeletal Dysplasias: Growing Therapy for Growing Bones. Front Pharmacol 8: 79.

96. Quentin E, Gladen A, Rodén L, Kresse H (1990) A genetic defect in the biosynthesis of dermatan sulfate proteoglycan: galactosyltransferase I deficiency in fibroblasts from a patient with a progeroid syndrome. Proc Natl Acad Sci U S A 87: 1342-1346.
97. T. Okajima, Fukumoto S, Furukawa K, T. U (1999) Molecular Basis for the Progeroid Variant of Ehlers-Danlos Syndrome:IDENTIFICATION AND CHARACTERIZATION OF TWO MUTATIONS IN GALACTOSYLTRANSFERASE I GENE. The Journal of biological chemistry 274: 28841–28844.
98. Baasanjav S, Al-Gazali L, Hashiguchi T, Mizumoto S, Fischer B, et al. (2011) Faulty initiation of proteoglycan synthesis causes cardiac and joint defects. Am J Hum Genet 89: 15-27.
99. Saigoh K, Izumikawa T, Koike T, Shimizu J, Kitagawa H, et al. (2010) Chondroitin beta-1,4-N-acetylgalactosaminyltransferase-1 missense mutations are associated with neuropathies. Journal Of Human Genetics 56: 143.
100. Hiraoka S, Furuichi T, Nishimura G, Shibata S, Yanagishita M, et al. (2007) Nucleotide-sugar transporter SLC35D1 is critical to chondroitin sulfate synthesis in cartilage and skeletal development in mouse and human. Nat Med 13: 1363-1367.
101. Furuichi T, Kayserili H, Hiraoka S, Nishimura G, Ohashi H, et al. (2009) Identification of loss-of-function mutations of SLC35D1 in patients with Schneckenbecken dysplasia, but not with other severe spondylodysplastic dysplasias group diseases. J Med Genet 46: 562-568.
102. Huber C, Oules B, Bertoli M, Chami M, Fradin M, et al. (2009) Identification of CANT1 mutations in Desbuquois dysplasia. Am J Hum Genet 85: 706-710.
103. Faden M, Al-Zahrani F, Arafah D, Alkuraya FS (2010) Mutation of CANT1 causes Desbuquois dysplasia. Am J Med Genet A 152A: 1157-1160.
104. Nizon M, Huber C, De Leonardis F, Merrina R, Forlino A, et al. (2012) Further delineation of CANT1 phenotypic spectrum and demonstration of its role in proteoglycan synthesis. Hum Mutat 33: 1261-1266.
105. Balasubramanian K, Li B, Krakow D, Nevarez L, Ho PJ, et al. (2017) MED resulting from recessively inherited mutations in the gene encoding calcium-activated nucleotidase CANT1. Am J Med Genet A 173: 2415-2421.
106. Laccone F, Schoner K, Krabichler B, Kluge B, Schwerdtfeger R, et al. (2011) Desbuquois dysplasia type I and fetal hydrops due to novel mutations in the CANT1 gene. Eur J Hum Genet 19: 1133-1137.
107. Desbuquois G, Greiner B, Michel J, Rossignol C (1966) Nanisme chondrodystrophique avec ossification anarchique et polymalformations chez deux soeurs. Arch Fr Pediatr 23: 573-587.
108. Le Merrer M, Young ID, Stanescu V, Maroteaux P (1991) Desbuquois syndrome. Eur J Pediatr 150: 793-796.
109. Faivre L, Cormier-Daire V, Eliott AM, Field F, Munnich A, et al. (2004) Desbuquois dysplasia, a reevaluation with abnormal and "normal" hands: radiographic manifestations. Am J Med Genet A 124A: 48-53.

110. Bui C, Huber C, Tuysuz B, Alanay Y, Bole-Feysot C, et al. (2014) XYLT1 mutations in Desbuquois dysplasia type 2. Am J Hum Genet 94: 405-414.
111. Yang M, Horii K, Herr AB, Kirley TL (2006) Calcium-dependent dimerization of human soluble calcium activated nucleotidase: characterization of the dimer interface. J Biol Chem 281: 28307-28317.
112. Harden TK, Sesma JI, Fricks IP, Lazarowski ER (2010) Signalling and pharmacological properties of the P2Y receptor. Acta Physiol (Oxf) 199: 149-160.
113. Superti-Furga A, Hästbacka J, Wilcox WR, Cohn DH, van der Harten HJ, et al. (1996) Achondrogenesis type IB is caused by mutations in the diastrophic dysplasia sulphate transporter gene. Nat Genet 12: 100-102.
114. Rossi A, van der Harten HJ, Beemer FA, Kleijer WJ, Gitzelmann R, et al. (1996) Phenotypic and genotypic overlap between atelosteogenesis type 2 and diastrophic dysplasia. Hum Genet 98: 657-661.
115. Walker BA, Scott CI, Hall JG, Murdoch JL, McKusick VA (1972) Diastrophic dwarfism. Medicine (Baltimore) 51: 41-59.
116. Horton WA, Rimoin DL, Lachman RS, Skovby F, Hollister DW, et al. (1978) The phenotypic variability of diastrophic dysplasia. J Pediatr 93: 609-613.
117. Gollop TR, Eigier A (1987) Prenatal ultrasound diagnosis of diastrophic dysplasia at 16 weeks. Am J Med Genet 27: 321-324.
118. Forlino A, Piazza R, Tiveron C, Della Torre S, Tatangelo L, et al. (2005) A diastrophic dysplasia sulfate transporter (SLC26A2) mutant mouse: morphological and biochemical characterization of the resulting chondrodysplasia phenotype. Hum Mol Genet 14: 859-871.
119. Superti-Furga A, Neumann L, Riebel T, Eich G, Steinmann B, et al. (1999) Recessively inherited multiple epiphyseal dysplasia with normal stature, club foot, and double layered patella caused by a DTDST mutation. J Med Genet 36: 621-624.
120. Ahmad M, Haque MF, Ahmad W, Abbas H, Haque S, et al. (1998) Distinct, autosomal recessive form of spondyloepimetaphyseal dysplasia segregating in an inbred Pakistani kindred. Am J Med Genet 78: 468-473.
121. Wikstrom B, Engfeldt B, Heinegard D, Hjerpe A (1985) Proteoglycans and glycosaminoglycans in cartilage from the brachymorphic (bm/bm) mouse. Coll Relat Res 5: 193-204.
122. Miyake N, Elcioglu NH, Iida A, Isguven P, Dai J, et al. (2012) PAPSS2 mutations cause autosomal recessive brachyolmia. J Med Genet 49: 533-538.
123. Thiele H, Sakano M, Kitagawa H, Sugahara K, Rajab A, et al. (2004) Loss of chondroitin 6-O-sulfotransferase-1 function results in severe human chondrodysplasia with progressive spinal involvement. Proc Natl Acad Sci U S A 101: 10155-10160.
124. van Roij MH, Mizumoto S, Yamada S, Morgan T, Tan-Sindhunata MB, et al. (2008) Spondyloepiphyseal dysplasia, Omani type: further definition of the phenotype. Am J Med Genet A 146A: 2376-2384.

125. Tuysuz B, Mizumoto S, Sugahara K, Celebi A, Mundlos S, et al. (2009) Omani-type spondyloepiphyseal dysplasia with cardiac involvement caused by a missense mutation in CHST3. Clin Genet 75: 375-383.
126. Hermanns P, Unger S, Rossi A, Perez-Aytes A, Cortina H, et al. (2008) Congenital joint dislocations caused by carbohydrate sulfotransferase 3 deficiency in recessive Larsen syndrome and humero-spinal dysostosis. Am J Hum Genet 82: 1368-1374.
127. Unger S, Lausch E, Rossi A, Megarbane A, Sillence D, et al. (2010) Phenotypic features of carbohydrate sulfotransferase 3 (CHST3) deficiency in 24 patients: congenital dislocations and vertebral changes as principal diagnostic features. Am J Med Genet A 152A: 2543-2549.
128. K. U, K. K, H. M, H. I, E. N, et al. (1999) Disruption of the mouse chondroitin 6-sulfotransferase gene. Glycoconj J 16: S13.
129. Malfait F, Syx D, Vlummens P, Symoens S, Nampoothiri S, et al. (2010) Musculocontractural Ehlers-Danlos Syndrome (former EDS type VIB) and adducted thumb clubfoot syndrome (ATCS) represent a single clinical entity caused by mutations in the dermatan-4-sulfotransferase 1 encoding CHST14 gene. Hum Mutat 31: 1233-1239.
130. Sohaskey ML, Yu J, Diaz MA, Plaas AH, Harland RM (2008) JAWS coordinates chondrogenesis and synovial joint positioning. Development 135: 2215-2220.
131. Zhang Z, Lutz B (2002) Cre recombinase-mediated inversion using lox66 and lox71: method to introduce conditional point mutations into the CREB-binding protein. Nucleic Acids Res 30: e90.
132. Araki K, Okada Y, Araki M, Yamamura K (2010) Comparative analysis of right element mutant lox sites on recombination efficiency in embryonic stem cells. BMC Biotechnol 10: 29.
131. Rossi, A., Kaitila I, Wilcox WR, Rimoin DL, Steinmann B, Cetta G, Superti-Furga A. (1998)Proteoglycan sulfation in cartilage and cell cultures from patients with sulfate transporter chondrodysplasias: relationship to clinical severity and indications on the role of intracellular sulfate production. Matrix Biol;17, 361-369.
132. Pacifici, M. (1990) Independent secretion of proteoglycans and collagens in chick chondrocyte cultures during acute ascorbic acid treatment. Biochem J 272, 193-199.
133. Farndale, R.W., Buttle, D.J. & Barrett, A.J. (1986) Improved quantitation and discrimination of sulphated glycosaminoglycans by use of dimethylmethylene blue. Biochim Biophys Acta 883, 173-177.
134. Sobue, M., Habuchi H, Ito K, Yonekura H, Oguri K, Sakurai K, Kamohara S, Ueno Y, Noyori R, Suzuki S (1987) beta-D-xylosides and their analogues as artificial initiators of glycosaminoglycan chain synthesis. Aglycone-related variation in their effectiveness in vitro and in ovo. Biochem J 241, 591-601.
135. Ng HY, Alvin Lee KX, Shen YF. (2017)Articular Cartilage: Structure, Composition, Injuries and Repair. JSM Bone and Joint Dis 1(2): 1010.

136. Usami, Y., Gunawardena, A.T., Iwamoto, M. & Enomoto-Iwamoto, M. (2016) Wnt signaling in cartilage development and diseases: lessons from animal studies. Lab Invest 96, 186-196.
137. Wilusz RE, Guilak F. (2014)High resistance of the mechanical properties of the chondrocyte pericellular matrix to proteoglycan digestion by chondroitinase, aggrecanase, or hyaluronidase. J Mech Behav Biomed Mater.38:183-97. doi: 10.1016/.
138. Theocharis AD, Skandalis SS, Gialeli C, Karamanos NK. . (2016) Extracellular matrix structure. Adv Drug Deliv Rev;97:4-27. doi: 10.1016.
139. Taylor K.R., and Gallo R.L. (2006) FASEB journal : official publication of the Federation of American Societies for Experimental Biology 20, 9-22
140. Roughley PJ, Mort JS. (2014) The role of aggrecan in normal and osteoarthritic cartilage. J Exp Orthop. 1(1):8. doi: 10.1186
141. Araki K, Okada Y, Araki M, Yamamura K. (2010) Comparative analysis of right element mutant lox sites on recombination efficiency in embryonic stem cells. BMC Biotechnol.10:29. Epub 2010/04/02. doi: 10.1186/1472-6750-10-29.
142. Mitchell KJ, Pinson KI, Kelly OG, Brennan J, Zupicich J, Scherz P, Leighton PA, Goodrich LV, Lu X, Avery BJ, Tate P, Dill K, Pangilinan E, Wakenight P, Tessier-Lavigne M, Skarnes WC. (2001) Functional analysis of secreted and transmembrane proteins critical to mouse development. Nat Genet.28:241–249
143. Zhang Z, Lutz B. (2002) Cre recombinase-mediated inversion using lox66 and lox71: method to introduce conditional point mutations into the CREB-binding protein. Nucleic Acids Res.30(17).
144. Hunziker EB, Herrmann W, Schenk RK. (1983) Ruthenium hexammine trichloride (RHT)-mediated interaction between plasmalemmal components and pericellular matrix proteoglycans is responsible for the preservation of chondrocytic plasma membranes in situ during cartilage fixation. J Histochem Cytochem.31(6):717-27.
145. Mis E.K., Liem K.F., Kong Y., Schwartz N.B.,Domowicz M., Weatherbee S.D. (2014) Forward genetics defines Xylt1 as a key, conserved regulator of early chondrocyte maturation and skeletal length. Deve.Bio.385(1),pp. 67-82
146. Watanabe Y, Takeuchi K, Higa Onaga S, Sato M, Tsujita M, Abe M, Natsume R, Li M, Furuichi T, Saeki M, Izumikawa T, Hasegawa A, Yokoyama M, Ikegawa S, Sakimura K, Amizuka N, Kitagawa H, Igarashi M. (2010) Chondroitin sulfate N-acetylgalactosaminyltransferase-1 is required for normal cartilage development. Biochem J. 15;432(1):47-55

APPENDIX

BRIEF REPORT

Human Mutation

OFFICIAL JOURNAL HGVS HUMAN GENOME VARIATION SOCIETY www.hgvs.org

Chondroitin Sulfate *N*-acetylgalactosaminyltransferase-1 (CSGalNAcT-1) Deficiency Results in a Mild Skeletal Dysplasia and Joint Laxity

Julia Vodopiutz,[1]* Shuji Mizumoto,[2] Ekkehart Lausch,[3] Antonio Rossi,[4] Sheila Unger,[5] Nikolaus Janocha,[3] Rossella Costantini,[4] Rainer Seidl,[1] Susanne Greber-Platzer,[1] Shuhei Yamada,[2] Thomas Müller,[6] Bernd Jilma,[7] Rudolf Ganger,[8] Andrea Superti-Furga,[9] Shiro Ikegawa,[10] Kazuyuki Sugahara,[2†] and Andreas R. Janecke[6,11†]

[1]Department of Pediatrics and Adolescent Medicine, Medical University of Vienna, Vienna, Austria; [2]Department of Pathobiochemistry, Faculty of Pharmacy, Meijo University, Tempaku ku, Nagoya, Aichi, Japan; [3]Department of Pediatrics, Medical Center, Faculty of Medicine, University of Freiburg, Freiburg, Germany; [4]Department of Molecular Medicine, Unit of Biochemistry, University of Pavia, Pavia, Italy; [5]Department of Medical Genetics, Centre Hospitalier Universitaire Vaudois, University of Lausanne, Lausanne, Switzerland; [6]Department of Pediatrics I, Medical University of Innsbruck, Innsbruck, Austria; [7]Department of Clinical Pharmacology, Medical University of Vienna, Vienna, Austria; [8]Paediatric Department, Orthopaedic Hospital of Speising, Vienna, Austria; [9]Department of Pediatrics, Centre Hospitalier Universitaire Vaudois, University of Lausanne, Lausanne, Switzerland; [10]Laboratory for Bone and Joint Diseases, Center for Integrative Medical Sciences, RIKEN, Tokyo, Japan; [11]Division of Human Genetics, Medical University of Innsbruck, Innsbruck, Austria

Communicated by Jürgen Horst

Received 15 June 2016; accepted revised manuscript 29 August 2016.
Published online 7 September 2016 in Wiley Online Library (www.wiley.com/humanmutation). DOI: 10.1002/humu.23070

ABSTRACT: Mutations in genes encoding enzymes responsible for the biosynthesis and structural diversity of glycosaminoglycans (GAGs) cause a variety of disorders affecting bone and connective tissues, including Desbuquois dysplasia (DD). In an infant with prenatal-onset disproportionate short stature, joint laxity, and radiographic findings typical for DD compound-heterozygosity for a large intragenic deletion, and a p.Pro384Arg missense mutation in *CSGALNACT1* was found. *CSGALNACT1* encodes chondroitin sulfate *N*-acetylgalactosaminyltransferase-1 (CSGalNAcT-1, ChGn-1), which initiates chondroitin sulfate (CS) chain biosynthesis on the so-called GAG-protein linker region tetrasaccharide. Biochemical studies revealed a reduced GalNAc-transferase activity of the Arg-384 mutant protein, whereas no differences in proteoglycan synthesis in fibroblasts and the GAG content in the urine were found between patient and controls. This is the first description of bi-allelic loss-of-function mutations in *CSGALNACT1* that produce a skeletal dysplasia reminiscent of the skeletal dysplasia of *Csgalnact1*$^{-/-}$ mice, and adds to the genetic heterogeneity of DD.

Hum Mutat 00:1–5, 2016. © 2016 Wiley Periodicals, Inc.

KEY WORDS: *CSGALNACT1*; chondroitin sulfate *N*-acetylgalactosaminyltransferase-1; skeletal dysplasia; glycosaminoglycan; proteoglycan

Skeletal dysplasias represent a large group of genetic disorders of the skeleton, currently comprising 436 different clinical entities, which are associated with mutations in 364 different genes [Bonafe et al., 2015b]. A subset of these genes encodes enzymes responsible for the biosynthesis and structural diversity of sulfated glycosaminoglycans (GAGs) [Mizumoto et al., 2015b]. GAGs are linear polysaccharides that form the side chains of proteoglycans (PGs) and have been classified into chondroitin sulfate (CS), dermatan sulfate (DS), and heparan sulfate (HS), based on their structural units. The biosynthesis of GAGs starts with the formation of a common tetrasaccharide linker region, which is covalently attached to the serine residues of the PG core proteins [Lindahl and Rodén, 1965]. This is followed by the polymerization of either HS or CS/DS disaccharide chains. The first hexosamine addition to the linker region is critical in determining whether HS or CS/DS is selectively assembled. CS *N*-acetylgalactosaminyltransferase-1 (CSGalNAcT-1, ChGn-1) encoded by *CSGALNACT1* (MIM# 616615) catalyzes the transfer of a GalNAc residue onto the linker region and is therefore critical for initiation of CS/DS synthesis [Uyama et al., 2002; Izumikawa et al., 2015]. Here, we report bi-allelic loss-of-function mutations in *CSGALNACT1*, resulting in a skeletal dysplasia that features the radiographic pattern of Desbuquois dysplasia (DD; MIM# 251450) with mild joint laxity. DD is an autosomal recessive chondrodysplasia, characterized by pre- and postnatal micromelic short stature, brachydactyly, facial dysmorphism, joint laxity with multiple dislocations, and the mandatory skeletal features of advanced carpotarsal bone age and shortness of long bones with a so-called Swedish key appearance of the proximal femur. So far, *CANT1* (calcium activated nucleotidase 1 gene; MIM# 613165) [Nizon et al., 2012], *XYLT1* (xylosyltransferase I; MIM# 608124) [Bui et al., 2014], and *IMPAD1* (inositol monophosphatase domain containing 1; MIM# 614010) [Vissers et al., 2011] mutations have been shown to result in DD. The proteins encoded by these DD genes are involved in CS

Additional Supporting Information may be found in the online version of this article.

†The authors wish it to be known that, in their opinion, the last two authors should be regarded as joint Senior Authors.

*Correspondence to: Julia Vodopiutz, Department of Pediatrics and Adolescent Medicine, Medical University of Vienna, Währinger Gürtel 18–20, A-1090 Wien. E-mail: julia.vodopiutz@meduniwien.ac.at

Contract Grant Sponsors: Austrian Society of Pediatrics (ÖGKJ); Department of Pediatrics and Adolescent Medicine of the Medical University of Vienna; Jubiläumsfonds der Österreichischen Nationalbank (15627); Japan Society for the Promotion of Science (JSPS) (23790066, 16K08251); Research Institute of Meijo University; Nakatomi Foundation; German Ministry of Education and Research (FACE Consortium); European Community's Seventh Framework Programme (602300).

biosynthesis, and thus provide evidence for abnormal CS biosynthesis in DD.

Twenty previously unreported patients (Supp. Table S1) with a clinical diagnosis of DD were examined by consultants specialized in pediatrics, radiology, and clinical genetics. Written informed consent for genetic and metabolic research investigations was obtained from all participants, and the study was approved by the ethics committees of the Medical University of Innsbruck, Austria and the University of Freiburg, Germany. Genomic DNA was extracted from peripheral blood from all participants by standard procedures. Patients' samples were subjected to Sanger sequencing of the complete coding regions and splice sites of the known DD genes (Supp. Methods), and mutations in these genes were identified in 10 patients (data not shown). In order to classify the skeletal dysplasia in one patient without mutation (patient 1; Fig. 1), a chromosomal microarray analysis was performed. Using a genome-wide Human SNP Array 6.0, genotyping console 4.0, and ChAS 1.2.2 software (Affymetrix), a heterozygous deletion of approximately 55-kb in size on chromosome 8p21.3 encompassing exons 5 to 8 of the 10 exons of *CSGALNACT1* was indicated, based on signal intensities of 57 markers in this region. Based on chromosomal microarray data, the junction fragment was PCR-amplified (Supp. Methods), confirming a deletion of 55,290 bp in size with the breakpoints at hg19 positions 19,269,401 and 19,324,691 bp (Fig. 2A). Inspection of sequences surrounding the deletion breakpoints identified identical 20-bp sequences shared between *CSGALNACT1* introns 4 and 8 (Fig. 2B), which likely caused a non-allelic homologous recombination (NAHR) event. This deletion predicted frameshift and premature termination of the reading frame, p.(G212*fs**30), and the triggering of nonsense-mediated mRNA decay. Indeed, fibroblast RNA analysis (Supp. Methods) revealed that no transcript is produced from this allele (Supp. Fig. S1). Assuming autosomal recessive inheritance of CSGalNAcT-1 deficiency, Sanger sequencing of the coding exons of *CSGALNACT1* was performed (Supp. Table S2) and identified a hemizygous missense mutation c.1151C>G (g.19,276,243G>C, p.Pro384Arg) in patient 1 (Fig. 2B). A pathogenic effect of the p.Pro384Arg mutation on the function of the encoded enzyme is predicted by SIFT (score 0.00, not tolerated) and PolyPhen-2 (score 1.00, probably damaging) (Supp. Methods), as Pro-384 is an invariantly conserved amino acid residue (Fig. 2C). The c.1151C>G mutation is very rare as it is not listed in the 1,000 Genomes, dbSNP, and ESP databases, and it is present on three of 120,290 alleles listed in the EXAC database. The intragenic deletion was inherited from the mother and the missense mutation from the healthy father, and the patient was a compound-heterozygote (Fig. 2D). Exome sequencing (Supp. Methods) did not reveal potentially pathogenic mutations in any of the known skeletal dysplasia genes in this patient, further emphasizing *CSGALNACT1* as the disease-causing gene. Both mutations have been submitted to a locus-specific mutation database (http://databases.lovd.nl/shared/genes/CSGALNACT1). In order to identify additional mutations in unrelated patients and to confirm that *CSGALNACT1* mutations cause a skeletal dysplasia in humans, Sanger sequencing of the *CSGALNACT1* coding region was performed in our cohort of previously unreported patients with a diagnosis of DD, but no additional *CSGALNACT1* mutations were identified.

Patient 1 is the second child of non-consanguineous Caucasian parents. In the mother's second pregnancy, shortness of long bones and a flat facial profile were noted in the fetus on a routine ultrasound scan by 28 weeks of gestation. The pregnancy was otherwise uneventful and the girl was born at term with head circumference (HC) 34.0 cm (P54), weight 2.826 g (P16), length 46.5 cm (P8), and Apgar scores of 9/10/10. She presented with non-proportionate and micromelic stature, brachydactyly, and round face with midface hypoplasia (Fig. 1). Skeletal radiograms indicated a diagnosis of DD (Fig. 1). Clinical examination at the age of 3½ years showed a girl with HC 49.5 cm (P55), height 95 cm (P13), weight 14.8 kg (P15), mild micromelic and non-proportionate stature, hyperlordosis, pes planus, and mild facial dysmorphism consisting of midface hypoplasia, flat nasal bridge, short nose, anteverted nares, long philtrum, and microretrognathia. Neurological status was normal and psychomotor development appropriate for age. Mild joint laxity was noted. Magnetic resonance imaging showed a normal brain and normal structures of the upper spine and spinal cord at the age of 2 years. Family history is uneventful except for three episodes of unexplained Bell's palsy in the mother at 11 and 30 years of age. Nerve conduction velocity studies and electromyography were normal after the last episode of Bell's paralysis. Neurological investigation was normal except for spontaneous fasciculations in the face at 32 years of age.

To examine whether the mutation p.Pro384Arg in CSGalNAcT-1 causes a reduction of the GalNAc-transferase activity, the soluble FLAG-tagged CSGalNAcT-1 was expressed in COS-7 cells (Supp. Methods). The expression level of the mutant enzyme, Arg384-CSGalNAcT-1, in the conditioned medium was considerably lower than that of the wild-type enzyme (Supp. Fig. S2A). Therefore, a large amount of the conditioned media from the Arg384-CSGalNAcT-1-expressing COS-7 cells were collected and utilized for the GalNAc-transferase assay. Western blotting analysis showed comparable amounts of both recombinant proteins (Fig. 2E). To compare GalNAc-transferase activity of the wild-type with that of the Arg384-mutant enzyme, the enzymatic activity was measured using those recombinant enzymes, UDP-[^{3}H]GalNAc, and polymer chondroitin as the enzyme sources, donor substrate, and acceptor substrate, respectively. The GalNAc-transferase activity of the Arg384-mutant was significantly decreased compared with that of the wild-type enzyme, and was nearly equal to that of the mock transfectant (Fig. 2F). These data indicate that the mutation in CSGalNAcT-1 resulted in a loss of enzyme function.

As CSGalNAcT-1 plays a role in CS and DS synthesis, we investigated whether its deficiency had an effect on the level of PG synthesis in fibroblasts. For this purpose, we metabolically labeled patient and control fibroblasts for 24 hr with $Na_2[^{35}S]O_4$, with and without addition of β-D-xyloside. We observed some variability among controls, patient, and a heterozygous carrier for a *CSGALNACT1* mutation, but no significant differences in PG synthesis were observed (Supp. Fig. S3A and B). Likewise, urinary GAG analysis in the patient with bi-allelic *CSGALNACT1* alterations did not indicate evidence for altered PG metabolism (data not shown).

In sum, we identified compound-heterozygosity for two *CSGALNACT1* alterations that result in complete loss of the encoded enzyme's activity as the plausible disease cause in patient 1 with a mild skeletal dysplasia with shortness of long bones of prenatal onset, and radiographic features typical for DD. This 3½-year-old patient's psychomotor development is normal, and additional anomalies that occur in DD, that is, maternal hydramnios, cardial septal defect, lung hypoplasia, congenital glaucoma, severe postnatal short stature, joint dislocations, scoliosis, and limited ambulation [Nizon et al., 2012] were not present. Sanger sequencing excluded mutations in the known DD genes, and whole-exome sequencing excluded mutations in all known skeletal dysplasia genes [Bonafe et al., 2015a] as causing the disease in this patient, emphasizing *CSGALNACT1* as a novel human skeletal dysplasia gene.

CSGalNAcT-1 plays a critical role in CS biosynthesis in cartilage [Sakai et al., 2007], and we hypothesized that a loss of CSGalNAcT-1 function might result in the clinical symptoms of a skeletal

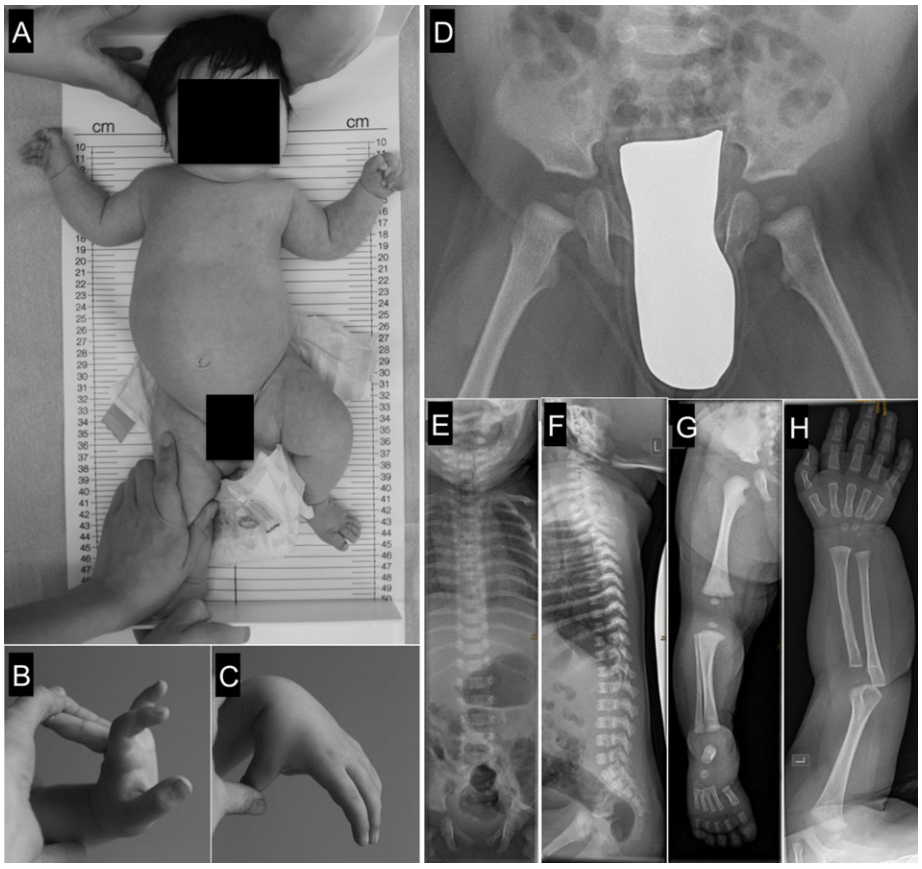

Figure 1. Clinical and skeletal features associated with *CSGALNACT1* mutations in patient 1. Note the short limbs and round face at 6 weeks of age (**A**) and laxity of fingers at 3.5 years of age (**B and C**). Radiographs performed at birth (**E–G**) and at 5 months of age (**D and H**) show flat acetabular roofs and enlargement of the lesser trochanter with metaphyseal beaking resulting in Swedish key appearance of the femur (**D**), coronal and sagittal clefting of the vertebrae (**E and F**) and mild advanced carpotarsal bone age (**G and H**), constituting the mandatory pattern of Desbuquois dysplasia.

dysplasia by a reduction of CS and possibly also DS in affected tissues. However, no differences were observed in the total PG synthesis between *CSGALNACT1*-mutated patient fibroblasts and controls. These results contrast with reductions of PG synthesis seen in fibroblasts from DD patients with mutations in *CANT1* [Nizon et al., 2012]. The total PG synthesis in fibroblasts might inappropriately reflect the GAG synthesis in chondrocytes in our patient with mild clinical affection. Moreover, PG synthesis varies greatly among cultures depending on tissue source of the cells, the in vitro age of the culture and as yet unidentified factors, all hindering the detection of especially subtle changes in PG synthesis [Harper et al., 1987].

Support for our hypothesis that loss of CSGalNAcT-1 function causes the dysplasia in our patient comes from mouse studies. *Csgalnact1*-null mice have shorter limbs and axial skeleton and a thinner growth plate in cartilage than wild-type mice, which results in a slightly shorter body length and smaller body weight. The skeletal phenotype in our patient is reminiscent of the *Csgalnact1*-null mouse, which is viable and has a normal lifespan and fertility. *Csgalnact1*-null mice produce a smaller amount as well as a shorter length of CS chains in cartilage than their wild-type littermates [Watanabe et al., 2010; Sato et al., 2011]. The reduction in CS supposedly affects normal chondrogenesis and formation of type II collagen fibers [Watanabe et al., 2010]. The mouse studies suggested that CSGalNAcT1 is essential for the differentiation and maturation of cartilage.

Two rare, heterozygous loss-of-function mutations in *CSGALNACT1*, p.His234Arg and p.Met509Arg were previously identified in two patients with neuropathies. One patient had adult-onset, irreversible hemi-facial palsy, without any family history of neuropathies. The other patient had childhood-onset hereditary motor and sensory neuropathy [Saigoh et al., 2011]. These mutations were identified upon *CSGALNACT1* sequence analysis of a very heterogeneous cohort of patients affected with diverse neuropathies. Interestingly, recurrent episodes of Bell's palsy had occurred in the mother of our patient. These observations suggest that reduced or altered amounts of CS chains on PGs in the nervous system may lead to peripheral neuropathies. How these neuropathies develop is unknown, but it was speculated that they develop subsequent to traumatic nerve damage. CS is produced in the central nervous system mainly by reactive astrocytes and CS–PGs function as barrier-forming molecules during axonal regeneration [Carulli et al., 2005; Properzi et al., 2005], but may be physiologically necessary to minimize inflammation after trauma of the peripheral nerve by inhibiting invasion of macrophages [Takeuchi et al., 2013]. Similarly, heterozygosity for the *CSGALNACT1* loss-of-function variant p.Ser126Leu was associated with a slower disease course of Multiple Sclerosis [Saigoh et al., 2016], supposedly resulting in decreased synthesis of CS–PGs that might inhibit the recovery from neural injuries. Intriguingly, the downregulation and upregulation of CS and HS biosynthesis, respectively, in the scars of *Csgalnact1*$^{-/-}$ mice

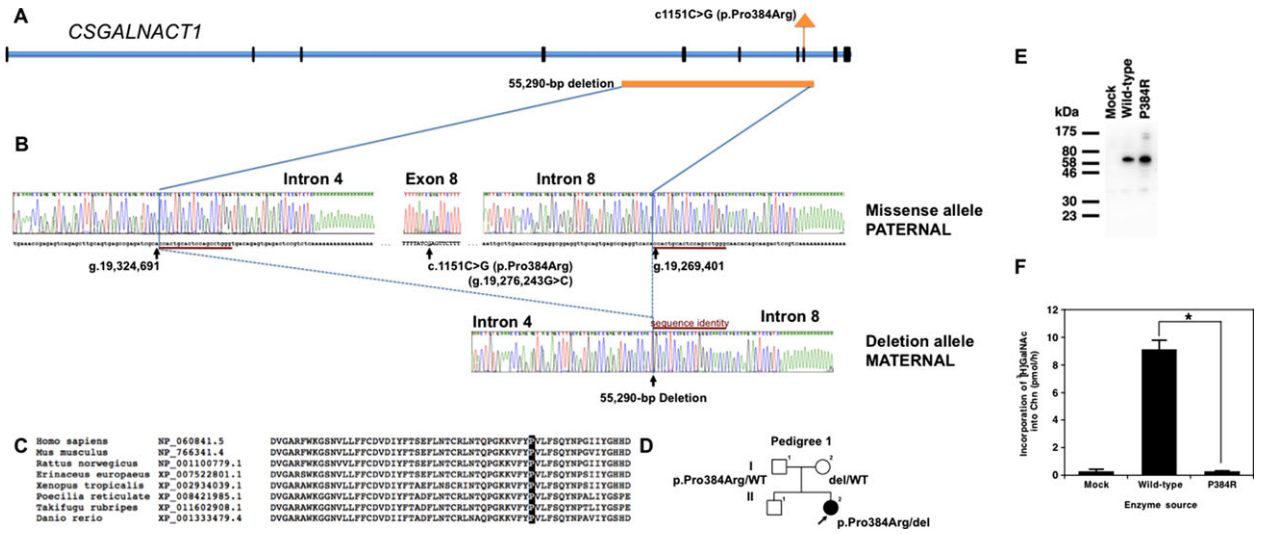

Figure 2. *CSGALNACT1* mutation detection and functional characterization. **A**: Schematic representation of *CSGALNACT1* with exons displayed as black boxes and locations of the identified *CSGALNACT1* mutation and intragenic deletion. **B**: Sequence chromatograms of *CSGALNACT1* in the patient displaying the hemizygous c.1151C>G mutation on the paternal allele (upper panel) and the 55.3-kbp deletion on the maternal allele (lower panel). The deletion boundaries are indicated by blue lines, and the identical 20-bp sequences in introns 4 and 8 at the deletion breakpoints are indicated by red lines. **C**: The p.Pro384Arg mutation affects an invariantly conserved amino acid in CSGalNAcT-1 orthologues. **D**: Simplified pedigree and segregation of the *CSGALNACT1* mutation and deletion. The non-affected sibling is not a compound-heterozygote. **E**: The purified recombinant wild-type- and Pro384Arg-CSGalNAcT-1 (0.4 and 4 ml, respectively) from the conditioned medium separated by SDS-PAGE was detected with the horseradish peroxidase-conjugated anti-FLAG antibody by Western blot analysis. The signals of the FLAG-tagged CSGalNAcT-1 were detected at ~60 kDa. The comparable amounts of both recombinant proteins were detected by estimate the bands by densitometric scanning using ImageQuant TL software (GE Healthcare). "Mock" indicates the enzyme source from the COS-7 cells transfected with an empty vector. **F**: GalNAc-transferase activity was examined using the partially purified recombinant mutant and wild-type enzymes, UDP-[^{3}H]GalNAc as the donor substrate, and polymer chondroitin as the acceptor substrate. GalNAc-transferase activity was determined by incorporation of [^{3}H]GalNAc into the polymer chondroitin. "Mock" indicates the enzyme source from the COS-7 cells transfected with an empty vector. Values are the means ± SE ($n = 3$). $^*P < 0.0001$ versus wild-type was calculated by the ANOVA Dunnett test.

led to better recovery from injuries in the nervous system than in wild type animals.

A number of genetic disorders are caused by mutations in the genes encoding enzymes responsible for the synthesis of GAG, side chains of a large number of PGs. As a major component of the extracellular matrix, PGs influence the mechanical properties of connective tissue and play an important role in cell–cell and cell–matrix interactions. They interact with major signaling pathways, influencing developmental processes and regulating cell adhesion, motility, proliferation, differentiation, and morphogenesis [Haltiwanger and Lowe, 2004; Mizumoto et al., 2015a]. Genetic defects of PG biosynthesis lead to multi-system disorders, often prominently affecting the skeletal system and skin [Mizumoto et al., 2013]. Specific deficiencies in the enzymes involved in the biosynthesis of the linkage region between the core of the PG protein and its GAG side chains are known as linkeropathies [Nakajima et al., 2013; Mizumoto et al., 2015b]. Although the linkage region is the identical tetrasaccharide sequence for all PGs in all tissues, bi-allelic mutation in the genes encoding the four linkage-synthesizing enzymes are associated with clinically different symptoms of skeletal system and skin. However, all these diseases share short stature, prominent forehead and eyes, pectus abnormalities, joint laxity and dislocations, broad fingertips, foot abnormalities, hypotonia, and developmental delays. Other features that are present in some linkeropathies are cardiac defects, radio-ulnar synostosis, monkey wrench or Swedish key appearance of the femora, and atrophic scars. These phenotypic differences may be due to varying levels of gene expression in different tissues [Nakajima et al., 2013]. Mutations in one linkage-synthesizing gene, *XYLT1*, cause DD (MIM# 615777), which has been reported in nine patients to-date [Bui et al., 2014; Schreml et al., 2014]. Mutations in the linkage-synthesizing genes galactosyltransferase II (*B3GALT6*) and glucuronosyltransferase I (*B3GAT3*) were reported in 21 patients with spondyloepimetaphyseal dysplasia with joint laxity, type 1 (MIM# 271640) and Ehlers-Danlos syndrome-like disorder [Malfait et al., 2013; Nakajima et al., 2013; Alazami et al., 2016], and with Larsen-like syndrome and multiple joint dislocations (MIM# 245600) in three families [Baasanjav et al., 2011; von Oettingen et al., 2014; Jones et al., 2015], respectively. The clinical features in our patient with GalNAcT-1 deficiency are milder than those in linkeropathies, which are located "upstream" in GAG synthesis, and they are also milder than in diseases caused by "downstream" localizing enzyme deficiencies of CS and DS synthesis, respectively, such as CHST3 (carbohydrate sulfotransferase 3; MIM# 603799) and CHST14 (carbohydrate [*N*-acetylgalactosamine 4–*O*] sulfotransferase 14; MIM# 608429), which are characterized by more severe skeletal [Unger et al., 2010] and skin involvement, by congenital malformations and coagulation abnormalities [Dundar et al., 2009; Janecke et al., 2016]. The milder phenotype in our patient as compared with other GAG synthesis defects might be explained by the presence of two functionally partly redundant enzymes in fibroblasts and chondrocytes, *CSGALNACT1* and *CSGALNACT2* (MIM# 616616). In vitro studies indicated that CSGalNAcT-1 and CSGalNAcT-2 both exhibit GalNAc-transferase activities, however, CSGalNAcT-1 predominantly initiates CS chain synthesis by transfer of the first GalNAc residue, whereas CSGalNAcT-2 elongates CS chains by transfer of the second and subsequent GalNAc residues in the

repeating disaccharide of CS, -GlcUA-GalNAc- (Uyama et al., 2002; Uyama et al., 2003). In addition, differential expression of *CSGALNACT1* and *CSGALNACT2* might exist in different tissues. Furthermore, a phosphorylated tetrasaccharide linkage structure was recently identified to be present in cartilage of *Csgalnact1*$^{-/-}$ mice, and this was the preferred substrate for CSGalNAcT-1 in vitro, supporting a unique role of CSGalNAcT-1 in regulating the number of CS chains and the total amount of CS in growth plate cartilage [Izumikawa et al., 2015]. Concluding, this is the first report of biallelic loss-of-function mutations in *CSGALNACT1* resulting in a mild skeletal dysplasia with joint laxity and the radiological features of DD. This provides further evidence for the role of CS biosynthesis in the pathophysiology of skeletal and connective disorders.

Acknowledgment

The authors thank Dr. Malvina Herceg (Medical University of Vienna) for performing nerve conduction studies.

Ethics Approval

The work was carried out in accordance with study protocols approved by the ethics committees of the Medical University of Innsbruck, Austria and the University of Freiburg, Germany.

Disclosure statement: The authors declare no conflict of interest.

References

Alazami AM, Al-Qattan SM, Faqeih E, Alhashem A, Alshammari M, Alzahrani F, Al-Dosari MS, Patel N, Alsagheir A, Binabbas B, Alzaidan H, Alsiddiky A, et al. 2016. Expanding the clinical and genetic heterogeneity of hereditary disorders of connective tissue. Hum Genet 135:525–540.

Baasanjav S, Al-Gazali L, Hashiguchi T, Mizumoto S, Fischer B, Horn D, Seelow D, Ali BR, Aziz SA, Langer R, Saleh AA, Becker C, et al. 2011. Faulty initiation of proteoglycan synthesis causes cardiac and joint defects. Am J Hum Genet 89:15–27.

Bonafe L, Cormier-Daire V, Hall C, Lachman R, Mortier G, Mundlos S, Nishimura G, Sangiorgi L, Savarirayan R, Sillence D, Spranger J, Superti-Furga A, et al. 2015a. Nosology and classification of genetic skeletal disorders: 2015 revision. Am J Med Genet A 167A:2869–2892.

Bonafe L, Cormier-Daire V, Hall C, Lachman R, Mortier G, Mundlos S, Nishimura G, Sangiorgi L, Savarirayan R, Sillence D, Spranger J, Superti-Furga A, et al. 2015b. Nosology and classification of genetic skeletal disorders: 2015 revision. Am J Med Genet A 167A:2869–2892.

Bui C, Huber C, Tuysuz B, Alanay Y, Bole-Feysot C, Leroy JG, Mortier G, Nitschke P, Munnich A, Cormier-Daire V. 2014. XYLT1 mutations in Desbuquois dysplasia type 2. Am J Hum Genet 94:405–414.

Carulli D, Laabs T, Geller HM, Fawcett JW. 2005. Chondroitin sulfate proteoglycans in neural development and regeneration. Curr Opin Neurobiol 15:116–120.

Dundar M, Muller T, Zhang Q, Pan J, Steinmann B, Vodopiutz J, Gruber R, Sonoda T, Krabichler B, Utermann G, Baenziger JU, Zhang L, et al. 2009. Loss of dermatan-4-sulfotransferase 1 function results in adducted thumb-clubfoot syndrome. Am J Hum Genet 85:873–882.

Haltiwanger RS, Lowe JB. 2004. Role of glycosylation in development. Annu Rev Biochem 73:491–537.

Harper GS, Hascall VC, Yanagishita M, Gahl WA. 1987. Proteoglycan synthesis in normal and Lowe syndrome fibroblasts. J Biol Chem 262:5637–5643.

Izumikawa T, Sato B, Mikami T, Tamura J, Igarashi M, Kitagawa H. 2015. GlcUAbeta1-3Galbeta1-3Galbeta1-4Xyl(2-O-phosphate) is the preferred substrate for chondroitin N-acetylgalactosaminyltransferase-1. J Biol Chem 290:5438–5448.

Janecke AR, Li B, Boehm M, Krabichler B, Rohrbach M, Muller T, Fuchs I, Golas G, Katagiri Y, Ziegler SG, Gahl WA, Wilnai Y, et al. 2016. The phenotype of the musculocontractural type of Ehlers-Danlos syndrome due to CHST14 mutations. Am J Med Genet A 170:103–115.

Jones KL, Schwarze U, Adam MP, Byers PH, Mefford HC. 2015. A homozygous B3GAT3 mutation causes a severe syndrome with multiple fractures, expanding the phenotype of linkeropathy syndromes. Am J Med Genet A 167A:2691–2696.

Lindahl U, Rodén L. 1965. The role of galactose and xylose in the linkage of heparin to protein. J Biol Chem 240:2821–2826.

Malfait F, Kariminejad A, Van Damme T, Gauche C, Syx D, Merhi-Soussi F, Gulberti S, Symoens S, Vanhauwaert S, Willaert A, Bozorgmehr B, Kariminejad MH, et al. 2013. Defective initiation of glycosaminoglycan synthesis due to B3GALT6 mutations causes a pleiotropic Ehlers-Danlos-syndrome-like connective tissue disorder. Am J Hum Genet 92:935–945.

Mizumoto S, Ikegawa S, Sugahara K. 2013. Human genetic disorders caused by mutations in genes encoding biosynthetic enzymes for sulfated glycosaminoglycans. J Biol Chem 288:10953–10961.

Mizumoto S, Yamada S, Sugahara K. 2015a. Molecular interactions between chondroitin-dermatan sulfate and growth factors/receptors/matrix proteins. Curr Opin Struct Biol 34:35–42.

Mizumoto S, Yamada S, Sugahara K. 2015b. Mutations in biosynthetic enzymes for the protein linker region of chondroitin/dermatan/heparan sulfate cause skeletal and skin dysplasias. Biomed Res Int 2015:861752.

Nakajima M, Mizumoto S, Miyake N, Kogawa R, Iida A, Ito H, Kitoh H, Hirayama A, Mitsubuchi H, Miyazaki O, Kosaki R, Horikawa R, et al. 2013. Mutations in B3GALT6, which encodes a glycosaminoglycan linker region enzyme, cause a spectrum of skeletal and connective tissue disorders. Am J Hum Genet 92:927–934.

Nizon M, Huber C, De Leonardis F, Merrina R, Forlino A, Fradin M, Tuysuz B, Abu-Libdeh BY, Alanay Y, Albrecht B, Al-Gazali L, Basaran SY, et al. 2012. Further delineation of CANT1 phenotypic spectrum and demonstration of its role in proteoglycan synthesis. Hum Mutat 33:1261–1266.

Properzi F, Carulli D, Asher RA, Muir E, Camargo LM, van Kuppevelt TH, ten Dam GB, Furukawa Y, Mikami T, Sugahara K, Toida T, Geller HM, et al. 2005. Chondroitin 6-sulphate synthesis is up-regulated in injured CNS, induced by injury-related cytokines and enhanced in axon-growth inhibitory glia. Eur J Neurosci 21:378–390.

Saigoh K, Izumikawa T, Koike T, Shimizu J, Kitagawa H, Kusunoki S. 2011. Chondroitin beta-1,4-N-acetylgalactosaminyltransferase-1 missense mutations are associated with neuropathies. J Hum Genet 56:143–146.

Saigoh K, Yoshimura S, Izumikawa T, Miyata S, Tabara Y, Matsushita T, Miki T, Miyamoto K, Hirano M, Kitagawa H, Kira JI, Kusunoki S. 2016. Chondroitin sulfate beta-1,4-N-acetylgalactosaminyltransferase-1 (ChGn-1) polymorphism: association with progression of multiple sclerosis. Neurosci Res 108:55–59.

Sakai K, Kimata K, Sato T, Gotoh M, Narimatsu H, Shinomiya K, Watanabe H. 2007. Chondroitin sulfate N-acetylgalactosaminyltransferase-1 plays a critical role in chondroitin sulfate synthesis in cartilage. J Biol Chem 282:4152–4161.

Sato T, Kudo T, Ikehara Y, Ogawa H, Hirano T, Kiyohara K, Hagiwara K, Togayachi A, Ema M, Takahashi S, Kimata K, Watanabe H, et al. 2011. Chondroitin sulfate N-acetylgalactosaminyltransferase 1 is necessary for normal endochondral ossification and aggrecan metabolism. J Biol Chem 286:5803–5812.

Schreml J, Durmaz B, Cogulu O, Keupp K, Beleggia F, Pohl E, Milz E, Coker M, Ucar SK, Nurnberg G, Nurnberg P, Kuhn J, et al. 2014. The missing "link": an autosomal recessive short stature syndrome caused by a hypofunctional XYLT1 mutation. Hum Genet 133:29–39.

Takeuchi K, Yoshioka N, Higa Onaga S, Watanabe Y, Miyata S, Wada Y, Kudo C, Okada M, Ohko K, Oda K, Sato T, Yokoyama M, et al. 2013. Chondroitin sulphate N-acetylgalactosaminyl-transferase-1 inhibits recovery from neural injury. Nat Commun 4:2740.

Unger S, Lausch E, Rossi A, Megarbane A, Sillence D, Alcausin M, Aytes A, Mendoza-Londono R, Nampoothiri S, Afroze B, Hall B, Lo IF, et al. 2010. Phenotypic features of carbohydrate sulfotransferase 3 (CHST3) deficiency in 24 patients: congenital dislocations and vertebral changes as principal diagnostic features. Am J Med Genet A 152A:2543–2549.

Uyama T, Kitagawa H, Tamura Ji J, Sugahara K. 2002. Molecular cloning and expression of human chondroitin N-acetylgalactosaminyltransferase: the key enzyme for chain initiation and elongation of chondroitin/dermatan sulfate on the protein linkage region tetrasaccharide shared by heparin/heparan sulfate. J Biol Chem 277:8841–8846.

Uyama T, Kitagawa H, Tanaka J, Tamura J, Ogawa T, Sugahara K. 2003. Molecular cloning and expression of a second chondroitin N-acetylgalactosaminyltransferase involved in the initiation and elongation of chondroitin/dermatan sulfate. J Biol Chem 278:3072–3078.

Vissers LE, Lausch E, Unger S, Campos-Xavier AB, Gilissen C, Rossi A, Del Rosario M, Venselaar H, Knoll U, Nampoothiri S, Nair M, Spranger J, et al. 2011. Chondrodysplasia and abnormal joint development associated with mutations in IMPAD1, encoding the Golgi-resident nucleotide phosphatase, gPAPP. Am J Hum Genet 88:608–615.

von Oettingen JE, Tan WH, Dauber A. 2014. Skeletal dysplasia, global developmental delay, and multiple congenital anomalies in a 5-year-old boy-report of the second family with B3GAT3 mutation and expansion of the phenotype. Am J Med Genet A 164A:1580–1586.

Watanabe Y, Takeuchi K, Higa Onaga S, Sato M, Tsujita M, Abe M, Natsume R, Li M, Furuichi T, Saeki M, Izumikawa T, Hasegawa A, et al. 2010. Chondroitin sulfate N-acetylgalactosaminyltransferase-1 is required for normal cartilage development. Biochem J 432:47–55.

ACCEPTED FOR PUBLICATION IN SPRINGER

Analysis of proteoglycan synthesis and secretion in cell culture systems

Running head: Proteoglycan synthesis and secretion

Chiara Paganini, Rossella Costantini and Antonio Rossi*

Department of Molecular Medicine, Biochemistry Unit, University of Pavia, 27100 Pavia, Italy.

*Corresponding author: Department of Molecular Medicine, Biochemistry Unit, University of Pavia, Via Taramelli 3B, 27100 Pavia, Italy. E-mail: antrossi@unipv.it

Analysis of proteoglycan synthesis and secretion in cell culture systems

Chiara Paganini, Rossella Costantini and Antonio Rossi

Abstract

Experimental protocols for the synthesis and secretion of proteoglycans in cell culture models are important to study specific biosynthetic steps or disorders in which a defect in proteoglycans is expected. We describe a method using ^{35}S-sulfate to metabolically label newly synthesised proteoglycans from cell cultures in order to measure proteoglycan synthesis and secretion. The method is set up for fibroblast and chondrocyte cultures, but can be extended to other cell types.

Keywords: proteoglycan, glycosaminoglycan, metabolic labelling, protein secretion, ion exchange chromatography, gel filtration chromatography.

1. Introduction

Proteoglycans (PGs) are present in the extracellular matrices (ECMs) and in the cell membranes. They are composed of a core protein to which glycosaminoglycans (GAGs), linear polysaccharide chains, are attached. GAG chains may vary in number and size in different PGs [1,2]. PG biosynthesis is a complex mechanism that involves several enzymes and transporters. This process is divided in four main steps: core protein biosynthesis in the rough endoplasmic reticulum, GAG biosynthesis and GAG sulfation in the Golgi apparatus and PG secretion [1].

Defects in enzymes or transporters involved in this complex process may lead to defects in PG biosynthesis resulting in different genetic disorders. Indeed, several skeletal dysplasias

are caused by defects in the core protein or in GAG biosynthesis or sulfation [3-6]. Moreover, due to the complexity of the synthesis process and to the heterogeneity of PGs, little is known regarding the mechanisms involved in their intracellular quality control and secretion in the ECMs. Thus, experimental protocols for the synthesis and secretion of PGs using cell cultures are important to study specific biosynthetic steps or for a preliminary screening in disorders in which a defect in PGs is expected. There are several assays for fast measurement of the proteoglycan content based on 1,9-dimethylmethylene blue or safranin O; these assays are useful for tissue analysis and eventually in specific cell culture systems [7,8]. However quite often few cells are available from patients and in some instances, they can not be expanded in order to avoid their de-differentiation (i.e. chondrocytes or osteoblasts); for this reason more sensitive methods using radioactive labelling are required.

We describe a method to metabolically label with ^{35}S-sulfate newly synthesised PGs from cell cultures in order to measure PG synthesis and secretion in the ECM. The method is set up for fibroblast and chondrocyte cultures, but can be extended to other cell types. Moreover labelled PGs recovered from the purification step might be used for further analysis (i.e. identification of the different GAG species or GAG hydrodynamic size). In order to enhance the biosynthetic defect at the GAG level, if present, metabolic labelling is performed in basal medium or in basal medium containing 1 mM 4-nitrophenyl β-D-xylopyranoside a compound that acts as a chain initiator and boosts GAG biosynthesis [9,4,10].

2. Materials

Prepare all solutions using Milli-Q water and analytical grade reagents. Follow the waste disposal regulations for cell culture and for radioactive waste materials. Protect yourself with gloves and with personal protective equipment.

2.1. Cell culture and cell labelling

1. Minimal essential medium (MEM): 9.6 g/l MEM (cat. n. M0268, Sigma), 2.2 g/l sodium bicarbonate ($NaHCO_3$), 1x antibiotic solution (Penicillin/Streptomycin 100x cat. n. ECB3001D, EuroClone) and 10% foetal calf serum (FCS) heat inactivated. Weight 9.6 g MEM and 2.2 g $NaHCO_3$ and transfer in a cylinder, add Milli-Q water and dissolve powder. Make up to 1 l and filter to sterilize the solution. Under the laminar flow cabinet add 10 ml of sterile 100x Penicillin/Streptomycin solution and 100 ml FCS. Store at 4°C.
2. 50 mM β-D-xyloside: dissolve 13.56 mg 4-nitrophenyl β-D-xylopyranoside (β-D-xyloside) (cat. n. N2132, Sigma) in 1 ml solution 1:1 dimethyl sulfoxide (DMSO): MEM (0.5 ml DMSO and 0.5 ml MEM) and filter to sterilize the solution. Store at -20°C.
3. Pre-labelling MEM containing 250 µM Na_2SO_4: 2.5 ml 100x MEM vitamin solution (cat. n. M6895, Sigma), 5 ml 50x MEM amino acid solution (cat. n. M5550, Sigma), 25 ml 10x Earle's balanced salt solution (EBSS) (cat. n. E7510, Sigma), 2.5 ml 200 mM glutamine, 625 µl 100 mM Na_2SO_4, 0.55 g $NaHCO_3$. Make up to 250 ml and filter to sterilize the solution. Store at 4°C (*see* **Note 1**).
4. Labelling MEM 50 µCi/ml $Na_2[^{35}S]O_4$: add 625 µl of 2 mCi/ml $Na_2[^{35}S]O_4$ (cat. n. NEX041H, Perkin Elmer) to 24.3 ml of MEM containing 250 µM Na_2SO_4, used for the pre-labelling step (*see* **Note 1**).
5. Pre-labelling and labelling MEM containing 1 mM β-D-xyloside: add 20 µl 50 mM β-D-xyloside in DMSO/MEM (1:1) for each ml of pre-labelling and labelling MEM containing 250 µM Na_2SO_4.
6. Labelling MEM 100 µCi/ml $Na_2[^{35}S]O_4$: add 375 µl of 2 mCi/ml $Na_2[^{35}S]O_4$ (cat. n. NEX041H, Perkin Elmer) to 7.2 ml of MEM containing 250 µM Na_2SO_4, used for the pre-labelling step (*see* **Note 1**).

7. MEM for chase containing 5 mM Na_2SO_4: 2.5 ml 100x MEM vitamin solution, 5 ml 50x MEM amino acid solution, 25 ml 10x EBSS, 2.5 ml 200 mM glutamine, 12.5 ml 100 mM Na_2SO_4, 0.55 g $NaHCO_3$. Make up to 250 ml and filter to sterilize the solution. Store at 4°C (*see* **Note 2**).
8. 1x phosphate buffered saline (PBS): 137 mM NaCl, 2.7 mM KCl, 8.1 mM Na_2HPO_4, 1.5 mM KH_2PO_4, pH 7.4. Weight 8 g NaCl, 0.2 g KCl, 1.15 g Na_2HPO_4 and 0.2 g KH_2PO_4. Add Milli-Q water and dissolve. Make up to 1 l and adjust to pH 7.4 with diluted phosphoric acid or NaOH. Store at 4°C.

2.2. Analysis of proteoglycan synthesis

1. Buffer for harvest medium and cell layer: 8 M urea, 4% Triton X-100, 20 mM ethylenediaminetetraacetic acid (EDTA), 20 mM N-ethylmaleimide (NEM), 1 mM phenylmethylsulfonyl fluoride (PMSF), 0.1 M 6-aminocaproic acid, 100 mM sodium acetate, pH 5.8. Weigh 24 g urea, 125 mg NEM and 0.66 g 6-aminocaproic acid. Add 5 ml 1 M sodium acetate, pH 6.0, 2 ml 0.5 M EDTA, 2 ml Triton X-100, 250 µl 0.2 M PMSF in 96% ethanol and make up to 50 ml. Adjust the pH to 5.8 with diluted acetic acid or sodium hydroxide (NaOH), if necessary and store at 4°C.
2. Cell lysis buffer: 2 M urea, 2% Triton X-100, 50 mM sodium acetate buffer, pH 5.8. Weigh 6.0 g urea, add 2.5 ml 1 M sodium acetate buffer, pH 6.0 and 1 ml Triton X-100. Make up to 50 ml, adjust the pH to 5.8 with diluted acetic acid or NaOH, if necessary and store at 4°C (*see* **Note 3**).
3. DEAE Sephacel for ion exchange chromatography (cat. n. 17-0500-01, GE Healthcare).
4. Starting buffer for DEAE Sephacel chromatography: 8 M urea, 0.5% Triton X-100, 10 mM EDTA, 10 mM NEM, 0.5 mM PMSF, 0.15 M sodium chloride (NaCl), 0.1 M 6-aminocaproic acid, 50 mM sodium acetate, pH 6.0. Weigh 288.28 g urea, 5.25 g NaCl,

0.75 g NEM and 7.87 g 6-aminocaproic acid. Add 30 ml 1 M sodium acetate buffer, pH 6.0, 12 ml 0.5 M EDTA, 1.5 ml 0.2 M PMSF in 96% ethanol and 3 ml Triton X-100. Make up to 600 ml, adjust the pH to 6.0 with diluted acetic acid or NaOH, if necessary and store at 4°C.

5. Regenerating buffer for DEAE Sephacel chromatography: starting buffer for DEAE Sephacel chromatography with 2 M NaCl. Dissolve 10.80 g NaCl in 100 ml starting buffer (previously prepared). Store at 4°C.
6. Eluting buffer for DEAE Sephacel chromatography: starting buffer for DEAE Sephacel chromatography with 1 M NaCl. Dissolve 4.96 g NaCl in 100 ml starting buffer (previously prepared). Store at 4°C.
7. Bicinchoninic acid (BCA) protein assay kit (cat. n. 23225, Thermo Scientific).
8. Scintillation cocktail (Emulsifier Scintillator Plus, cat. n. 6013099, PerkinElmer).

2.3. Analysis of proteoglycan secretion

1. Buffer for harvest medium: 8 M guanidinium chloride (GuHCl) (cat. n. 1.04220.1000, Merck), 2% Triton X-100, 0.2 M sodium acetate, pH 5.8. Weigh 15.28 g GuHCl, add 2 ml 1 M sodium acetate buffer, pH 5.8, and 0.4 ml Triton X-100. Make up to 20 ml, adjust the pH to 5.8 with diluted acetic acid or NaOH, if necessary and store at 4°C.
2. Cell lysis buffer: 4 M GuHCl, 2% Triton X-100, 0.1 M sodium acetate, pH 5.8. Weigh 19.10 g GuHCl, add 5 ml 1 M sodium acetate, pH 5.8, and 1 ml Triton X-100. Make up to 50 ml, adjust the pH to 5.8 with diluted acetic acid or NaOH, if necessary and store at 4°C.
3. 10x proteinase inhibitors: 0.1 M benzamidine hydrochloride, 40 mM EDTA and 2.5 mg/ml NEM. Weigh 1.57 g benzamidine hydrochloride, 1.49 g EDTA disodium salt and

250 mg NEM, dissolve in 100 ml PBS and adjust pH at 7.4 with diluted phosphoric acid or NaOH. Store at -20°C.

4. Eluting buffer for gel filtration chromatography: 4 M GuHCl, 0.5% Triton X-100, 50 mM sodium acetate, pH 6.0. Weigh 382.12 g GuHCl, add 50 ml 1 M sodium acetate, pH 6.0, and 5 ml Triton X-100. Make up to 1 l, adjust the pH to 6.0 with diluted acetic acid or NaOH, if necessary and store at 4°C.
5. PD Miditrap G-25 column (cat. n. 28-9180-08, GE Healthcare) for gel filtration chromatography.
6. Scintillation cocktail (Emulsifier Scintillator Plus, cat. n. 6013099, PerkinElmer).

3. Methods

3.1. Analysis of proteoglycan synthesis

Fibroblasts, chondrocytes or other cells are metabolically labelled with ^{35}S-sulfate for 24 hours in order to analyse the amount of newly synthesised PGs. After 24 hours labelling, PGs are purified from medium and cell layer by ion exchange chromatography (DEAE Sephacel) and their amount is normalised to the protein content of the cell layer. Metabolic labelling can be performed also in basal medium containing 1 mM β-D-xyloside, an enhancer of glycosaminoglycan synthesis, in order to highlight potential defects in proteoglycan metabolism that in basal conditions might not be detectable.

1. Plate 2.5×10^5 fibroblast or chondrocyte cells in each well of a 6 well-plate in 2.5 ml of MEM with 10% FCS and incubate at 37°C in 5% CO_2 (*see* **Note 4**). Plate each cell line in 2 different wells if the analysis is performed in medium with or without β-D-xyloside (*see* **Note 5** and **Note 6**).

2. After 48 hours, wash the cell layer with 1.5 ml of pre-labelling MEM (*see* **Note 7**).
3. Before the labelling step, pre-incubate one well with 1.5 ml pre-labelling MEM and the other one with 1.5 ml pre-labelling MEM containing 1 mM β-D-xyloside. Incubate cells at 37°C in 5% CO_2 for 2 hours.
4. Label cells with 1 ml of labelling MEM 50 µCi/ml $Na_2[^{35}S]O_4$ with or without β-D-xyloside for 24 hours at 37°C in 5% CO_2. Cells preincubated with β-D-xyloside are labelled in presence of the same drug.
5. At the end of the labelling period, transfer the well plates on ice and harvest the medium in disposable plastic tubes containing 1.1 ml buffer for harvest medium and cell layer. Wash the cell layer with 100 µl PBS and add to the medium sample. Freeze the medium fraction immediately at -20°C.
6. Add to the cell layer 1 ml of cell lysis buffer to lyse cells and scrape with a cell scraper. Harvest the cell lysates in Eppendorf tubes.
7. Collect 2 aliquots 100 µl each to measure the protein content by the BCA protein assay (*see* **Note 8**).
8. Add the remaining cell layer solution (0.8 ml) to the frozen medium fraction and then add 0.4 ml starting buffer (*see* **Note 9**); freeze immediately at -20°C.
9. Thaw samples on ice and load on DEAE Sephacel columns previously packed and equilibrated (*see* **Note 10**); discard the eluates.
10. Wash the columns with 7 ml of starting buffer and discard the eluates.
11. Elute PGs with 3 ml eluting buffer collecting the eluate in a pre-weight centrifuge tube (*see* **Note 11**).
12. Add to the eluates 9 volumes of 96% ethanol to precipitate PGs at 4°C overnight.
13. Centrifuge samples at 17,300 × g for 50 minutes at 4°C.
14. Discard supernatant and wash the pellet with 20 ml 70% ethanol.

15. Centrifuge samples at 17,300 × g for 10 minutes at 4°C.
16. Discard supernatant and solubilize the pellet with 3 ml Milli-Q water (PG fraction).
17. Transfer 100 µl of sample in a scintillation vial and measure ^{35}S-activity to determine the total radioactivity of samples (*see* **Note 12**) and normalize to the protein content (*see* **Note 13**).

3.2. Analysis of proteoglycan secretion

To analyse proteoglycan secretion cells are metabolically labelled with ^{35}S-sulfate for 2 hours. At the end of the labelling period, the medium is removed and replaced with new medium containing an excess of cold sulfate in order to avoid further labelling with ^{35}S-sulfate. At different time points from medium replacement, proteoglycans are purified from medium and cell layer by gel filtration chromatography and the relative amount of secreted proteoglycans (PGs in medium) to total synthesised proteoglycans (PGs in medium and cell layer) is calculated.

1. Plate 5×10^4 fibroblast or chondrocyte cells in each well of a 24 well-plate in 1 ml of MEM with 10% FCS for each well and incubate at 37°C in 5% CO_2 (*see* **Note 4**). Prepare one plate with all cell lines to be studied for each pulse chase time point (0 min, 30 min, 2.5 h and 5 h) (*see* **Note 6**).
2. After 48 hours, wash cells with 1 ml pre-labelling MEM (*see* **Note 7**).
3. Pre-label cells with 1 ml pre-labelling MEM and incubate at 37°C in 5% CO_2 for 2 hours.
4. Label cells with 0.3 ml of labelling MEM 100 µCi/ml $Na_2[^{35}S]O_4$ for 2 hours at 37°C in 5% CO_2.
5. At the end of labelling period, immediately harvest the plate at chase time point 0 min, while wash other plates twice with 1 ml pre-warmed MEM for chase at 37°C and discard

the medium. Then incubate cells with 0.3 ml pre-warmed MEM for chase at 37°C in 5% CO_2 for different chase time points (30 min, 2.5 h and 5 h).

6. At each chase time point immediately place the plate on ice, harvest the medium in an Eppendorf tube containing 80 µl of 10x proteinase inhibitors and 0.4 ml buffer for harvest medium.
7. Wash cell layer with 100 µl PBS and add to the medium fraction.
8. Wash again the cell layer with 1 ml cold PBS and discard.
9. Lyse cells in the well with 0.6 ml cell lysis buffer and add 60 µl 10x proteinase inhibitors (cell layer fraction).
10. Load medium fraction (total volume 880 µl) on PD Miditrap G-25 column, equilibrated previously with 15 ml eluting buffer and discard the eluate.
11. Add 120 µl eluting buffer and collect the eluate in a 8 ml scintillation vial (fraction 1) (*see* **Note 14**).
12. Elute with 0.7 + 0.7 ml eluting buffer and collect the eluate in 8 ml scintillation vials (fraction 2 and 3, respectively).
13. Discard columns.
14. Load cell layer fraction (total volume 660 µl) on PD Miditrap G-25 column, equilibrated previously with 15 ml eluting buffer and discard the eluate.
15. Wash the well with 170 µl eluting buffer, add to the column and discard the eluate.
16. Add 170 µl eluting buffer and collect in a 8 ml scintillation vial (fraction 1) (*see* **Note 14**).
17. Elute with 0.7 + 0.7 ml eluting buffer and collect the eluate in 8 ml scintillation vials (fraction 2 and 3, respectively).
18. Discard columns.
19. Add to all vials 6 ml scintillation cocktail and measure the ^{35}S-activity using a liquid scintillation counter (*see* **Note 15**).

20. Calculate for each chase time point the percentage of ^{35}S-activity in medium to the total counts (medium and cell layer) (*see* **Note 16**) and plot against time to draw the secretion curve (Fig. 1).

4. Notes

1. In the pre-labelling and labelling step a culture medium with a low concentration of Na_2SO_4 (250 µM) is used in order to increase the specific activity and favour metabolic labelling with ^{35}S-sulfate.
2. During the chase, cells are incubated in MEM with a high concentration of cold sulfate (5 mM) in order to dilute the residual ^{35}S-sulfate and avoid its incorporation in PGs.
3. The cell lysis buffer contains 2 M urea in order to avoid interference in the BCA protein assay.
4. If there are wells in the plate without cells, put the same volume of medium also in these wells. Depending on the number of cell lines to be studied, 6 well-plates might be replaced by 35 mm tissue culture dishes.
5. β-D-xyloside is an analog of xylose, the first GAG sugar attached to serine residues of the core protein. β-D-xyloside is used in cell cultures to boost GAG synthesis [9]. In this condition, it is possible to enhance defects in GAG synthesis that in basal conditions might not be observed.
6. Prepare an appropriate number of plates in order to perform the analysis in triplicate.
7. This step is necessary to remove all residual serum in wells before the pre-labelling and labelling steps.

8. Collect 100 µl of cell layer and measure the protein content with a BCA protein assay using bovine serum albumin (BSA) as standard curve in the working range 5-250 µg/ml. Perform the protein assay in duplicate.
9. Since the cell lysis buffer contains 2 M urea, a low urea concentration for DEAE Sephacel chromatography, it is necessary to add starting buffer for DEAE Sephacel chromatography in order to increase the urea concentration up to 4 M.
10. Package 1 ml of DEAE Sephacel in disposable polypropylene columns (cat. n. 731-1550, Bio-Rad Laboratories). Regenerate each column with 2 ml regenerating buffer for DEAE Sephacel chromatography and equilibrate with 5 ml of starting buffer.
11. In order to determine the exact volume of 96% ethanol required to precipitate PGs, the eluate from DEAE Sephacel column is collected in a pre-weighted tube. After elution the gross weight of the tube is measured and the volume of the eluate is calculated by subtraction. Use centrifuge tubes with a maximum capacity of 40-50 ml.
12. Add to 100 µl of sample 5 ml of scintillation cocktail and measure the ^{35}S-activity using a liquid scintillation counter.
13. The purified labelled PGs can be used also to study several features of PGs or GAGs such as the hydrodynamic size by gel filtration chromatography, the GAG composition or the core protein by western blot [4].
14. In fraction 1 ^{35}S-activity should not be present. This fraction is counted in order to check the column performance: if the column has been packed and equilibrated properly no activity should be present.
15. When using some scintillation cocktails a precipitate might be observed in the vials since the volume of the aqueous sample is high. To avoid this problem add 400 µl of 96% ethanol and mix properly until the precipitate disappear. If not, aliquot the

aqueous sample in more vials or use 20 ml vials if they fit with the liquid scintillation counter.

16. Labelled PGs are present in fractions 2 and 3, thus the activity in these fractions is summed up in order to get the total ^{35}S-activity of PGs in medium or cell layer fraction.

Acknowledgements

Work supported by the European Community's Seventh Framework Programme

under grant agreement no. 602300 (SYBIL).

References

1. Vynios DH (2014) Metabolism of cartilage proteoglycans in health and disease. Biomed Res Int 2014:452315

2. Heinegård D (2009) Fell-Muir Lecture: Proteoglycans and more--from molecules to biology. Int J Exp Pathol 90 (6):575-586

3. Stattin EL, Wiklund F, Lindblom K, Onnerfjord P, Jonsson BA, Tegner Y, Sasaki T, Struglics A, Lohmander S, Dahl N, Heinegard D, Aspberg A (2010) A missense mutation in the aggrecan C-type lectin domain disrupts extracellular matrix interactions and causes dominant familial osteochondritis dissecans. Am J Hum Genet 86 (2):126-137

4. Nizon M, Huber C, De Leonardis F, Merrina R, Forlino A, Fradin M, Tuysuz B, Abu-Libdeh BY, Alanay Y, Albrecht B, Al-Gazali L, Basaran SY, Clayton-Smith J, Desir J, Gill H, Greally MT, Koparir E, van Maarle MC, MacKay S, Mortier G, Morton J, Sillence D, Vilain C, Young I, Zerres K, Le Merrer M, Munnich A, Le Goff C, Rossi A, Cormier-Daire

V (2012) Further Delineation of CANT1 Phenotypic Spectrum and Demonstration of Its Role in Proteoglycan Synthesis. Human Mutation 33 (8):1261-1266

5. Rossi A, Superti-Furga A (2001) Mutations in the diastrophic dysplasia sulfate transporter (DTDST) gene (SLC26A2): 22 Novel mutations, mutation review, associated skeletal phenotypes, and diagnostic relevance. Human Mutation 17 (3):159-171.

6. Mizumoto S, Ikegawa S, Sugahara K (2014) Human genetic disorders caused by mutations in genes encoding biosynthetic enzymes for sulfated glycosaminoglycans. J Biol Chem 288 (16):10953-10961

7. Farndale RW, Buttle DJ, Barrett AJ (1986) Improved quantitation and discrimination of sulphated glycosaminoglycans by use of dimethylmethylene blue. Biochim Biophys Acta 883 (2):173-177

8. Carrino DA, Arias JL, Caplan AI (1991) A spectrophotometric modification of a sensitive densitometric Safranin O assay for glycosaminoglycans. Biochem Int 24 (3):485-495

9. Sobue M, Habuchi H, Ito K, Yonekura H, Oguri K, Sakurai K, Kamohara S, Ueno Y, Noyori R, Suzuki S (1987) beta-D-xylosides and their analogues as artificial initiators of glycosaminoglycan chain synthesis. Aglycone-related variation in their effectiveness in vitro and in ovo. Biochem J 241 (2):591-601

10. Rossi A, Kaitila I, Wilcox WR, Rimoin DL, Steinmann B, Cetta G, Superti-Furga A (1998) Proteoglycan sulfation in cartilage and cell cultures from patients with sulfate transporter chondrodysplasias: relationship to clinical severity and indications on the role of intracellular sulfate production. Matrix Biol 17 (5):361-369

Figure legend

Fig. 1 Analysis of PG secretion using primary chondrocyte cultures. Chondrocytes were metabolically labelled with 100 µCi/ml $Na_2[^{35}S]O_4$ for 2 hours. At the end of the labelling period cells were incubated with MEM containing 5 mM Na_2SO_4 and medium and cell layer were harvested at different chase time points (0, 0.5, 2.5 and 5 hours). For each chase time point the percentage of secreted PGs was determined based on the ^{35}S-activity in the medium to the total counts (medium and cell layer).

Calcium activated nucleotidase 1 (CANT1) is critical for glycosaminoglycan biosynthesis in cartilage and endochondral ossification

Chiara Paganini[a,b,†], Luca Monti[a,†], Rossella Costantini[a], Roberta Besio[a], Silvia Lecci[a], Marco Biggiogera[c], Kun Tian[d], Jean-Marc Schwartz[d], Céline Huber[e], Valérie Cormier-Daire[e], Beth G. Gibson[f], Katarzyna A. Pirog[f], Antonella Forlino[a] and Antonio Rossi[a]

***a* - Department of Molecular Medicine,** *Unit of Biochemistry, University of Pavia, Pavia, Italy*
***b* - Scuola Universitaria Superiore IUSS,** *Pavia, Italy*
***c* - Department of Biology & Biotechnology,** *University of Pavia, Pavia, Italy*
***d* - Faculty of Biology, Medicine and Health**, *University of Manchester, Manchester, UK*
***e* - Department of Genetics,** *INSERM UMR1163, Université Paris Descartes-Sorbonne Paris Cité, Institut Imagine, AP-HP, Hôpital Necker Enfants Malades, Paris, France*
***f* - Institute of Genetic Medicine,** *Newcastle University, Newcastle upon Tyne, UK*

Correspondence to Antonio Rossi: *at: Dipartimento di Medicina Molecolare, Unità di Biochimica "Alessandro Castellani", Via Taramelli, 3/B, I-27100 Pavia, Italy. antrossi@unipv.it.*
https://doi.org/10.1016/j.matbio.2018.11.002

Abstract

Desbuquois dysplasia type 1 (DBQD1) is a chondrodysplasia caused by mutations in *CANT1* gene encoding an ER/Golgi calcium activated nucleotidase 1 that hydrolyses UDP. Here, using *Cant1* knock-in and knock-out mice recapitulating DBQD1 phenotype, we report that CANT1 plays a crucial role in cartilage proteoglycan synthesis and in endochondral ossification. Specifically, the glycosaminoglycan synthesis was decreased in chondrocytes from *Cant1* knock-out mice and their hydrodynamic size was reduced, whilst the sulfation was increased and the overall proteoglycan secretion was delayed. Interestingly, knock-out chondrocytes had dilated ER cisternae suggesting delayed protein secretion and cellular stress; however, no canonical ER stress response was detected using microarray analysis, Xbp1 splicing and protein levels of BiP and ATF4. The observed proteoglycan defects caused deregulated chondrocyte proliferation and maturation in the growth plate resulting in the reduced skeletal growth. In conclusion, the pathogenic mechanism of DBQD1 comprises deregulated chondrocyte performance due to defective intracellular proteoglycan synthesis and altered proteoglycan properties in the extracellular matrix.

Introduction

Proteoglycans (PGs) are a complex class of macromolecules ubiquitously distributed in the extracellular matrix (ECM) and on the cell surface. They are composed of a core protein to which a variable number of glycosaminoglycan (GAG) side chains are covalently attached [1]. GAGs are linear polysaccharides classified according to the composition of their disaccharide units in chondroitin sulfate, dermatan sulfate, keratan sulfate and heparan sulfate. In addition, sugar moieties are modified by sulfation at various hydroxyl groups and by epimerization of uronic acid. These features give rise to a tremendous diversity, crucial for the structural properties of the ECM and for a wide range of biological events, including cell signaling, cell proliferation, tissue morphogenesis and growth factor interactions [2,3]. The biosynthesis of GAGs involves a great number of glycosyltransferases,

Please cite this article as: C. Paganini, L. Monti, R. Costantini, et al., Calcium activated nucleotidase 1 (CANT1) is critical for glycosaminoglycan biosynthesis in cartilage and endoc..., Matrix Biology, https://doi.org/10.1016/j.matbio.2018.11.002

epimerases and sulfotransferases well orchestrated in the Golgi apparatus and, in addition, enzymes and transporters involved in providing the building components such as activated sugars and sulfate. A deficiency or malfunction of any enzyme involved in PG biosynthesis may lead to disorders of varying severity. Most of these disorders affect the skeleton and in some instances the skin [4]. The biosynthesis of defective PGs may affect their charge density or their interactions with other extracellular components, thus affecting the overall ECM structure and properties [5].

According to the most recent nosology and classification of skeletal disorders there are >400 different clinical phenotypes classified in 42 groups [6]; the skeletal abnormalities resulting from defects in GAG synthesis are: chondrodysplasia, short stature, decreased bone density, digit patterning defects, brachydactyly, multiple joint dislocations and advanced carpal ossification.

Desbuquois dysplasia (DBQD) is a rare autosomal recessive chondrodysplasia characterized by short stature, joint laxity, short extremities and round face; the radiological features include "Swedish key" appearance of the proximal femur, advanced carpal and tarsal bone age and progressive scoliosis. Two forms of DBQD have been described: type 1 (DBQD1) with additional hand anomalies (extra ossification centre distal to the second metacarpal, delta phalanx, bifid distal phalanx of the thumb and phalangeal dislocations) and type 2 (DBQD2) without additional hand anomalies [7]. DBQD1 is caused by mutations in *CANT1* gene, encoding for Calcium Activated Nucleotidase 1, while DBQD2 is caused by mutations in *XYLT1* gene, encoding for Xylosyltransferase 1 [8,9]. XYLT1 is involved in the very first step of GAG biosynthesis: it transfers a Xyl residue from UDP-Xyl to the specific serine residues in the newly synthesised core protein of PGs [2]. CANT1 is a nucleotidase present in the endoplasmic reticulum (ER) and Golgi that preferentially hydrolyses UDP to UMP and phosphate [10]. Due to its substrate preference and its localization, it has been suggested that CANT1 might play a role in PG synthesis through the hydrolysis of UDP, a product of glycosyltransferase reactions [8]. UDP removal is essential for the glycosyltransferases, preventing their reaction inhibition and allowing the exchange of UMP with the cytosolic UDP-sugars through an antiporter exchanger. Interestingly, fibroblasts from DBQD1 patients showed reduced PG synthesis, in particular when cells were incubated with β-D-xyloside, a compound that increases GAG synthesis [11].

CANT1 is a member of the apyrase family with sequence homology to apyrases present in the saliva of hematophagous arthropods that hydrolyse extracellular nucleotides, such as ATP and ADP, acting as anti-hemostatic agents [12]. Although the role of apyrases has been elucidated in blood-feeding arthropods, the exact physiological function of CANT1 in human tissues remains to be determined. In 2002, two different groups characterized two forms of the same enzyme, a membrane bound and a soluble secreted form [10,13]. Thus, unlike apyrases found in the blood-feeding arthropods, the substrate preference and subcellular localization of the enzyme suggest very different functions in mammals. In fact, CANT1 is likely involved in the intracellular glycosylation reactions and, in addiction, in protein quality control and folding as demonstrated in neuroblastoma cell lines [14]. Moreover, since uridine nucleotides as well as UDP-sugars are also recognized as extracellular signaling molecules, the presence of the soluble secreted form of CANT1 suggests that the enzyme may also modulate cellular responses to extracellular UDP *via* specific pyrimidinergic receptors (P2Y family) [15].

Overall, results to date suggest that CANT1 has several biological functions *in vitro,* depending on the cell type. Interestingly, mutations in CANT1 leading to a partial or total loss of the enzyme function primarily affect the skeleton *in vivo*, as demonstrated by the clinical phenotype of DBQD1 patients. Unfortunately, since skeletal tissue biopsies from DBQD1 patients are rarely available, a detailed picture of the biochemical, molecular and cellular events in the DBQD1 cartilage and bone, ultimately resulting in dwarfism, progressive joint disease and malformed skeleton, is far from complete.

To provide new insight on the role of CANT1 in the development and homeostasis of the skeleton and to contribute to the understanding of the disease-causing mechanism of *CANT1* mutations in DBQD1, we have generated novel *Cant1* knock-in and knock-out murine strains. We show that both strains present with a skeletal and connective tissue phenotype that recapitulates human DBQD1. Moreover, biochemical studies of knock-out cartilage samples and primary chondrocytes demonstrate that CANT1 defects not only affect GAG synthesis, but also GAG elongation, sulfation and PG secretion.

Results

Generation of the *Cant1* knock-in and knock-out mice

We generated transgenic knock-in mice harbouring the p.R302H substitution, which is homologous to the p.R300H substitution in the active site of human CANT1 using a gene targeting approach (Fig. 1). The p.R300H CANT1 mutation has been detected at the homozygous state in two patients of

Please cite this article as: C. Paganini, L. Monti, R. Costantini, et al., Calcium activated nucleotidase 1 (CANT1) is critical for glycosaminoglycan biosynthesis in cartilage and endoc..., Matrix Biology, https://doi.org/10.1016/j.matbio.2018.11.002

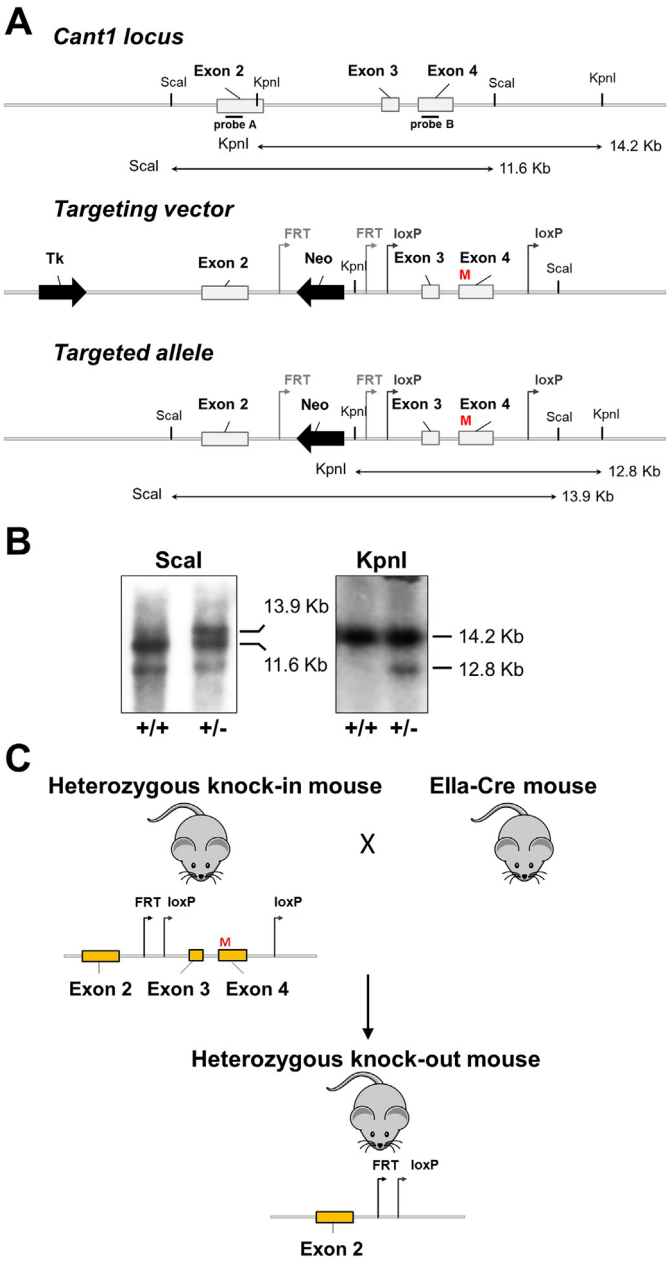

Fig. 1. Generation of *Cant1* knock-in and knock-out mice. (A) Schematic representation of *Cant1* locus and targeting vector used for the generation of *Cant1* knock-in (*Cant1*$^{R302H/R302H}$) and knock-out (*Cant1*$^{-/-}$) mice. A c.G905A transition (M) causing the R302H substitution was inserted in *Cant1* exon 4 to generate the *Cant1* knock-in mouse, whilst exon 3 and 4 were flanked by loxP sites to allow the generation of the *Cant1* knock-out mouse by Cre recombinase excision. (B) Southern blot analysis to identify embryonic stem clones that had undergone homologous recombination. The 13.9 kb *ScaI* fragment and the 12.8 kb *KpnI* fragment indicate proper 5′ and 3′ targeting of the *Cant1* locus. (C) Schematic diagram of heterozygous *Cant1* knock-out mouse generation by the excision of exon 3 and 4 obtained mating heterozygous *Cant1* knock-in mice with EIIa-Cre deleter mice (B6.FVB-Tg(EIIa-cre)C5379Lmgd).

different ethnic origin affected by a moderate form of DBQD1 [8]. To knock-in the missense mutation we introduced a c.G905A transition in a cloned fragment containing exon 4 of the murine *Cant1* gene by site directed mutagenesis. In addition, the gene targeting vector for the generation of the knock-in line was designed to allow a *Cant1* deletion, leading to a knock-out line, by flanking the exon 3 and 4, encoding for the enzyme active site, with loxP sequences (Fig. 1A, C).

The gene targeting vector was electroporated into Sv129/Bl6 embryonic stem (ES) cells. ES clones that had undergone homologous recombination were identified by Southern blot analysis using probes for the 5′ and 3′ end of the targeted region (Fig. 1B). We used two independent ES clones with an euploid karyotype to produce male chimeras; germline transmission of the targeted allele was achieved by breeding the chimeric males with C57Bl/6 J females. Offspring were mated to an Flp deleter mouse strain to remove the positive selection cassette leading to the generation of heterozygous *Cant1* knock-in mice (*Cant1*$^{+/R302H}$ mouse) bearing the R302H missense mutation.

Heterozygous *Cant1* knock-out mice (*Cant1*$^{+/-}$ mouse) were generated by mating heterozygous knock-in animals with a Cre deleter murine strain (Fig. 1C). Deletion of exon 3 and 4 and lack of expression of *Cant1* mRNA in homozygous knock-out mice was confirmed by real time PCR on total

Please cite this article as: C. Paganini, L. Monti, R. Costantini, et al., Calcium activated nucleotidase 1 (CANT1) is critical for glycosaminoglycan biosynthesis in cartilage and endoc..., Matrix Biology, https://doi.org/10.1016/j.matbio.2018.11.002

RNA from skin of newborn mice (relative quantitation: 1.11 ± 0.16, 0.57 ± 0.12 and 0.0003 ± 0.0001 in wild-type, heterozygous and homozygous mice, respectively; $n = 3$; $P < 0.001$ homozygous knock-out *vs.* heterozygous knock-out and wild-type).

Cant1 knock-in and knock-out animals present with skeletal abnormalities reminiscent of human DBQD1 phenotype

Cant1 knock-in and knock-out mice were morphologically characterized to validate them as animal models of DBQD1. Heterozygous *Cant1* knock-in and knock-out mice did not present with an overt phenotype, similar to human heterozygous carriers of *CANT1* mutations. Specifically, their body weights were normal and no skeletal defects were observed by double staining with alcian blue and alizarin red; for this reason we did not study these animals further.

By mating heterozygous knock-in mice, we obtained animals homozygous for the R302H substitution in the CANT1 catalytic domain. At postnatal days (P)60 the homozygous mutant mice demonstrated a skeletal phenotype characterized by reduced size and a moderate thoracic kyphosis (Fig. 2A, B). Moreover, we observed a medial deviation of the first digit in the extremities of *Cant1*$^{R302H/R302H}$ mice with the formation of an additional rudimentary phalanx, so called "delta phalanx" (Fig. 2C), a typical feature in the DBQD1 patients [11].

By mating heterozygous knock-out mice, we obtained litters with the normal mendelian ratio of homozygous, heterozygous and wild type animals. We analysed the skeletal phenotype of the knock-out and wild type offspring at different ages from birth to P60 by double staining of cartilage and bone and by X-ray analysis. Alcian blue and alizarin red skeletal preparations from P1 to P21 showed that knock-out (*Cant1*$^{-/-}$) mice were smaller when compared with the wild type littermates (*Cant1*$^{+/+}$), demonstrating a skeletal growth defect (Fig. 3A). In addition, adult *Cant1*$^{-/-}$ mice at P60 were also smaller than the age matched wild type animals (Fig. 3B). Starting from P21, a moderate thoracic kyphosis was evident in the knock-out mice (Suppl. Fig. 1). Moreover, we observed a "delta phalanx" at the extremities of hind limbs of P7, P14 and P21 *Cant1*$^{-/-}$ mice (Fig. 3C), similar to the *Cant1* knock-in mice.

Overall, these data demonstrated a skeletal phenotype with growth retardation and abnormalities in bone extremities reminiscent of the clinical features of DBQD1 in both mouse lines. Since the skeletal phenotype of the knock-in and knock-out mouse lines was similar, in order to study the pathophysiology of *CANT1* mutations in DBQD1 and the role of CANT1 in skeletal homeostasis, we prioritised the deep characterization of the *Cant1*$^{-/-}$ mouse at the biochemical, histological and molecular level.

Defects in endochondral ossification are present in *Cant1* knock-out mice

We performed morphometric analysis of representative long bones (tibia, femur and ilium) in skeleton preparations of wild type and *Cant1* knock-out mice stained with alcian blue and alizarin red from birth to P21 (Fig. 3A). In knock-out newborn mice the widths of the tibiae and femurs were significantly decreased compared with the age and sex matched wild type bones. At P7, P14 and P21 both length and width of tibiae and femurs were significantly decreased in *Cant1*$^{-/-}$ mice compared with wild type animals. Moreover, a significant reduction in the length and width of the ilium was found in mutant animals compared with wild type littermates at all ages (Fig. 4).

Bone morphometric measurements confirmed the reduced growth of *Cant1*$^{-/-}$ long bones, suggesting a defect in endochondral ossification; we therefore decided to deeply phenotype the tibial growth plate. The overall architecture of the growth plate in *Cant1*$^{-/-}$ mice was maintained, with well-delineated resting, proliferative and hypertrophic zones. In addition, the columnar alignments of chondrocytes in the proliferative and hypertrophic zones were unaffected (Fig. 5). In *Cant1*$^{-/-}$ and wild type animals the height of the growth plate decreased from P7 to P21 following the formation of the secondary ossification centre. However, the height of the proliferative zone in P7 *Cant1*$^{-/-}$ growth plates and of the hypertrophic zone in P7 and P14 *Cant1*$^{-/-}$ cartilage was reduced compared with control animals. The area of proliferative and hypertrophic zones showed a similar trend, with a significant difference in both at P7 and in the hypertrophic zone at P14 (Table 1). No disruptions of growth plate organisation were observed in *Cant1*$^{-/-}$ mice at P21.

The number of columns in a standardized area, the number of cells per column and the column height were measured in proliferative and hypertrophic zones. Interestingly, most differences were observed in the first two weeks of life. At P7, the mutant mice showed a higher number of columns per area in the proliferative zone, but the columns were shorter and with fewer cells compared with wild type growth plates. These changes were also present in the hypertrophic zone at P7, whilst at P14 only the heights of the columns in the proliferative and hypertrophic zones of *Cant1*$^{-/-}$ mice were decreased compared with wild type animals. At P21 no differences between mutant and wild type mice were evident by morphometric analysis (Table 1).

Interestingly, at P7 the relative proliferative zone area was significantly increased in mutant compared with wild type mice and, correspondingly, the relative hypertrophic zone area was markedly decreased, suggesting an imbalance between the two growth

Please cite this article as: C. Paganini, L. Monti, R. Costantini, et al., Calcium activated nucleotidase 1 (CANT1) is critical for glycosaminoglycan biosynthesis in cartilage and endoc..., Matrix Biology, https://doi.org/10.1016/j.matbio.2018.11.002

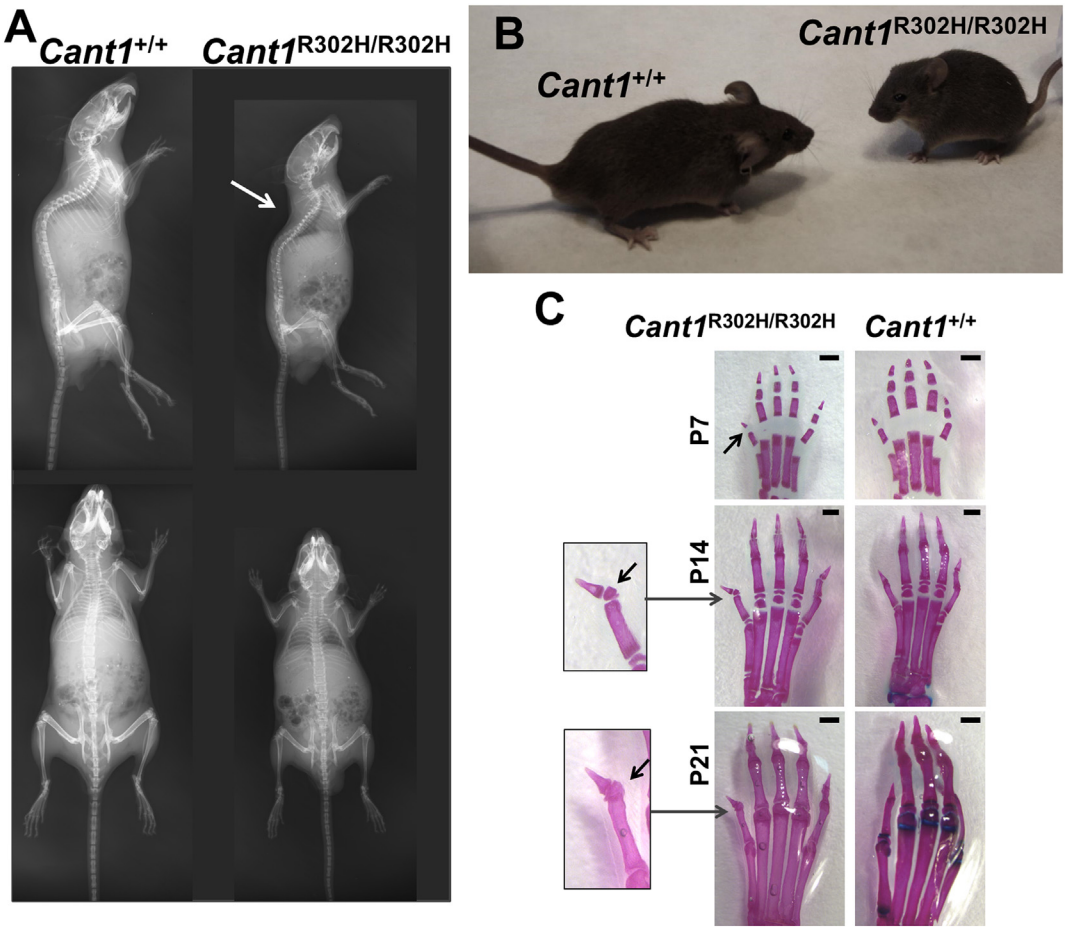

Fig. 2. *Cant1* knock-in mice show a skeletal phenotype reminiscent of the human DBQD1. (A) X-ray images of two month old *Cant1* knock-in (*Cant1*$^{R302H/R302H}$) mice showed reduced growth compared with wild type (*Cant1*$^{+/+}$) animals. Moderate thoracic kyphosis (arrow) was present in *Cant1*$^{R302H/R302H}$ mouse. (B) Gross morphology of a two month old *Cant1*$^{R302H/R302H}$ and *Cant1*$^{+/+}$ mice showing growth retardation in the mutant littermate. (C) Alcian blue and alizarin red staining of the hind limb extremities at different ages showed the presence of a delta phalanx (arrow) in *Cant1*$^{R302H/R302H}$ mice. Scale bars = 0.5 mm. (For interpretation of the references to colour in this figure legend, the reader is referred to the web version of this article.)

plate zones, whilst at other age points no significant differences were observed (Table 1). Longitudinal bone growth is dependent on cell proliferation and on the volume and height that the hypertrophic chondrocytes achieve during terminal differentiation [16,17]. Interestingly, in *Cant1*$^{-/-}$ growth plate the average height of the most terminal hypertrophic chondrocytes was decreased compared with wild type mice at all ages (Table 1). Finally, a delay in the formation of secondary ossification centre was evident in mutant mice at all ages compared with the wild type animals, providing an additional proof of skeletal growth retardation (Fig. 5).

Proliferation and apoptosis imbalance in growth plates of *Cant1* knock-out mice

To investigate whether the growth plate defects in *Cant1*$^{-/-}$ mice were due to changes in cell proliferation, differentiation and viability, we studied chondrocyte proliferation and apoptosis by 5′-bromo-2′-deoxyuridine (BrdU) labelling and by a TUNEL assay, respectively.

BrdU-labelled cells were detected only in the proliferative zone and the ratio of proliferating cells (BrdU positive cells) to the total cell number (haematoxylin positive cells) was calculated. In *Cant1*$^{-/-}$ mice the percentage of proliferating chondrocytes was significantly increased compared with wild type animals at P7 (15.72 ± 0.66% and 13.12 ± 1.84%, respectively; $P < 0.001$, $n = 3$) and P14 (14.87 ± 3.60 and 11.43 ± 3.55%, respectively; $P < 0.05$, n = 3), whilst no differences were detected in P21 *Cant1*$^{-/-}$ mice (Fig. 6A, B).

We measured apoptosis in the proliferative and hypertrophic zones of *Cant1*$^{-/-}$ and wild type mice at P7 and P14. The percentage of apoptotic chondrocytes in the proliferative zone of P7 *Cant1*$^{-/-}$ mice

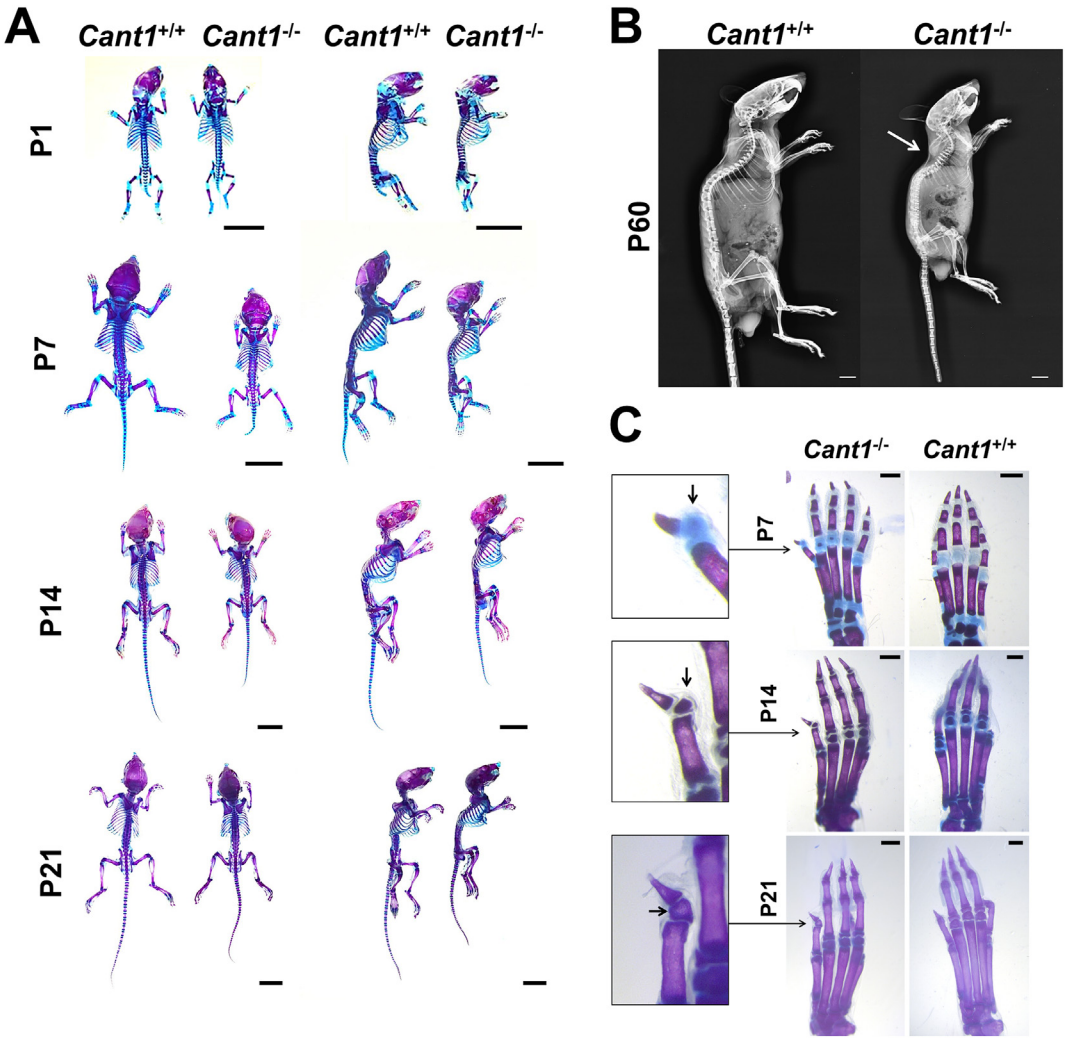

Fig. 3. Skeletal phenotype of *Cant1* knock-out mice is reminiscent of the DBQD1 patients' phenotype. (A) Alcian blue and alizarin red staining of full skeletons from birth to P21 showed that *Cant1*$^{-/-}$ mice were smaller compared with age matched wild type (*Cant1*$^{+/+}$) controls. Scale bars = 1 cm. (B) X-ray analysis of two month old (P60) *Cant1*$^{-/-}$ and *Cant1*$^{+/+}$ mice showed reduced growth of *Cant1*$^{-/-}$ compared with wild type animals. Moreover, a moderate thoracic kyphosis (arrow) was observed in *Cant1*$^{-/-}$ mice. Scale bars = 1 cm. (C) Alcian blue and alizarin red staining of the hind limb extremities at different ages revealed the presence of a delta phalanx (arrow) in *Cant1*$^{-/-}$ mice at all ages. Scale bars = 1 mm. (For interpretation of the references to colour in this figure legend, the reader is referred to the web version of this article.)

was increased compared with wild type mice (0.04 ± 0.01% and 0.01 ± 0.01%, respectively; $P < 0.05$, n = 3), whereas no difference was detected in the hypertrophic zone of P7 and P14 mice (Fig. 6C, D).

Overall, these results demonstrated an imbalance between proliferation and apoptosis in *Cant1*$^{-/-}$ growth plate consistent with the defects detected by morphometric analysis in the proliferative and hypertrophic zones (Table 1).

Proteoglycan synthesis is reduced in *Cant1* knock-out mice

It has been hypothesised that CANT1 plays a role in PG synthesis through the hydrolysis of UDP produced by glycosyltransferases. We therefore decided to study the PG metabolism and synthesis in primary chondrocyte cultures from rib cartilage of mutant and wild type mice at P4 by metabolic labelling with ^{35}S-sulfate.

In basal conditions (MEM), PG synthesis was reduced in *Cant1*$^{-/-}$ chondrocytes compared with wild type cells ($P < 0.01$, n = 3). This defect was even more enhanced when the cells were metabolically labelled in MEM containing *p*-nitrophenyl-β-D-xylopyranoside (β-D-xyloside) ($P < 0.001$, n = 3) (Fig. 7A, B).

To evaluate if CANT1 defect affects PG synthesis *in vivo*, we analysed the GAG content of cartilage from mutant and wild type mice. Femoral head

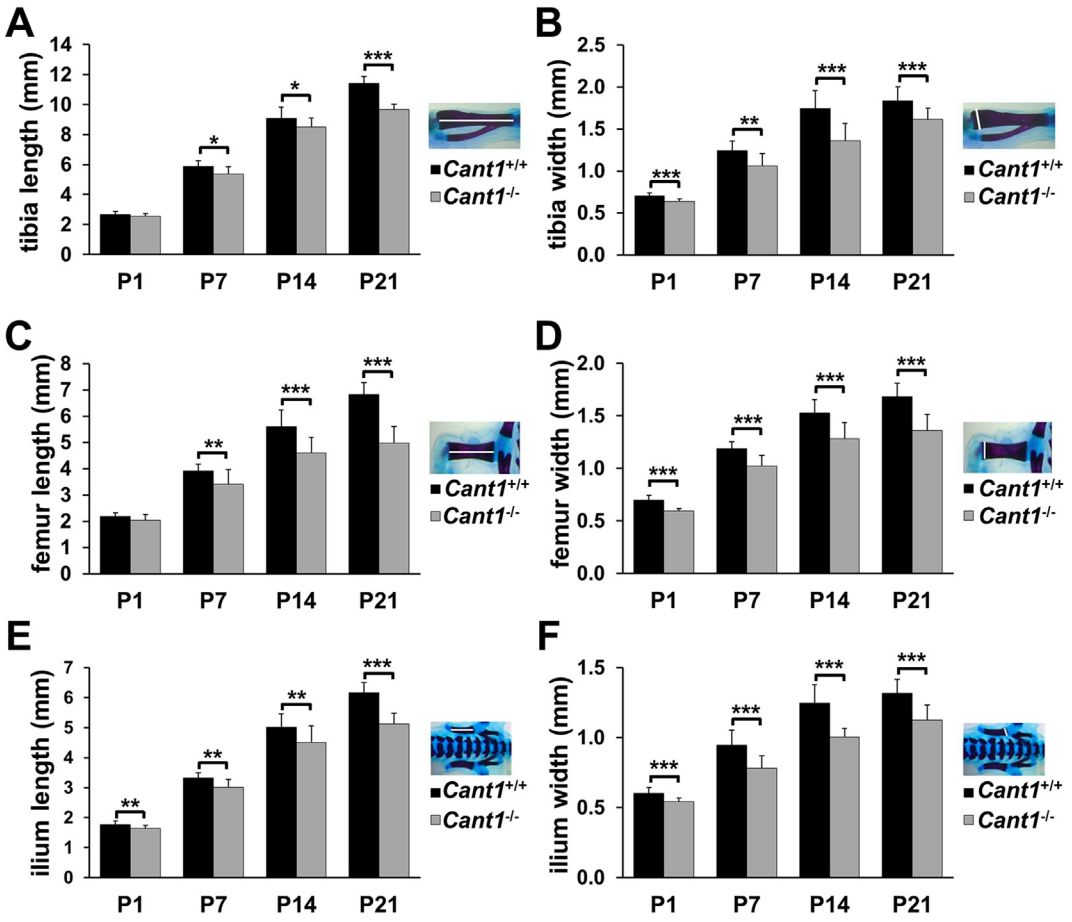

Fig. 4. Endochondral ossification is affected in *Cant1*$^{-/-}$ mice. (A – F) Morphometric analysis of alcian blue and alizarin red skeletal preparations. (A) Tibia length was significantly decreased in *Cant1*$^{-/-}$ mice starting from one week of life (P7), whilst (B) tibia width was reduced from birth. Similar changes were observed in (C, D) the femur, whereas (E) both the ilium length and (F) width were significantly decreased in *Cant1*$^{-/-}$ mice from birth. Data are presented as mean ± SD, significance was determined by Student's *t*-test, * $P < 0.05$; ** $P < 0.01$; *** $P < 0.001$; $n = 5$. (For interpretation of the references to colour in this figure legend, the reader is referred to the web version of this article.)

cartilage of P4 mice was digested with proteinase K to remove proteins and release GAGs. The GAG content, quantified by the dimethylmethylene blue (DMMB) assay and normalised to DNA, was reduced in *Cant1*$^{-/-}$ mice compared with control animals ($P < 0.01$, $n = 10$) (Fig. 7C).

In conclusion, the PG content was reduced in *Cant1*$^{-/-}$ chondrocyte cultures and in *Cant1*$^{-/-}$ cartilage.

Glycosaminoglycans are oversulfated and show reduced hydrodynamic size in *Cant1* knock-out cartilage

To assess whether CANT1 defect affects other structural properties of PGs, we analysed GAG sulfation in primary chondrocytes by HPLC analysis of chondroitin sulfate disaccharides. The percentage of monosulfated disaccharides (ΔDi-4S and ΔDi-6S) relative to the total amount of disaccharides (ΔDi-0S, ΔDi-4S and ΔDi-6S) was increased in *Cant1*$^{-/-}$ chondrocytes compared with *Cant1*$^{+/+}$ cells, in both cell layer (88.43 ± 1.91% and 76.92 ± 3.47%, respectively; $P < 0.01$, $n = 3$) and medium fractions (92.22 ± 1.36% and 73.62 ± 3.03%, respectively; $P < 0.001$, n = 3), demonstrating chondroitin sulfate oversulfation in *Cant1*$^{-/-}$ chondrocytes compared with wild type cells (Fig. 8A).

To confirm this result *in vivo*, we analysed sulfation of chondroitin sulfate from femoral head cartilage of P4 *Cant1*$^{-/-}$ and wild type mice by HPLC. There was a significant increase in the relative amount of monosulfated disaccharides in *Cant1*$^{-/-}$ mice compared with wild type controls (94.05 ± 0.56% and 86.01 ± 0.49%, respectively; $P < 0.001$, $n = 6$), indicating PG oversulfation in *Cant1*$^{-/-}$ mouse cartilage (Fig. 8B).

Please cite this article as: C. Paganini, L. Monti, R. Costantini, et al., Calcium activated nucleotidase 1 (CANT1) is critical for glycosaminoglycan biosynthesis in cartilage and endoc..., Matrix Biology, https://doi.org/10.1016/j.matbio.2018.11.002

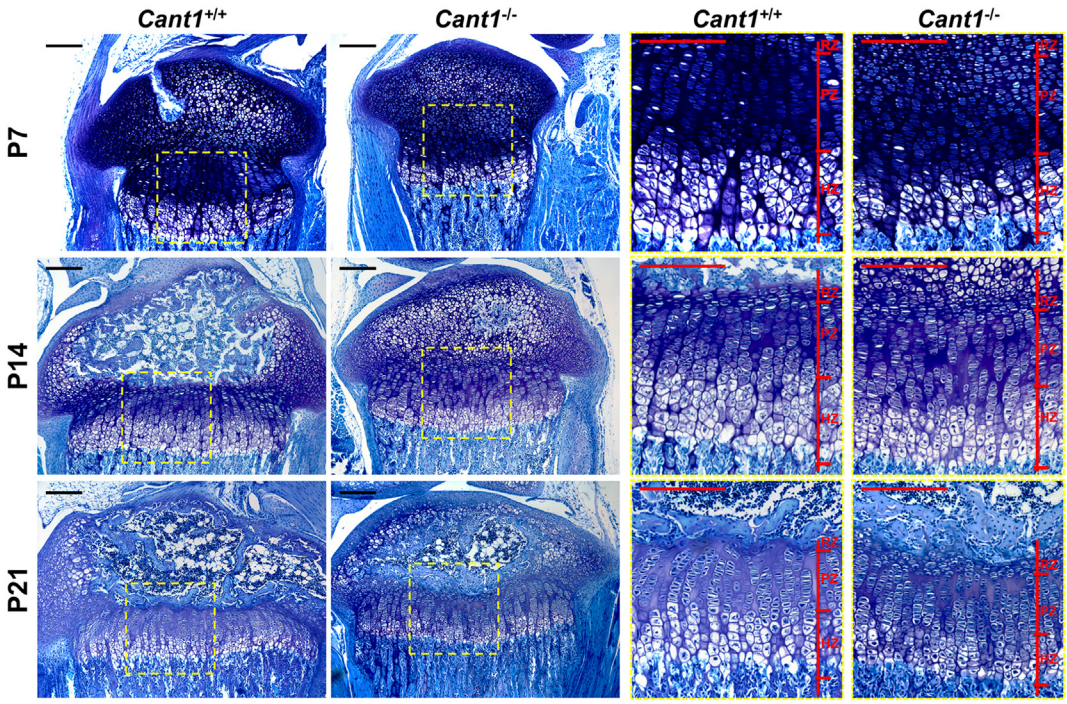

Fig. 5. A delay in the formation of secondary ossification centre is observed in *Cant1*$^{-/-}$ mice. Proximal tibia sections of P7, P14 and P21 *Cant1*$^{-/-}$ and *Cant1*$^{+/+}$ mice were stained with toluidine blue. Areas enclosed in the yellow dashed boxes are shown at higher magnification in the right panel. RZ = resting zone; PZ = proliferative zone; HZ = hypertrophic zone; scale bar = 200 μm. (For interpretation of the references to colour in this figure legend, the reader is referred to the web version of this article.)

Table 1. Morphometric analysis of the tibia growth plate.

	P7		P14		P21	
	Cant1$^{+/+}$	*Cant1*$^{-/-}$	*Cant1*$^{+/+}$	*Cant1*$^{-/-}$	*Cant1*$^{+/+}$	*Cant1*$^{-/-}$
RZ area (μm^2)	n.d.	n.d.	20,574.93 ± 7008.57	16,979.34 ± 3186.25	26,390.30 ± 9892.46	22,189.23 ± 13,319.88
PZ area (μm^2)	208,067.47 ± 15,822.06	155,870.54 ± 30,219.71***	222,002.16 ± 71,476.72	186,545.80 ± 40,461.79	154,103.78 ± 27,144.13	135,134.71 ± 35,629.46
HZ area (μm^2)	156,959.08 ± 13,340.36	89,508.58 ± 12,386.65***	201,043.21 ± 37,338.63	141,589.18 ± 16,126.29**	162,727.19 ± 14,671.09	139,185.84 ± 46,788.93
Relative RZ area (%)	n.d.	n.d.	4.72 ± 1.56	4.93 ± 0.60	7.62 ± 2.66	7.42 ± 2.83
Relative PZ area (%)	56.99 ± 3.07	63.22 ± 5.19*	49.30 ± 8.92	53.63 ± 4.20	44.65 ± 4.49	46.05 ± 4.75
Relative HZ area (%)	43.01 ± 3.07	36.78 ± 5.19*	45.97 ± 7.82	41.44 ± 4.34	47.73 ± 5.70	46.53 ± 4.82
RZ height (μm)			23.87 ± 4.09	23.26 ± 4.53	24.95 ± 5.02	22.10 ± 7.96
PZ height (μm)	268.68 ± 28.06	231.42 ± 30.78*	197.03 ± 63.52	196.06 ± 44.45	113.08 ± 24.53	107.13 ± 25.07
HZ height (μm)	177.06 ± 11.53	128.28 ± 24.22***	168.84 ± 23.58	140.80 ± 10.12*	119.26 ± 11.51	108.23 ± 33.47
Number of column in a 4×10^4 μm^2 area in the PZ	39.43 ± 6.85	50.89 ± 6.06*	28.08 ± 3.29	32.12 ± 4.07	56.66 ± 6.79	60.05 ± 7.48
Number of cell per column in the PZ	8.57 ± 0.93	6.76 ± 0.46**	9.70 ± 0.54	8.68 ± 0.72	7.15 ± 1.12	7.84 ± 0.71
Height of column in the PZ (μm)	45.56 ± 5.38	33.65 ± 3.20**	62.47 ± 5.10	52.08 ± 6.53*	43.92 ± 4.08	46.33 ± 7.17
Number of column in a 4×10^4 μm^2 area in the HZ	12.22 ± 2.21	18.30 ± 8.94	12.51 ± 2.38	14.87 ± 3.40	33.97 ± 4.44	38.77 ± 4.03
Number of cell per column in the HZ	10.18 ± 0.93	7.94 ± 0.77**	11.41 ± 1.78	10.29 ± 1.08	7.93 ± 0.92	7.80 ± 1.53
Height of column in the HZ (μm)	136.08 ± 17.64	88.23 ± 7.25***	150.38 ± 8.23	111.14 ± 7.23***	109.11 ± 6.91	95.43 ± 22.67
Height of the most terminal HCs (μm)	25.43 ± 2.77	19.49 ± 0.85**	24.08 ± 0.78	19.42 ± 0.38*	23.27 ± 0.99	19.89 ± 2.05**

All measurements (mean ± SD) were performed on an average of five sections stained with toluidine blue as shown in Fig. 5 and three mice in each group were analysed. Student's *t*-test was performed, * $P < 0.05$; ** $P < 0.01$; *** $P < 0.001$; RZ = resting zone; PZ = proliferative zone; HZ = hypertrophic zone; n.d. = not determined.

Please cite this article as: C. Paganini, L. Monti, R. Costantini, et al., Calcium activated nucleotidase 1 (CANT1) is critical for glycosaminoglycan biosynthesis in cartilage and endoc..., Matrix Biology, https://doi.org/10.1016/j.matbio.2018.11.002

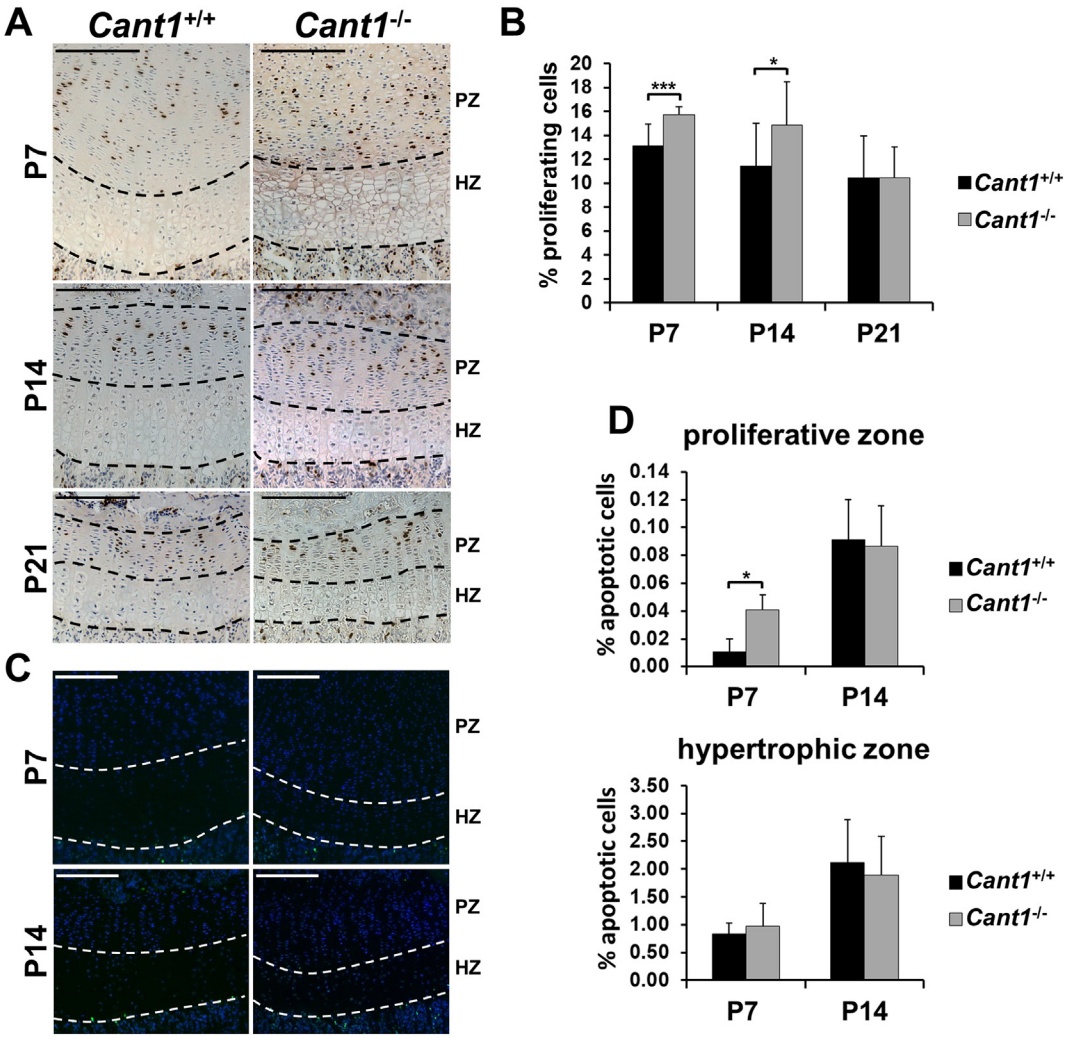

Fig. 6. Proliferation and apoptosis are imbalanced in *Cant1*$^{-/-}$ growth plate. (A) BrdU assay on proximal tibia sections of *Cant1*$^{-/-}$ and *Cant1*$^{+/+}$ mice. BrdU positive cells (brown) were only found in the proliferative zone. PZ = proliferative zone; HZ = hypertrophic zone; scale bar = 200 μm. (B) The percentage of proliferating chondrocytes was higher in P7 and P14 *Cant1*$^{-/-}$ proliferative zone. An average of five sections per animal were analysed. Data are reported as mean ± SD and significance was determined by Student's *t*-test, * $P < 0.05$; *** $P < 0.001$; $n = 3$. (C) Fluorescent TUNEL assay on proximal tibia sections of *Cant1*$^{-/-}$ and *Cant1*$^{+/+}$ mice. TUNEL positive cells showed a green nucleus profile, while total cells were stained in blue by DAPI. PZ = proliferative zone; HZ = hypertrophic zone; scale bar = 200 μm. (D) The percentage of apoptotic chondrocytes was increased only in P7 *Cant1*$^{-/-}$ proliferative zone. An average of five sections per animal was analysed. Data are reported as mean ± SD and Student's t-test was performed, * $P < 0.05$; $n = 3$. (For interpretation of the references to colour in this figure legend, the reader is referred to the web version of this article.)

To analyse whether the increased sulfation in mutant mice was due to an overexpression of chondroitin sulfotransferases, we performed expression studies using RNA from rib cartilage of P4 *Cant1*$^{-/-}$ and wild type mice on an Affymetrix genechip microarray. No significant differences between *Cant1*$^{-/-}$ and wild type animals were detected with a fold expression change set to ±2 (Suppl. Table 1).

Since both the GAG content and the sulfation were altered in cartilage and in chondrocyte cultures from *Cant1*$^{-/-}$ mice, we also considered the hydrodynamic size of the GAGs. When chondrocytes were incubated in basal medium (MEM), the hydrodynamic size of GAG chains in *Cant1*$^{-/-}$ and *Cant1*$^{+/+}$ cells was similar (K_{av} 0.50 and 0.53, respectively; $n = 3$), even if a slight peak broadening toward the total volume (V_t) was evident in *Cant1*$^{-/-}$ chromatograms, indicating a fraction of GAGs with lower molecular mass compared with wild type controls (Fig. 9A). Interestingly, when cells were metabolically labelled in MEM containing β-D-xyloside, GAGs from *Cant1*$^{-/-}$ chondrocytes showed a significant shift toward the V_t compared with wild type cells (K_{av} 0.81 ± 0.02 and

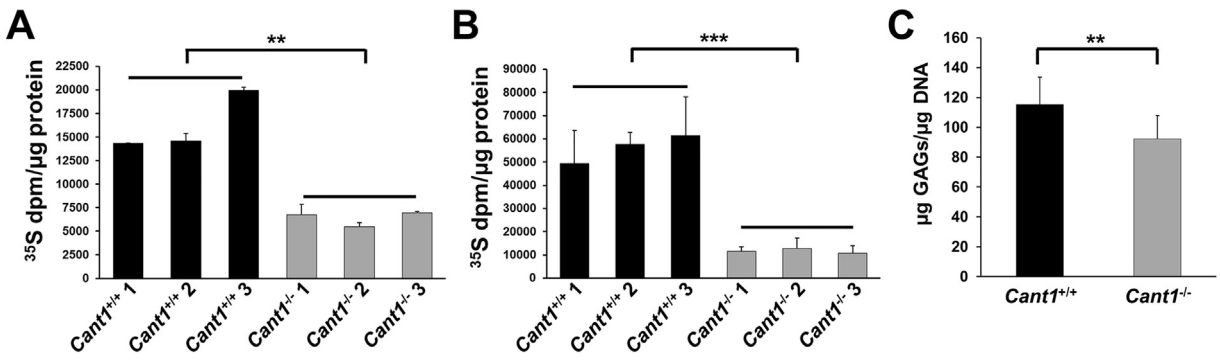

Fig. 7. Proteoglycan synthesis is reduced in *Cant1*$^{-/-}$ mice. (A) Rib chondrocyte cultures were metabolically labelled with ^{35}S-sulfate for 24 h in basal medium. The amount of newly synthesised PGs was determined on the basis of ^{35}S-activity and normalised to the protein content, demonstrating that *Cant1*$^{-/-}$ chondrocytes produced less PGs compared with wild type cells. Data are representative of two independent experiments and reported as mean ± SD. Significance was determined by Student's *t*-test; ** $P < 0.01$. (B) Rib chondrocyte cultures were metabolically labelled with ^{35}S-sulfate for 24 h in basal medium containing 1 mM *p*-nitrophenyl-β-D-xylopyranoside. Samples were analysed as described in 7A, demonstrating that the reduced PG synthesis in *Cant1*$^{-/-}$ chondrocytes was more evident in presence of β-D-xyloside. Data are representative of two independent experiments and reported as mean ± SD. Student's t-test was performed, *** $P < 0.001$. (C) The GAG content in femoral head cartilage from 4 day old mice was analysed by dimethylmethylene blue assay and normalised to DNA content, showing reduced GAG content in *Cant1*$^{-/-}$ cartilage. Data are representative of three independent experiments and reported as mean ± SD. Student's t-test was performed, ** $P < 0.01$; $n = 10$.

0.63 ± 0.05, respectively; $P < 0.01$, n = 3), (Fig. 9B). This result demonstrated the smaller size of newly synthesised GAGs in *Cant1*$^{-/-}$ chondrocytes compared with control cells when oligosaccharide synthesis was enhanced.

In summary, these results demonstrated that when CANT1 was impaired, beyond reduced synthesis of PGs, GAG sulfation pattern and hydrodynamic size were also altered.

Proteoglycan secretion is reduced in *Cant1* knock-out mice

Results described above demonstrated defects in different steps of PG biosynthesis in *Cant1*$^{-/-}$ chondrocytes that could impact on PG secretion. We therefore investigated PG secretion by a pulse chase experiment in primary rib chondrocytes.

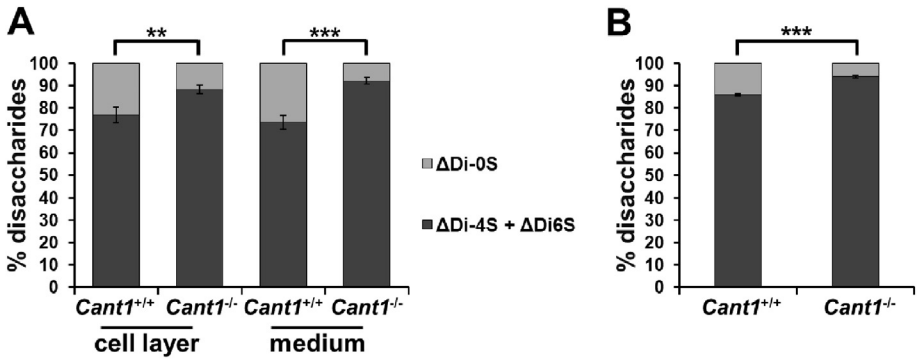

Fig. 8. Chondroitin sulfate proteoglycans are oversulfated in *Cant1*$^{-/-}$ mice. (A) Sulfation of chondroitin sulfate proteoglycans extracted from cell layer and medium of *Cant1*$^{-/-}$ and *Cant1*$^{+/+}$ chondrocyte cultures was analysed by reverse-phase HPLC after digestion with chondroitinase ABC and ACII. The percentage of monosulfated disaccharides (ΔDi-4S and ΔDi-6S) was significantly increased in *Cant1*$^{-/-}$ cells compared with wild type controls. Data are reported as mean ± SD and significance was determined by Student's *t*-test, ** $P < 0.01$, *** $P < 0.001$; $n = 3$. (B) Chondroitin sulfate proteoglycans were extracted from P4 *Cant1*$^{-/-}$ and *Cant1*$^{+/+}$ femoral head cartilage and their sulfation was analysed by reverse-phase HPLC after digestion with chondroitinase ABC and ACII. The percentage of monosulfated disaccharides (ΔDi-4S and ΔDi-6S) was significantly increased and correspondingly the percentage of non-sulfated disaccharides (ΔDi-0S) was reduced in *Cant1*$^{-/-}$ cartilage compared with wild types. Data are reported as mean ± SD and Student's *t*-test was performed, *** $P < 0.001$; $n = 6$.

Please cite this article as: C. Paganini, L. Monti, R. Costantini, et al., Calcium activated nucleotidase 1 (CANT1) is critical for glycosaminoglycan biosynthesis in cartilage and endoc..., Matrix Biology, https://doi.org/10.1016/j.matbio.2018.11.002

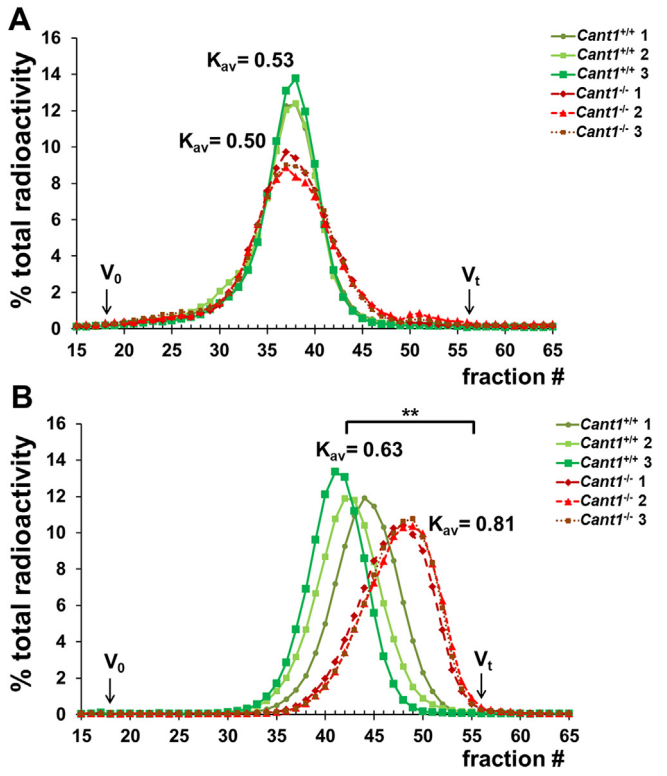

Fig. 9. GAG hydrodynamic size is reduced in *Cant1*$^{-/-}$ mice. (A) Chondrocyte cultures were metabolically labelled with ^{35}S-sulfate for 24 h in basal medium. GAGs were released from PGs by β-elimination and their hydrodynamic size was analysed by gel filtration chromatography. GAG hydrodynamic size of *Cant1*$^{-/-}$ chondrocytes was comparable with *Cant1*$^{+/+}$ cells even if a slight peak broadening toward the total volume (V_t) was observed. Data are representative of two independent experiments. (B) *Cant1*$^{-/-}$ and *Cant1*$^{+/+}$ chondrocyte cultures were metabolically labelled with ^{35}S-sulfate in basal medium containing 1 mM *p*-nitrophenyl-β-D-xylopyranoside, an enhancer of GAG synthesis. GAG hydrodynamic size was analysed by gel filtration chromatography. A marked shift toward the V_t was found in *Cant1*$^{-/-}$ chromatograms demonstrating that *Cant1*$^{-/-}$ GAGs have reduced size compared with wild type controls. Data are representative of two independent experiments and K_{av} is reported as mean. Significance was determined by Student's t-test, ** $P < 0.01$. (For interpretation of the references to colour in this figure legend, the reader is referred to the web version of this article.)

A significant impairment of PG secretion was demonstrated in mutant chondrocytes compared with wild type cells ($P < 0.05$, $n = 3$) (Fig. 10).

The defects in PG synthesis and secretion, detected *in vitro*, suggested the study of chondrocytes at the ultrastructural level by transmission electron microscopy (TEM). In *Cant1*$^{-/-}$ cartilage sections of P4 mice, chondrocytes showed ER enlargement with retained proteinaceous material, as previously shown in patient fibroblasts [8] (Fig. 11). Interestingly, the *Cant1*$^{-/-}$ femoral head cartilage sections at P4 also showed a less dense ECM compared with wild type samples (Fig. 11), consistent with reduced GAG content in *Cant1*$^{-/-}$ cartilage observed by the DMMB assay (Fig. 7C).

Taken together these results further confirmed the biochemical data demonstrating defects in PG metabolism and secretion in *Cant1*$^{-/-}$ cartilage.

Despite the dilated ER cisternae, ER stress is not present in *Cant1* knock-out chondrocytes

The enlargement of the ER observed by TEM analysis in mutant mice suggested protein retention and possibly ER stress in *Cant1*$^{-/-}$ chondrocytes. Indeed, retention of proteins and accumulation of unfolded proteins in the ER leading to increased ER volume and activation of the unfolded protein response (UPR) have been previously demonstrated in several skeletal disorders [18,19]. Therefore, we performed expression studies in rib cartilage of P4 *Cant1*$^{-/-}$ and wild type mice using an Affymetrix genechip microarray in order to investigate ER stress and UPR activation in *Cant1*$^{-/-}$ chondrocytes. The analysis of microarray data, focused on genes related to ER stress and UPR, indicated no differences between *Cant1*$^{-/-}$ and wild type animals

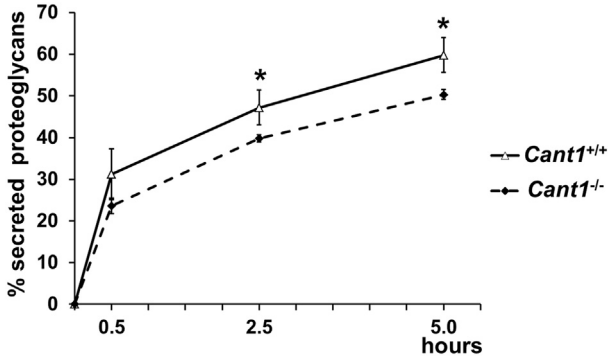

Fig. 10. Proteoglycan secretion is delayed in *Cant1*$^{-/-}$ mice. Chondrocyte cultures were metabolically labelled with ^{35}S-sulfate for 2 h and cells were harvested after 0.5, 2.5 and 5 h. The percentage of ^{35}S-PGs in the medium to total labelled PGs (in medium and cell layer) was calculated and showed a delayed secretion of PGs in *Cant1*$^{-/-}$ chondrocytes. Data are reported as mean ± SD and significance was determined by Student's *t*-test, * $P < 0.05$; $n = 3$.

Please cite this article as: C. Paganini, L. Monti, R. Costantini, et al., Calcium activated nucleotidase 1 (CANT1) is critical for glycosaminoglycan biosynthesis in cartilage and endoc..., Matrix Biology, https://doi.org/10.1016/j.matbio.2018.11.002

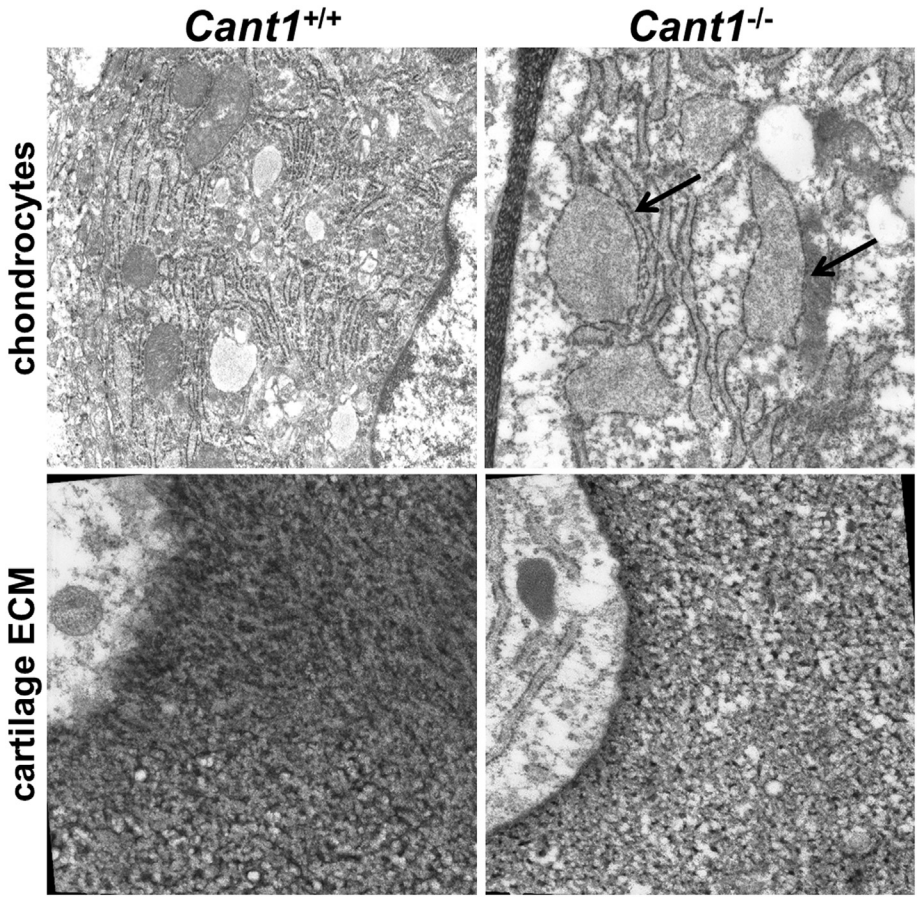

Fig. 11. ER enlargement is present in *Cant1*$^{-/-}$ cartilage. Femoral head cartilage sections of P4 *Cant1*$^{-/-}$ and *Cant1*$^{+/+}$ mice were analysed by TEM. In *Cant1*$^{-/-}$ samples the presence of ER enlargement in chondrocytes (arrows) and a less dense cartilage ECM compared with wild type sections were observed. Three animals for each genotype were analysed. Magnification in chondrocyte images: 12,000× and in cartilage images: 20,000×.

(Suppl. Table 2). These results suggested that the UPR was not activated in *Cant1*$^{-/-}$ chondrocytes.

To confirm these data at the protein level, we analysed the expression of Binding immunoglobulin Protein (BiP), a master regulator of the UPR, and of Activating Transcription Factor 4 (ATF4), a crucial UPR transcription factor, by western blot of cell lysates from *Cant1*$^{-/-}$ and wild type primary rib chondrocyte cultures. Western blots showed no difference in the levels of BiP and ATF4 between *Cant1*$^{-/-}$ and wild type cells (Fig. 12A, B, C), supporting the expression studies.

The activation of the Inositol-Requiring Enzyme 1 (IRE1) branch of UPR results in splicing of X-box binding protein 1 (Xbp1) mRNA to the Xbp1s form that is translated into a transcription factor [20]. In both *Cant1*$^{-/-}$ and wild type chondrocytes only the unspliced form of Xbp1 was found (Fig. 12D), providing a further proof that UPR was not activated in *Cant1*$^{-/-}$ chondrocytes.

Overall, these results demonstrated that ER stress was not present in *Cant1*$^{-/-}$ mice, even though ER enlargement and delayed PG secretion were observed (Figs. 10, 11).

Discussion

The molecular mechanisms underlying the genetic diseases are often quite complex and involve deregulation and misfunction of several genes. Even for monogenic disorders understanding the genotype to phenotype correlation is difficult when the gene involved is poorly understood. A *Cant1*$^{-/-}$ mouse was generated by the excision of exon 3 and 4 encoding for the active site of the enzyme in order to define the physiological role of CANT1 and to better understand the pathophysiology of DBQD1 (Fig. 1). The chondrodysplastic phenotype in mutant mice recapitulated that of the DBQD1 patients. The skeletal growth of mutant mice was reduced

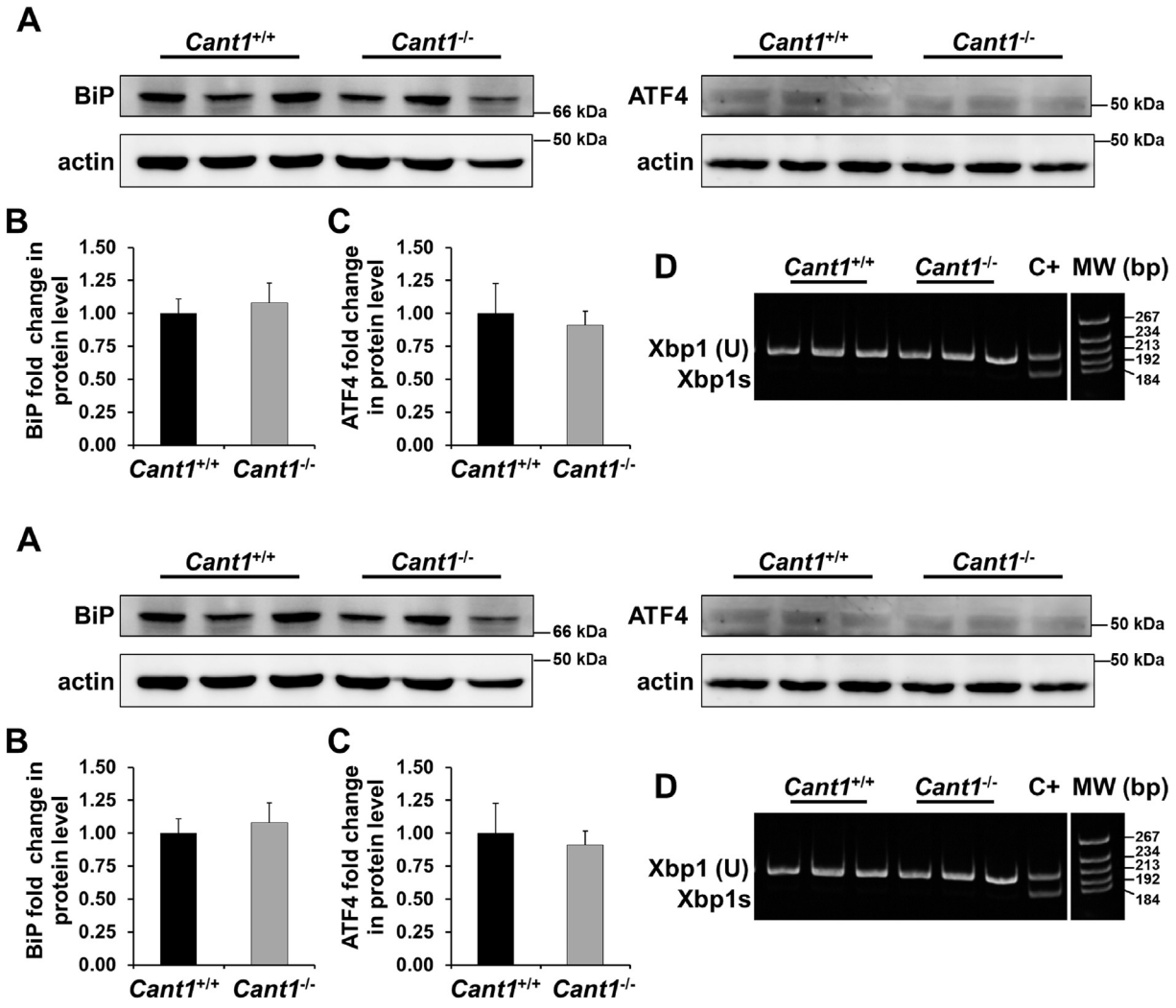

Fig. 12. Canonical ER stress is not present in *Cant1*$^{-/-}$ chondrocytes. (A) BiP and ATF4 western blot of *Cant1*$^{-/-}$ and *Cant1*$^{+/+}$ chondrocytes. Actin was used as internal control and data are representative of three independent experiments. (B) BiP protein level of *Cant1*$^{-/-}$ and *Cant1*$^{+/+}$ chondrocytes. The intensity of the wild type band was set to one and the expression of mutant samples was expressed as fold change. Data are representative of three experiments and reported as mean ± SD. Significance was determined by Student's *t*-test, $P > 0.05$; $n = 3$. (C) ATF4 protein level of *Cant1*$^{-/-}$ and *Cant1*$^{+/+}$ chondrocytes. The intensity of the wild type band was set to one and the expression of mutant samples was expressed as fold change. Data are representative of three experiments and reported as mean ± SD. Student's t-test was performed, $P > 0.05$; n = 3. (D) The spliced form of Xbp1 (Xbp1s) was analysed by RT-PCR and results were separated on acrylamide gel. Only the unspliced form of Xbp1 (U) was present in both *Cant1*$^{-/-}$ and *Cant1*$^{+/+}$ chondrocytes demonstrating that ER stress was not present. Positive control (C+): wild type chondrocytes incubated with tunicamycin overnight to induce ER stress showed both unspliced and spliced form of Xbp1.

compared with wild types and a "delta phalanx", a typical hand abnormality described in DBQD1 patients [8], was present at the extremities of *Cant1*$^{-/-}$ mice (Fig. 3).

Endochondral ossification defects

Morphometric analysis of long bones demonstrated reduced size and growth retardation in mutant mice (Fig. 4). In *Cant1*$^{-/-}$ mice, the height and area of the proliferative and hypertrophic zones of the growth plate were markedly reduced (Table 1). Chondrocyte proliferation was increased in *Cant1*$^{-/-}$ mice compared with the wild type animals at P7 and P14, whilst a higher percentage of apoptotic chondrocytes was only detected in the proliferative zone of P7 *Cant1*$^{-/-}$ mice (Fig. 6). Thus, the high chondrocyte proliferation rate in *Cant1*$^{-/-}$ mice was balanced by the increased apoptosis in the first week of life when significant differences in growth plate morphology were observed.

Please cite this article as: C. Paganini, L. Monti, R. Costantini, et al., Calcium activated nucleotidase 1 (CANT1) is critical for glycosaminoglycan biosynthesis in cartilage and endoc..., Matrix Biology, https://doi.org/10.1016/j.matbio.2018.11.002

During hypertrophy, chondrocytes undergo terminal differentiation and their height and volume increase fourfold and tenfold, respectively [16,17]. In *Cant1*$^{-/-}$ mice we observed an impairment of the terminal chondrocyte differentiation at P7, P14 and P21, indicated by the decreased height of the most terminal hypertrophic chondrocytes compared with wild type animals (Table 1).

The growth plate defects described in *Cant1*$^{-/-}$ mice are consistent with the putative role of CANT1 in GAG biosynthesis. A disorganized growth plate as well as alterations in the orientation of chondrocyte columns and in chondrocyte function has previously been described in animal models with altered synthesis, length or sulfation of GAGs [21–24]. Thus, we speculate that the structural defects of PGs present in *Cant1*$^{-/-}$ ECM can lead to altered binding of growth factors, thus increasing the proliferation of growth plate chondrocytes and impairing chondrocyte differentiation. Alternatively, the high cell proliferation rate could be a compensative process in order to restore defects caused by impaired terminal differentiation of chondrocytes.

Glycosaminoglycan synthesis defects

Since PGs play a crucial role in the cartilage growth plate development and homeostasis [25], we therefore investigated the role of CANT1 in PG biosynthesis using mouse tissues and primary cultures of rib chondrocytes from *Cant1* mutant and wild type mice. *Cant1*$^{-/-}$ chondrocytes synthesised less PGs compared with the wild type cells both *in vitro* and *in vivo* (Fig. 7); moreover, GAG chains in the *Cant1*$^{-/-}$ chondrocytes were smaller in size and oversulfated compared with wild type controls (Fig. 8A, 9). Increased GAG sulfation was further confirmed in the cartilage of mutant mice (Fig. 8B). The defects in different intracellular steps of GAG biosynthesis caused a reduction of PG secretion in *Cant1*$^{-/-}$ chondrocytes compared with wild type cells (Fig. 10). Interestingly, we demonstrated that in the absence of CANT1, GAG chains are oversulfated both *in vitro* and *in vivo,* even though increased expression of sulfotransferases was excluded by microarray analysis (Suppl. Table 1). Thus, we postulate that the oversulfation of chondroitin sulfate chains in cartilage of mutant mice is caused by the delay of PG secretion. In particular, we hypothesise that PGs spend more time in the Golgi apparatus of the *Cant1*$^{-/-}$ chondrocytes, where sulfotransferases have more time to catalyse GAG sulfation. This observation parallels what has been observed in the dominant forms of Osteogenesis Imperfecta, in which several glycine substitutions in type I collagen triple helix cause a delay in triple helix folding, allowing a longer activity of hydroxylases and glycosyltransferases of the ER and leading to increased level of post-translational modifications [26,27].

Reduced PG synthesis detected in mutant mice was previously observed in fibroblast cultures from DBQD1 patients [11], thus confirming the phenotypic similarities of *Cant1*$^{-/-}$ mice with the disorder in humans at the biochemical level. Overall, these data provide a definitive evidence of CANT1 involvement in PG biosynthesis in cartilage.

ER enlargement and potential cellular stress

To further investigate the molecular basis of the defect in PG secretion, sections of mutant cartilage were analysed by TEM. *Cant1*$^{-/-}$ chondrocytes showed dilated ER cisternae with retained electrodense material, suggesting intracellular protein retention (Fig. 11). This finding further validated *Cant1*$^{-/-}$ mice as a model of DBQD1, since ER enlargement has previously been reported in patients' fibroblasts [8]. Delayed PG secretion and ER enlargement suggested that ER stress might contribute to the skeletal phenotype. ER stress often triggers a cell response, the UPR, involving the expression of specific transcription factors and chaperones [28]. However, the expression of the main ER stress markers was normal in *Cant1*$^{-/-}$ mice (Suppl. Table 2). This finding was supported by normal protein levels of BiP, a master regulator of the UPR [28], and of ATF4 (downstream of Protein kinase R-like ER Kinase, PERK); in addition the alternatively spliced form of Xbp1 mRNA (downstream of IRE1) was not detected in *Cant1*$^{-/-}$ cartilage (Fig. 12). Overall, these data support ER enlargement without canonical ER stress in chondrocytes, when CANT1, a Golgi protein, is impaired. This observation is consistent with previous data from an Osteogenesis Imperfecta mouse model bearing the G610C substitution in the procollagen α2(I) chain whereby the resulting procollagen triple helix misfolding leads to an unusual form of cellular stress not linked to the conventional UPR [29].

Altered ER structures have been described as a consequence of defects in proteins involved in the ER/Golgi trafficking. Mutations affecting trafficking protein particle complex 2 (TRAPPC2 or Sedlin) and dymeclin, thought to have roles in protein transport between ER and Golgi, also cause nonlethal skeletal dysplasias, X-linked spondyloepiphyseal dysplasia tarda and Dyggve-Melchior-Clausen syndrome, respectively [30–32]. Therefore, ER swelling does not result exclusively from structural defects in the secreted matrix proteins [18], but also from defects in the components of the secretory pathway and in the cross-talk between ER and Golgi. Interestingly, ER stress has not been described in sedlin or dymeclin mutant cells [30,31].

Chondrocytes produce several highly modified PGs, the most abundant of which is aggrecan, a

Please cite this article as: C. Paganini, L. Monti, R. Costantini, et al., Calcium activated nucleotidase 1 (CANT1) is critical for glycosaminoglycan biosynthesis in cartilage and endoc..., Matrix Biology, https://doi.org/10.1016/j.matbio.2018.11.002

very large macromolecule that contains more than a hundred GAG chains whose synthesis occurs in the Golgi [19,33]. Therefore, it is not surprising that defects in GAG synthesis may result in defects in organelle autoregulation leading to altered organelle structures.

Role of glycosaminoglycan defects in DBQD1 pathology

The finding of defective GAG synthesis in the pathogenesis of DBQD1 comports well with the current understanding of cartilage function. In normal cartilage, the chondrocytes synthesise and deposit large amounts of sulphated PGs in the extracellular matrix, where these macromolecules are crucial for the mechanical and biological functions of cartilage.

PGs constitute a major regulatory point of chondrocyte activity providing structural support to chondrocytes and creating a milieu, which affects diffusion of growth factors, signaling molecules and nutrients [33,34]. It is well known that structural defects in the ECM macromolecules affect the properties of tissues, including cartilage. Interestingly, in transgenic mice expressing a mutated form of thyroglobulin, a protein not expressed in the growth plate, it has been demonstrated that mutant protein retention and intracellular stress *per se* directly disturb chondrocyte performance without altering secretion and assembly of ECM proteins [35]. This observation suggests that cell performance is not only affected by structural defects in ECM proteins, but also by proteins (including enzymes and transporters) involved in post-translational modifications, folding and quality control. Furthermore, increased post-translational modifications and delayed type I collagen secretion have been demonstrated in recessive forms of Osteogenesis Imperfecta, where the enzymes involved in collagen folding and post-translational modifications are defective (*i.e.* cartilage associated protein, prolyl 3-hydroxylase, serpin H1 and FKBP65) [26,36]. We therefore postulate that the pathomolecular mechanism of DBQD1 comprises of an intracellular (GAG synthesis defects, ER/Golgi enlargement and impaired PG secretion) and extracellular (PG structural defects) component.

It is interesting to note that the clinical abnormalities in DBQD1 are restricted to cartilage and bone, even though *CANT1* appears to be widely expressed. Cartilage-producing cells are thought to have a vastly greater requirement of sugars for PG synthesis than any other tissue [37] and the physiological consequences of altered GAG synthesis in such tissue may be much more profound. However, we cannot exclude that other tissues may have alternative strategies for their modest Golgi glycosylation requirements, including different nucleotidases.

To conclude, the *Cant1*$^{-/-}$ mouse is an appropriate animal model of DBQD1 and it recapitulates the typical clinical features observed in DBQD1 patients. Moreover, GAG synthesis is decreased and PG secretion is reduced in mutant cartilage, demonstrating that CANT1 plays a role in PG metabolism. The PG defects cause deregulated chondrocyte proliferation and maturation in the cartilage growth plate. Further studies of the cellular pathways involved in the defective ER Golgi cross-talk and organelle autoregulation will be crucial in order to elucidate the molecular basis of the disease and to pave the way for developing therapeutic strategies for this rare chondrodysplasia.

Materials and methods

Preparation of the gene targeting vector

The short and long arm of the gene targeting vector were generated by PCR amplification of the *Cant1* gene targeting vector CANT1 PG00123_Y_1_H12 from Helmholtz Zentrum Munchen, Germany (https://www.eummcr.org). The sequence of the gene targeting vector is available at https://www.i-dcc.org/imits/targ_rep/alleles/10068/targeting-vector-genbank-file. The main components of the vector are the 5′ and 3′ homology arms that mediate homologous recombination at the murine *Cant1* locus and a central targeting cassette that disrupts gene function and reports gene expression with a lacZ reporter. The targeting cassette is flanked by FRT recombination sites, which allows the removal of the targeting cassette with Flp recombinase. In addition, exon 3 and 4 of the murine *Cant1* gene are flanked by a pair of loxP recombination sites for conditional gene inactivation by deleting the two exons with Cre recombinase.

The 5′arm containing the 5′ Cant1 homologous region, exon 2 and an FRT recombination site was amplified by high fidelity PCR (PfuUltra II fusion HS DNA Polymerase, Agilent Technologies). The sense and antisense primers were designed according to the nucleotide sequence of the CANT1 PG00123_Y_1_H12 plasmid vector and contained the *HindIII* restriction site (5′-AGCAGG**AAGCTT**TGACTTGGTGAGGCTCCC-3′ and 5′-TCACAA**AAGCTT**CTTCTGTTAGTCCCAACCC-3′, respectively). The amplified 4.1 kb 5′ arm after *HindIII* (Promega) digestion was cloned in the *HindIII* multiple cloning site 1 of the NTKV1902 vector (pKO Scrambler NTKV, Stratagene), a gene targeting vector containing the herpes simplex *thymidine kinase* (*Tk*) gene, driven by the polyoma virus thymidine kinase (MC1) promoter, and *neomycin* gene, driven by the phosphoglycerate kinase (PGK)

Please cite this article as: C. Paganini, L. Monti, R. Costantini, et al., Calcium activated nucleotidase 1 (CANT1) is critical for glycosaminoglycan biosynthesis in cartilage and endoc..., Matrix Biology, https://doi.org/10.1016/j.matbio.2018.11.002

promoter, for negative and positive selection, respectively.

Likewise, the 3′arm was amplified by high fidelity PCR using sense and antisense primers containing the *SacII* restriction site (5′-CTGGAT**CCGCGG**GTACCGCGTCG-3′ and 5′-ACAT-GA**CCGCGG**CTGCTTCTGGGGTTGG-3′, respectively). Then the 7.5 kb 3′arm containing a FRT site and exon 3 and 4 flanked by loxP sites was cloned in pBluescript II KS (pBS3′arm). The c.905G > A transition causing the R302H substitution in *Cant1* was introduced in the pBS3'arm by site-directed mutagenesis with the QuickChange II XL Site-Directed Mutagenesis Kit (Agilent Technologies), according to the manufacturer instructions. Finally, the mutated 3'arm was cloned in the *SacII* restriction site of the multiple cloning site 2 of the gene targeting vector.

Generation of Cant1 targeted embryonic stem cells and mice

Electroporation of the linearized targeting vector (Fig. 1A) into ES cells with C57Bl/6J × 129/SV background was performed by the Core Facility for Conditional Mutagenesis (Dibit, San Raffaele Hospital, Milan, Italy) and was followed by transfected ES cells exposure to G418 and ganciclovir. Selected colonies were isolated and screened by Southern blot analysis for the recombinant allele. Correct 5′ targeting was confirmed by DNA digestion with *ScaI* and membrane hybridization with a PCR probe spanning *Cant1* exon 2. Correct 3′ targeting was confirmed by DNA digestion with *KpnI* and membrane hybridization with a PCR probe spanning a *Cant1* exon 4 fragment. The 5′ end probe detected a 13.9 kb *ScaI* fragment specific for the targeting allele and a 11.6 kb fragment for the wild-type allele; the 3′ end probe detected a 12.8 kb *KpnI* fragment for the targeted allele and a 14.2 kb fragment for the wild-type allele (Fig. 1B). The presence of the mutation was confirmed by direct sequencing and two positive clones were injected in C57Bl/6J × 129/SV mouse blastocysts. The resulting chimeric male mice were mated with a Flp recombinase transgenic strain (B6.129S4-Gt(ROSA)26Sor$^{tm1(FLP1)Dym}$, Jackson Laboratory) to delete the frt-flanked neomycin selection cassette. Offspring heterozygous for the mutation were used to generate the *Cant1* p.R302H knock-in mice (*Cant1*$^{R302H/R302H}$).

To generate the *Cant1* knock-out strain (*Cant1*$^{-/-}$), heterozygous knock-in animals were mated with a Cre mouse strain (B6.FVB-Tg(EIIa-cre)C5379Lmgd) to delete exon 3 and 4 that were flanked by the loxP recombination sites (Fig. 1C).

Animal care

Animals were bred with free access to water and standard pelleted food. Care and use of mice complied with relevant animal welfare institutional guidelines and protocols were approved by the Animal Care and Use Committee of the University of Pavia and the Ministry of Health (Licence n. 95/2017-PR).

Mouse genotyping.

Mice were genotyped by PCR using genomic DNA from mouse tail clips. PCR primers to genotype homozygous knock-in mice (*Cant1*$^{R302H/R302H}$ mice) from heterozygous and wild type animals were CAN18 (5'-CCTGTGGAGGTTGGGATTCC- 3′) and CAN47 (5'-CAAATGAGGCCCAGGAAGTG- 3′), whilst CAN18, CAN47 and CANFRT3 (5'-AAATGAT-CACTGCCTTGTCCTG- 3′) primers were used for genotyping homozygous knock-out mice (*Cant1*$^{-/-}$ mice) from heterozygous and wild type animals.

Real time PCR

Total RNA was extracted from skin by QIAzol® Lysis Reagent (QIAGEN) according to manufacturer instructions. RNA (2 μg) was reverse transcribed using the High Capacity cDNA Reverse Transcription kit (Applied Biosystems) following manufacturer's recommendation. Relative quantitative real time PCR experiments were performed using the Quanti-Fast SYBR Green PCR Kit (QIAGEN) with QuantiTect Primer Assay (QIAGEN) for *Cant1* (QT01041789) and TATA box binding protein (QT00198443) as housekeeping gene for expression normalization. Each sample was run in triplicate in 96 well plates in three independent experiments with the MX3000P (Stratagene) apparatus. Three mice for each genotype were analysed and relative *Cant1* expression was determined with the ΔΔCt method.

Skeletal staining with alcian blue and alizarin red

Skeletal characterization of mice was performed by double staining with alcian blue and alizarin red to stain cartilage and bone, respectively, as described previously [38]. Images of skeletal preparations were acquired by a Leica DFC425 C digital camera connected to a Leica M165 FC stereomicroscope. Skeletal morphometric analysis were performed using the LAS 4.5 software (Leica) by two different observers blinded to genotype.

X-ray analysis

A Faxitron MX-20 cabinet X-ray system (Faxitron Bioptics) was used for X-ray images of mice. The exposure was set to 27 kV for 19 s with 2-fold magnification for adult mice. Kodak DirectView Elite CR System (Carestream Health) was used to capture X-ray images.

Please cite this article as: C. Paganini, L. Monti, R. Costantini, et al., Calcium activated nucleotidase 1 (CANT1) is critical for glycosaminoglycan biosynthesis in cartilage and endoc..., Matrix Biology, https://doi.org/10.1016/j.matbio.2018.11.002

Histological staining and morphometric analysis

For histological study, hind limbs were dissected immediately after sacrifice, fixed with 10% formalin in PBS (Sigma-Aldrich) and processed for light microscopy according to standard procedures after decalcification in 14% ethylenediaminetetraacetic acid (EDTA) pH 7.1 at room temperature for 2–4 weeks depending on the age of the mice.

For histomorphometric analysis, slides were stained with toluidine blue as described previously [21] and images of sections were acquired using a DM5500 B microscope (Leica) connected to a Leica DFC 480 camera. All morphometric measurement were performed by LAS V4.5 software (Leica). The resting, proliferative and hypertrophic zones were defined on the basis of cell morphology as reported in literature [39]. To determine the height of each zone at least five measurements per zone per section were performed. To determine the number of cells per column and the height of columns in different zones at least 20 columns per zone per sections were analysed. An average of five sections per animal was considered. All measurements were performed by two different observers blinded to genotype.

Proliferation and apoptosis analysis

For immunohistochemical detection of proliferative cells in the growth plate, mice were intraperitoneally injected with 100 mg/kg 5′-bromo-2′-deoxyuridine (BrdU) (Sigma-Aldrich) as previously reported [39]. Mice were sacrificed 2 h post injection; hind limbs were harvested and processed according to standard procedure. 6 μm sections were analysed using the BrdU Staining Kit (Invitrogen) according to the manufacturer suggestions. Images of sections were acquired using a DM5500 B microscope (Leica) connected to a Leica DFC 480 camera. All measurements were performed using LAS V4.5 software (Leica).

For the immunohistochemical detection of apoptotic chondrocytes in the growth plate, the DeadEnd™ Fluorometric TUNEL System (Promega) was used on 6 μm sections according to manufacturer's instructions. Images of sections were captured by a fluorescence microscope Axioimager.Z2 (Zeiss) and all measurements were performed using Image J software.

Proliferating and apoptotic cell measurements were performed by two different observers blinded to genotype.

Primary chondrocyte cultures

To establish primary chondrocyte cultures, thoracic cage of P4 mice was harvested and digested with 2 mg/ml collagenase type II (Invitrogen) in Dulbecco's modified Eagle's medium (DMEM) (Sigma-Aldrich) at 37 °C for 90 min. The cartilage was dissected from each rib under the microscope and digested with 2 mg/ml collagenase type II at 37 °C for 3 h. The released chondrocytes were plated and cultured in DMEM with 10% foetal calf serum (FCS) (EuroClone) at 37 °C in a humidified atmosphere containing 5% CO_2.

Metabolic labelling of chondrocyte cultures and PG synthesis analysis

Chondrocyte cultures were preincubated with or without 1 mM *p*-nitrophenyl β-D-xylopyranoside (Sigma-Aldrich) in minimal essential medium (MEM) (Sigma-Aldrich) containing 250 μM cold Na_2SO_4 without FCS at 37 °C in 5% CO_2 for 2 h. Cells were then labelled with 50 μCi/ml $Na_2[^{35}SO_4]$ (38.8–59.2 TBq/mmol, PerkinElmer) in the same medium for 24 h as described previously [40]. At the end of the labelling period, an equal volume of 100 mM sodium acetate buffer, pH 5.8, containing 8 M urea, 4% Triton X-100, 20 mM EDTA, 20 mM N-ethylmalemide (NEM), 0.1 M 6-aminocaproic acid and 1 mM phenylmethylsulfonyl fluoride (PMSF) was added to the medium. The cell layer was lysed in 50 mM sodium acetate buffer, pH 5.8, containing 2 M urea and 2% Triton X-100, an aliquot was used to determine the protein content by the BCA Protein Assay (Pierce) and the rest was added to the medium. Samples were loaded on 1 ml DEAE Sephacel columns and, after column washing with 50 mM sodium acetate, pH 6.0, containing 8 M urea, 0.15 M NaCl, 0.5% Triton X-100, 10 mM EDTA, 10 mM NEM, 0.1 M 6-aminocaproic acid and 0.5 mM PMSF, PGs were eluted with 1 M NaCl in the same buffer. The PGs were then precipitated with 9 volumes of 96% ethanol at 4 °C overnight and centrifuged at 17,300 ×*g* at 4 °C for 50 min. The pellet was washed with 70% ethanol and then solubilized in water. PGs were quantified by measuring the ^{35}S-activity using a liquid scintillation counter and normalised to the protein content.

Size exclusion chromatography of GAG chain

Labelled PGs synthesised by chondrocytes and purified as described above were β-eliminated by alkaline digestion with 0.125 M NaOH followed by reduction with 1 M $NaBH_4$ at room temperature overnight to release GAG chains. After neutralization with acetic acid, samples were lyophilized and dissolved in 50 mM sodium acetate, pH 6.0, containing 4 M guanidinium chloride (GuHCl) and 0.5% Triton X-100. Samples were loaded on a Superose 6 10/300GL column (GE Healthcare) and eluted in the same buffer at 0.2 ml/min. Fraction of 0.4 ml were

Please cite this article as: C. Paganini, L. Monti, R. Costantini, et al., Calcium activated nucleotidase 1 (CANT1) is critical for glycosaminoglycan biosynthesis in cartilage and endoc..., Matrix Biology, https://doi.org/10.1016/j.matbio.2018.11.002

collected and ^{35}S-activity was measured by scintillation counting.

Analysis of PG secretion

In a pulse chase experiment, primary chondrocytes were labelled with MEM without FCS containing 100 μCi/ml $Na_2[^{35}SO_4]$ at 37 °C in 5% CO_2 for 2 h. At the end of the labelling period, the medium was removed, cells were washed with MEM without FCS containing 2.5 mM cold sulfate and incubated in the same medium for different chase times (0, 0.5, 2.5 and 5 h) as described previously [41]. At each time point, the cell layer and medium were collected separately. To each medium the same volume of 0.2 M sodium acetate, pH 5.8, containing 8 M GuHCl, 2% Triton X-100 and protease inhibitors (4 mM EDTA, 10 mM benzamidine, 1.9 mM NEM) was added, whilst the cell layer was scraped in 0.1 M sodium acetate, pH 5.8, containing 4 M GuHCl, 2% Triton X-100 and protease inhibitors. Each medium and cell layer were desalted to remove free ^{35}S-sulfate with PD Miditrap G-25 columns (GE Healthcare) equilibrated and eluted with 50 mM sodium acetate, pH 6.0, containing 4 M GuHCl and 0.5% Triton X-100. The V_0 from each gel filtration column was collected and ^{35}S-activity was measured by scintillation counting. For each time point, the percentage of ^{35}S-activity in the medium to the total counts (medium and cell layer) was calculated.

Glycosaminoglycan content assay

GAG content was measured in the femoral head cartilage of P4 mice using the dimethylmethylene blue (DMMB) assay [42]. Briefly, femoral head cartilages were dissected and digested with 300 μl of 1.67 mg/ml proteinase K (Sigma-Aldrich) in 0.1 M ammonium acetate, pH 7.35, containing 5 mM EDTA at 55 °C overnight. Then samples were incubated at 100 °C for 10 min to denature proteinase K. The DMMB assay was performed on 60 μl of digested samples adding 1 ml of DMMB solution (10.7 mg/l DMMB (Sigma-Aldrich) in 55 mM formic acid, pH 3.3). Sample absorbance was read at 520 nm immediately after DMMB addition. To determine the GAG concentration, a standard curve containing up to 6 μg chondroitin sulfate in the sample buffer was used. GAG content was normalised to DNA amount analysed on digested samples by the Quant-iT™ PicoGreen® dsDNA Assay Kit (Invitrogen), according to the manufacturer's instructions.

Proteoglycan sulfation analysis

For PG sulfation analysis, GAGs were extracted from cartilage and primary chondrocyte cultures. GAGs from femoral head cartilage of P4 mice were obtained by proteinase K digestion of the tissue as described above. Chondrocyte cultures were incubated with basal medium without FCS at 37 °C in 5% CO_2 for 24 h. Then, the medium was made 0.1 M sodium acetate, pH 5.6, 5 mM EDTA and 5 mM cysteine and 20 U of papain (Sigma) were added, while the cell layer was scraped in papain digestion buffer (0.1 M sodium acetate, pH 5.6, 5 mM EDTA and 5 mM cysteine) and digested with 20 U of papain. Digestion was performed at 65 °C overnight.

Papain and proteinase K in all digested samples (from cell cultures or from femoral head cartilage) were inactivated at 100 °C for 10 min and released GAGs were recovered and analysed by HPLC after 2-aminoacridone derivatization as previously described [43].

Transmission electron microscopy analysis

Femoral head cartilages were processed for transmission electron microscopy as reported previously [44]. Briefly, cartilage was dissected and fixed with 2% (v/v) glutaraldehyde and 0.7% (w/v) ruthenium hexamine trichloride (RHT) in 0.1 M cacodylate buffer, pH 7.4, at room temperature for 3 h. The samples were then washed with 0.7% RHT in 0.1 M cacodylate buffer, pH 7.4. Samples were post-fixed in 0.7% RHT and 2% (w/v) osmium tetroxide (OsO_4) in 0.1 M cacodylate buffer at room temperature for 2 h, rinsed in distilled water, dehydrated in ethanol and infiltrated with LR White acrylic resin. Thin sections (60–70 nm tick) were cut on a Reichert OM-U3 ultramicrotome, stained with saturated aqueous uranyl acetate followed by lead citrate and observed with a Zeiss EM900 electron microscope at 80 kV.

Microarray analysis

Total RNA was extracted from rib cartilage for microarray analysis. Thoracic cage of P4 mice was dissected, digested with 2 mg/ml collagenase type II in DMEM at 37 °C for 90 min and costal cartilages were harvested from each rib under the dissection microscope. The RNA then was purified from costal cartilage using RNeasy Plus Mini kit (QIAGEN) according to manufacturer's protocol. RNA quality was analysed by Agilent 2100 Bioanalyzer (Agilent Technologies) using the RNA Nano chip kit (Agilent Technologies), while RNA concentration was determined by the NanoDrop ND-1000 spectrophotometer.

The GeneChip® Mouse Genome 430A 2.0 microarray (Affymetrix) was used and processed with the GeneChip® 3' IVT PLUS Reagent Kit and the GeneChip® Hybridisation Wash and Stain Kit. The microarray analysis was performed by the Center for Genome Research of the University of Modena and Reggio Emilia, Italy. The fold change threshold between *Cant1*$^{-/-}$ and *Cant1*$^{+/+}$ mice was set ±2.

Please cite this article as: C. Paganini, L. Monti, R. Costantini, et al., Calcium activated nucleotidase 1 (CANT1) is critical for glycosaminoglycan biosynthesis in cartilage and endoc..., Matrix Biology, https://doi.org/10.1016/j.matbio.2018.11.002

RT-PCR analysis

Total RNA was extracted from chondrocytes by QIAzol® Lysis Reagent (QIAGEN) according to manufacturer instructions. Then cDNA was obtained from purified RNA by SuperScript™ IV First-Strand Synthesis System (Invitrogen) in accordance with manufacturer's protocol. The presence of the Xbp1 spliced form was analysed by RT-PCR as described in literature [16] using the following primers: XBP1 forward (5′-GAACCAGGAGTTAAGAACACG- 3′) and XBP1 reverse (5′-AGGCAACAGTGTCA-GAGTCC- 3′).

Briefly, 5 μl cDNA was subjected to PCR as follows: 3 min at 95 °C, followed by 35 cycles of 95 °C for 40 s, 60 °C for 45 s and 72 °C for 40 s and then 10 min of extension at 72 °C. PCR products were separated by electrophoresis on 8% acrylamide gel in TBE buffer. The Xbp1 unspliced form band was 205 bp long, while the Xbp1 spliced form band was 179 bp long.

Western blot analysis

For western blot analysis, 2×10^6 chondrocytes were plated in 60 mm diameter culture dishes with DMEM and 10% FCS and incubated at 37 °C in 5% CO_2. After 3 days, the cells were scraped in PBS and centrifuged at 1,200 ×*g* for 15 min. The cell pellets were lysed and analysed by western blot as previously described [45]. SDS-PAGE was carried out on 10% polyacrylamide gels. Primary antibodies to BiP (rabbit monoclonal antibody, Cell Signaling), to ATF-4 (rabbit monoclonal antibody, Cell Signaling), to actin (goat polyclonal antibody, Santa Cruz Biotechnology) and the appropriate HRP secondary antibody (goat anti-rabbit polyclonal antibody, Cell Signaling and donkey anti-goat polyclonal antibody, Santa Cruz Biotechnology) were used. The ImageQuant TL software was used for densitometry analysis and the intensity of the wild type band was set to 1 and the expression of mutant samples was expressed as fold change.

Statistical analysis

Statistical analysis was performed using Microsoft Excel software. All values are expressed as mean ± standard deviation (SD). Statistical difference between different groups was evaluated using Student's *t*-test and a p-value < 0.05 was considered statistically significant.

Acknowledgments

We thank Drs. Lorenza Ronfani, Rosanna Rinaldi and Luisa Pintonello from the Core Facility for Conditional Mutagenesis (CFCM), Biotechnology Department (Dibit), San Raffaele Scientific Institute, Milan, Italy, for electroporation of ES cells and generation of mouse chimeras. We also thank Dr. Elena Tenedini from the Center for Genome Research of the University of Modena and Reggio Emilia, Italy, for microarray experiments.

This work was supported by Fondazione Telethon (grant n. GGP11079 to AR), European Commission Seventh Framework Programme under grant agreement n. 602300 (SYBIL) (to JMS, VC-D, KAP, AF and AR) and MIUR "Dipartimenti di Eccellenza 2018-2022" (to AF and AR).

Author contributions

CP, LM and AR designed and performed the majority of the experiments. RC, RB and SL performed the rest of the experiments. CP, BGG, KAP and AR performed growth plate studies. MB did electron microscopy. CH and VC-D provided medical background on the disease. KT and JMS analysed microarray data. CP, MB, VC-D, KAP, AF and AR analysed data, wrote and reviewed the manuscript.

Declarations of interest

None.

Appendix A. Supplementary data

Supplementary data to this article can be found online at https://doi.org/10.1016/j.matbio.2018.11.002.

Received 21 September 2018;
Received in revised form 5 November 2018;
Accepted 5 November 2018
Available online xxxx

Keywords:
Calcium activated nucleotidase 1;
Cartilage;
Glycosaminoglycan;
Growth plate;
Proteoglycan;
Skeletal dysplasia

†These authors contributed equally.

Abbreviations used:
BrdU, 5′-bromo-2′-deoxyuridine; CANT1, calcium activated nucleotidase 1; DBQD1, Desbuquois dysplasia type 1; DMMB, dimethylmethylene blue; GAG, glycosaminoglycan; PG, proteoglycan; β-D-xyloside, *p*-nitrophenyl-β-D-xylopyranoside; ΔDi-0S, 3-*O*-β(D-gluc-4-eneuronosyl)-*N*-

acetylgalactosamine; ΔDi-4S and ΔDi-6S, derivatives of ΔDi-0S with a sulfate at the 4 or 6 position of hexosamine moiety respectively.

References

[1] H.E. Bulow, O. Hobert, The molecular diversity of glycosaminoglycans shapes animal development, Annu. Rev. Cell Dev. Biol. 22 (2006) 375–407.

[2] D.H. Vynios, Metabolism of cartilage proteoglycans in health and disease, Biomed. Res. Int. 2014 (2014) 452315.

[3] R.V. Iozzo, L. Schaefer, Proteoglycan form and function: a comprehensive nomenclature of proteoglycans, Matrix Biol. 42 (2015) 11–55.

[4] S. Mizumoto, K. Sugahara, Bone and skin disorders caused by a disturbance in the biosynthesis of chondroitin sulfate and dermatan sulfate, in: K. Nikos (Ed.), Extracellular Matrix: Pathobiology and Signaling, Walter de Gruyter, Berlin, Germany 2012, pp. 97–118.

[5] S. Mizumoto, S. Yamada, K. Sugahara, Human genetic disorders and knockout mice deficient in glycosaminoglycan, Biomed. Res. Int. 2014 (495764) (2014) 495764.

[6] L. Bonafe, V. Cormier-Daire, C. Hall, R. Lachman, G. Mortier, S. Mundlos, G. Nishimura, L. Sangiorgi, R. Savarirayan, D. Sillence, J. Spranger, A. Superti-Furga, M. Warman, S. Unger, Nosology and classification of genetic skeletal disorders: 2015 revision, Am. J. Med. Genet. A 167 (12) (2015) 2869–2892.

[7] L. Faivre, V. Cormier-Daire, A.M. Eliott, F. Field, A. Munnich, P. Maroteaux, M. Le Merrer, R. Lachman, Desbuquois dysplasia, a reevaluation with abnormal and “normal” hands: radiographic manifestations, Am. J. Med. Genet. A 124A (1) (2004) 48–53.

[8] C. Huber, B. Oules, M. Bertoli, M. Chami, M. Fradin, Y. Alanay, L.I. Al-Gazali, M.G. Ausems, P. Bitoun, D.P. Cavalcanti, A. Krebs, M. Le Merrer, G. Mortier, Y. Shafeghati, A. Superti-Furga, S.P. Robertson, C. Le Goff, A.O. Muda, P. Paterlini-Brechot, A. Munnich, V. Cormier-Daire, Identification of CANT1 mutations in Desbuquois dysplasia, Am. J. Hum. Genet. 85 (5) (2009) 706–710.

[9] C. Bui, C. Huber, B. Tuysuz, Y. Alanay, C. Bole-Feysot, J.G. Leroy, G. Mortier, P. Nitschke, A. Munnich, V. Cormier-Daire, XYLT1 mutations in Desbuquois dysplasia type 2, Am. J. Hum. Genet. 94 (3) (2014) 405–414.

[10] B.U. Failer, N. Braun, H. Zimmermann, Cloning, expression, and functional characterization of a Ca(2+)-dependent endoplasmic reticulum nucleoside diphosphatase, J. Biol. Chem. 277 (40) (2002) 36978–36986.

[11] M. Nizon, C. Huber, F. De Leonardis, R. Merrina, A. Forlino, M. Fradin, B. Tuysuz, B.Y. Abu-Libdeh, Y. Alanay, B. Albrecht, L. Al-Gazali, S.Y. Basaran, J. Clayton-Smith, J. Desir, H. Gill, M.T. Greally, E. Koparir, M.C. van Maarle, S. MacKay, G. Mortier, J. Morton, D. Sillence, C. Vilain, I. Young, K. Zerres, M. Le Merrer, A. Munnich, C. Le Goff, A. Rossi, V. Cormier-Daire, Further delineation of CANT1 phenotypic spectrum and demonstration of its role in proteoglycan synthesis, Hum. Mutat. 33 (8) (2012) 1261–1266.

[12] T.M. Smith, T.L. Kirley, The calcium activated nucleotidases: a diverse family of soluble and membrane associated nucleotide hydrolyzing enzymes, Purinergic Signal 2 (2) (2006) 327–333.

[13] T.M. Smith, C.A. Hicks-Berger, S. Kim, T.L. Kirley, Cloning, expression, and characterization of a soluble calcium-activated nucleotidase, a human enzyme belonging to a new family of extracellular nucleotidases, Arch. Biochem. Biophys. 406 (1) (2002) 105–115.

[14] T. Cali, L. Fedrizzi, D. Ottolini, R. Gomez-Villafuertes, B. Mellstrom, J.R. Naranjo, E. Carafoli, M. Brini, Ca2+–activatted nucleotidase 1, a novel target gene for the transcriptional repressor DREAM (downstream regulatory element antagonist modulator), is involved in protein folding and degradation, J. Biol. Chem. 287 (22) (2012) 18478–18491.

[15] T.K. Harden, J.I. Sesma, I.P. Fricks, E.R. Lazarowski, Signalling and pharmacological properties of the P2Y receptor, Acta Physiol (Oxford) 199 (2) (2010) 149–160.

[16] M. Forouhan, K. Mori, R.P. Boot-Handford, Paradoxical roles of ATF6α and ATF6β in modulating disease severity caused by mutations in collagen X, Matrix Biol. 70 (2018) 50–71.

[17] E.B. Hunziker, R.K. Schenk, L.M. Cruz-Orive, Quantitation of chondrocyte performance in growth-plate cartilage during longitudinal bone growth, J. Bone Joint Surg. Am. 69 (2) (1987) 162–173.

[18] M.D. Briggs, P.A. Bell, K.A. Pirog, The utility of mouse models to provide information regarding the pathomolecular mechanisms in human genetic skeletal diseases: the emerging role of endoplasmic reticulum stress (review), Int. J. Mol. Med. 35 (6) (2015) 1483–1492.

[19] Y. Krishnan, A.J. Grodzinsky, Cartilage diseases, Matrix Biol. 71-72 (2018) 51–69.

[20] S.E. Patterson, C.N. Dealy, Mechanisms and models of endoplasmic reticulum stress in chondrodysplasia, Dev. Dyn. 243 (7) (2014) 875–893.

[21] B. Gualeni, M. Facchini, F. De Leonardis, R. Tenni, G. Cetta, M. Viola, A. Passi, A. Superti-Furga, A. Forlino, A. Rossi, Defective proteoglycan sulfation of the growth plate zones causes reduced chondrocyte proliferation via an altered Indian hedgehog signalling, Matrix Biol. 29 (6) (2010) 453–460.

[22] S. Hiraoka, T. Furuichi, G. Nishimura, S. Shibata, M. Yanagishita, D.L. Rimoin, A. Superti-Furga, P.G. Nikkels, M. Ogawa, K. Katsuyama, H. Toyoda, A. Kinoshita-Toyoda, N. Ishida, K. Isono, Y. Sanai, D.H. Cohn, H. Koseki, S. Ikegawa, Nucleotide-sugar transporter SLC35D1 is critical to chondroitin sulfate synthesis in cartilage and skeletal development in mouse and human, Nat. Med. 13 (11) (2007) 1363–1367.

[23] D.G. Wilson, K. Phamluong, W.Y. Lin, K. Barck, R.A. Carano, L. Diehl, A.S. Peterson, F. Martin, M.J. Solloway, Chondroitin sulfate synthase 1 (Chsy1) is required for bone development and digit patterning, Dev. Biol. 363 (2) (2012) 413–425.

[24] M. Kluppel, T.N. Wight, C. Chan, A. Hinek, J.L. Wrana, Maintenance of chondroitin sulfation balance by chondroitin-4-sulfotransferase 1 is required for chondrocyte development and growth factor signaling during cartilage morphogenesis, Development 132 (17) (2005) 3989–4003.

[25] N.B. Schwartz, M. Domowicz, Chondrodysplasias due to proteoglycan defects, Glycobiology 12 (4) (2002) 57R–68R.

[26] J.C. Marini, A. Forlino, H.P. Bachinger, N.J. Bishop, P.H. Byers, A. Paepe, F. Fassier, N. Fratzl-Zelman, K.M. Kozloff, D. Krakow, K. Montpetit, O. Semler, Osteogenesis imperfecta, Nat Rev Dis Primers 3 (2017), 17052. .

[27] R. Morello, Osteogenesis imperfecta and therapeutics, Matrix Biol. 71–72 (2018) 294–312.

Please cite this article as: C. Paganini, L. Monti, R. Costantini, et al., Calcium activated nucleotidase 1 (CANT1) is critical for glycosaminoglycan biosynthesis in cartilage and endoc..., Matrix Biology, https://doi.org/10.1016/j.matbio.2018.11.002

[28] T.G. Lewy, J.M. Grabowski, M.E. Bloom, BiP: master regulator of the unfolded protein response and crucial factor in Flavivirus biology, Yale J Biol Med 90 (2) (2017) 291–300.
[29] L.S. Mirigian, E. Makareeva, E.L. Mertz, S. Omari, A.M. Roberts-Pilgrim, A.K. Oestreich, C.L. Phillips, S. Leikin, Osteoblast malfunction caused by cell stress response to procollagen Misfolding in α2(I)-G610C mouse model of osteogenesis imperfecta, J. Bone Miner. Res. 31 (8) (2016) 1608–1616.
[30] A.B. Osipovich, J.L. Jennings, Q. Lin, A.J. Link, H.E. Ruley, Dyggve-Melchior-Clausen syndrome: chondrodysplasia resulting from defects in intracellular vesicle traffic, Proc. Natl. Acad. Sci. U. S. A. 105 (42) (2008) 16171–16176.
[31] R. Venditti, T. Scanu, M. Santoro, G. Di Tullio, A. Spaar, R. Gaibisso, G.V. Beznoussenko, A.A. Mironov, A. Mironov Jr., L. Zelante, M.R. Piemontese, A. Notarangelo, V. Malhotra, B. M. Vertel, C. Wilson, M.A. De Matteis, Sedlin controls the ER export of procollagen by regulating the Sar1 cycle, Science 337 (6102) (2012) 1668–1672.
[32] G.E. Tiller, V.L. Hannig, D. Dozier, L. Carrel, K.C. Trevarthen, W.R. Wilcox, S. Mundlos, J.L. Haines, A.K. Gedeon, J. Gecz, A recurrent RNA-splicing mutation in the SEDL gene causes X-linked spondyloepiphyseal dysplasia tarda, Am. J. Hum. Genet. 68 (6) (2001) 1398–1407.
[33] C. Kiani, L. Chen, Y.J. Wu, A.J. Yee, B.B. Yang, Structure and function of aggrecan, Cell Res. 12 (1) (2002) 19–32.
[34] M.S. Domowicz, M. Cortes, J.G. Henry, N.B. Schwartz, Aggrecan modulation of growth plate morphogenesis, Dev. Biol. 329 (2) (2009) 242–257.
[35] B. Gualeni, M.H. Rajpar, A. Kellogg, P.A. Bell, P. Arvan, R.P. Boot-Handford, M.D. Briggs, A novel transgenic mouse model of growth plate dysplasia reveals that decreased chondrocyte proliferation due to chronic ER stress is a key factor in reduced bone growth, Dis. Model. Mech. 6 (6) (2013) 1414–1425.
[36] R. Morello, T.K. Bertin, Y. Chen, J. Hicks, L. Tonachini, M. Monticone, P. Castagnola, F. Rauch, F.H. Glorieux, J. Vranka, H.P. Bachinger, J.M. Pace, U. Schwarze, P.H. Byers, M. Weis, R.J. Fernandes, D.R. Eyre, Z. Yao, B.F. Boyce, B. Lee, CRTAP is required for prolyl 3-hydroxylation and mutations cause recessive osteogenesis imperfecta, Cell 127 (2) (2006) 291–304.
[37] C.W. Archer, P. Francis-West, The chondrocyte, Int. J. Biochem. Cell Biol. 35 (4) (2003) 401–404.
[38] A. Forlino, R. Piazza, C. Tiveron, S. Della Torre, L. Tatangelo, L. Bonafe, B. Gualeni, A. Romano, F. Pecora, A. Superti-Furga, G. Cetta, A. Rossi, A diastrophic dysplasia sulfate transporter (SLC26A2) mutant mouse: morphological and biochemical characterization of the resulting chondrodysplasia phenotype, Hum. Mol. Genet. 14 (6) (2005) 859–871.
[39] P. Vanky, U. Brockstedt, A. Hjerpe, B. Wikstrom, Kinetic studies on epiphyseal growth cartilage in the normal mouse, Bone 22 (4) (1998) 331–339.
[40] A. Rossi, I. Kaitila, W.R. Wilcox, D.L. Rimoin, B. Steinmann, G. Cetta, A. Superti-Furga, Proteoglycan sulfation in cartilage and cell cultures from patients with sulfate transporter chondrodysplasias: relationship to clinical severity and indications on the role of intracellular sulfate production, Matrix Biol. 17 (5) (1998) 361–369.
[41] M. Pacifici, Independent secretion of proteoglycans and collagens in chick chondrocyte cultures during acute ascorbic acid treatment, Biochem. J. 272 (1) (1990) 193–199.
[42] C.R. de Lima, R.Y. Baccarin, Y.M. Michelacci, Reliability of 1,9-dimethylmethylene blue tests in comparison to agarose gel electrophoresis for quantification of urinary glycosaminoglycans, Clin. Chim. Acta 378 (1–2) (2007) 206–215.
[43] L. Monti, C. Paganini, S. Lecci, F. De Leonardis, E. Hay, M. Cohen-Solal, S. Villani, A. Superti-Furga, R. Tenni, A. Forlino, A. Rossi, *N*-acetylcysteine treatment ameliorates the skeletal phenotype of a mouse model of diastrophic dysplasia, Hum. Mol. Genet. 24 (19) (2015) 5570–5580.
[44] E.B. Hunziker, W. Herrmann, R.K. Schenk, Ruthenium hexammine trichloride (RHT)-mediated interaction between plasmalemmal components and pericellular matrix proteoglycans is responsible for the preservation of chondrocytic plasma membranes in situ during cartilage fixation, J. Histochem. Cytochem. 31 (6) (1983) 717–727.
[45] R. Besio, G. Iula, N. Garibaldi, L. Cipolla, S. Sabbioneda, M. Biggiogera, J.C. Marini, A. Rossi, A. Forlino, 4-PBA ameliorates cellular homeostasis in fibroblasts from osteogenesis imperfecta patients by enhancing autophagy and stimulating protein secretion, Biochim. Biophys. Acta, Mol. Basis Dis. 1864 (5 Pt A) (2018) 1642–1652.

Please cite this article as: C. Paganini, L. Monti, R. Costantini, et al., Calcium activated nucleotidase 1 (CANT1) is critical for glycosaminoglycan biosynthesis in cartilage and endoc..., Matrix Biology, https://doi.org/10.1016/j.matbio.2018.11.002

SUBMITTED TO PLOSONE

Testing the Cre-mediated genetic switch for the generation of conditional knock-in mice

Mattia Capulli[1¶], Rossella Costantini[2¶], Stephan Sonntag[3,4], Antonio Maurizi[1], Chiara Paganini[2,5], Luca Monti[2], Antonella Forlino[2], Doron Shmerling[3], Anna Teti[1], Antonio Rossi[2]*

[1]Department of Biotechnological and Applied Clinical Sciences, University of L'Aquila, L'Aquila, Italy;

[2]Department of Molecular Medicine, Unit of Biochemistry, University of Pavia, Pavia, Italy;

[3]PolyGene AG, Rümlang, Switzerland;

[4]ETH Phenomics Center (EPIC), ETH Zürich, Zürich, Switzerland.

[5]Scuola Universitaria Superiore IUSS, Pavia, Italy.

[¶] These authors contributed equally to this work.

* Corresponding author:

E-mail: antrossi@unipv.it (AR)

Short title: Challenges in the generation of conditional knock-in mice

ABSTRACT

The Cre-mediated genetic switch combines the ability of Cre recombinase to stably invert or excise a DNA fragment depending upon the orientation of flanking mutant loxP sites. In this work, we have tested this strategy *in vivo* with the aim to generate two conditional knock-in mice for missense mutations in the *Impad1* and *Clcn7* genes causing two different skeletal dysplasias. Targeting constructs were generated in which the *Impad1* exon 2 and an inverted exon 2* and the *Clcn7* exon 7 and an inverted exon 7* containing the point mutations were flanked by mutant loxP sites in a head-to-head orientation. When the Cre recombinase is present, the DNA flanked by the mutant loxP sites is expected to be stably inverted leading to the activation of the mutated exon.

The targeting vectors were used to generate heterozygous floxed mice in which inversion of the wild-type with the mutant exon has not occurred yet. To generate *Impad1* and *Clcn7* knock-in mice, floxed animals were mated to a global Cre-deleter mouse strain for stable inversion and activation of the mutation. Unexpectedly the phenotype of homozygous *Impad1* knock-in animals overlaps with the lethal phenotype described previously in *Impad1* knock-out mice. Similarly, the phenotype of homozygous *Clcn7* floxed mice overlaps the one of *Clcn7* knock-out mice. Expression studies by qPCR and RT-PCR demonstrated that mutant mRNA underwent abnormal splicing leading to the synthesis of non-functional proteins. Thus, the skeletal phenotypes were not caused by the missense mutations, but by aberrant splicing. Our data demonstrate that the Cre mediated genetic switch strategy should be considered cautiously for the generation of conditional knock-in mice.

INTRODUCTION

In the era of big data the question for geneticists is often whether a mutation identified by next generation sequencing in a particular gene can explain the clinical phenotype of the patient. Indeed a crucial issue in biomedical research is to convert sequence information, -omics, analytical and clinical data into knowledge about gene function.

Skeletal dysplasias represent one of the largest classes of birth defects with 436 different disorders that have been clustered in 42 different groups depending on molecular and/or clinical features. More than 350 disease genes have been identified encoding for proteins involved in a wide spectrum of biological functions in cartilage and bone [1, 2]. To shed light on the molecular mechanisms of skeletal disorders, mechanistic studies using *in vitro* and *in vivo* approaches are necessary to elucidate the role of the disease gene in the disorder.

Cell cultures, or *in vitro* studies, provide the first important system to study human diseases, preserving the physiology of living cells and enabling the manipulation under controlled laboratory condition. Patient-derived cells including fibroblasts, induced pluripotent stem cells, primary chondrocytes, osteoblasts and osteoclasts are widely used to model congenital disorders of cartilage and bone [3]; however, their use does not always mirror the whole body condition.

Due to the complexity of skeletal pathologies *in vivo* models represent a need for the field. Recently, *Danio rerio* (Zebrafish) has become an appealing animal model to study skeletal development as well as to test drug's efficacy [4-6], nevertheless nowadays mouse models still represent the gold standard for disease of bone modeling since they are anatomically and physiologically close to humans. The mouse genome can be manipulated in many different ways in order to generate models that carry the same disease causing mutation detected in patients [7]. Moreover, patient specific mutations might be helpful to identify genotype-phenotype correlations and differences in the effects of particular mutations.

For more than 20 years the most suitable technique to generate animal models has been based on homologous recombination in murine embryonic stem cells to change the expression of an endogenous gene [8]. The gene-targeting technique has many advantages related to the fact that homologous recombination defines the site of integration and the genetic change in a very specific manner. Gene-targeting can be designed to introduce different genetic modifications that can be transmitted to successive generation such as gene deletions (knock-out), point mutations (knock-in), gene insertions in a certain locus or chromosomal rearrangements.

Knock-out mice can be also generated by the gene trap strategy, which is based on the disruption of an endogenous gene function by the random insertion of an intronic gene-trap cassette [9]. More recently, the genome-editing CRISPR/Cas9 technology has offered a new, quick and cheaper way to model genetic disorders [10].

Genetic changes in the germ line might be useful to track the gene function, but may also result in severe developmental consequences complicating or precluding the experimental analysis; example of these drawbacks is embryonic lethality in knock-outs. To overcome these limits related to constitutive expression of the targeting construct, conditional mice expressing the gene modification only at a specific developmental stage or in selected cells have been generated. Different conditional systems are available; among them, the tetracycline (tet) regulatory system and Cre/*loxP* or Flp/FRT recombination systems are the most widely used [11, 12]. Cre and Flp recombinases mediate different effects on their DNA target sequences including excision, duplication, integration, inversion and translocation depending on the orientation of their specific recognition sequence, namely *loxP* and FRT, respectively.

However, integration and inversion between wild-type *lox*P sites is inefficient due to activation of a vicious cycle of re-excision through intramolecular recombination. To overcome such limitation the left element/right element (LE/RE) mutant strategy using LE mutant *lox* carrying mutations in the left-inverted repeat region and RE mutant *lox* carrying mutations in the right-inverted repeat region can be used [13, 14]. Recombination between a LE mutant *lox* and a RE

mutant *lox* results in the generation of a double mutant *lox* site with mutations in both ends and a wild-type *loxP* site. The double mutant *lox* site is no longer a substrate for Cre recombinase; therefore, the recombination reaction proceeds only in the forward direction.

By combining the ability of Cre recombinase to invert or excise a DNA fragment and the use of wild-type and mutant *loxP* sites, an efficient and reliable Cre-mediated genetic switch has been proposed [15]. Through this strategy expression of a given gene can be turned off, while expression of another one can be simultaneously turned on. This innovative, flexible and powerful approach can be used to easily generate many genetic modifications in a conditional manner [16].

The genetic switch has also been proposed to invert a wild-type exon with a mutated one in order to generate conditional point mutations [14]. In the present work, we have tested this powerful tool to generate two conditional knock-in mice bearing patient specific missense mutations causative of two different skeletal disorders: chondrodysplasia with joint dislocations, gPAPP type and Autosomal Dominant Osteopetrosis Type 2 (ADO2).

MATERIALS AND METHODS

Preparation of the gene targeting vectors and generation of mutant mice

A vector for the stable inversion mediated by Cre-recombinase was generated by gene synthesis with a combination of *lox71* as LE mutant *loxP* (carrying mutations in the left-inverted repeat region) and *loxKR3* as RE mutant *loxP* (carrying mutations in the right-inverted repeat region) in a head-to-head orientation [13]. Different restriction sites were synthesized upstream, downstream and in between the lox sites, to allow insertion of different cassettes. To test the efficiency of the Cre-mediated irreversible inversion we took advantage of an FRT-flanked *neomycin* resistance cassette cloned between the *lox*-sites using *EcoRV* and *EcoRI*. The resulting vector was transformed in *E.coli* expressing Cre-recombinase where efficient recombination was confirmed by inversion *in vivo*.

Subsequently, the *lox71*/*loxKR3* vector was used for the assembly of the *Impad1* and *Clcn7* conditional knock-in gene targeting constructs. Briefly, the vectors contained homology arms for the *Impad1* or *Clcn7* genes of about 5 kb and 2.7 kb or 3.7 kb and 2.8 kb, respectively. The homologous sequences flanked by a duplicated region of the mutated and wild type exon (exon 2 for *Impad1* and exon 7 for *Clcn7*) were introduced in a head-to-head orientation. They were flanked by the head-to-head *lox71* and *loxKR3* sites and separated by an FRT-flanked neomycin cassette (Fig 1).

The missense mutation knocked in the *Impad1* gene was a c.726G>A transition (NM_177730.4) leading to substitution of p.Asp175>Asn in exon 2. This mutation corresponds to the p.Asp177>Asn mutation detected in a patient with chondrodysplasia with joint dislocations, gPAPP type [17]. In addition close to the mutation two silent mutations, c.716T>C and c.719C>T respectively, were inserted to generate a *ClaI* restriction site useful for animal genotyping.

The missense mutation knocked in the *Clcn7* gene was a g.14365G>A transition (NM_011930.4) leading to substitution of p.Gly213>Arg. This mutation corresponds to the most common human mutation, p.Gly215>Arg, detected in patients with ADO2 [18].

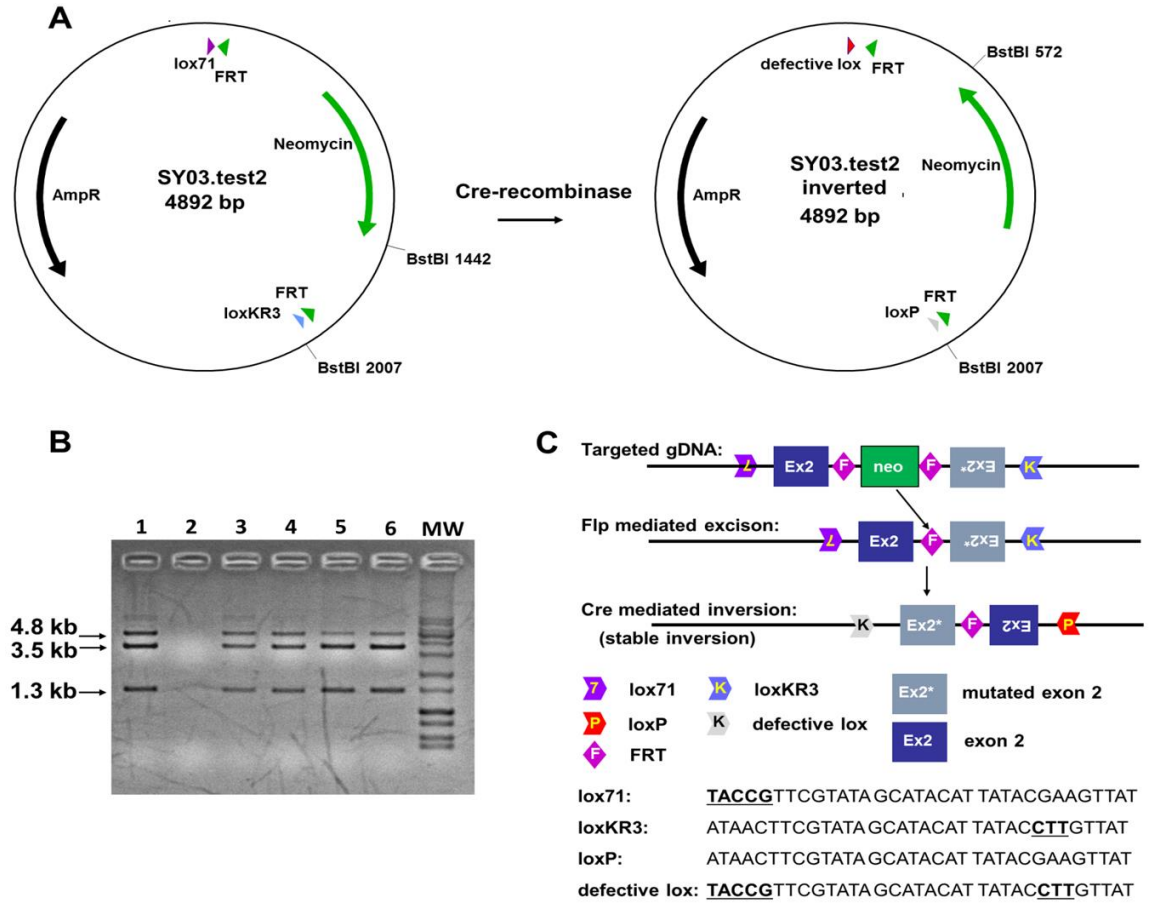

Fig 1. Strategy for conditional knock-in generation via inversion. (A) Scheme of the plasmid used to test recombination and stable inversion with *lox71* and *loxKR3*. Magenta arrowhead: *lox71*; light blue arrowhead: *loxKR3*; grey arrowhead: *loxP*; red arrowhead: double mutant *lox*; green arrowhead: *FRT* site. (B) Restriction fragment analysis with *BstBI* of the plasmid (4.8 kb) after transformation in Cre-expressing E.c*oli*. The correctly inverted plasmid results in restriction fragments of 3.5 kb and 1.3 kb. Lanes 1, 3-6: positive clones; lane 2: blank (water); MW: DNA molecular weight marker. (C) Two versions of the targeted exon (wild-type and mutated) are inserted in head-to-head orientation between a *loxKR3* and a *lox71* site. The two versions of the exon are separated by an FRT-flanked *neomycin* cassette. After targeting the *neomycin* cassette is deleted via Flp-mediated recombination *in vivo*. The mutation is activated by stable inversion of the

two exons mediated by Cre-recombinase. The targeted exon in the *Impad1* conditional knock-in is exon 2, as shown in the figure, while exon 7 is the targeted exon in the *Clcn7* conditional knock-in. The sequences of *lox* sites used in this study are reported and mutated sequences are indicated by bold and are underlined. *Lox71* carries mutations in the left element, while *loxKR3* carries mutations in the right element.

Generation of *Impad1* and *Clcn7* targeted embryonic stem cells and mice

The two targeting vectors bearing the *Impad1* or the *Clcn7* mutation were electroporated into 2 x 10^7 C57Bl/6N-based and 129Ola-based ES cells, respectively. After selection with 200 µg/ml neomycin (G418) for 8 days, about 400 ES cell clones were isolated and analyzed via PCR screening.

In both ES cell lines, positive ES cell clones in which correct homologous recombination has occurred were identified via long range PCR (data not shown) and confirmed by Southern blot analysis. A list of all primers used for PCR analyses and for the synthesis of the Southern blot probe (generated by PCR with primers Neo3-for and Neo4-rev) as well as for genotyping are reported in S1 Table.

For *Impad1* mouse generation, two positive ES cell clones were injected into grey C57Bl/6N derived blastocysts. The resulting chimeras were bred to C57Bl/6N-based Flp-deleter mice (B6gr-Tg(ACTFLPe)9205Dym/NPg) and the resulting black offspring was analyzed by PCR. Several positive mice that lost the FRT-flanked neomycin cassette via Flp-recombination were identified (here called "floxed" mice, $Impad1^{Flox/WT}$ mice). Deletion of the neomycin cassette was demonstrated by PCR using primers Neo3-for and Neo4-rev (S1 Table); moreover the presence of the floxed allele was confirmed by the presence of the *lox71* site checked by PCR with primers SY08.20 and SY08.21. $Impad1^{Flox/WT}$ mice were mated to a Cre mouse strain (B6.FVB-Tg(EIIa-cre)C5379Lmgd) to generate the heterozygous knock-in of the p.Asp175>Asn mutation ($Impad1^{D175N/WT}$ mouse). Correct Cre-mediated switch was checked taking advantage of the insertion of the *ClaI* restriction site close to the missense mutation. The 480bp PCR product of the

mutant allele obtained using Imp3 and Imp4 primers was digested by *ClaI* in two restriction fragments of 124bp and 356bp, respectively.

For *Clcn7* mouse generation, three positive clones were injected into blastocysts from black C57Bl/6N females. The resulting chimeras were bred to C57Bl/6N-based Flp-deleter (B6gr-Tg(ACTFLPe)9205Dym/NPg) mice. The resulting agouti offsprings were then genotyped and several positive mice showing deletion of the neomycin resistance cassette were identified (here called "floxed" mice, $Clcn7^{Flox/WT}$ mice). These were bred further with each other to generate homozygous floxed mice. For animal genotyping the insertion of the *lox71* site, used as marker of the mutant allele, was checked by PCR with primers flanking the insertion site (SY03.11 and SY03.12). Deletion of the *neomycin* cassette was demonstrated by PCR using primers Neo3-for and Neo4-rev (S1 Table).

Animals

Animals were bred with free access to water and standard pelleted food. Care and use of mice for this study was in compliance with relevant animal welfare institutional guidelines in agreement with EU Directive 2010/63/EU for animals and the Italian Legislative Decree 4.03.2014, n.26. The experimental protocol was approved by the Italian Ministry of Health (Animal protocol n. 844/2017-PR and n. 564/2016-PR). Mice were sacrificed by CO_2 inhalation. The Impad1 knock-out strain, generated by Frederick et al. [19] was provided by “The Jackson Laboratories”, Bar Harbor, Maine, USA.

Mouse genotyping

Mice were genotyped by PCR using genomic DNA from mouse tail or ear clips. For animal genotyping of the *Impad1* knock-in strain the mutant allele was detected by digestion with *ClaI* of a PCR product generated with primers Imp3 and Imp4. The 480bp PCR product of the mutant allele

was digested by *ClaI* in two restriction fragments of 124bp and 356bp, respectively. Genotyping of the *Impad1* knock-out strain was performed as described previously [19].

For animal genotyping of the *Clcn7* floxed strain SY03.11 and SY03.12 PCR primers were used to genotype homozygous mutant mice from heterozygous and wild type animals.

X-rays and image analysis

X-ray analyses were performed using a Faxitron MX-20 cabinet X-ray system (Faxitron Bioptics LLC, USA) and X-ray images were digitalized with a Kodak DirectView Elite CR System (Carestream Health Italia, Italy).

Micro Computed Tomography

Femurs from 3 week-old mice were fixed in 4% formaldehyde for 48 hours and then scanned by a μCT SkyScan 1174 (Bruker Italia, Italy). The scan was performed with 6.4 μm resolution at 50 kV. The Skyscan NRecon software was used to reconstruct images with a modified Feldkamp algorithm. Three-dimensional analysis was carried out employing a Marching Cubes type model with a rendered surface [20]. Threshold values were applied for segmenting trabecular bone. Bone trabecular and cortical variables were determined according to Bouxsein et al [21].

Differential skeletal staining with alcian blue and alizarin red

Skeletal staining of newborn mice were performed with alcian blue–alizarin red [22]. Briefly, pups were skinned, dehydrated in 96% ethanol, defatted in acetone and stained with alcian blue and alizarin red. Muscles were removed with 1% KOH in 20% glycerol and preparations were stored in glycerol. Mice were then photographed using a Leica M165 FC stereomicroscope connected to a Leica DFC425 C digital camera (Leica Microsystems, Italy).

qPCR and alternative splicing analysis

Skin from newborn mice was homogenized in 1 ml of QIAzol Lysis Reagent (QIAGEN, Italy) and total RNA was extracted according to the manufacturer's instructions. Reverse transcription of 1 µg RNA in a final volume of 20 µl was performed using the SuperScript IV First-Strand Synthesis System (Invitrogen, Thermo Fisher Scientific, Italy) according to the manufacturer's instructions.

For expression analyses by RT-qPCR, the QuantiFast Primer Assays with validated primer sets for *Impad1* and *Gapdh* (QIAGEN) were used with the QuantiTect SYBR Green PCR Kit (QIAGEN) according to the manufacturer's protocol. The primer set of *Impad1* span exon 2 and 3. Each sample was run in triplicate in 96 well plates in three independent experiments with the MX3000P apparatus (Stratagene, USA). The expression of *Impad1* relative to the housekeeping *Gapdh* gene was obtained by ΔΔCt method.

For alternative splicing detection, total RNA was used for RT-PCR analysis using primers in exon 1 and exon 5 of the *Impad1* gene. PCR products were analyzed by 1.5% agarose gels. For DNA sequencing of the spliced forms, the PCR products were cloned with the TA cloning kit (Invitrogen) followed by Sanger sequencing.

HPLC analysis of cartilage glycosaminoglycan sulfation

For cartilage disaccharide analysis, cartilage was obtained from the femoral heads of newborn mice by careful dissection under the dissection microscope and glycosaminoglycans (GAGs) were recovered by papain digestion and cetylpyridinium chloride precipitation as previously described [23]. Purified GAGs were digested with 30 mU of both chondroitinase ABC and chondroitinase ACII (Seikagaku Corp., Japan) in 0.1 M sodium acetate, pH 7.35 at 37°C overnight. Released disaccharides were lyophilized and redissolved in 40 µl of 12.5 mM 2-aminoacridone (Invitrogen) in 85% DMSO/15% acetic acid and incubated for 15 minutes at room temperature in the dark. Then, 40 µl of 1.25 M sodium cyanoborohydride in water was added and the mixture was incubated overnight at 37 °C. Disaccharides were fractioned with a ProntoSIL HPLC column (4.6 mm × 200 mm, Bischoff Chromatography, Germany) using a linear gradient (0 - 42% solvent B in 42 min);

mobile phases were 0.1 M ammonium acetate, pH 7.0, (Solvent A) and methanol (Solvent B). The analysis was carried out at room temperature with 0.7 ml/min flow rate and the elution profile was monitored by a fluorescence detector (2475 Multy λ Fluorescence Detector, Waters, Italy), with excitation and emission wavelengths of 425 and 525 nm, respectively.

Statistical analysis

Statistical analyses were carried out by the software Prism® by GraphPad v7.0 and the type of analysis is stated in the figure legends; all results are presented as mean ± SD.

RESULTS

Generation of the Cre mediated switch allele in mice.

In order to generate the two conditional knock-in mice, a combination of two partially mutated *lox* sites in the head-to-head orientation were used. This strategy guarantees stable inversion of DNA between the *lox* sites since after Cre recombination a wild-type *loxP* site and a double mutant *lox*, no longer recognized by the enzyme, are generated (Fig 1A). First the combination *lox71* and *loxKR3*, reported previously by Araki et al [13] in a head-to-head orientation was tested for recombination efficiency in a Cre expressing *E.coli* strain. Five clones were isolated from each transformation and analyzed via restriction analysis with *BstBI*. All clones showed the expected restriction pattern corresponding to the inverted version of the test vector (Fig 1B).

Two gene targeting vectors were generated based on the *lox71*/*loxKR3* construct. The first for an Impad1 mutation (p.Asp175>Asn) and the latter for a mutation in the Clcn7 (p.Gly213>Arg) (Fig 1C and Fig 2A and 2B).

Homologous recombination was performed in C57Bl/6N-based (Impad1) and 129Ola-based (Clcn7) ES cells and confirmed by Southern blot analysis (Fig 2C and 2E). Proper targeted ES cell clones were injected into C57Bl/6N blastocysts and the resulting chimeras were bred to FLP-deleter mice for *neomycin* cassette deletion. The heterozygous offsprings, here called "floxed" mice (*Impad1*$^{Flox/WT}$ mice and *Clcn7*$^{Flox/WT}$ mice, respectively), were then confirmed by the presence of the *lox71* site (Fig 2D and 2F) and the deletion of the *neomycin* cassette (not shown).

To generate heterozygous *Impad1* knock-in animals (*Impad1*$^{D175N/WT}$), *Impad1*$^{Flox/WT}$ mice were mated to a global Cre mouse strain for stable inversion and activation of the mutation.

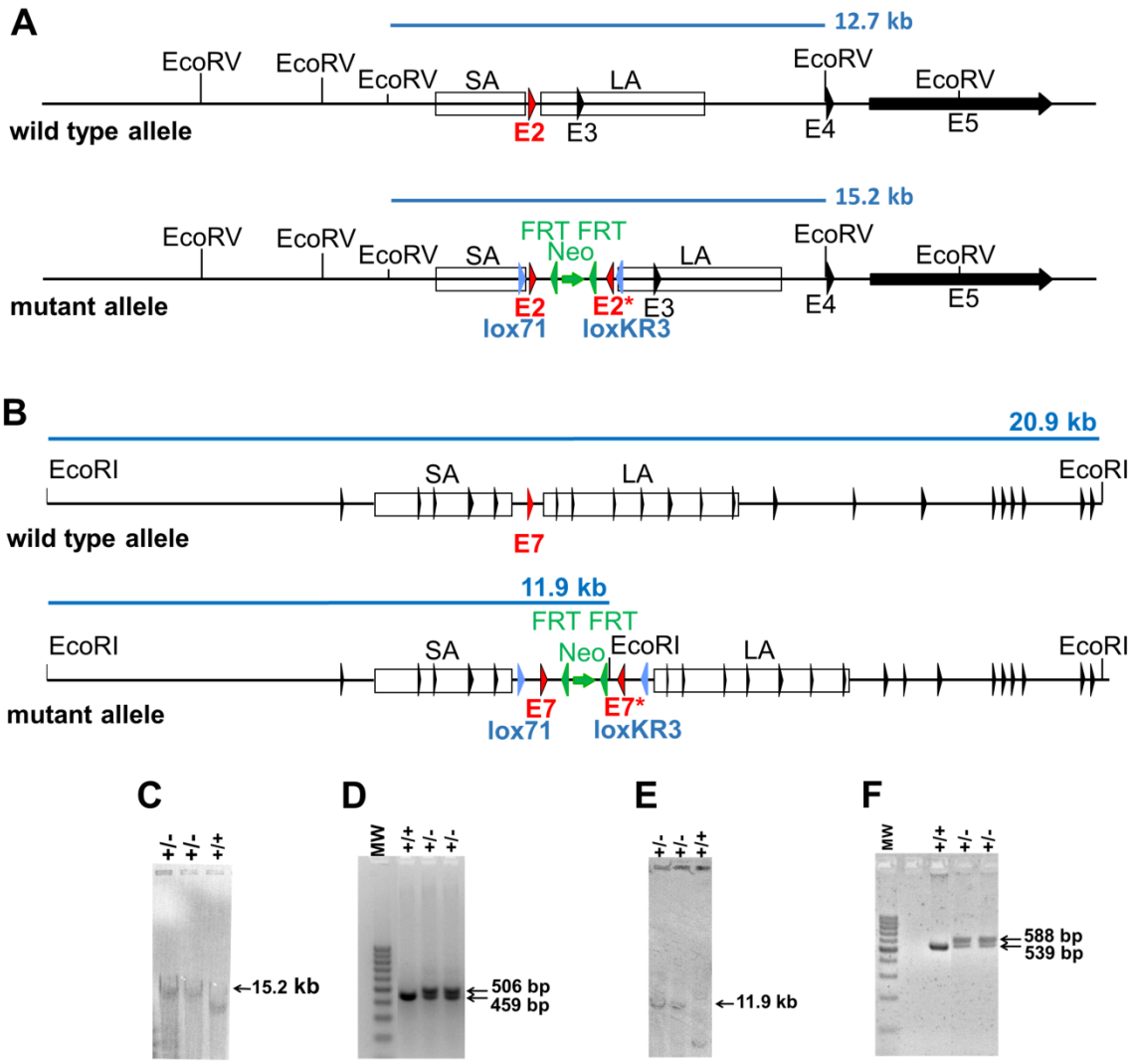

Fig 2. Generation of the *Clcn7* and *Impad1* mouse lines. (A) Schematic drawing of the wild type and targeted loci for *Impad1*. *EcoRV* restriction sites and fragments for Southern blot analyses are indicated in light blue. (B) Schematic drawings of the wild type and targeted loci for *Clcn7*. *EcoRI* restriction sites and fragments for Southern blot analyses are indicated in light blue. Exons, indicated by arrowheads, are not numbered to simplify the figure. (C) Southern blot analysis of *Impad1* targeted ES cells after *EcoRV* digestion using a *neomycin* specific probe; the 15.2 kb fragment corresponding to correct homologous recombination is indicated. (D) Genotyping PCR analysis for heterozygous *Impad1* floxed pups using primers SY08.20 and SY08.21 flanking the *lox71* site. The wild-type and floxed allele result in PCR products of 459 bp and 506 bp, respectively. (E) Southern blot analysis of *Clcn7* targeted ES cells after *EcoRI* digestion using a

neomycin specific probe; the 11.9 kb fragment corresponding to correct homologous recombination is indicated. (F) Genotyping PCR analysis for heterozygous *Clcn7* floxed pups using primers SY03.11 and SY03.12 flanking the *lox71* site. The wild-type and floxed allele result in PCR products of 539 bp and 588 bp, respectively. Black arrowhead: exon; green arrowhead: FRT site; light blue arrowhead: *lox71* or *loxKR3* site; red arrowhead: targeted exon 2 in *Impad1* or targeted exon 7 in *Clcn7*; green arrow: *neomycin* cassette; SA: short arm; LA: long arm; E#: exon number; MW: DNA molecular weight marker.

Phenotypic characterization of the *Impad1* knock-in mouse

Impad1$^{D175N/WT}$ mice did not show any phenotypic alteration by X-ray analysis and visual inspection as human carriers of *IMPAD1* mutations and were no further studied.

Homozygous mutant (*Impad1*$^{D175N/D175N}$) animals died at birth and were smaller compared to wild type and heterozygous littermates; visual inspection and X-ray analysis demonstrated growth retardation and skeletal defects (Fig 3A and 3B). Mutant animals showed severe hypoplasia of the skeleton; the length of the axial skeleton and of the limbs were reduced. By X-rays and alcian blue and alizarin red skeletal staining, the femur, tibia and fibula were markedly shorter compared to wild-type animals; furthermore, reduced sternal length and diminished rib spacing were evident (Fig 3B and 3D). Moreover, *Impad1*$^{D175N/D175N}$ mice showed cleft palate already observed in patients with chondrodysplasia with joint dislocations, gPAPP type (Fig 3C).

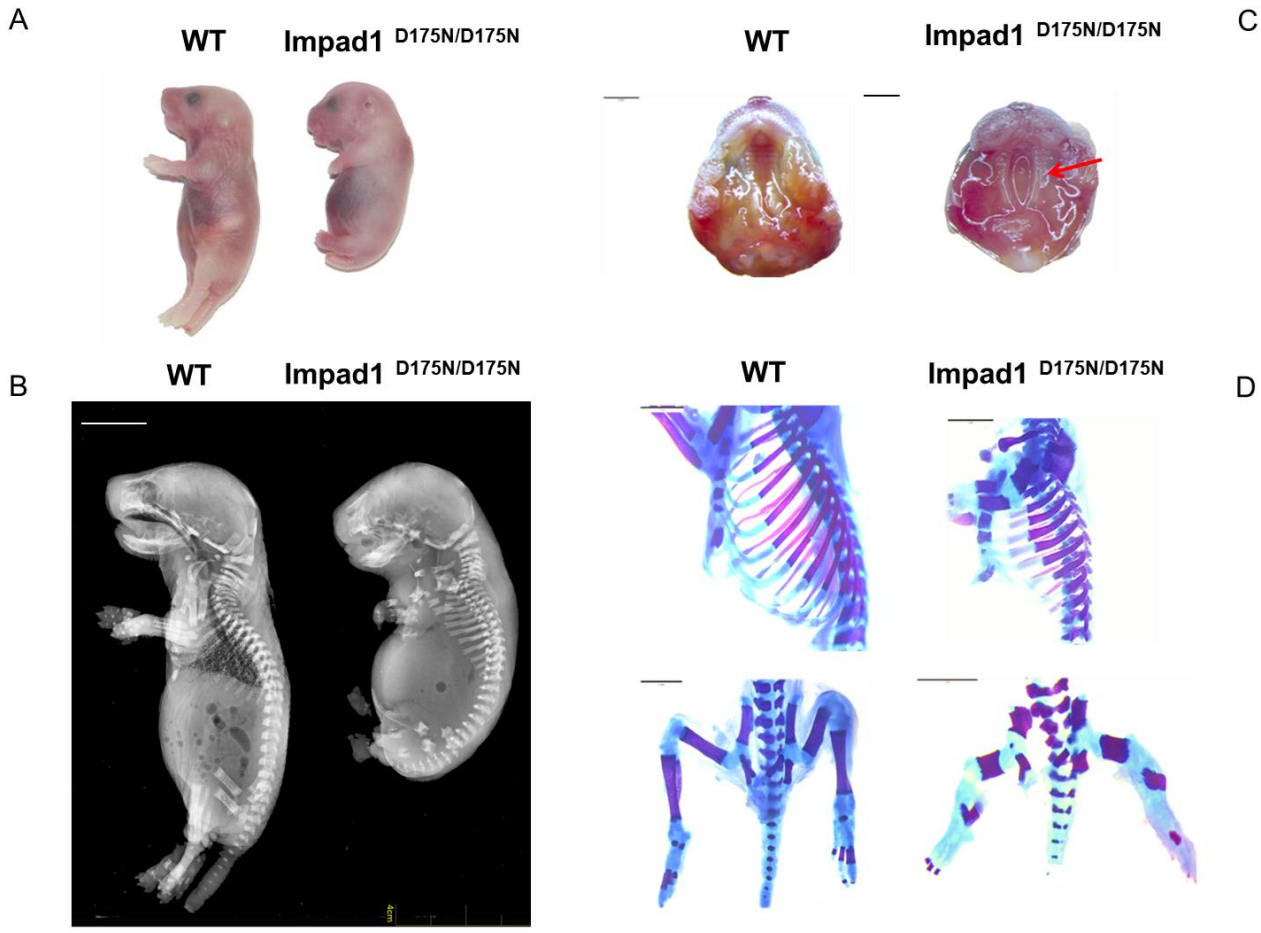

Fig 3. Phenotypic characterization of the *Impad1*$^{D175N/D175N}$ mouse. (A) Gross morphology of wild type and *Impad1*$^{D175N/D175N}$ newborn mice. Mutant animals die at birth and are considerably smaller than wild type littermates demonstrating severe growth retardation. (B) X-rays of wild type and mutant mice at birth. The mutant shows skeletal defects and growth retardation. (C) In *Impad1*$^{D175N/D175N}$ mice cleft palate is observed (arrow). Scale bars: 2 mm. (D) Alcian blue and alizarin red skeletal staining of *Impad1*$^{D175N/D175N}$ and wild type bones at birth; the femur, tibia and fibula are markedly shorter compared to wild-type animals; rib cages of mutant mice display skeletal defects characterized by reduced sternal length and diminished rib spacing. Scale bars: 2mm.

Surprisingly, the *Impad1*$^{D175N/D175N}$ mouse showed the same peculiar phenotype described previously in the *Impad1* knock-out mouse [19, 24]. Thus, we further investigated the molecular and biochemical basis causing neonatal lethality in our animal model.

Impad1 encodes for a Golgi 3'-phosphoadenosin 5'-phosphate phosphatase crucial for macromolecular sulfation. In whole embryo and in the limbs of the *Impad1* knock-out mouse severe undersulfation of chondroitin sulfate proteoglycans was demonstrated compared to wild-type mice [19, 24]. For this reason, proteoglycan sulfation was measured by HPLC disaccharide analysis in femoral head cartilage of wild type and $Impad1^{D175N/D175N}$ mice and, for comparison, in the Frederick's *Impad1* knock-out [19]. Glycosaminoglycans were purified by digestion of femoral head cartilage with papain. Then glycosaminoglycans were digested with chondroitinase ABC and ACII and released disaccharides separated by HPLC after derivatization with a fluorescent tag. A dramatic increase in the relative amount of the chondroitin non-sulfated disaccharide (ΔDi-0S) was observed in newborn $Impad1^{D175N/D175N}$ mice compared to wild-type animals indicating chondroitin sulfate undersulfation (61 ± 9.2% and 14 ± 1.6% ΔDi-0S, respectively; $P < 0.001$ n=3). Interestingly, the extent of proteoglycan undersulfation in mutant mice was similar to homozygous *Impad1* knock-out animals (63 ± 1.6% ΔDi-0S, n=3) (Fig 4).

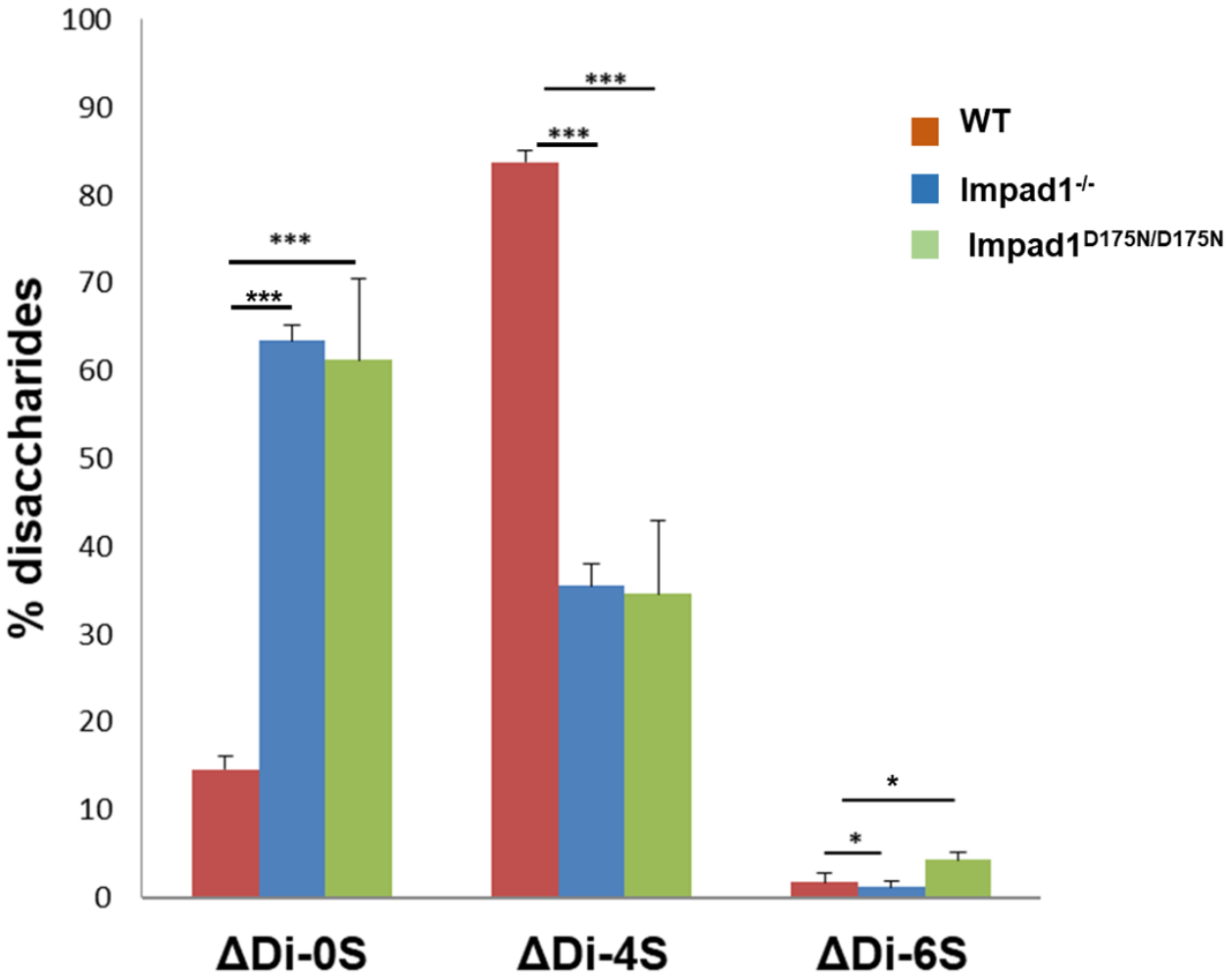

Fig 4. Sulfation of chondroitin sulfate proteoglycans from femoral head cartilage. Sulfation of proteoglycans was determined by HPLC disaccharide analysis after digestion by chondroitinase ABC and ACII of chondroitin sulfate proteoglycans from the femoral head cartilage of wild-type (WT) and *Impad1*$^{D175N/D175N}$ mice at birth. In parallel the same analysis was performed also in the *Impad1* knock-out (*Impad1*$^{-/-}$) mouse studied by Frederick [19]. The amount of non sulfated disaccharide (ΔDi-0S) relative to the total amount of disaccharides (ΔDi-0S, ΔDi-4S and ΔDi-6S) is significantly increased in mutant mice compared to the wild-types indicating proteoglycan undersulfation. Interestingly, the level of proteoglycan undersulfation in mutants is similar the Frederick's knock-out mouse. Three mice per group were used; data are reported as mean ± SD (Student's t-test, *p<0.05; ***p<0.001).

Since the clinical and biochemical phenotype of *Impad1*$^{D175N/D175N}$ animals overlap with *Impad1* knock-outs, the expression of *Impad1* was measured by qPCR with primers spanning exons

2 and 3. *Impad1* mRNA was barely detectable in *Impad1*$^{D175N/D175N}$ mice compared with wild-types; *Impad1* expression level in heterozygous mice was reduced by half (Fig 5).

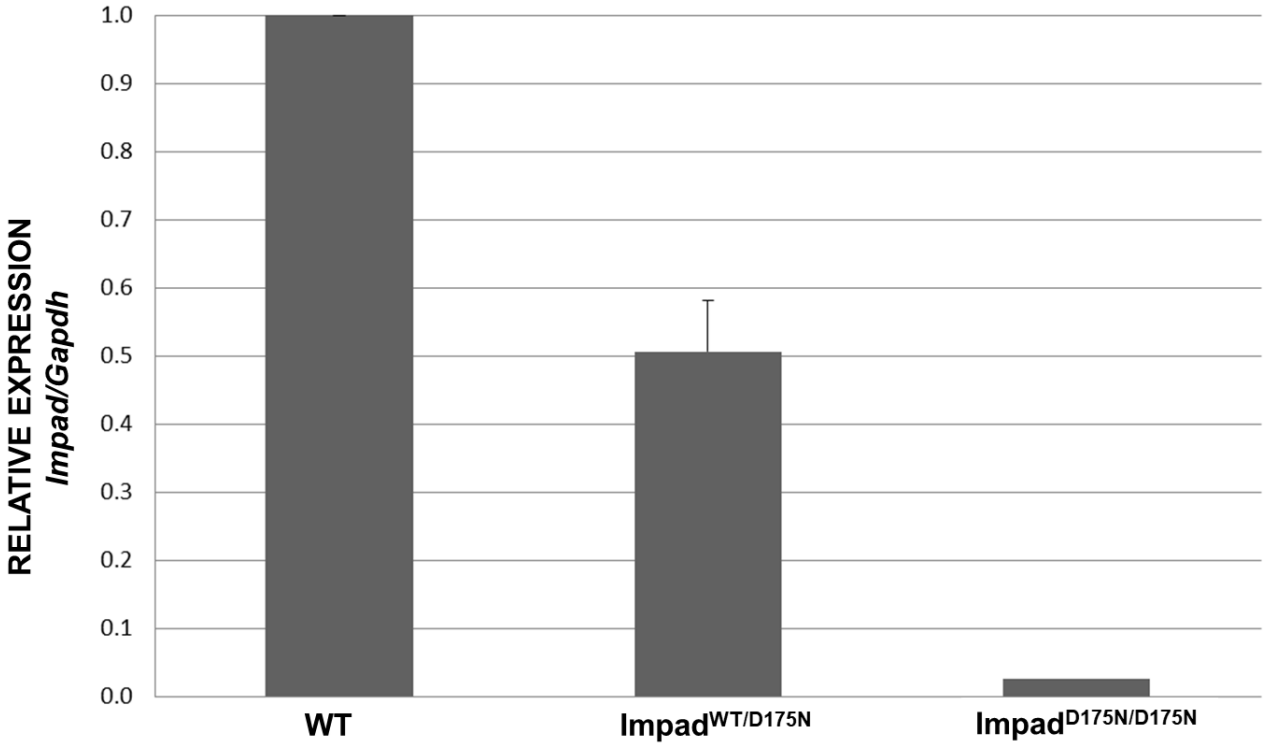

Fig 5. Relative expression analysis of the *Impad1* gene. RT-qPCR on total RNA isolated from skin of wild-type (WT), heterozygous (*Impad1*$^{WT/D175N}$) and *Impad1*$^{D175N/D175N}$ newborn mice was performed with primers spanning exon 2 and exon 3. Expression of *Impad1* mRNA normalized to *Gapdh* is absent in homozygous mutant animals compared to wild-types. Three mice per genotype were used; each sample was run in triplicate and three different experiments were performed.

Since in *Impad1*$^{D175N/D175N}$ mice no Impad1 transcript was detected by qPCR, we checked whether the modified *Impad1* locus impairs correct RNA splicing. Thus, we considered potential alternative splicing of *Impad1* exons by RT-PCR using two primers spanning exon 1 to 5 encompassing the whole coding sequence (Fig 6). Results showed that in wild-type animals one band, 639 bp long, corresponding to a unique transcript including the 5 coding exons was present. This band was not detected in *Impad1*$^{D175N/D175N}$ mice; conversely two different bands, 477 bp and 383 bp long, respectively were observed (Fig 6A). Sequencing of the two bands demonstrated that the two transcript variants lack exon 2 or exon 2 and exon 3 (Fig 6B) causing, if translated,

frameshift mutations leading to premature stop codons p.Ile128ArgfsX13 and p.Ile128LeufsX5, respectively.

Retrospectively we noted that *Impad1*$^{Flox/WT}$ cross breeding resulted in an unusual small litters size. The analysis of some pups found dead at birth revealed their homozygous *Impad1*$^{Flox/Flox}$ genotype. Furthermore, their X-ray showed the same severe skeletal phenotype observed in *Impad1*$^{D175N/D175N}$ mice (S1 Fig).

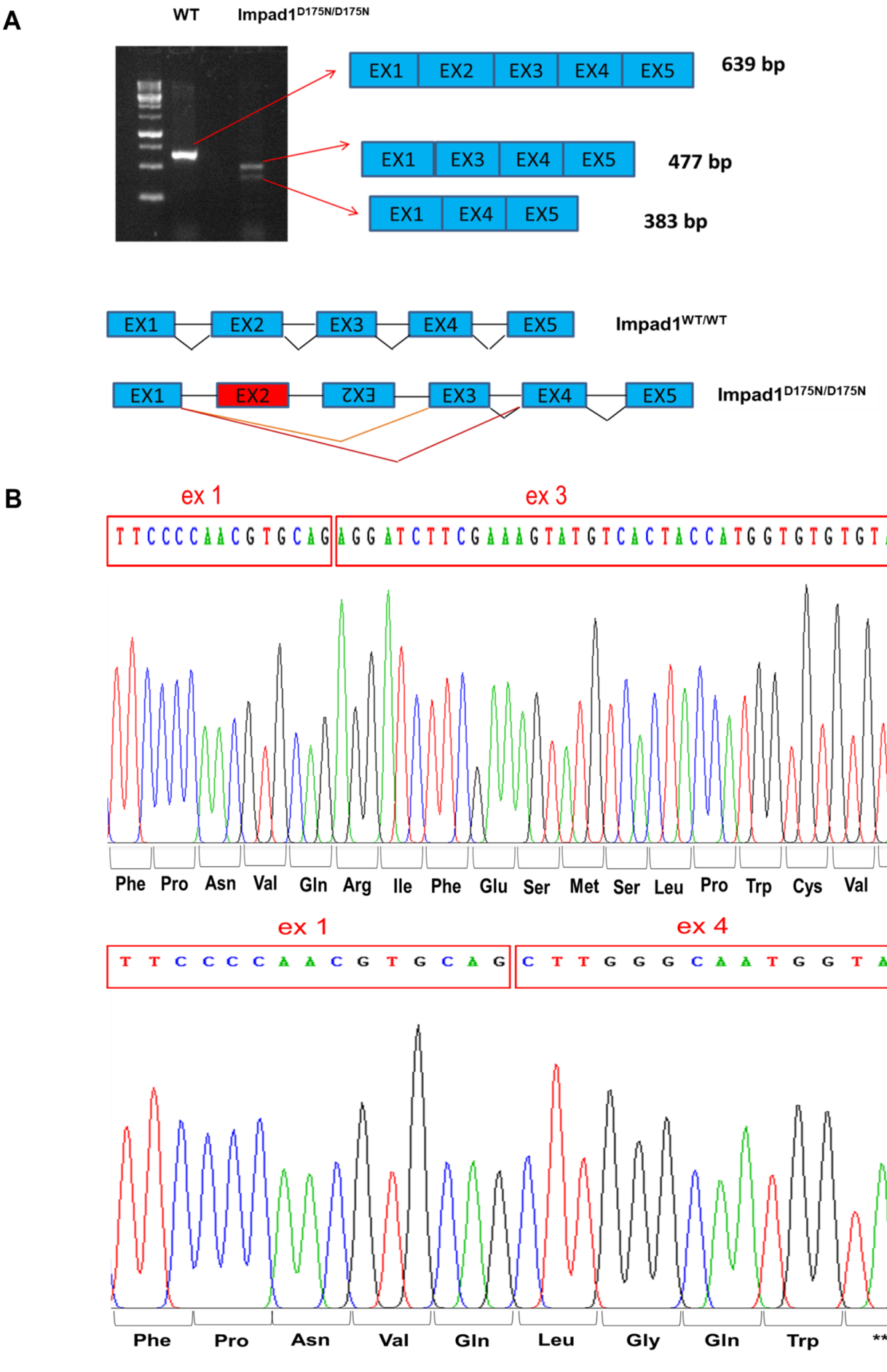
A
WT
Impad1D175N/D175N
EX1 EX2 EX3 EX4 EX5
639 bp
EX1 EX3 EX4 EX5
477 bp
EX1 EX4 EX5
383 bp
EX1 EX2 EX3 EX4 EX5
Impad1WT/WT
EX1 EX2 EX3 EX4 EX5
Impad1D175N/D175N
B
ex 1
ex 3
TTCCCCAACGTGCAG
AGGATCTTCGAAAGTATGTCACTACCATGGTGTGTGTAG
Phe Pro Asn Val Gln Arg Ile Phe Glu Ser Met Ser Leu Pro Trp Cys Val ***
ex 1
ex 4
TTCCCCAACGTGCAG
CTTGGGCAATGGTAG
Phe Pro Asn Val Gln Leu Gly Gln Trp ***

Fig 6. Alternative splicing analysis of Impad1 mRNA. (A) RT-PCR using primers that amplify a region spanning exon 1 to exon 5 was performed from skin total RNA of wild-type and *Impad1*$^{D175N/D175N}$ newborn mice and analysed by 1.5% agarose gel. In wild-type animals one band, 639 bp long, corresponding to the correctly spliced Impad1 transcript including the 5 coding exons is present. This band is not detected in mutant mice, conversely two different bands, 477 bp and 383 bp long, respectively are observed. (B) Sequencing of the two bands demonstrated that the two transcript variants lack exon 2 or both exon 2 and exon 3.

Phenotypic characterization of the *Clcn7* floxed mice

Since in *Impad1*$^{D175N/D175N}$ the phenotype was not due to the missense mutation, but by altered splicing of the modified *Impad1* allele, and that aberrant splicing was likely responsible for *Impad1*$^{Flox/Flox}$ mice unexpected lethal outcome, we checked whether similar modification affected also the *Clcn7*$^{Flox/Flox}$ mice. For this reason heterozygous *Clcn7* floxed mice (*Clcn7*$^{Flox/WT}$) were mated together to observe the phenotype in homozygous floxed mice (*Clcn7*$^{Flox/Flox}$). Since these mice were not mated yet to a Cre expressing murine strain, inversion of the mutated exon, bearing the p.Gly213>Arg mutation, was not yet occurred and thus no phenotype should have been observed. The *Clcn7*$^{Flox/Flox}$ mouse presented the phenotypic characteristic of Autosomal Recessive Osteopetrosis. In particular the *Clcn7*$^{Flox/Flox}$ displayed a phenotype resembling *Clcn7* knock-out mice [25], with reduced survival (Fig 7) and a normal Mendelian ratio of genotypes at birth. As expected, no significant changes in survival was found in the heterozygous *Clcn7*$^{Flox/WT}$ mice (Fig 7).

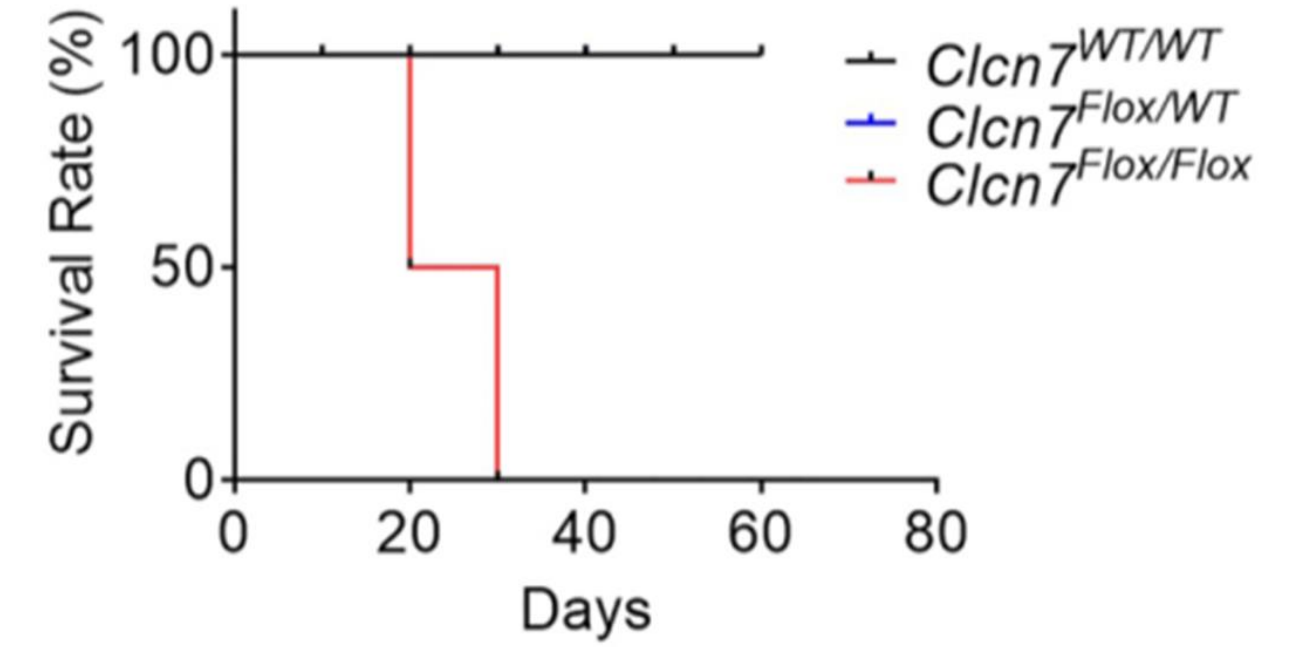

Fig 7. Survival rate of *Clcn7*$^{Flox/Flox}$ mice. Survival rates were calculated following *Clcn7*$^{WT/WT}$ (black line), *Clcn7*$^{Flox/WT}$ (blue line) and *Clcn7*$^{Flox/Flox}$ (red line) mice for 60 days. The *Clcn7*$^{WT/WT}$ and *Clcn7*$^{Flox/WT}$ survival rates overlap, for this reason the blue line is not visible in the graph. Survival rate of *Clcn7*$^{Flox/Flox}$ mice was dramatically reduced. Data are the mean ± SD of 5 mice for group (Mantel-Cox test).

Moreover, *Clcn7*$^{Flox/Flox}$ mice were shorter than heterozygous and wild-type littermates (Fig 8A) and showed no tooth eruption when compared with wild-type littermates (Fig 8B). Both features are clinical signs of Autosomal Recessive Osteopetrosis.

After gross evaluation, femoral bones were analyzed by X-ray and µCT that revealed the 3D architecture of the bones and confirmed a severe osteopetrotic phenotype in *Clcn7*$^{Flox/Flox}$ mice (Fig 9), with an extremely high bone volume/tissue volume (72 ± 4.3% in *Clcn7*$^{Flox/Flox}$ and 13 ± 3.2% in wild-type littermates).

Altogether, these results revealed that the *Clcn7*$^{Flox/Flox}$ mouse has not the expected phenotype, but rather recapitulates the loss-of-function model suggesting that the genomic modification results in a knock-out allele.

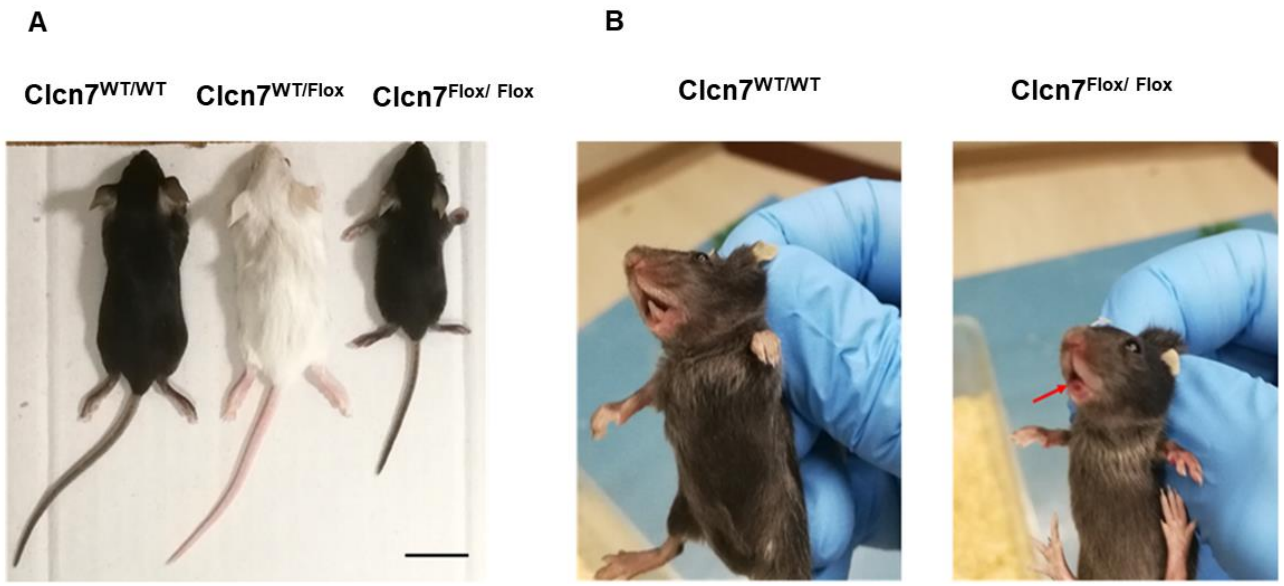

Fig 8. *Clcn7*$^{\text{Flox/Flox}}$ mouse phenotype. Twenty-one day old *Clcn7*$^{\text{WT/WT}}$, *Clcn7*$^{\text{Flox/WT}}$ and *Clcn7*$^{\text{Flox/Flox}}$ mice were evaluated for (A) gross appearance and (B) tooth eruption. *Clcn7*$^{\textit{Flox/Flox}}$ mice showed reduced skeletal growth and no tooth eruption (the red arrow points to the absence of teeth). Scale bar: 1cm

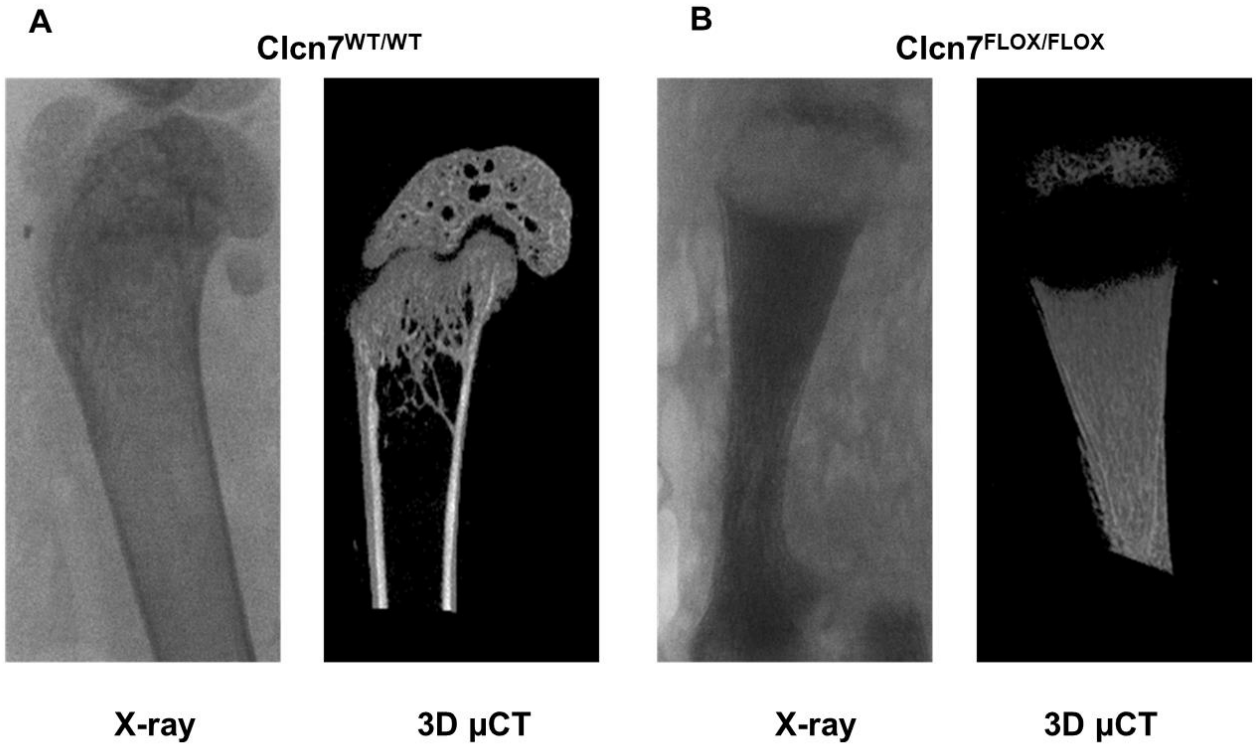

Fig 9. Bone phenotype of the *Clcn7*$^{Flox/Flox}$ mice. Twenty-one day old (**A**) *Clcn7*$^{WT/WT}$ and (**B**) *Clcn7*$^{Flox/Flox}$ mice were sacrificed and then X-ray and μCT imaging were performed on femurs. A severe osteopetrotic phenotype with high bone mass is present in mutant mice. Pictures are representative of 5 mice per group.

DISCUSSION

We have tested a Cre-mediated genetic switch combining the ability of Cre recombinase to invert a DNA fragment, depending upon the orientation of the flanking *loxP* sites, and the use of wild-type and mutant *loxP* sites in order to make recombination irreversible. The notion was that Cre recombinase-mediated inversion would place the exon bearing the missense mutation into a position where it would be spliced properly, while the inverted wild-type exon would be spliced out.

We have used this strategy to generate two conditional knock-in mice for the *Impad1* and *Clcn7* genes. Mutations in these genes cause in human two different skeletal disorders: chondrodysplasia with joint dislocations gPAPP type and autosomal dominant or recessive osteopetrosis, respectively. *Impad1* encodes for a Golgi resident adenosine 3',5'-bisphosphate phosphatase crucial for macromolecular sulfation[19, 24], while the *Clcn7* gene encodes for the ClC7 protein, a proton/chloride antiporter important in lysosomal acidification [26]. In bone, the ClC7 is expressed especially by osteoclasts and it has a pivotal role in bone resorption, charge-balancing the acidified osteoclast resorption lacuna. The missense mutation knocked-in the murine Impad1 was the p.Asp175>Asn corresponding to the p.Asp177>Asn detected previously in a patient [17]. The mutation knocked-in the murine Clc7 was the p.Gly213>Arg described previously in a patient with ADO2 [27, 28].

Both mouse models generated through this strategy resulted in an unexpected severe skeletal phenotype. Heterozygous floxed *Impad1* (*Impad1*$^{Flox/WT}$) mice were mated to a Cre deleter mouse strain in order to generate *Impad1*$^{D175N/WT}$ animals. *Impad1*$^{D175N/D175N}$ mice died at birth with severe hypoplasia of the skeleton and at the biochemical level cartilage proteoglycans were dramatically undersulfated. The phenotype overlapped with the lethal phenotype described previously in *Impad1* knock-out mice generated by a gene trap approach [19, 24]. Expression studies by qPCR and RT-PCR demonstrated that the mutant *Impad1* mRNA underwent abnormal splicing with loss of exon 2 or exons 2 and 3; no mutant full length mRNA spanning exons 1-5 as in normal *Impad1* mRNA was detected. This may results in activation of non-sense mediated decay or anyway to the synthesis

of transcript encoding for a non-functional enzyme since the active site of the phosphatase is encoded by exon 2.

A skeletal phenotype was observed also in homozygous *Clcn7*$^{Floxed/Floxed}$ mice before mating to Cre deleter mice, when the wild-type exon 7 was into a position where it would be spliced properly and thus a wild-type *Clcn7* mRNA would have been generated. The skeletal phenotype observed in these mice overlaps with the *Clcn7* knock-out reported previously [25], suggesting that also in this murine model abnormal splicing occurred generating a knock-out allele, likely because of the wild-type and mutant exon 7 in opposite orientation in the mutant *Clcn7*.

Thus in both animal models the skeletal phenotype parallels the phenotypes of their knock-out mice suggesting that the skeletal defects were not due to the missense mutations, but to aberrant splicing causing the synthesis of non-functional proteins. It is tempting to speculate that the two exons in opposite orientation generate a hairpin loop leading to the skipping of both exons.

A similar strategy was devised previously in order to generate a conditional knock-in of the cAMP response element binding protein (CBP) [14]. To achieve the Cre recombinase-mediated mutation CBP^{Tyr658Ala}, a targeting construct containing the wild-type exon 5 of the CBP and a mutated exon 5 (p.Tyr658>Ala) in an inverted orientation was generated. These sequences were flanked by two mutated *loxP* sites, which were positioned in a head-to-head orientation. The authors demonstrated that in ES cells the genetic switch worked properly when cells were transfected with a plasmid expressing Cre-recombinase, but unfortunately, no data were available regarding the expression at the mRNA or protein level. The generation and further characterization of transgenic animals from these ES cells has never been reported to date.

In conclusion, the Cre mediated genetic switch strategy has paved the way to the engineering of sophisticated genetic modifications including conditional point mutation, conditional rescue, conditional gene replacement and recombinase mediated cassette exchange which have been used successfully *in vitro*. However, it is worth noting that modifying the genome of eukaryotic cells to generate Cre mediated switch alleles may have some drawbacks. The repetition of endogenous

splicing sites in the antisense orientation may also induce the occurrence of aberrantly spliced mRNA. In any case, it is probably safe to reduce DNA repetitions as much as possible and to test for functionality in transiently transfected cells when possible, or in ES cell clones before further proceeding to blastocyst injections.

Author contributions

Conceptualization: Mattia Capulli, Rossella Costantini, Stephan Sonntag, Anna Teti, Antonio Rossi.

Formal analysis: Mattia Capulli, Rossella Costantini, Antonio Maurizi, Chiara Paganini, Luca Monti.

Funding acquisition: Mattia Capulli, Doron Shmerling, Antonella Forlino, Anna Teti, Antonio Rossi.

Investigation: Mattia Capulli, Rossella Costantini, Stephan Sonntag, Antonio Maurizi, Chiara Paganini, Luca Monti.

Methodology: Stephan Sonntag, Doron Shmerling.

Supervision: Mattia Capulli, Stephan Sonntag, Doron Shmerling, Anna Teti, Antonio Rossi.

Writing - original draft: Mattia Capulli, Rossella Costantini, Stephan Sonntag, Antonio Maurizi, Antonio Rossi.

Writing - review & editing: Mattia Capulli, Rossella Costantini, Stephan Sonntag, Antonio Maurizi, Chiara Paganini, Antonella Forlino, Doron Shmerling, Anna Teti, Antonio Rossi.

Funding

The research leading to these results has received funding from the European Community's Seventh Framework Programme under grant agreement n. 602300 (SYBIL) (to DS, AF, AT and AR), Fondazione Telethon, Italy (grant n. GEP15062 to AR and GGP14014 to AT), MIUR "Dipartimenti di Eccellenza 2018-2022" (to AF and AR), MIUR " Progetti di ricerca di rilevante interesse nazionale" (PRIN 2015F3JHMB to AT and AR) and "Fondo di finanziamento per le attività base di ricerca" (FFABR to MC).

References

1. Krakow D. Skeletal dysplasias. Clin Perinatol. 2015;42(2):301-19, viii. Epub 2015/06/05. doi: 10.1016/j.clp.2015.03.003. PubMed PMID: 26042906; PubMed Central PMCID: PMCPMC4456691.
2. Bonafe L, Cormier-Daire V, Hall C, Lachman R, Mortier G, Mundlos S, et al. Nosology and classification of genetic skeletal disorders: 2015 revision. Am J Med Genet A. 2015;167(12):2869-92. PubMed PMID: 26394607.
3. Neben CL, Roberts RR, Dipple KM, Merrill AE, Klein OD. Modeling craniofacial and skeletal congenital birth defects to advance therapies. Hum Mol Genet. 2016;25(R2):R86-r93. Epub 2016/06/28. doi: 10.1093/hmg/ddw171. PubMed PMID: 27346519; PubMed Central PMCID: PMCPMC5036869.
4. Gioia R, Tonelli F, Ceppi I, Biggiogera M, Leikin S, Fisher S, et al. The chaperone activity of 4PBA ameliorates the skeletal phenotype of Chihuahua, a zebrafish model for dominant osteogenesis imperfecta. Human Molecular Genetics. 2017;26(15):2897-911. doi: 10.1093/hmg/ddx171. PubMed PMID: WOS:000405706800008.
5. Fiedler I, Schmidt F, Wölfel E, Plumeyer C, Milovanovic P, Gioia R, et al. Severely Impaired Bone Material Quality in Chihuahua Zebrafish Resembles Classical Dominant Human Osteogenesis Imperfecta. Journal of Bone and Mineral Research. 2018;33(8):1489-99. doi: 10.1002/jbmr.3445.
6. de Andrea CE, Prins FA, Wiweger MI, Hogendoorn PC. Growth plate regulation and osteochondroma formation: insights from tracing proteoglycans in zebrafish models and human cartilage. J Pathol. 2011;224(2):160-8. Epub 2011/04/21. doi: 10.1002/path.2886. PubMed PMID: 21506131.
7. Garofalo S, Horton WA. Genetic-engineered models of skeletal diseases. II. Targeting mutations into transgenic mice chondrocytes. Methods Mol Biol. 2000;137:491-8. Epub 2000/08/19. doi: 10.1385/1-59259-066-7:491. PubMed PMID: 10948562.
8. Capecchi MR. Gene targeting in mice: functional analysis of the mammalian genome for the twenty-first century. Nat Rev Genet. 2005;6(6):507-12. Epub 2005/06/03. doi: 10.1038/nrg1619. PubMed PMID: 15931173.
9. Bradley A, Anastassiadis K, Ayadi A, Battey JF, Bell C, Birling MC, et al. The mammalian gene function resource: the International Knockout Mouse Consortium. Mamm Genome. 2012;23(9-10):580-6. Epub 2012/09/13. doi: 10.1007/s00335-012-9422-2. PubMed PMID: 22968824; PubMed Central PMCID: PMCPMC3463800.
10. Birling MC, Herault Y, Pavlovic G. Modeling human disease in rodents by CRISPR/Cas9 genome editing. Mamm Genome. 2017;28(7-8):291-301. Epub 2017/07/06. doi: 10.1007/s00335-017-9703-x. PubMed PMID: 28677007; PubMed Central PMCID: PMCPMC5569124.
11. Bockamp E, Maringer M, Spangenberg C, Fees S, Fraser S, Eshkind L, et al. Of mice and models: improved animal models for biomedical research. Physiol Genomics. 2002;11(3):115-32. Epub 2002/12/05. doi: 10.1152/physiolgenomics.00067.2002. PubMed PMID: 12464688.
12. Bockamp E, Sprengel R, Eshkind L, Lehmann T, Braun JM, Emmrich F, et al. Conditional transgenic mouse models: from the basics to genome-wide sets of knockouts and current studies of tissue regeneration. Regen Med. 2008;3(2):217-35. Epub 2008/03/01. doi: 10.2217/17460751.3.2.217. PubMed PMID: 18307405.
13. Araki K, Okada Y, Araki M, Yamamura K. Comparative analysis of right element mutant lox sites on recombination efficiency in embryonic stem cells. BMC Biotechnol. 2010;10:29. Epub 2010/04/02. doi: 10.1186/1472-6750-10-29. PubMed PMID: 20356367; PubMed Central PMCID: PMCPMC2865440.
14. Zhang Z, Lutz B. Cre recombinase-mediated inversion using lox66 and lox71: method to introduce conditional point mutations into the CREB-binding protein. Nucleic Acids Res. 2002;30(17):e90. Epub 2002/08/31. PubMed PMID: 12202778; PubMed Central PMCID: PMCPMC137435.
15. Schnutgen F, Doerflinger N, Calleja C, Wendling O, Chambon P, Ghyselinck NB. A directional strategy for monitoring Cre-mediated recombination at the cellular level in the mouse. Nat Biotechnol. 21. United States2003. p. 562-5.

16. Schnutgen F, Ghyselinck NB. Adopting the good reFLEXes when generating conditional alterations in the mouse genome. Transgenic Res. 2007;16(4):405-13. Epub 2007/04/07. doi: 10.1007/s11248-007-9089-8. PubMed PMID: 17415672.
17. Vissers LE, Lausch E, Unger S, Campos-Xavier AB, Gilissen C, Rossi A, et al. Chondrodysplasia and abnormal joint development associated with mutations in IMPAD1, encoding the Golgi-resident nucleotide phosphatase, gPAPP. Am J Hum Genet. 2011;88(5):608-15. PubMed PMID: 21549340.
18. Alam I, Gray AK, Chu K, Ichikawa S, Mohammad KS, Capannolo M, et al. Generation of the first autosomal dominant osteopetrosis type II (ADO2) disease models. Bone. 2014;59:66-75. Epub 2013/11/05. doi: 10.1016/j.bone.2013.10.021. PubMed PMID: 24185277; PubMed Central PMCID: PMCPMC3889206.
19. Frederick JP, Tafari AT, Wu SM, Megosh LC, Chiou ST, Irving RP, et al. A role for a lithium-inhibited Golgi nucleotidase in skeletal development and sulfation. Proc Natl Acad Sci U S A. 2008;105(33):11605-12. PubMed PMID: 18695242.
20. Lorensen WE, Cline HE. Marching cubes: A high resolution 3D surface construction algorithm. A*CM SIGGRAPH Comput Graph*. 1987;21:163-9.
21. Bouxsein ML, Boyd SK, Christiansen BA, Guldberg RE, Jepsen KJ, Muller R. Guidelines for assessment of bone microstructure in rodents using micro-computed tomography. J Bone Miner Res. 2010;25(7):1468-86. Epub 2010/06/10. doi: 10.1002/jbmr.141. PubMed PMID: 20533309.
22. Forlino A, Piazza R, Tiveron C, Della Torre S, Tatangelo L, Bonafe L, et al. A diastrophic dysplasia sulfate transporter (SLC26A2) mutant mouse: morphological and biochemical characterization of the resulting chondrodysplasia phenotype. Hum Mol Genet. 2005;14(6):859-71. PubMed PMID: 15703192.
23. Monti L, Paganini C, Lecci S, De Leonardis F, Hay E, Cohen-Solal M, et al. N-acetylcysteine treatment ameliorates the skeletal phenotype of a mouse model of diastrophic dysplasia. Human Molecular Genetics. 2015;24(19):5570-80. doi: 10.1093/hmg/ddv289. PubMed PMID: WOS:000363018100015.
24. Sohaskey ML, Yu J, Diaz MA, Plaas AH, Harland RM. JAWS coordinates chondrogenesis and synovial joint positioning. Development. 2008;135(13):2215-20. PubMed PMID: 18539921.
25. Kornak U, Kasper D, Bosl MR, Kaiser E, Schweizer M, Schulz A, et al. Loss of the ClC-7 chloride channel leads to osteopetrosis in mice and man. Cell. 2001;104(2):205-15. Epub 2001/02/24. PubMed PMID: 11207362.
26. Graves AR, Curran PK, Smith CL, Mindell JA. The Cl-/H+ antiporter ClC-7 is the primary chloride permeation pathway in lysosomes. Nature. 2008;453(7196):788-92. Epub 2008/05/02. doi: 10.1038/nature06907. PubMed PMID: 18449189.
27. Waguespack SG, Koller DL, White KE, Fishburn T, Carn G, Buckwalter KA, et al. Chloride channel 7 (ClCN7) gene mutations and autosomal dominant osteopetrosis, type II. J Bone Miner Res. 2003;18(8):1513-8. Epub 2003/08/22. doi: 10.1359/jbmr.2003.18.8.1513. PubMed PMID: 12929941.
28. Capulli M, Maurizi A, Ventura L, Rucci N, Teti A. Effective Small Interfering RNA Therapy to Treat CLCN7-dependent Autosomal Dominant Osteopetrosis Type 2. Mol Ther Nucleic Acids. 2015;4:e248. Epub 2015/09/02. doi: 10.1038/mtna.2015.21. PubMed PMID: 26325626; PubMed Central PMCID: PMCPMC4877447.

SUPPORTING INFORMATION

Testing the Cre-mediated genetic switch for the generation of conditional knock-in mice

Mattia Capulli, Rossella Costantini, Stephan Sonntag, Antonio Maurizi, Chiara Paganini, Luca Monti, Antonella Forlino, Doron Shmerling, Anna Teti, Antonio Rossi

S1 Table. PCR primers used in this study.

SY08.18 5’-TCCTACTGTAGATACAGAATTAC-3’
SY08.19 5’-GCAAATAAGCAGTTACAGAATATG-3’

Neo3-for: 5’-CAAGCTCTTCAGCAATATCACGGG-3’
Neo4-rev: 5’-CCTGTCCGGTGCCCTGAATGAACT-3’

SY08.20: 5’-TGGCCTGAGACACATTCC-3’
SY08.21: 5’-CTGCTGGTACCTCCTTAG-3’

SY03.11: 5’-CTCTTGGCCACCCAATTC-3’
SY03.12: 5’-GGACAGAGCCTCTACAAC-3’

IMP3: 5’-GTTAGATTAGAAAGTACTTGAAG-3’
IMP8: 5’-CTAGTCTGCTTGTCTGGAAACC-3’

S1 Fig. X-rays of the *Impad1*$^{Flox/Flox}$ mouse. The newborn mutant shows severe underdevelopment of the skeleton compared to the wild-type mouse.